Quantitative GTPase affinity purification identifies Rho family protein interaction partners

Paul, F. and Zauber, H. and von Berg, L. and Rocks, O. and Daumke, O. and Selbach, M.

Molecular & Cellular Proteomics
2017 JAN 01 ; 16(1): 73-85
Doi: 10.1074/mcp.M116.061531

Publisher: American Society for Biochemistry and Molecular Biology

Quantitative GTPase Affinity Purification Identifies Rho Family Protein Interaction Partners*[S]

Florian Paul‡, Henrik Zauber‡, Laura von Berg§, Oliver Rocks§, Oliver Daumke¶, and Matthias Selbach‡‖

Although Rho GTPases are essential molecular switches involved in many cellular processes, an unbiased experimental comparison of their interaction partners was not yet performed. Here, we develop quantitative GTPase affinity purification (qGAP) to systematically identify interaction partners of six Rho GTPases (Cdc42, Rac1, RhoA, RhoB, RhoC, and RhoD), depending on their nucleotide loading state. The method works with cell line or tissue-derived protein lysates in combination with SILAC-based or label-free quantification, respectively. We demonstrate that qGAP identifies known and novel binding partners that can be validated in an independent assay. Our interaction network for six Rho GTPases contains many novel binding partners, reveals highly promiscuous interaction of several effectors, and mirrors evolutionary relationships among Rho GTPases. ***Molecular & Cellular Proteomics 16: 10.1074/mcp.M116.061531, 73–85, 2017.***

The Ras superfamily of small guanosine triphosphatases (Ras GTPases) consists of more than 150 members in mammals and conserved orthologs in all eukaryotes (1). As molecular switches, they cycle between an active GTP- and an inactive GDP-bound state. GTPase-activating proteins (GAPs)[1] stimulate the slow intrinsic GTPase activity, which inactivates the GTPase. Conversely, guanine nucleotide exchange factors (GEFs) promote release of GDP, which is replaced by GTP, thereby transforming the GTPase into the active state. The GTP-bound form binds to downstream effector proteins to initiate their specific cellular function. In this manner, GTPases control numerous biological processes, including cytoskeletal rearrangements, membrane dynamics, and gene expression. Rho GTPases form a subfamily of the Ras superfamily (2). Of its 22 mammalian members, RhoA, Rac1, and Cdc42 have been studied most intensively and are best known for their role in regulating the actin cytoskeleton (3).

Identifying effector proteins is key to understanding Rho GTPase function. More than 70 effector proteins have already been identified for each of the three prototypical family members, RhoA, Rac1, and Cdc42 (4). However, new effector proteins are still being discovered, and little is known about effectors of less well studied family members. Systematic screens for GTPase effectors employed the yeast two-hybrid approach (5) or immobilized GTPases for affinity purification (6, 7). However, these approaches are semiquantitative at best, which makes it difficult to distinguish loading-state-specific binders from constitutive interactors and nonspecific contaminants. Due to these challenges, an unbiased interactor screen for multiple Rho GTPases has not yet been reported.

We sought to systematically identify proteins that interact with Rho GTPases in a loading-state-specific manner. Quantitative affinity purification combined with mass spectrometry is a powerful technology that can be used to identify protein–protein interactions (PPIs) in an unbiased way (8–11). Here, we develop quantitative GTPase affinity purification (qGAP) as a novel variant of quantitative affinity purification combined with mass spectrometry to systematically identify Rho GTPase interaction partners. We then employ qGAP to screen for interaction partners of the three prototypical Rho GTPases (Cdc42, Rac1, RhoA) and three additional family members (RhoB, RhoC, RhoD). We employ qGAP in a SILAC-dependent way with lysates of cultured cells (SILAC-qGAP) and a label-free manner (LF-qGAP) with tissue samples. We show that qGAP identifies many well-known effectors and dozens of potential new interaction partners. Importantly, new inter-

From the ‡Proteome Dynamics, §Spatio-Temporal Control of Rho GTPase Signaling, ¶Crystallography, Max Delbrück Center for Molecular Medicine, Robert-Rössle-Str. 10, D-13092 Berlin, Germany

Received June 7, 2016, and in revised form, October 27, 2016
Published, MCP Papers in Press, November 16, 2016, DOI 10.1074/mcp.M116.061531
Author contributions: O.R., O.D., and M.S. designed the research; F.E.P. and L.V. performed research; O.R. and O.D. contributed new reagents or analytic tools; F.E.P. and H.Z. analyzed data; and F.E.P., H.Z., and M.S. wrote the paper.

[1] The abbreviations used are: GAP, GTPase-activating protein; CRIB, Cdc42/Rac interactive binding; GEF, GTPase exchange factor; GDP, guanosine diphosphate; GTP, guanosine triphosphate; GTPase, guanosine triphosphatases, HIPPIE, human integrated protein–protein interaction reference; LFQ, label-free quantification; PLA, proximity ligation assay; PPI, protein–protein interaction; qGAP, quantitative GTPase affinity purification; Ras, rat sarcoma; Rho, Ras homolog; SILAC, stable isotope labeling by/with amino acids in cell culture; CNF, cytotoxic necrotizing factor.

action partners can be validated with a high success rate in an independent assay. Our interaction network reflects evolutionary relationships among Rho GTPases and reveals promiscuous binding of several known effectors.

RESULTS

Establishing SILAC-qGAP—Quantitative affinity purification combined with mass spectrometry can be used to study cellular dynamics of PPIs (8, 9, 11–13). The principle is to compare the abundance of proteins copurifying with the bait to an internal control. The approach can thus distinguish specific interaction partners from nonspecific contaminants: While true interaction partners are more abundant in the bait sample, nonspecific contaminants show a 1:1 ratio. This strategy has been successfully employed to identify both constitutive PPIs and dynamic PPIs that are regulated by cellular signaling events and/or posttranslational modifications (14–17).

We reasoned that quantitative affinity purification combined with mass spectrometry should also allow us to identify GTPase effector proteins in an unbiased manner (Fig. 1 *A*). To establish the method, we recombinantly expressed Rho GTPases as GST-fusion proteins in *Escherichia coli* and purified them to homogeneity. In order to test whether or not purified recombinant GTPases were enzymatically active, we initially monitored the intrinsic GTPase activities of RhoA, Cdc42, and Rac1 by an HPLC-based method. All three Rho GTPases showed GTP-hydrolysis activity (Fig. S1) with rate constants similar to previously published data (18–21). To further evaluate their functionality, we added HEK cell lysates to the reactions overexpressing citrine-labeled GAPs specific for each GTPase (22–24). Lysates of citrine-expressing control cells increased GTP hydrolysis, presumably due to the presence of endogenously expressed GAPs in the lysate (Fig. S1). The presence of citrine-labeled GAPs dramatically increased GTP hydrolysis (Fig. S1). These data clearly show that the purified recombinant GTPases used in our experiments were fully active and capable of interacting with known interaction partners.

In order to test whether or not we can identify activation state-specific binders, we loaded recombinant Cdc42 with GDP or GTPγS, a GTP-analog that is inefficiently hydrolyzed (25). Differentially loaded fusion proteins were then covalently coupled to N-hydroxysuccinimide-activated Sepharose beads. These beads were used to pull-down interacting proteins from differentially SILAC-labeled HeLa cell lysates. After washing, proteins were combined, eluted, and analyzed by high resolution shotgun proteomics and MaxQuant (26). In total, we identified over 1,000 proteins (Fig. 1*B*). As expected, the vast majority of these proteins had SILAC log2 fold changes around 0, indicating that they do not interact with Cdc42 in a loading-state-specific way. We then selected significant outliers in the distribution of log2 fold changes as putative specific interaction partners of the GTP- and GDP-loaded forms (calculation with the software package Perseus, "significance B," Benjamini Hochberg false discovery rate $< 5\%$ (26)). Most of these putative binders showed preferential interaction with the GTPγS-loaded form. This is consistent with the idea that the GTP-bound form mediates most downstream functions (27, 28). As an additional control, we also performed a label swap experiment (Fig. 1*C*). We then plotted the log2 fold changes from both experiments against each other (Fig. 1*D*). Specific binders were required to be significant outliers in both experiments and to show inverted ratios. Note that the same heavy and light lysates were used for both the forward and reverse experiment. Therefore, requiring an inverted ratio in the label swap eliminates proteins that deviate from the 1:1 ratio already in the lysate. According to these criteria, 25 proteins were defined as loading-state-specific binders. All of them showed preferential binding to the GTPγS-loaded form. The list contains several well-known Cdc42 interactors like Cdc42 binding proteins (CDCBPA and CDC42BPB), Cdc42 effector proteins (CDC42EP1, 2, 3, and 4) as well as BAIAP2. Collectively, these data indicate that our assay can reliably identify Cdc42 effectors.

Establishing LF-qGAP—One limitation of the experiments described above is that they are based on lysate derived from HeLa cells. Hence, proteins that are not expressed in this cell line cannot be detected. We therefore sought to employ lysate derived from tissues as broader source of proteins for our qGAP assay (Fig. 2*A*). We chose mouse brain lysate since five of the six Rho GTPases studied here are expressed in this tissue (only RhoC seems to be expressed in macrophages or glandular cell types (29)). In addition, different cell types are present in brain, which should lead to a large number of potential binding proteins being available in the lysate. For quantification, we chose a label-free approach that was used previously to study interaction partners of GFP-fusion proteins (30, 31).

To test the performance of (LF-qGAP, we repeated pull-downs with Cdc42 using protein lysate prepared from mouse cerebellum (Figs. 2*A* and 2*B*). In total, we performed six pull-downs—three with the GDP-loaded form and three with the GTPγS-loaded form. After proteomic analysis of all six samples, we used label-free quantification by MaxQuant (32) and displayed the data as a volcano plot (Fig. 2*B*). We accepted proteins as loading-state-specific binders based on a combination of the *t* test *p* value and the fold change at a permutation-based false discovery rate of 0.05 (30). In total, these experiments identified 42 and two potential interactors of the GTPγS- and GDP-loaded form, respectively. The increased number of identified interaction partners compared with the SILAC data (Fig. 2*C*) is probably due to a combination of technical (experimental setup, data analysis) and biological factors (different protein levels, cofactors, and posttranslational modifications). For example, we observed that interaction partners that we exclusively found in brain tissue pull-downs tend to be more abundant in brain tissue than in HeLa

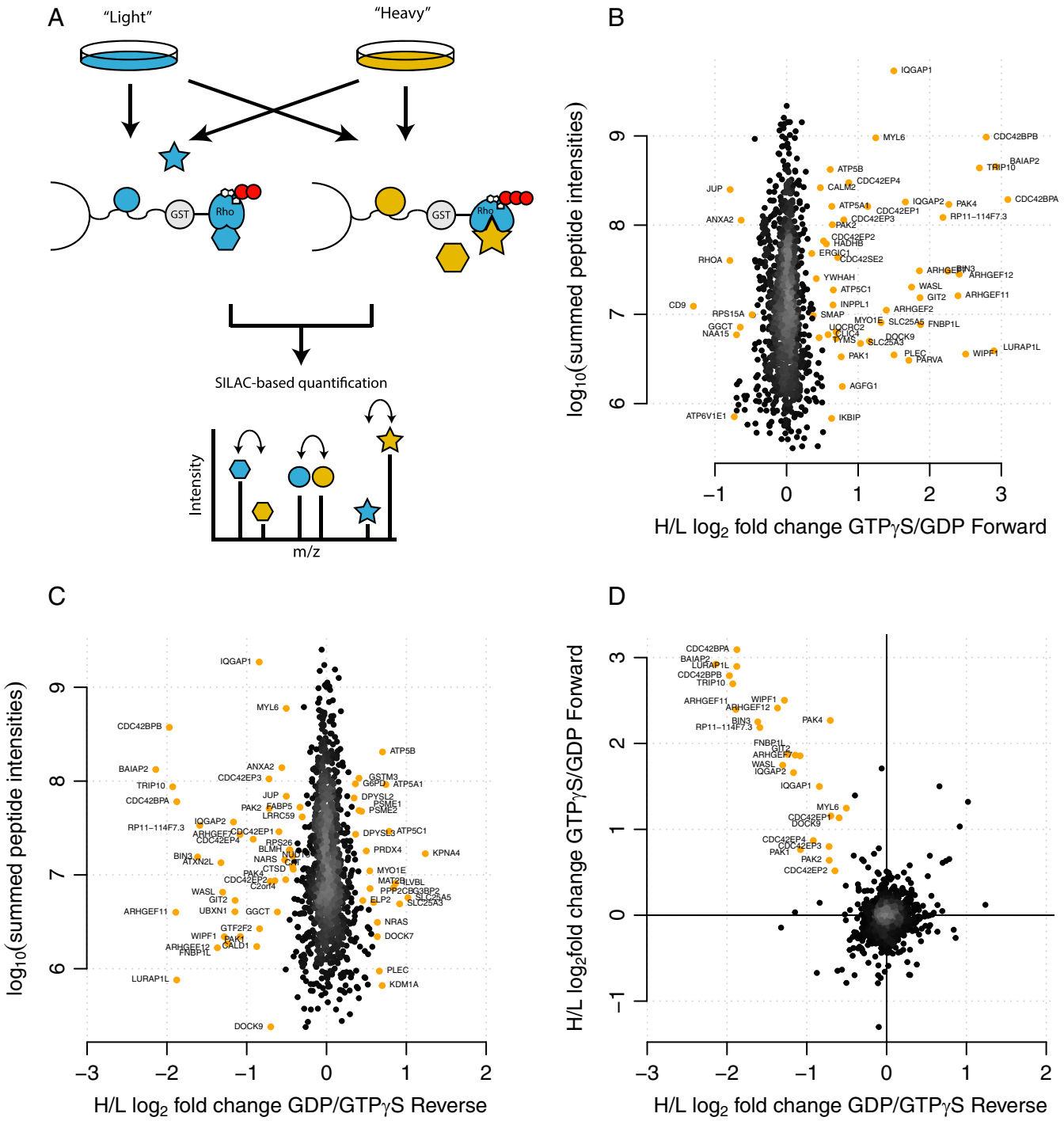

FIG. 1. **Identification of Cdc42 interaction partners with SILAC-qGAP.** (*A*) Rho GTPases were expressed, purified, loaded with either GDP or GTPγS, and bound to a Sepharose matrix. Protein samples were obtained from SILAC-labeled cells. Proteins from H- and L-labeled cells were pulled down with Cdc42GTPγS and Cdc42GDP in a forward (*arrows*) and reverse experiment. Bound proteins were eluted and analyzed via mass spectrometry. Significant outliers were calculated (labeled in *orange*) for the forward (*B*) and reverse (*C*) experiment. Proteins that are significant outliers in the forward and reverse experiment and that were specific to one nucleotide form in both experiments are considered specific interaction partners of Cdc42 (*D*, labeled in *orange*).

cell lysate (data not shown). Thus, LF-qGAP is not necessarily superior to the SILAC-qGAP. The choice of the lysate should generally be guided by the biological question.

LF-qGAP for Six Rho GTPases—Encouraged by these results, we used LF-qGAP to screen for interaction partners of Rac1, Cdc42, RhoA, RhoB, RhoC, and RhoD (Fig. 3 and Fig.

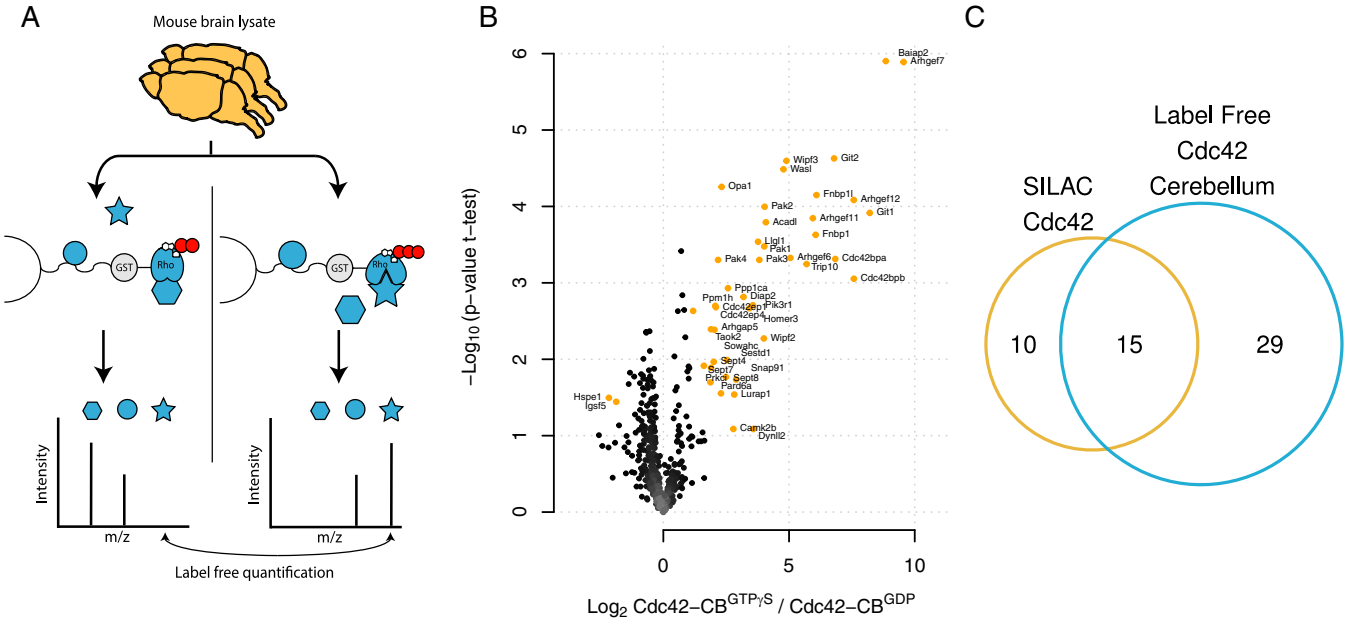

FIG. 2. **Identification of Cdc42 interaction partners with LF-qGAP from mouse cerebellum.** (*A*) Protein lysates from mouse cerebellum ($n = 3$ independent samples) were incubated with Cdc42GTPγS or Cdc42GDP coupled to beads. Bound proteins were eluted and analyzed via mass spectrometry in triplicates. Differences in intensities between runs (Log2 Cdc42GTPγS/Cdc42GDP) and statistical significance (-Log10(*p* value *t* test)) were calculated. (*B*) Specific interactors are distinguished from background proteins based on a combination of the log2 fold change and the *t* test *p* value (significantly different proteins in *orange*), Cdc42GTPγS (*right*) or Cdc42GDP (*left*) (colored in *red*). (*C*) We identified more interaction partners for LF-qGAP (44 proteins) than for SILAC-qGAP (25) with a significant overlap (15).

S2). For Rac1, Cdc42, and RhoA, we also used lysates derived from different brain regions (cerebellum, cerebrum, and hippocampus) while whole brain lysates were used for RhoB, RhoC, and RhoD. Every experiment was performed in biological triplicates. We performed ten experiments (six Rho GTPases and varying brain tissues) with six pull-downs for each experiment (three replicates for GDP and GTP each, *i.e.* a total number of 60 individual pull-downs). From these, we generated an unbiased map of Rho GTPase interaction partners. For each GTPase, we identified between 24 and 73 potential interactors. In total, this amounted to 293 interactions (Supplemental Table 1). Most of them were specific for the GTPγS-loaded form, consistent with the idea that the GTP-loaded form mediates most downstream functions. Many of the proteins we identified as GTPγS-specific binders are well-known effectors (like N-WASP for Cdc42, Rhotekin for RhoA and RhoB) while others are novel (such as mitotic spindle organizing protein 2 for Cdc42). Similarly, some of the GDP-specific interactions are known (*e.g.* Tiam2-Rac1) and some are new (*e.g.* Traf7-Rac1).

The analysis above is based on the direct comparison of the GTPγS and the GDP-loaded form of an individual Rho GTPase. While this is the most relevant control strategy, we would like to point out that our data can be analyzed in different ways. For example, differences in interactors between GTP-loaded forms of two different GTPases could be identified by directly comparing them to each other (*e.g.* Rac1- GTPγS with Cdc42-GTPγS).

Comparison to Published Data—To systematically compare our data with known interactors, we used an integrated protein interaction database, HIPPIE, as a reference (33). We found that known targets are highly significantly overrepresented in our dataset (Fig. 4, *p* values between 7×10^{-4} and 3×10^{-31}, p(X ≥ x), hypergeometric test). Since several literature-described Rho GTPase interaction partners are not in the reference database (*e.g.* Plekhg5 for RhoA (34) and Arhgap5 for Rac1 (35)) but were identified in our screen, we expect the number of true positive identifications of qGAP to be even higher. In addition, our data also contain proteins that are probably indirect binders. For example, we found association of lethal giant larvae homolog 1 with Cdc42, which is probably mediated via the complex of PAR-6A and atypical protein kinase C (aPKC-lambda/iota) that were also both identified. Whether or not detection of indirect interactors is a strength or weakness is a matter of perspective. In any case, our data show that qGAP hits are highly enriched for proteins involved in Rho GTPase biology.

Validation—For each Rho GTPase, we identified dozens of novel interaction partners (see also colored lines in Fig. 6*A*). Thus, our dataset provides a valuable resource for exploring Rho GTPase biology. However, since qGAP is an *in vitro* assay, it is not clear if identified potential interactors also associate with their respective Rho GTPase in living cells. We therefore sought to validate qGAP hits using an independent method. Ideally, this method should (i) assess interactions of endogenous untagged proteins *in vivo*, (ii) provide an unbi-

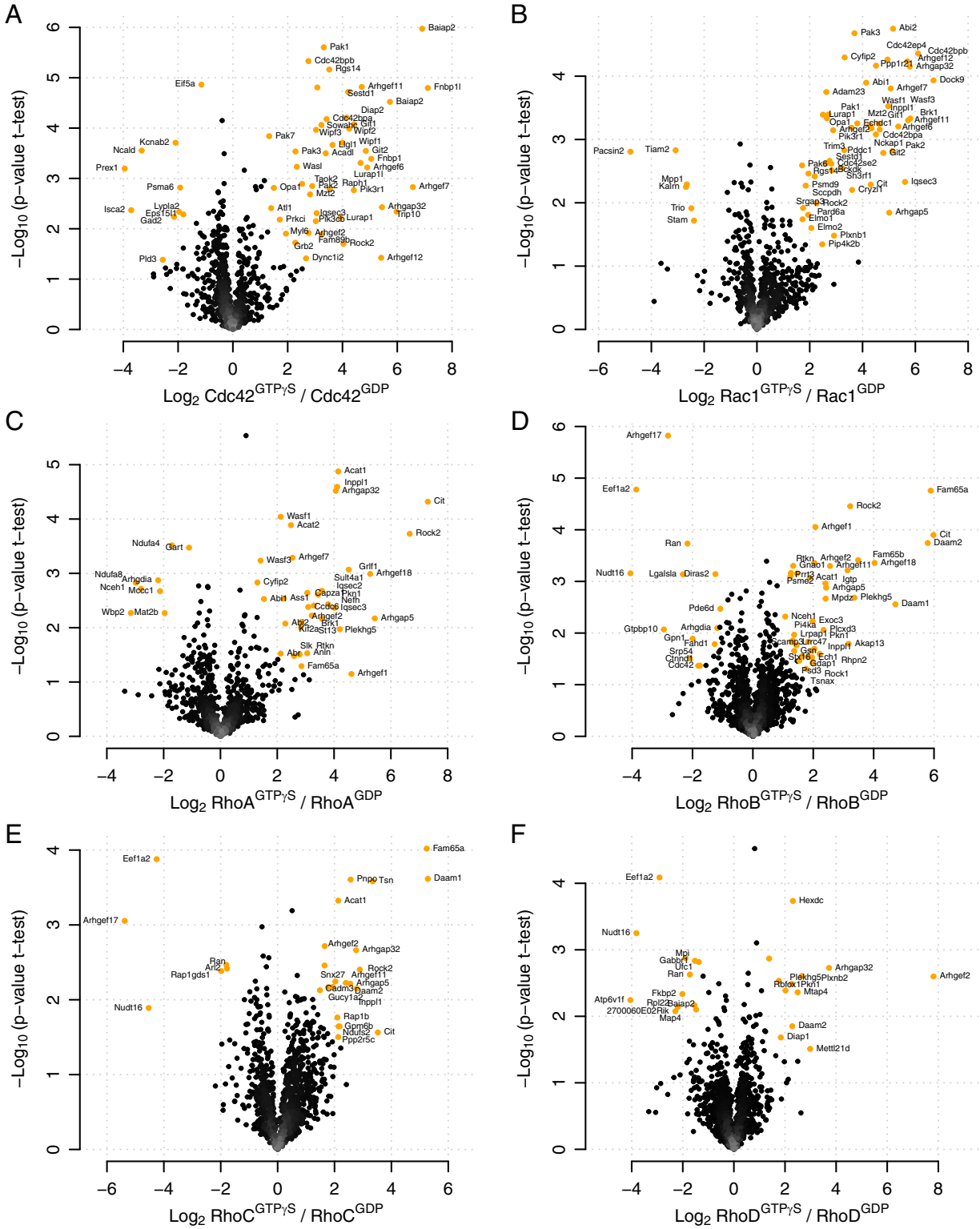

FIG. 3. **LF-qGAP from brain lysates for six Rho GTPases.** Cerebrum pull-downs for (*A*) Cdc42, (*B*) Rac1, (*C*) RhoA. Pull-downs from whole brain lysates for (*D*) RhoB, (*E*) RhoC, (*F*) RhoD. As before, specific interactors (colored in orange) are distinguished from background proteins based on a combination of the log2 fold change and the *t* test *p* value. GTPγS-specific interactors are expected in the *upper right corner*, interactors of the GDP-form in the *upper left corner*.

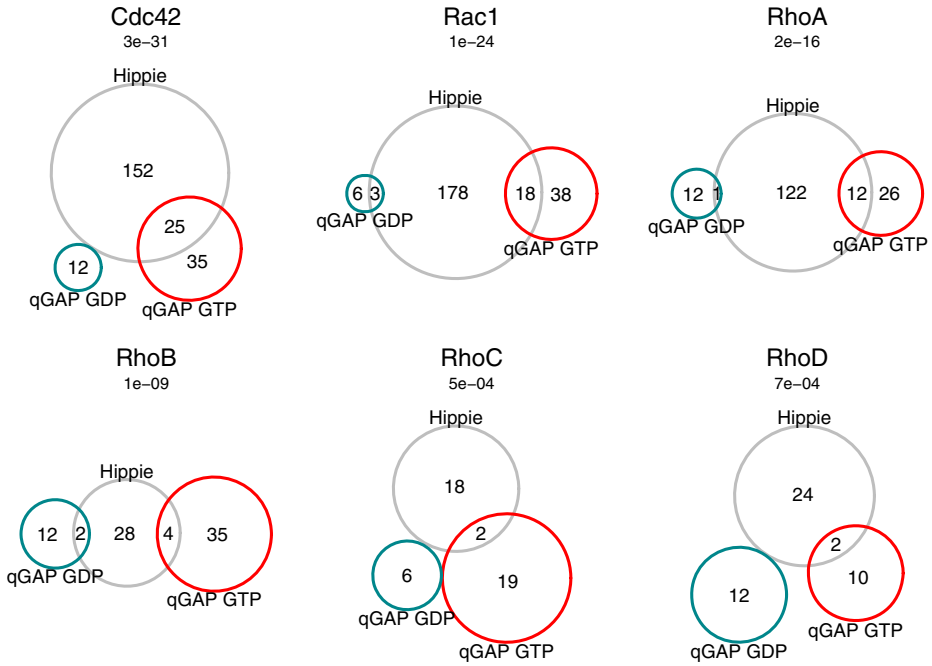

FIG. 4. **Overlap with published interactions.** Interactors identified by qGAP (GDP specific interactors in *turquoise*; GTPγS specific interactors in *red*) with interactors listed in the HIPPIE protein-protein interaction Database (*gray circle*). *p* values indicate significance of the enrichment of overlapping interactors between qGAP and HIPPIE and are given above each Venn diagram.

ased quantitative read out, and (iii) differentiate between the GTP- and the GDP-loaded form of the Rho GTPase. The proximity ligation assay (PLA) uses oligonucleotides attached to antibodies against two target proteins that guide the formation of circular DNA strands when bound in close proximity (36). The DNA can be amplified and visualized, which enables unbiased quantification of endogenous protein complexes at single-molecule resolution. The GTP-loading state of endogenous Rho GTPases can be manipulated with the bacterial toxins CNF_Y and CNF1 (37, 38). These toxins deamidate a single glutamine residue that is required for GTPase activity. Thus, toxin treatment locks the endogenous Rho GTPases in the GTP-bound state. CNF1 targets RhoA at Gln63 and Rac1 and Cdc42 at Gln61 while CNF_Y is specific for RhoA (39–41).

We reasoned that combining PLA with CNF1 or CNF_Y treatment should allow us to validate qGAP interaction partners *in situ*. HeLa cells were serum starved, treated with the toxin or vehicle control for 1 h, and fixed. We then used PLA to assess the proximity of Rho GTPases with identified interaction partners using specific antibodies. The PLA signal between RhoA and the known effector Rho-associated protein kinase 2 (Rock2) increased upon toxin treatment, indicating that Rock2 associates with activated RhoA (Fig. 5*A*, *left*). Rock2 was originally described to be specific for RhoA (42). Interestingly, qGAP also detected association of Rock2 with Rac1 and Cdc42, and this was validated by our PLA-based approach (Figs. 5*A* *center* and 5*B*). PLA also validated interaction of Cdc42 with IQSEC3 (Fig. 5*A*, *right*). In total, our PLA-based method validated 9/11 tested novel interactions (Fig. 5*B* and Fig. S3). The data suggest that most of the novel qGAP interactors also associate with their cognate Rho GTPase in a loading-state-specific manner *in situ*.

A Protein–Protein Interaction Map for Rho GTPases—To provide a global overview, we assembled our data into the first protein–protein interaction network for multiple Rho GTPases (Fig. 6*A*). Many proteins were found to interact only with a single Rho GTPase. However, several proteins such as Rock2, Arhgef2, and Arhgap5 were surprisingly promiscuous. For Rock2, promiscuous association with Rac1 and Cdc42 was also validated with the proximity ligation assay (Fig. 5). The number of shared effectors is probably even higher since proteins may have escaped detection in individual experiments. Thus, our data indicate extensive crosstalk between Rho GTPases. Our network also shows that Rac1 and Cdc42 share more interaction partners with each other than with RhoA, B, C, and D. This is consistent with the higher level of sequence homology between Rac1 and Cdc42. Intriguingly, hierarchical clustering of the six Rho GTPases based on our interaction network results in a dendrogram that resembles their phylogenetic relationships (Fig. 6*B*). Hence, closely related family members share more interaction partners than distantly related ones. It is tempting to speculate that orthologs of some of the shared targets already interacted with their common ancestor.

DISCUSSION

Rho proteins are key regulators of the actin cytoskeleton and involved in a plethora of biological processes. However, a

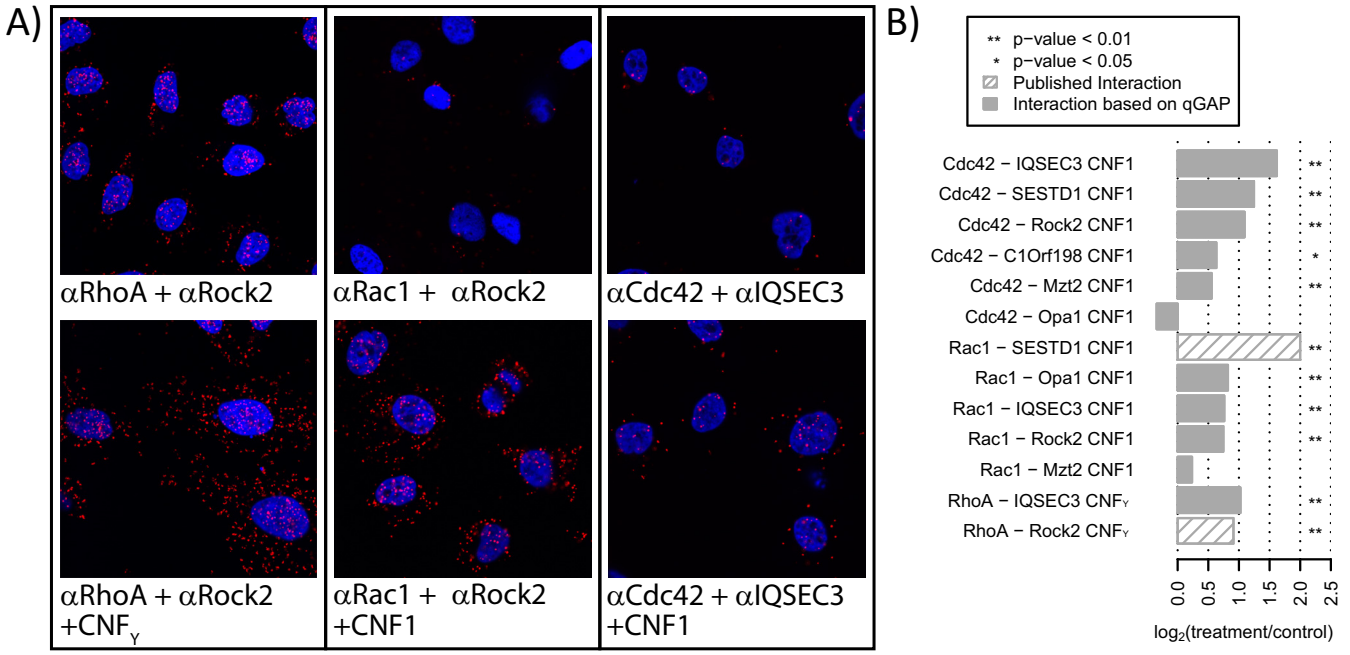

FIG. 5. **Validation of loading-state-dependent interactions *in situ* with the proximity ligation assay (PLA).** (*A*) Cells were treated with CNF_Y (for RhoA activation) or with CNF1 (Cdc42 and Rac1 activation), fixed, costained with oligonucleotide-coupled antibodies against the Rho GTPase and interactors. The basal PLA signal (*red*) increased upon toxin treatment for RhoA-Rock2 (known interaction), Rac1-Rock2 and Cdc42-IQSEC3 (both novel). (*B*) Automated quantification shows that toxin treatment significantly increased PLA signals for 9/11 tested novel interactions.

quantitative screen for interaction partners of multiple Rho GTPases has not yet been published. This is probably mainly due to the technical challenges involved. For example, while the yeast two-hybrid approach was used to screen for interaction partners of Cdc42 and Rac1 (5), this method cannot distinguish between the GTP- and the GDP-loaded forms of the GTPase. Moreover, previous attempts to identify interactors in pull-down assays required huge amounts of input material (*e.g.* 14 bovine brains for one experiment) and were not quantitative (6, 7). Here, we combined the pull-down assay with SILAC-based or label-free quantification to establish qGAP as a novel means to identify Rho GTPase interaction partners. We expect that this method is also applicable to the other ~150 proteins of the Ras superfamily. Using qGAP, we generate the first extensive Rho interaction network including the representative family members RhoA, Rac1, Cdc42, RhoB, RhoC, and RhoD. Our network reveals that several effectors such as Rock2 bind highly promiscuously. The network also reflects phylogenetic relationships between Rho family members. Hence, the specificity of individual effectors appears to mirror the evolution of Rho GTPase signaling. Finally, we report many novel Rho GTPase interaction partners and thus provide a useful resource for the community.

Despite the advantages of the qGAP method, it is important to also keep limitations in mind. First, the method is based on an *in vitro* pull-down. It is therefore not clear if identified interactions also occur in living cells. While 9 out of 11 tested interactions were validated using the proximity ligation assay and bacterial toxins (Fig. 5), we cannot provide independent evidence for all novel interactions. A second limitation is that we can only detect interactions of proteins that are present in the lysate used for the pull-down assay. The comparison of interaction partners identified in HeLa cell lysate and brain lysate shows that tissue choice is an important factor (Fig. 2). It should also be noted that differences in experimental design for some bait proteins might influence our interaction network (Fig. 6). Finally, qGAP detects both direct and indirect interactions. This can be seen as an advantage or a disadvantage of the method. In any case, it is important to keep this point in mind when interpreting the data.

It is also important to note that experiments with HeLa and brain lysate differ in several ways (choice of tissue, SILAC *versus* LFQ, statistical analysis, mass spectrometers used). This paper does not intend to compare both approaches. The choice of the biological system and therefore also the method for quantification will typically depend on the biological question of interest: Cell-culture-based systems lend themselves to SILAC-based quantification while studying *in vivo* systems is usually easier with label-free methods. Our results show that qGAP works with both.

Following up on the biological significance of novel interactors is beyond the scope of this manuscript. However, we would like to point at a number of interesting observations that could be addressed in future studies. One remarkable finding is that ARHGEF 1, 2, 6, 7, 11, 12, and 18 consistently

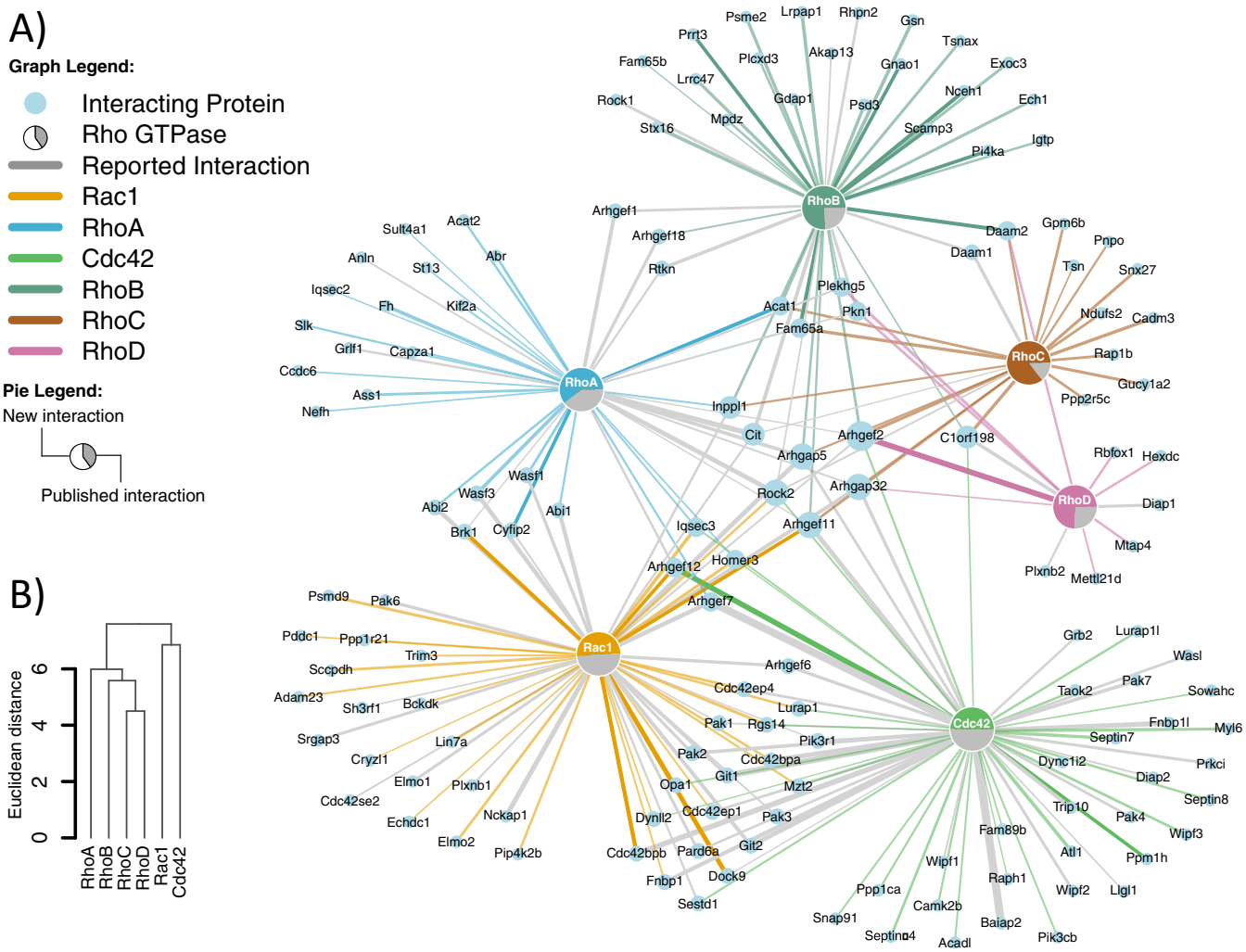

FIG. 6. (*A*) Interaction network between Rho GTPases and identified binding partners of the GTPγS-loaded form. Known (*gray*) and new (*colored*) interactions are visualized by *line colors* and the *pie charts* for every Rho GTPase. The width of edges corresponds to relative intensity ratio between GDP- and GTPγS-bound Rho GTPase. (*B*) Clustering Rho GTPases based on shared binding partners mirrors their phylogenetic relationships.

associated with the GTPγS-bound form of the respective Rho protein. It is well known that catalytic domains of GEFs preferentially bind to the nucleotide-free form of small GTPases (43). However, several GEF proteins have been previously shown to bind to the GTP-bound form of their GTPase via adjacent domains, like PH (Pleckstrin homolgy domain) domains (44). In fact, all of the above-mentioned GEFs have been reported to associate with GTP-loaded GTPases (44, 45). Hence, our data corroborate the previously postulated noncanonical binding mode.

Our data for RhoB, RhoC, and RhoD are particularly informative since these GTPases are less well characterized. RhoB and RhoC are closely related to RhoA, yet they have different effects on cell shape and migration (46). Our interaction data may therefore help to understand their nonredundant function. For example, we detect Rhophilin-2 only in the RhoB-GTPγS pull-downs, and this protein was previously shown to be specific for RhoB (47). Similarly, we also see AKAP13 (the lymphoid blast crisis oncogene) only in RhoB pull-downs. This is intriguing since both AKAP13 and RhoB are specifically involved in apoptosis induction by farnesyl transferase inhibitors (48, 49).

In summary, we develop qGAP, to identify interaction partners of Rho GTPases dependent on the loading state. We present the first extensive screen for Rho GTPase interaction partners with many new potential binding partners that can be validated with a high success rate by an orthogonal method. Our first systematic comparison of Rho GTPase effectors provides a rich resource for the community that has so far been lacking.

EXPERIMENTAL PROCEDURES

Experimental Design and Statistical Rationale—For SILAC experiments, protein samples were obtained from adherent

HeLa cell culture. Pull-downs were performed with lysate from one dish (15 cm), and beads from one heavy and one light experiment were mixed before elution (see Fig. 1). A label swap experiment was carried out. Label-free experiments were performed as biological triplicates for each nucleotide form of a Rho GTPase. This allowed us to do a *t* test on the obtained data. Additionally, several tissues were examined (hippocampus, cerebellum, cerebrum, whole brain, see Fig. 2).

Protein Expression and Purification—N-terminal GST-fusion proteins of RhoA, RhoB, RhoC, RhoD, Rac1, and Cdc42 were expressed in *E. coli* BL21 (DE3) Rosetta. N-terminal GST-tagged CNF1 and CNF_Y were expressed in *E. coli* Tuner pLysS. Bacteria were grown at 37 °C in TB medium supplemented with 100 μg/ml ampicillin and 34 μg/ml chloramphenicol until an OD_{600} of 0.4. Subsequently, protein expression was induced by addition of 40 μM isopropyl β-D-1-thiogalactopyranoside and bacteria grown at 18 °C and 180 rpm shaking for at least 15 h. Bacteria were lysed by either passing at least twice through a microfluidizer or by 6 $\times$ 10 s of sonication (UP200S, 0.85 amplitude, 0.5 s cycle time, sonotrode DRH-S2) with cooling steps in between. The lysate was cleared from debris by centrifugation (50,000 *g*, 4 °C, 45 min, JA-12 rotor) and filtered through a 0.2 μm pore size filter.

Affinity purification was performed with GSH Sepharose columns at a flow rate of 1 ml/min. The column was equilibrated with 6 CV (column volumes) equilibration buffer (20 mM HEPES, pH 7.5, 150 mM NaCl, 5 mM $MgCl_2$, 2.5 mM DTT). The filtered bacteria lysate was applied, the column was washed with 30 CV washing buffer (20 mM HEPES, pH 7.5, 300 mM NaCl, 5 mM $MgCl_2$, 2.5 mM DTT) followed by 5 CV equilibration buffer and bound proteins were finally eluted with 5 CV elution buffer (20 mM HEPES, pH 7.5, 150 mM NaCl, 5 mM $MgCl_2$, 2.5 mM DTT, 20 mM glutathione). Size exclusion chromatography was performed for RhoA, Rac1, and Cdc42 with concentrated protein solutions with a Superdex 200 16/60 column equilibrated with 2 CV equilibration buffer. The peak fractions containing the protein of interest were pooled and concentrated.

Nucleotide exchange was performed by EDTA-driven Mg^{2+}-depletion as described previously (50). 200 μM of the respective Rho GTPase were incubated with 15 mM EDTA, 150 mM NH_4SO_4, and 10 mM of GDP or 2 mM GTPγS (in 1 M HEPES, pH 7.5) overnight at 4 °C. The exchange reaction was stopped by addition of 30 mM $MgCl_2$. Excess nucleotide was removed by Amicon concentrator or buffer exchange via FPLC. Determination of bound nucleotide was followed standard HPLC protocols (51). GST-CNF1 and CNF_Y were stored at −20 °C in 50 mM Tris, pH 7.5, 50% glycerol.

GTPase Activity Assays—GTPase activity of RhoA, Cdc42, and Rac1 was determined by monitoring GTP to GDP ratios over time by HPLC measurements (52, 53). GTPases were loaded with GTP prior to measurements. Nucleotide exchange of RhoA was performed by EDTA-driven Mg^{2+}-depletion (50). Due to the fast intrinsic GTP hydrolysis rates of Cdc42 and Rac1, nucleotide-free forms of GTPase were generated prior to GTP loading as described before (53, 54).

For monitoring RhoA activity 50–100 μM GTP loaded GTPase was quickly thawed and diluted in assay buffer (20 mM HEPES, 150 mM NaCl, 5 mM $MgCl_2$, 2.5 mM DTT, pH 7.5) or prepared cell lysates in a 1:5 ratio. Hydrolysis reaction was assayed at room temperature and stopped by adding trichloroacetic acid (final concentration of 20%). Samples were centrifuged and neutralized. HPLC measurements were carried out using a reversed-phase C18 column (Reversed-phase ODS-2 Hypersil HPLC column, Thermo Scientific) and a precolumn (Hypersil ODS guard column, Agilent Technologies) for adsorbing residual denatured protein. Measurements were carried out in HPLC-buffer containing 10 mM tetrabutylammoniumbromide and 100 mM potassium phosphate (pH 6,5) with 7.5% acetonitrile. Nucleotide peaks were detected by measuring adsorption at 254 nm and quantified by integration.

GTPase activity of Cdc42 and Rac1 was monitored as described (18). Briefly, 50–100 μM nucleotide-free GTPase was quickly mixed with 50 μM GTP in GAP buffer (30 mM Tris, 10 mM $MgCl_2$, 3 mM DTT, 10 mM K_2HPO_4/KH_2PO_4, pH 7.5). Subsequently, assay buffer or prepared cell lysate was added in a 1:5 ratio. Samples were collected as described for RhoA and subjected to HPLC analysis.

Preparation of Cell Lysates for GTPase Activity Assays—HEK 293T cells were cultivated at 37 °C with 5% CO_2 in DMEM culture media supplemented with 5% fetal calf serum (FCS) and 1% penicillin/streptomycin. For GTPase activity assays lysates of cells transfected with GAP proteins with a known activity toward the respective GTPase (RhoA: STARD13, Cdc42: CDGAP; Rac1: ChimerinH206K; all encoded as mCitrine fusion proteins on pLP-mCitrine C1 SP vectors) were used. Transfection was mediated using the polyethylenimine-mediated DNA transfer method. Cells were lysed in Nonidet P-40 lysis buffer (1% Nonidet P-40, 10% glycerol, 20 mM Tris-HCl (pH 7.5), 150 mM NaCl, 1 mM EGTA, 5 mM NaF, Pefabloc, Benzonase), centrifuged, and the supernatant was washed three times in a VWR 15 ml concentrator (10 kDa cut-off) with assay buffer. The total protein concentration of the lysate was adjusted to 10 μg/μl. Lysates were immediately used in a GAP assay.

Preparation of Mouse Brain Lysate—Mouse brains were dissected from female BL/6 mice at an age of 12 weeks (kind gift of Dr. Ibanez-Tallon, MDC Berlin). Brains were either used as a whole (RhoB, RhoC, RhoD) or separated into a hippocampal (Cdc42), cerebellar (Cdc42, Rac1, RhoA), and remaining cerebrum fraction (Cdc42, Rac1, RhoA). The tissue samples were lysed in lysis buffer (50 mM Tris-HCl, pH 7.4, 150 mM NaCl, 1% Triton X-100, 1 mM EDTA, 1 mM EGTA, and protease inhibitors (Roche)) by application of 50–100 strokes in a dounce homogenizer on ice. The lysate was cleared from debris by two subsequent centrifugation steps at 20,000 *g* (4 °C, 20 min) and directly used for experiments. The input for a single pull-down was 500 μg (SILAC), 90 μg (hippocampus-

LFQ), 700 μg (cerebellum-LFQ), 1400 μg cerebrum-LFQ), and 1500 μg (whole-brain-LFQ).

Pull-Down Assays—For pull-down assays cell lysates were freshly prepared from mouse brains. Experiments were conducted as triplicates, resulting in six single pull-downs per Rho GTPase (three for the GDP and three for the GTPγS-loaded protein). Each pull-down was analyzed separately by mass spectrometry and quantified using label-free quantification (see below). For SILAC experiments, lysate was prepared from labeled HeLa cells in adherent culture. The same lysis buffer as for mice brains was used. Sepharose beads with an active N-hydroxysuccinimide group were used for covalent coupling of recombinant proteins (GE Healthcare). 150 μl of bead slurry were used per single pull-down. Storage solution was removed from bead slurry by centrifugation (1000 *g*, 2 min). Beads were washed in ice-cold equilibration (1 mM HCl) buffer and incubated with 500 μg of the recombinant protein for at least 2 h at room temperature. The beads were subsequently washed in buffer A (0.5 M ethanolamine, pH 8.3, 0.5 M NaCl), buffer B (0.1 M sodium acetate, pH 4.0, 0.5 M NaCl) and incubated in buffer A for 30 min. After wash steps with buffers B, A, and again B, the cell lysate was added to the beads and incubation was performed for 30 min at 4 °C. The supernatant was removed, the beads washed in pull-down wash buffer (50 mM Tris, pH 7.4, 300 mM NaCl, 5 mM $MgCl_2$) twice, and bound proteins were eluted with 200 μl U/T buffer (10 mM HEPES, pH 8.0, 6 M urea, 2 M thiourea) by shaking at 1400 rpm on an Thermo shaker (Eppendorf) for 15 min. Eluted proteins were precipitated in 70% ethanol.

Proximity Ligation Assay—HeLa cells were seeded on poly-L-lysine coated 18-well μ-slides (ibidi, Martinsried, Germany) for 1 day in standard cell culture medium (450 cells/well). After 24 h, the medium was replaced by starvation medium (0.2% FCS) and cells were cultivated for another 24 h. Purified cytotoxic necrotizing factors (0.4 g/l CNF1-GST or CNFY-GST in 50 mM Tris, pH 7.5, 50% glycerol) were dissolved in prewarmed PBS. Cells were then incubated for 1 h with either toxin at a final concentration of 0.4 μg/ml or the glycerol/PBS vehicle control. Cells were briefly washed in PBS, fixed with 4% paraformaldehyde and permeabilized with 0.1% Triton X-100 in PBS. Cells were washed in PBS, and unspecific binding of antibodies was blocked by incubation in PBS containing 1% BSA, 0.05% Tween20 for 20 min. Reagents for PLA were obtained from Olink Bioscience (Duolink® *in situ* orange starter kit). The primary antibody solution was applied for 1 h at 37 °C in a humidity chamber. Antibodies were combinations of one from mouse and one from rabbit donors. The two PLA probes were mixed, diluted 1:5 in antibody diluent buffer, and left for 20 min. The primary antibody was removed from the chamber slide. The slide was washed once; the PLA probe solution was added and incubated for 1 h at 37 °C. The probes were removed, the slide was washed twice for 5 min under gentle agitation, and the ligation–ligase solution was added to each sample and incubated in a preheated humidity chamber for 30 min at 37 °C. For amplification, the slide was washed twice for 2 min and the amplification–polymerase solution was added and incubated for 100 min in a preheated humidity chamber for 80 min at 37 °C. Finally, the slides were washed, dried, and In Situ Mounting Medium, including DAPI was added. Nonspecific signals were assessed by single primary antibody staining. Information about the antibodies used and their dilution can be found in Supplemental Table 2.

Microscopy and Processing of Images—Images were taken with a Leica TCS SP5 confocal microscope (Leica Microsystems, Wetzlar, Germany) using a 63x objective and Leica LAS AF software. Standard parameters were: pinhole of 2.5 AE, resolution of 2048 × 2048 pixels, line average of 4. Pictures were processed with ImageJ (version 1.44, Bethesda, MD) using the LOCI plugin. Pictures were imported without autoscale, threshold was set with a minimum of 30 and a maximum of 255, and "analyze particle" function was used for counting of spots.

Sample Preparation and Mass Spectrometry—Protein pellets were redissolved in U/T buffer and subsequently reduced with dithiothreitol and alkylated with iodoacetamide. Proteins were digested with LysC and trypsin. The peptides were desalted off-line and analyzed by online LC-MS on an EASY-nLC system (Thermo Scientific) coupled to a Q-Exactive-Orbitrap (Thermo Fisher Scientific, Waltham MA) for cerebrum and whole-brain samples or an LTQ-Orbitrap-Velos (Thermo Fisher Scientific) for hippocampus and cerebellum samples. SILAC samples were analyzed on an LTQ-Orbitrap XL (Thermo Fisher Scientific) system. 5 μl peptide samples were loaded onto a fritless microcolumn (75 μm inner diameter packed in-house with ReproSil-Pur C18-AQ 3-μm resin, Dr. Maisch GmbH). Peptides were eluted with an 8–60% acetonitrile gradient and 0.5% formic acid. Runs were performed as 4 h gradients at a flow rate of 200 nl/min. Peptides were ionized at currents of 2.2 kV (Q-Exactive and Orbitrap XL) and 2.3 kV (Orbitrap Velos). The Q-Exactive Orbitrap device was operated in data-dependent mode with a TOP10 method as previously described (55). One full scan (*m/z* range = 300 - 1650, r = 70,000, target value: 10^6 ions, maximum injection time = 20 ms) was used to detect precursor ions. The 10 most intense ions with a charge state greater than1 were selected for fragmentation (r = 17,500, target value = 10^6 ions, isolation window = 3 *m/z*, maximum injection time = 60 ms). Dynamic exclusion time for fragmented precursor ions was set to 30 s. The Velos Orbitrap was operated in the data-dependent mode with a standard TOP20 method. One full scan (*m/z* range = 300 - 1700, r = 60,000, target value = 10^6 ions) was used to detect precursor ions. The 20 most intense ions with a charge state greater than 1 were selected for fragmentation (target value 3000 ions, isolation window = 2 *m/z*). Dynamic exclusion time for fragmented precursor ions was set to 60 s.

The Orbitrap XL operated in data-dependent mode with one full scan in the Orbitrap analyzer (m/z = 300–1700; resolution = 60,000; target value = 10^6 ions). The five most intense ions with a charge state greater than 1 were selected (target value = 5,000) and fragmented in the linear trap quadrupole using CID (collision induced dissociation) (35% normalized collision energy and wideband activation enabled). Dynamic exclusion for selected precursor ions was 60 s.

Data Analysis and Label-Free Quantification with MaxQuant and Perseus—MS raw data files were analyzed with the MaxQuant software package (version 1.3.0.5) that includes the search engine Andromeda, using default settings (26). Carbamidomethylation on cysteines was used as fixed modification and oxidation on methionine and acetylated N terminus as variable modifications. Trypsin was used as protease, including cleavage between arginine or lysine and proline. Missed cleavages were set to two. Peptides were identified with 6 ppm precursor mass deviation and 20 ppm fragment mass deviation for Orbitrap Q Exactive devices. Samples from the LTQ-Orbitrap XL and Velos Orbitrap were allowed to have up to 6 ppm precursor mass deviation and 0.5 Da fragment mass deviation. Proteins were searched against the Uniprot mouse database (version June 2012, 59,377 entries) for LF-qGAP and Uniprot human database (version June 2012, 86,898 entries) for SILAC-qGAP. Identifications were filtered to a false discovery rate of 0.01 at the PSM (peptide spectrum match) and protein level using the target–decoy approach. The available Requantify option in MaxQuant was enabled. For label-free quantification, we directly compared peptide peak intensities between corresponding runs (match between runs enabled, LFQ min ratio count = 2) using the label-free quantification algorithm (LFQ) implemented in MaxQuant. Files produced by MaxQuant were further processed using the Perseus software package (version 1.3.0.4). The "LFQ Intensity" for each experiment was selected as expression value. The matrix was filtered for columns "Only identified by site," "Contaminant," and "Reverse hits." For each set of experiments, we only accepted proteins that were quantified in all three replicates of either the GTPγS- or GDP-bound form. The logarithm to the base of 10 was taken from LFQ intensities and missing values imputed by sampling from a normal distribution (width 0.3, downshift 1.8). Assuming that mainly low abundant peaks are the cause for missing data in shotgun proteomics, the imputation settings aim to simulate the distribution of low abundant peaks. Missing data were imputed in each experiment individually (column per column). The Gaussian distribution used for imputation was modified by using 0.3 width (in standard deviation of the real data) and a 1.8 fold downshift (in standard deviation units of the valid data).

The significance of the difference in protein abundance between the GTPγS and GDP pull-downs was calculated with a two-sided t test. Specific interactors were then selected based on the combination of the t test p values and the log2 fold differences as previously described (false discovery rate 5%, s0 = 0.5) (56–58). Most interaction partners had at least two unique peptides. For five potential interactors that were identified by a single unique peptide, we provide annotated spectra in Fig. S4 (Cit, Fnbp1l, Pak3, Rps27, Syp). Arhgef7 is listed with zero unique peptides due to the presence of several splice variants in the Uniprot database. The interaction network was plotted using the igraph R-package (59). Enrichment of known Rho GTPase interactions in identified binding partners was tested against HIPPIE Database (33) using the hypergeometric test functions phyper and dhyper from R (version 3.2.2).

The mass spectrometry proteomics data have been deposited to the ProteomeXchange Consortium (http://proteomecentral.proteomexchange.org) via the PRIDE partner repository with the dataset identifier PXD004190.

Acknowledgments—We thank Martha Hergeselle, Christian Sommer, and Sabine Werner for excellent technical assistance. Anne Ridley (Cancer Research UK), Gudula Schmidt (Freiburg University), and Alfred Wittinghofer (MPI of Molecular Physiology) kindly provided constructs.

* This project was supported by the German Research Foundation (SFB958, Scaffolding of Membranes) and the Helmholtz Association.

[S] This article contains supplemental material.

‖ To whom correspondence should be addressed: Max Delbrück Center for Molecular Medicine, Robert-Rössle-Str. 10, D-13092 Berlin, Germany, Tel.: +49 30 9406 3574, Fax.: +49 30 9406 2394; Email: matthias.selbach@mdc-berlin.de.

The authors declare that they have no conflict of interest.

REFERENCES

1. Wennerberg, K., Rossman, K. L., and Der, C. J. (2005) The Ras superfamily at a glance. *J. Cell Sci.* **118,** 843–846
2. Jaffe, A. B., and Hall, A. (2005) Rho GTPases: Biochemistry and biology. *Annu. Rev. Cell Dev. Biol*. **21,** 247–269
3. Ridley, A. J. (2006) Rho GTPases and actin dynamics in membrane protrusions and vesicle trafficking. *Trends Cell Biol.* **16,** 522–529
4. Bustelo, X. R., Sauzeau, V., and Berenjeno, I. M. (2007) GTP-binding proteins of the Rho/Rac family: Regulation, effectors and functions *in vivo*. *Bioessays* **29,** 356–370
5. Aspenström, P., Lindberg, U., and Hall, A. (1996) Two GTPases, Cdc42 and Rac, bind directly to a protein implicated in the immunodeficiency disorder Wiskott–Aldrich syndrome. *Curr. Biol*. **6,** 70–75
6. Kato, K., Yazawa, T., Taki, K., Mori, K., Wang, S., Nishioka, T., Hamaguchi, T., Itoh, T., Takenawa, T., Kataoka, C., Matsuura, Y., Amano, M., Murohara, T., and Kaibuchi, K. (2012) The inositol 5-phosphatase SHIP2 is an effector of RhoA and is involved in cell polarity and migration. *Mol. Biol. Cell*. **23,** 2593–2604
7. Christoforidis, S., and Zerial, M. (2000) Purification and identification of novel Rab effectors using affinity chromatography. *Methods* **20,** 403–410
8. Paul, F. E., Hosp, F., and Selbach, M. (2011) Analyzing protein–protein interactions by quantitative mass spectrometry. *Methods* **54,** 387–395
9. Vermeulen, M., Hubner, N. C., and Mann, M. (2008) High confidence determination of specific protein–protein interactions using quantitative mass spectrometry. *Curr. Opin. Biotechnol*. **19,** 331–337
10. Meyer, K., and Selbach, M. (2015) Quantitative affinity purification mass spectrometry: a versatile technology to study protein–protein interactions. *Front. Genet*. **6,** 237
11. Gingras, A. C., Gstaiger, M., Raught, B., and Aebersold R. (2007) Analysis of protein complexes using mass spectrometry. *Nat. Rev. Mol. Cell Biol*. **8,** 645–654
12. Gavin, A. C., Maeda, K., and Kühner, S. (2011) Recent advances in charting protein–protein interaction: Mass spectrometry-based approaches. *Curr. Opin. Biotechnol*. **22,** 42–49

13. Zinn, N., Hopf, C., Drewes, G., and Bantscheff, M. (2012) Mass spectrometry approaches to monitor protein–drug interactions. *Methods* **57,** 430–440
14. Tinti, M., Kiemer, L., Costa, S., Miller, M. L., Sacco, F., Olsen, J. V., Carducci, M., Paoluzi, S., Langone, F., Workman, C. T., Blom, N., Machida, K., Thompson, C. M., Schutkowski, M., Brunak, S., Mann, M., Mayer, B. J., Castagnoli, L., and Cesareni, G. (2013) The SH2 domain interaction landscape. *Cell Rep.* **3,** 1293–1305
15. Selbach, M., and Mann, M. (2006) Protein interaction screening by quantitative immunoprecipitation combined with knockdown (QUICK). *Nat. Methods* **3,** 981–983
16. Vermeulen, M., Eberl, H. C., Matarese, F., Marks, H., Denissov, S., Butter, F., Lee, K. K., Olsen, J. V., Hyman, A. A., Stunnenberg, H. G., and Mann, M. (2010) Quantitative interaction proteomics and genome-wide profiling of epigenetic histone marks and their readers. *Cell* **142,** 967–980
17. Selbach, M., Paul, F. E, Brandt, S. Guye, P., Daumke, O., Backert, S., Dehio, C., and Mann, M. (2009) Host cell interactome of tyrosine-phosphorylated bacterial proteins. *Cell Host Microbe* **5,** 397–403
18. Jaiswal, M., Fansa, E. K., Dvorsky, R., and Ahmadian, M. R. (2013) New insight into the molecular switch mechanism of human Rho family proteins: Shifting a paradigm. *Biol. Chem.* **394,** 89–95
19. Eberth, A., Dvorsky, R., Becker, C. F., Beste, A., Goody, R. S., and Ahmadian, M. R. (2005) Monitoring the real-time kinetics of the hydrolysis reaction of guanine nucleotide-binding proteins. *Biol. Chem.* **386,** 1105–1114
20. Mazhab-Jafari, M. T., et al. (2010) Real-time NMR study of three small GTPases reveals that fluorescent 2′(3′)-O-(N-methylanthraniloyl)-tagged nucleotides alter hydrolysis and exchange kinetics. *J. Biol. Chem.* **285,** 5132–5136
21. Zhang, B., Wang, Z. X., and Zheng, Y. (1997) Characterization of the interactions between the small GTPase Cdc42 and its GTPase-activating proteins and putative effectors. Comparison of kinetic properties of Cdc42 binding to the Cdc42-interactive domains. *J. Biol. Chem.* **272,** 21999–22007
22. Ching, Y. P., Wong, C. M., Chan, S. F., Leung, T. H., Ng, D. C., Jin, D. Y., and Ng, I. O. (2003) Deleted in liver cancer (DLC) 2 encodes a RhoGAP protein with growth suppressor function and is underexpressed in hepatocellular carcinoma. *J. Biol. Chem.* **278,** 10824–10830
23. Lamarche-Vane, N., and Hall, A. (1998) CdGAP, a novel proline-rich GTPase-activating protein for Cdc42 and Rac. *J. Biol. Chem.* **273,** 29172–29177
24. Wegmeyer, H., Egea, J., Rabe, N., Gezelius, H., Filosa, A., Enjin, A., Varoqueaux, F., Deininger, K., Schnütgen, F., Brose, N., Klein, R., Kullander, K., and Betz, A. (2007) EphA4-dependent axon guidance is mediated by the RacGAP alpha2-chimaerin. *Neuron* **55,** 756–767
25. Cherfils, J., Ménétrey, J., Le Bras, G., Janoueix-Lerosey, I., de Gunzburg, J., Garel, J. R., and Auzat, I. (1997) Crystal structures of the small G protein Rap2A in complex with its substrate GTP, with GDP and with GTPgammaS. *EMBO J.* **16,** 5582–5591
26. Cox, J., and Mann, M. (2008) MaxQuant enables high peptide identification rates, individualized p. p. b.-range mass accuracies and proteome-wide protein quantification. *Nat. Biotechnol.* **26,** 1367–1372
27. Etienne-Manneville, S., and Hall, A. (2002) Rho GTPases in cell biology. *Nature* **420,** 629–635
28. Ridley, A. J. (2001) Rho GTPases and cell migration. *J. Cell Sci.* **114**, 2713–2722
29. Uhlen, M., Oksvold, P., Fagerberg, L., Lundberg, E., Jonasson, K., Forsberg, M., Zwahlen, M., Kampf, C., Wester, K., Hober, S., Wernerus, H., Björling, L., and Ponten, F. (2010) Towards a knowledge-based Human Protein Atlas. *Nat. Biotechnol.* **28,** 1248–1250
30. Hubner, N. C., Bird, A. W., Cox, J., Splettstoesser, B., Bandilla, P., Poser, I., Hyman, A., and Mann, M. (2009) Quantitative proteomics combined with BAC TransgeneOmics reveals in vivo protein interactions. *J. Cell Biol*. **189,** 739–754
31. Hein, M. Y., Hubner, N. C., Poser, I., Cox, J., Nagaraj, N., Toyoda, Y., Gak, I. A., Weisswange, I., Mansfeld, J., Buchholz, F., Hyman, A. A., and Mann, M. (2015) A human interactome in three quantitative dimensions organized by stoichiometries and abundances. *Cell* **163,** 712–723
32. Cox, J., Matic, I., Hilger, M., Nagaraj, N., Selbach, M., Olsen, J. V., and Mann, M. (2009) A practical guide to the MaxQuant computational platform for SILAC-based quantitative proteomics. *Nat. Protoc*. **4,** 698–705
33. Schaefer, M. H., Fontaine, J. F., Vinayagam, A., Porras, P., Wanker, E. E., and Andrade-Navarro, M. A. (2012) HIPPIE: Integrating protein interaction networks with experiment based quality scores. *PLoS ONE* **7,** e31826
34. De Toledo, M., Coulon, V., Schmidt, S., Fort, P., and Blangy, A. (2001) The gene for a new brain specific RhoA exchange factor maps to the highly unstable chromosomal region 1p36.2–1p36.3. *Oncogene* **20,** 7307–7317
35. Burbelo, P. D., Miyamoto, S., Utani, A., Brill, S., Yamada, K. M., Hall, A., and Yamada, Y. (1995) p190-B, a new member of the Rho GAP family, and Rho are induced to cluster after integrin cross-linking. *J. Biol. Chem.* **270,** 30919–30926
36. Söderberg, O., Gullberg, M., Jarvius, M., Ridderstråle, K., Leuchowius, K. J., Jarvius, J., Wester, K., Hydbring, P., Bahram, F., Larsson, L. G., and Landegren, U. (2006) Direct observation of individual endogenous protein complexes in situ by proximity ligation. *Nat. Methods* **3,** 995–1000
37. Aktories, K., and Baribieri, J. T. (2005) Bacterial cytotoxins: Targeting eukaryotic switches. *Nat. Rev. Microbiol*. **3,** 397–410
38. Munro, P., and Lemichez, E. (2005) Bacterial toxins activating Rho GTPases. *Curr. Top. Microbiol. Immunol.* **291,** 177–190
39. Schmidt, G., Sehr, P., Wilm, M., Selzer, J., Mann, M., and Aktories, K. (1997) Gln 63 of Rho is deamidated by *Escherichia coli* cytotoxic necrotizing factor-1. *Nature* **387,** 725–729
40. Lerm, M., Selzer, J., Hoffmeyer, A., Rapp, U. R., Aktories, K., and Schmidt, G. (1999) Deamidation of Cdc42 and Rac by *Escherichia coli* cytotoxic necrotizing factor 1: Activation of c-Jun N-terminal kinase in HeLa cells. *Infect. Immun*. **67,** 496–503
41. Hoffmann, C., Pop, M., Leemhuis, J. Schirmer, J., Aktories, K., and Schmidt, G. (2004) The Yersinia pseudotuberculosis cytotoxic necrotizing factor (CNFY) selectively activates RhoA. *J. Biol. Chem.* **279,** 16026–16032
42. Leung, T., Manser, E., Tan, L., and Lim, L. (1995) A novel serine/threonine kinase binding the Ras-related RhoA GTPase which translocates the kinase to peripheral membranes. *J. Biol. Chem.* **270,** 29051–29054
43. Bos, J. L., Rehmann, H., and Wittinghofer, A. (2007) GEFs and GAPs: Critical elements in the control of small G proteins. *Cell* **129,** 865–877
44. Medina, F., Carter, A. M., Dada, O., Gutowski, S., Hadas, J., Chen, Z., and Sternweis, P. C. (2013) Activated RhoA is a positive feedback regulator of the Lbc family of Rho guanine nucleotide exchange factor proteins. *J. Biol. Chem.* **288,** 11325–11333
45. Baird, D., Feng, Q., and Cerione, R. A. (2005) The Cool-2/alpha-Pix protein mediates a Cdc42-Rac signaling cascade. *Curr. Biol.* **15,** 1–10
46. Ridley, A. J. (2013) RhoA, RhoB and RhoC have different roles in cancer cell migration. *J. Microsc.* **251,** 242–249
47. Mircescu, H., Steuve, S., Savonet, V., Degraef, C., Mellor, H., Dumont, J. E., Maenhaut, C., and Pirson, I. (2002) Identification and characterization of a novel activated RhoB binding protein containing a PDZ domain whose expression is specifically modulated in thyroid cells by cAMP. *Eur. J. Biochem.* **269,** 6241–6249
48. Prendergast, G. C. (2001) Actin' up: RhoB in cancer and apoptosis. *Nat. Rev. Cancer* **1,** 162–168
49. Raponi, M., Harousseau, J. L., Lancet, J. E., Löwenberg, B., Stone, R., Zhang, Y., Rackoff, W., Wang, Y., and Atkins, D. (2007) Identification of molecular predictors of response in a study of tipifarnib treatment in relapsed and refractory acute myelogenous leukemia. *Clin. Cancer Res*. **13,** 2254–2260
50. Tucker, J., Sczakiel, G., Feuerstein, J., John, J., Goody, R. S., and Wittinghofer, A. (1986) Expression of p21 proteins in *Escherichia coli* and stereochemistry of the nucleotide-binding site. *EMBO J*. **5,** 1351–1358
51. Lenzen, C., Cool, R. H., and Wittinghofer, A. (1995) Analysis of intrinsic and CDC25-stimulated guanine nucleotide exchange of p21ras-nucleotide complexes by fluorescence measurements. *Meth. Enzymol*. **255,** 95–109
52. Eberth, A., and Ahmadian, M. R. (2009) In vitro GEF and GAP assays. *Curr. Protoc. Cell Biol*. **43,** 14.9.1–14.9.25
53. Jaiswal, M., Dubey, B. N., Koessmeier, K. T., Gremer, L., and Ahmadian, M. R. (2012) Biochemical assays to characterize Rho GTPases. *Meth. Mol. Biol.* **827,** 37–58
54. John, J., Sohmen, R., Feuerstein, J., Linke, R., Wittinghofer, A., and Goody, R. S. (1990) Kinetics of interaction of nucleotides with nucleotide-free H-ras p21. *Biochemistry* **29,** 6058–6065

55. Kelstrup, C. D., Young, C., Lavallee, R., Nielsen, M. L., and Olsen, J. V. (2012) Optimized fast and sensitive acquisition methods for shotgun proteomics on a quadrupole Orbitrap mass spectrometer. *J. Proteome Res.*
56. Tusher, V. G., Tibshirani, R., and Chu, G. (2001) Significance analysis of microarrays applied to the ionizing radiation response. *Proc. Natl. Acad. Sci. U.S.A.* **98,** 5116–5121
57. Cox, J., Hein, M. Y., Luber, C. A., Paron, I., Nagaraj, N., and Mann, M. (2014) Accurate proteome-wide label-free quantification by delayed normalization and maximal peptide ratio extraction, termed MaxLFQ. *Mol. Cell. Proteomics* **13,** 2513–2526
58. Tyanova, S., Temu, T., Sinitcyn, P., Carlson, A., Hein, M. Y., Geiger, T., Mann, M., and Cox, J. (2016) The Perseus computational platform for comprehensive analysis of (prote)omics data. *Nat. Methods* **13,** 731–740
59. Csardi, G., and Nepusz, T. (2006) The igraph Software Package for Complex Network Research. *InterJournal Complex Systems* **1695,** 1–9

ASBMB MOLECULAR & CELLULAR PROTEOMICS MCP

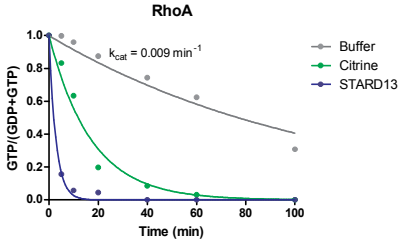
RhoA
k_{cat} = 0.009 min^{-1}
Buffer
Citrine
STARD13
GTP/(GDP+GTP)
1.0
0.8
0.6
0.4
0.2
0.0
0
20
40
60
80
100
Time (min)

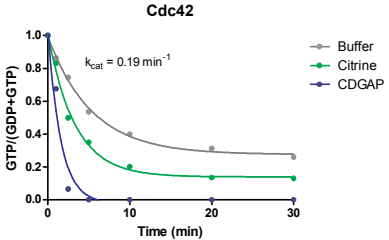
Cdc42
k_{cat} = 0.19 min^{-1}
Buffer
Citrine
CDGAP
GTP/(GDP+GTP)
1.0
0.8
0.6
0.4
0.2
0.0
0
10
20
30
Time (min)

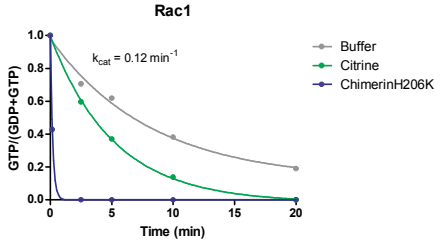
Rac1
k_{cat} = 0.12 min^{-1}
Buffer
Citrine
ChimerinH206K
GTP/(GDP+GTP)
1.0
0.8
0.6
0.4
0.2
0.0
0
5
10
15
20
Time (min)

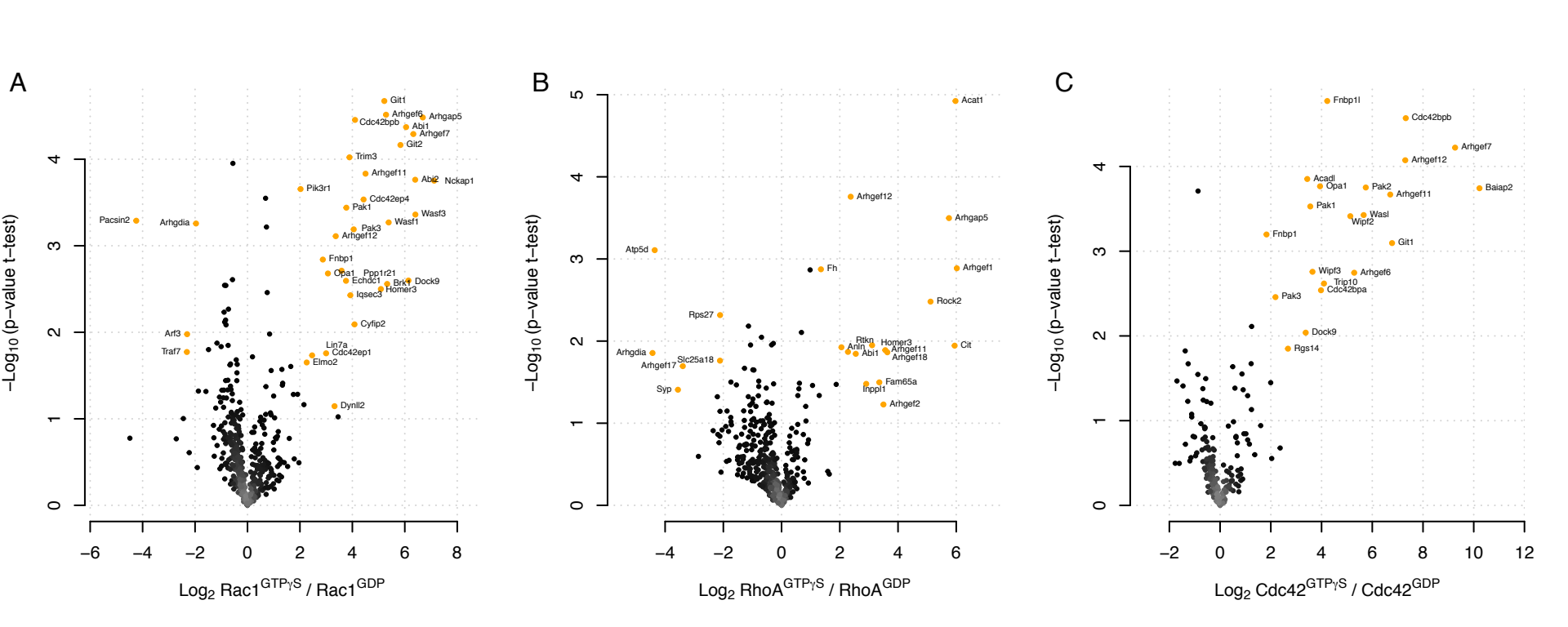
A
Git1
Arhgef6
Arhgap5
Cdc42bpb
Abi1
Arhgef7
Git2
Trim3
Arhgef11
Abi2
Nckap1
Pik3r1
Cdc42ep4
Pak1
Wasf3
Pacsin2
Arhgdia
Wasf1
Pak3
Arhgef12
Fnbp1
Opa1
Ppp1r21
Echdc1
Brk1
Dock9
Homer3
Iqsec3
Cyfip2
Arf3
Lin7a
Traf7
Cdc42ep1
Elmo2
Dynll2
−Log10 (p−value t−test)
Log2 Rac1GTPγS / Rac1GDP
B
Acat1
Arhgef12
Arhgap5
Atp5d
Fh
Arhgef1
Rock2
Rps27
Rtkn
Homer3
Anln
Arhgef11
Abi1
Cit
Arhgdia
Arhgef18
Slc25a18
Arhgef17
Fam65a
Inppl1
Syp
Arhgef2
−Log10 (p−value t−test)
Log2 RhoAGTPγS / RhoAGDP
C
Fnbp1l
Cdc42bpb
Arhgef7
Arhgef12
Acadl
Opa1
Pak2
Baiap2
Arhgef11
Pak1
Wasl
Wipf2
Fnbp1
Git1
Wipf3
Arhgef6
Trip10
Cdc42bpa
Pak3
Dock9
Rgs14
−Log10 (p−value t−test)
Log2 Cdc42GTPγS / Cdc42GDP

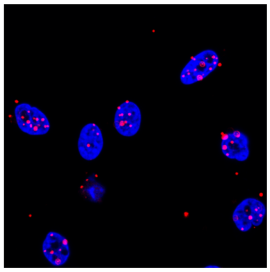

αRhoA + αIQSEC3

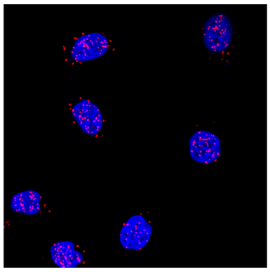

αRhoA + αACAT1

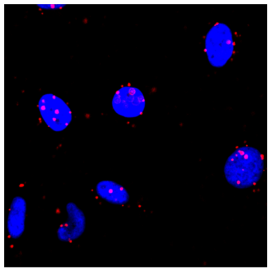

αRac1 + αSESTD1

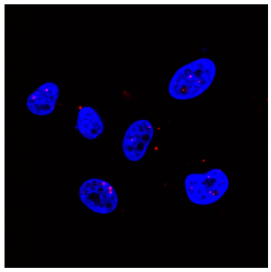

αRac1 + αOpa1

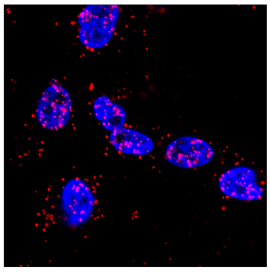

αRhoA + αIQSEC3 +CNF$_Y$

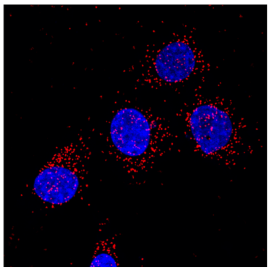

αRhoA + αACAT1 +CNF$_Y$

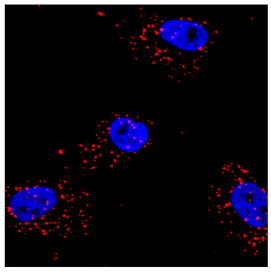

αRac1 + αSESTD1 +CNF1

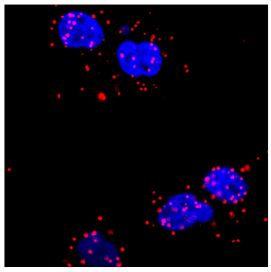

αRac1 + αOpa1 +CNF1

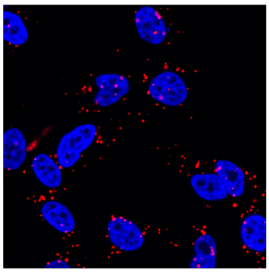

αRac1 + αMzt1/2

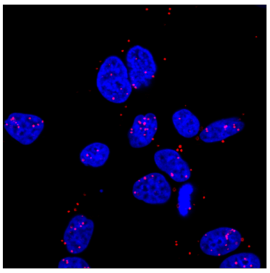

αRac1 + αIQSEC3

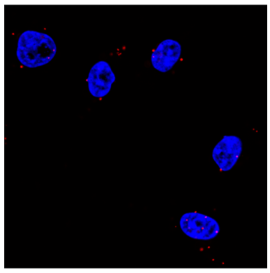

αCdc42 + αSESTD1

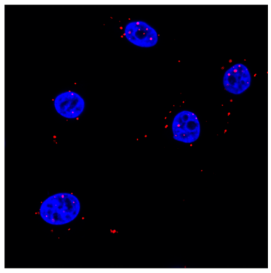

αCdc42 + αRock2

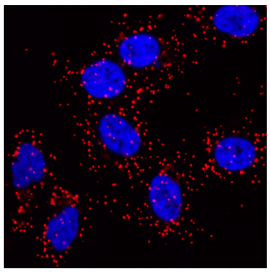

αRac1 + αMzt1/2 +CNF1

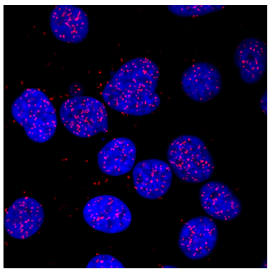

αRac1 + αIQSEC3 +CNF1

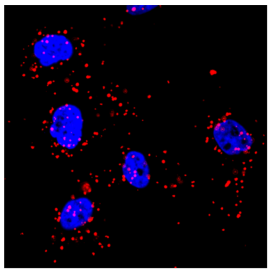

αCdc42 + αSESTD1 +CNF1

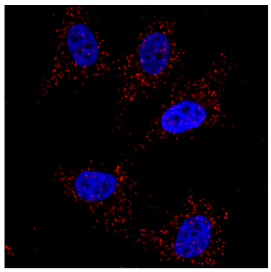

αCdc42 + αRock2 +CNF1

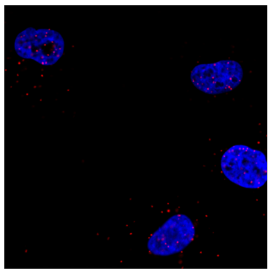

αCdc42 + αOpa1

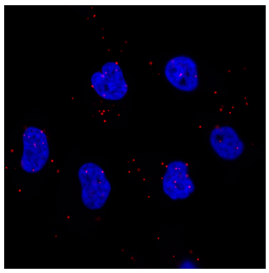

αCdc42 + αC1Orf198

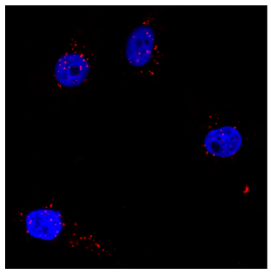

αCdc42 + αMzt2a/b

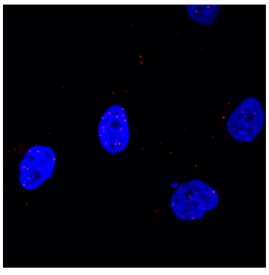

αCdc42 + αOpa1 +CNF1

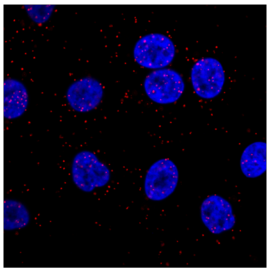

αCdc42 + αC1Orf198 +CNF1

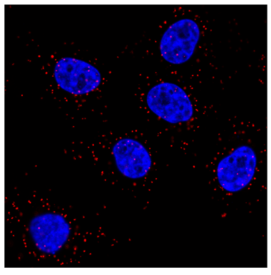

αCdc42 + αMzt2a/b +CNF1

SFDSLGSQSSHSR
Score: 222 ; 1393.6222 m/z; 697.81839 m/z; 0.30225 ppm; MULTI−MSMS

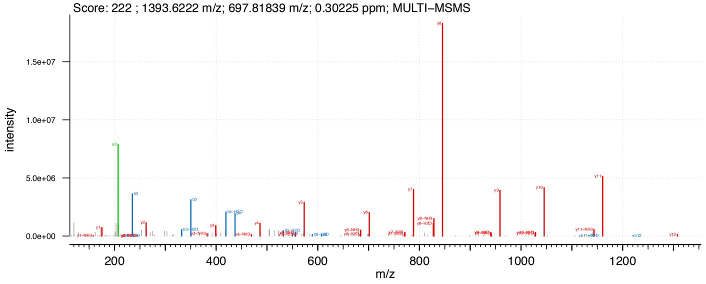

Raw File: Bibo_20111021_FEP_PD20111014_Cdc42_mouseCortex_LF_rep1_GTPgS
Scan Number: 3101
Proteins:
Q9ES28−2;Q9ES28−4;Q9ES28−6;Q9ES28;Q9ES28−7;Q9ES28−3;Q9ES28−5

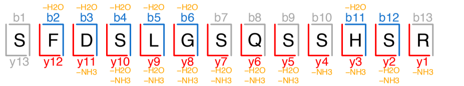

SFDSLGSQSSHSR
Score: 222 ; 1393.6222 m/z; 697.81839 m/z; 0.30225 ppm; MULTI−MSMS

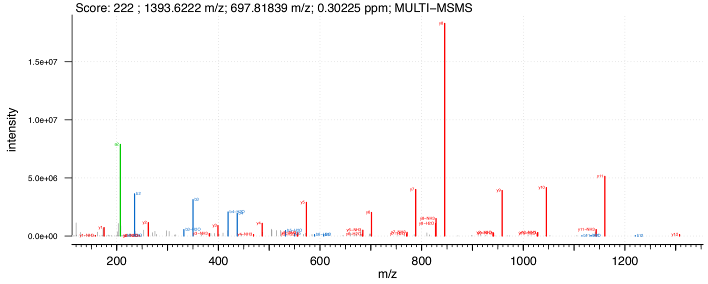

Raw File: Bibo_20111021_FEP_PD20111014_Cdc42_mouseCortex_LF_rep1_GTPgS
Scan Number: 3101
Proteins:
Q9ES28−2;Q9ES28−4;Q9ES28−6;Q9ES28;Q9ES28−7;Q9ES28−3;Q9ES28−5

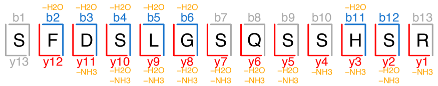

SFDSLGSQSSHSR
Score: 222 ; 1393.6222 m/z; 697.81839 m/z; 0.30225 ppm; MULTI−MSMS

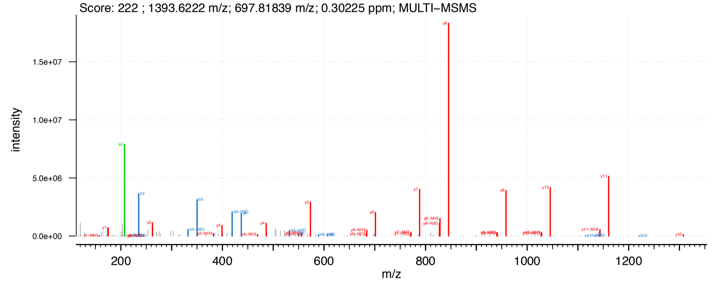

Raw File: Bibo_20111021_FEP_PD20111014_Cdc42_mouseCortex_LF_rep1_GTPgS
Scan Number: 3101
Proteins:
Q9ES28−2;Q9ES28−4;Q9ES28−6;Q9ES28;Q9ES28−7;Q9ES28−3;Q9ES28−5

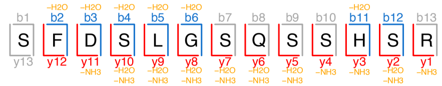

SFDSLGSQSSHSR
Score: 222 ; 1393.6222 m/z; 697.81839 m/z; 0.30225 ppm; MULTI−MSMS

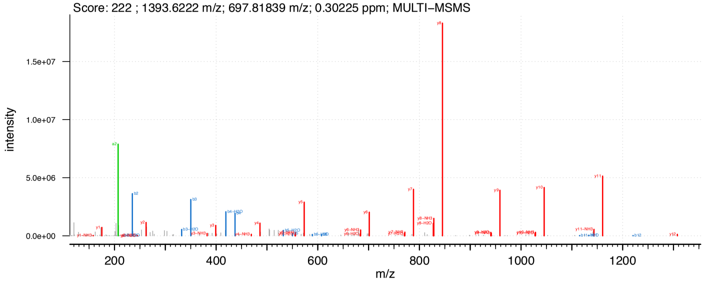

Raw File: Bibo_20111021_FEP_PD20111014_Cdc42_mouseCortex_LF_rep1_GTPgS
Scan Number: 3101
Proteins:
Q9ES28−2;Q9ES28−4;Q9ES28−6;Q9ES28;Q9ES28−7;Q9ES28−3;Q9ES28−5

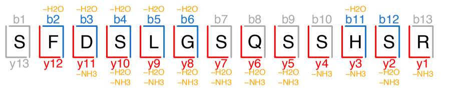

SFDSLGSQSSHSR
Score: 222 ; 1393.6222 m/z; 697.81839 m/z; 0.30225 ppm; MULTI−MSMS

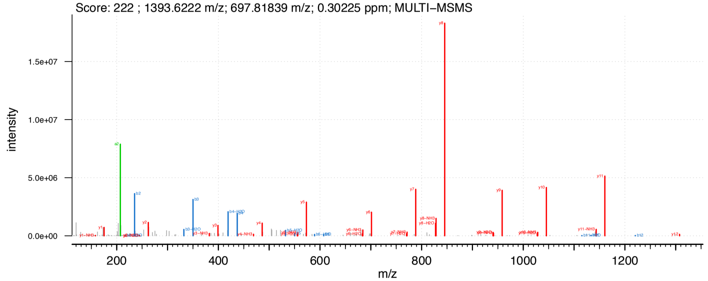

Raw File: Bibo_20111021_FEP_PD20111014_Cdc42_mouseCortex_LF_rep1_GTPgS
Scan Number: 3101
Proteins:
Q9ES28−2;Q9ES28−4;Q9ES28−6;Q9ES28;Q9ES28−7;Q9ES28−3;Q9ES28−5

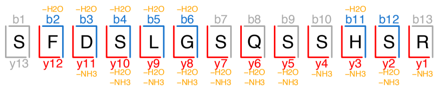

SFDSLGSQSSHSR
Score: 222 ; 1393.6222 m/z; 697.81839 m/z; 0.30225 ppm; MULTI−MSMS

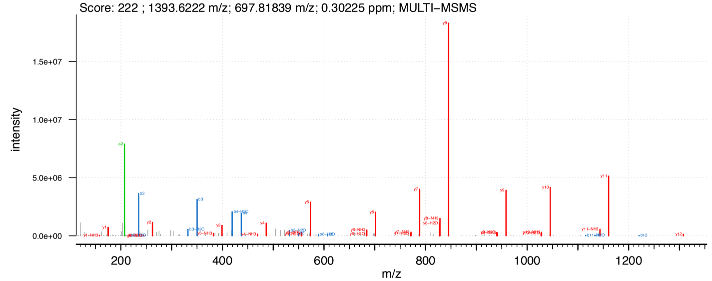

Raw File: Bibo_20111021_FEP_PD20111014_Cdc42_mouseCortex_LF_rep1_GTPgS
Scan Number: 3101
Proteins:
Q9ES28−2;Q9ES28−4;Q9ES28−6;Q9ES28;Q9ES28−7;Q9ES28−3;Q9ES28−5

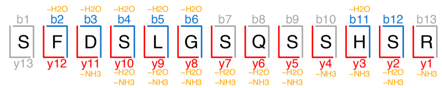

SFDSLGSQSSHSR
Score: 222 ; 1393.6222 m/z; 697.81839 m/z; 0.30225 ppm; MULTI−MSMS

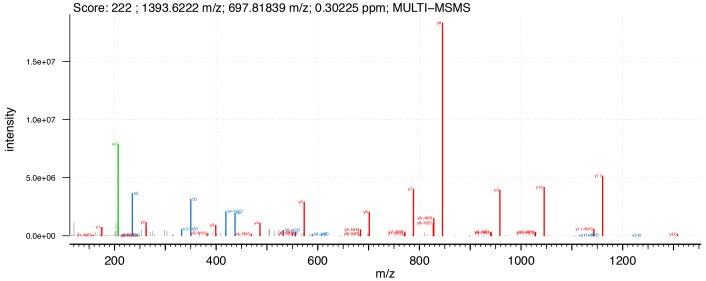

Raw File: Bibo_20111021_FEP_PD20111014_Cdc42_mouseCortex_LF_rep1_GTPgS
Scan Number: 3101
Proteins:
Q9ES28−2;Q9ES28−4;Q9ES28−6;Q9ES28;Q9ES28−7;Q9ES28−3;Q9ES28−5

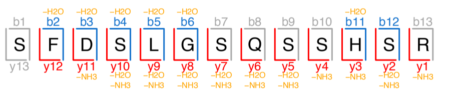

SFDSLGSQSSHSR
Score: 222 ; 1393.6222 m/z; 697.81839 m/z; 0.30225 ppm; MULTI−MSMS

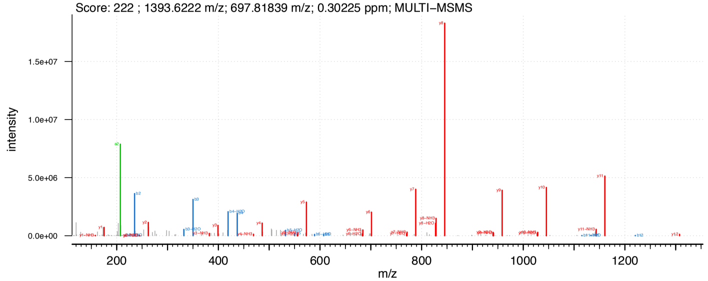

Raw File: Bibo_20111021_FEP_PD20111014_Cdc42_mouseCortex_LF_rep1_GTPgS
Scan Number: 3101
Proteins:
Q9ES28−2;Q9ES28−4;Q9ES28−6;Q9ES28;Q9ES28−7;Q9ES28−3;Q9ES28−5

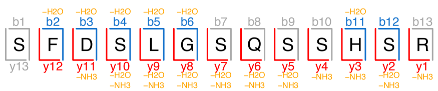

SFDSLGSQSSHSR
Score: 222 ; 1393.6222 m/z; 697.81839 m/z; 0.30225 ppm; MULTI−MSMS

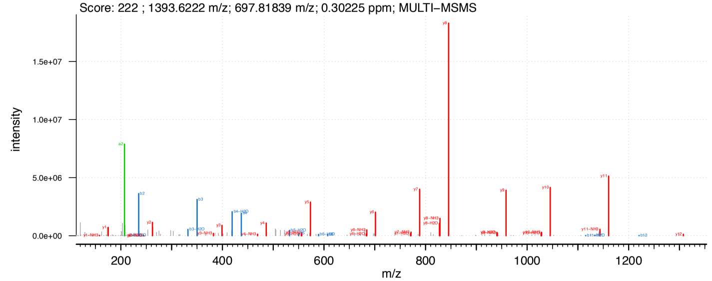

Raw File: Bibo_20111021_FEP_PD20111014_Cdc42_mouseCortex_LF_rep1_GTPgS
Scan Number: 3101
Proteins:
Q9ES28−2;Q9ES28−4;Q9ES28−6;Q9ES28;Q9ES28−7;Q9ES28−3;Q9ES28−5

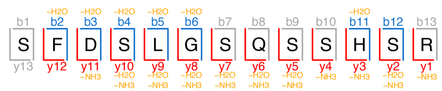

ALYLIATNGTPELQNPER
Score: 257 ; 1999.0375 m/z; 1000.526 m/z; −0.59187 ppm; MULTI−MSMS

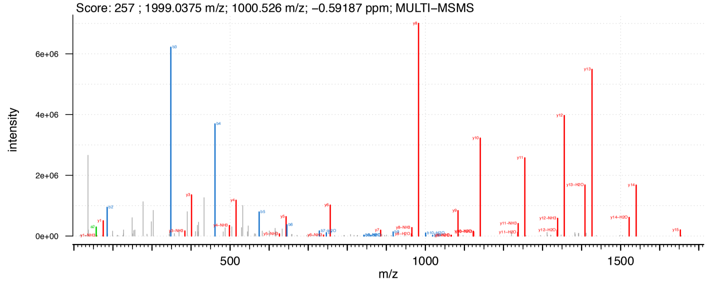

Raw File: Bibo_20111021_FEP_PD20111014_Cdc42_mouseCortex_LF_rep1_GTPgS
Scan Number: 28163
Proteins:
B1GX81;A3KGC0;Q61036;B1GX80;A3KGC1;Q61036−2

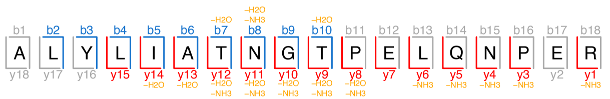

ALYLIATNGTPELQNPER
Score: 257 ; 1999.0375 m/z; 1000.526 m/z; −0.59187 ppm; MULTI−MSMS

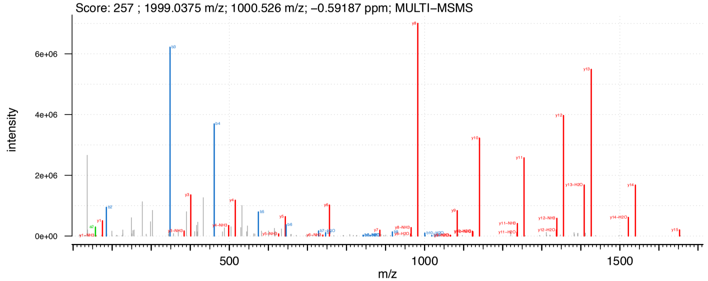

Raw File: Bibo_20111021_FEP_PD20111014_Cdc42_mouseCortex_LF_rep1_GTPgS
Scan Number: 28163
Proteins:
B1GX81;A3KGC0;Q61036;B1GX80;A3KGC1;Q61036−2

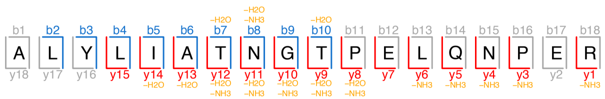

ALYLIATNGTPELQNPER
Score: 257 ; 1999.0375 m/z; 1000.526 m/z; −0.59187 ppm; MULTI−MSMS

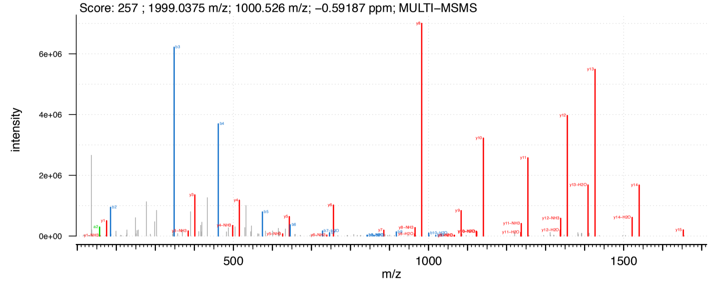

Raw File: Bibo_20111021_FEP_PD20111014_Cdc42_mouseCortex_LF_rep1_GTPgS
Scan Number: 28163
Proteins:
B1GX81;A3KGC0;Q61036;B1GX80;A3KGC1;Q61036−2

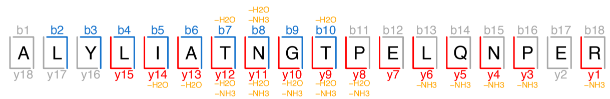

ALYLIATNGTPELQNPER
Score: 257 ; 1999.0375 m/z; 1000.526 m/z; −0.59187 ppm; MULTI−MSMS

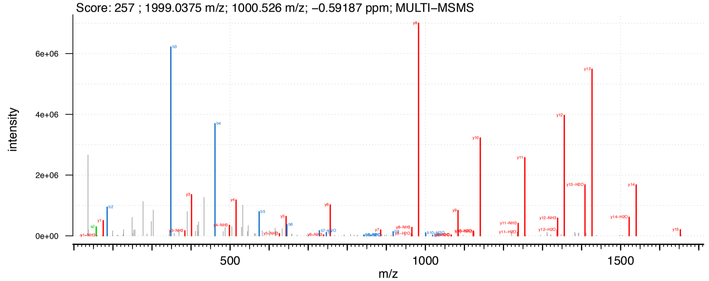

Raw File: Bibo_20111021_FEP_PD20111014_Cdc42_mouseCortex_LF_rep1_GTPgS
Scan Number: 28163
Proteins:
B1GX81;A3KGC0;Q61036;B1GX80;A3KGC1;Q61036−2

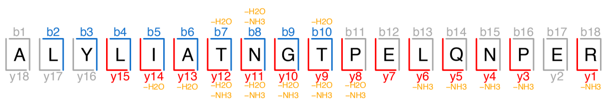

ALYLIATNGTPELQNPER
Score: 257 ; 1999.0375 m/z; 1000.526 m/z; −0.59187 ppm; MULTI−MSMS

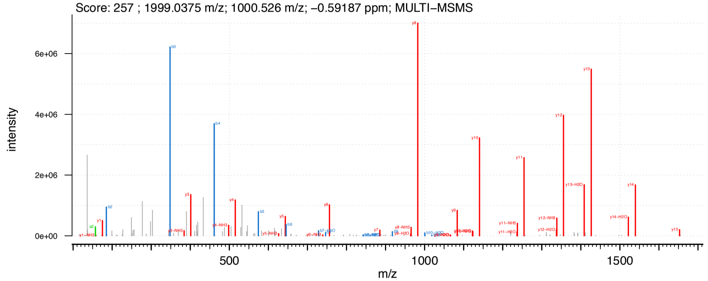

Raw File: Bibo_20111021_FEP_PD20111014_Cdc42_mouseCortex_LF_rep1_GTPgS
Scan Number: 28163
Proteins:
B1GX81;A3KGC0;Q61036;B1GX80;A3KGC1;Q61036−2

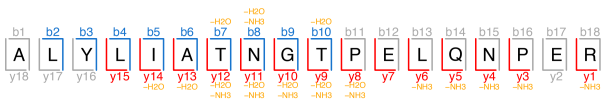

ALYLIATNGTPELQNPER
Score: 257 ; 1999.0375 m/z; 1000.526 m/z; −0.59187 ppm; MULTI−MSMS

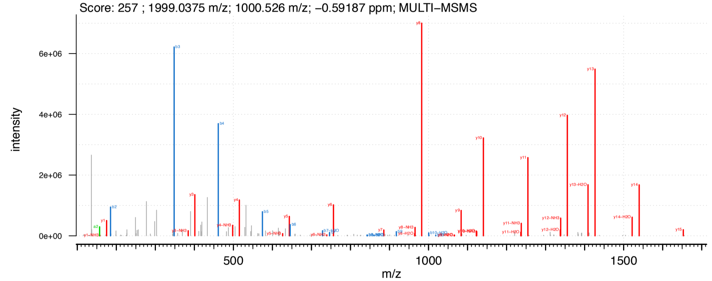

Raw File: Bibo_20111021_FEP_PD20111014_Cdc42_mouseCortex_LF_rep1_GTPgS
Scan Number: 28163
Proteins:
B1GX81;A3KGC0;Q61036;B1GX80;A3KGC1;Q61036−2

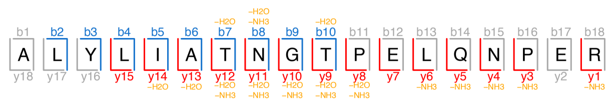

ALYLIATNGTPELQNPER
Score: 257 ; 1999.0375 m/z; 1000.526 m/z; −0.59187 ppm; MULTI−MSMS

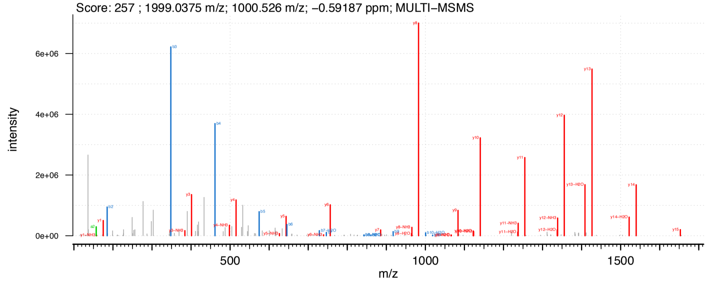

Raw File: Bibo_20111021_FEP_PD20111014_Cdc42_mouseCortex_LF_rep1_GTPgS
Scan Number: 28163
Proteins:
B1GX81;A3KGC0;Q61036;B1GX80;A3KGC1;Q61036−2

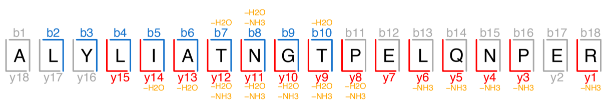

ALYLIATNGTPELQNPER
Score: 257 ; 1999.0375 m/z; 1000.526 m/z; −0.59187 ppm; MULTI−MSMS

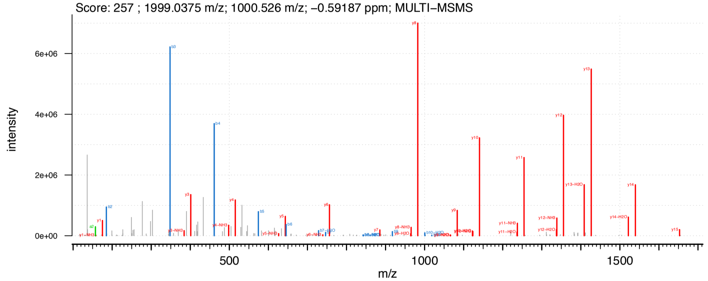

Raw File: Bibo_20111021_FEP_PD20111014_Cdc42_mouseCortex_LF_rep1_GTPgS
Scan Number: 28163
Proteins:
B1GX81;A3KGC0;Q61036;B1GX80;A3KGC1;Q61036−2

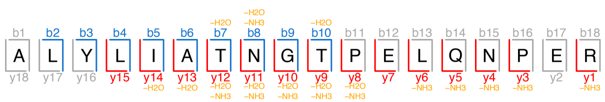

ALYLIATNGTPELQNPER
Score: 257 ; 1999.0375 m/z; 1000.526 m/z; −0.59187 ppm; MULTI−MSMS

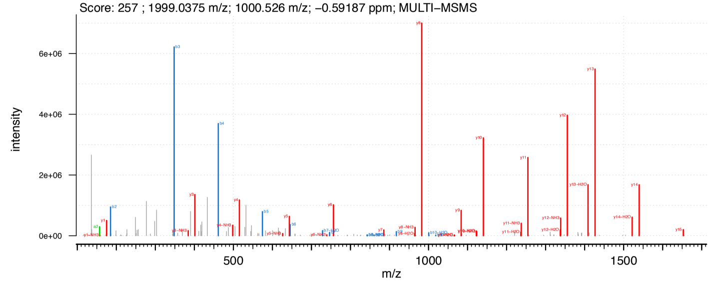

Raw File: Bibo_20111021_FEP_PD20111014_Cdc42_mouseCortex_LF_rep1_GTPgS
Scan Number: 28163
Proteins:
B1GX81;A3KGC0;Q61036;B1GX80;A3KGC1;Q61036−2

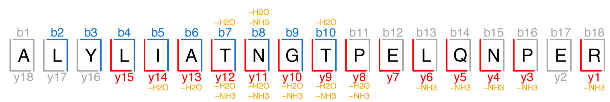

SVVESIASPAAPNKEDIPPSAENANSTTLYR
Score: 192 ; 3227.5946 m/z; 1076.8721 m/z; −0.82346 ppm; MULTI−MSMS

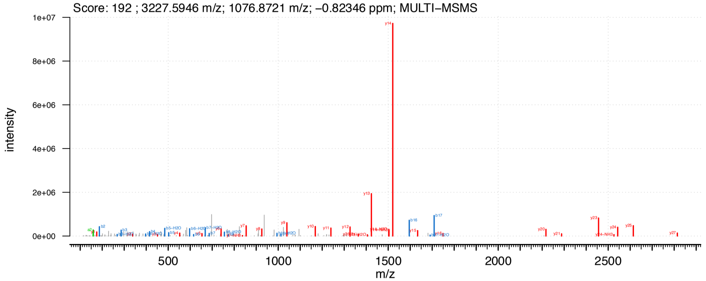

Raw File: Bibo_20111021_FEP_PD20111014_Cdc42_mouseCortex_LF_rep1_GTPgS
Scan Number: 18854
Proteins:
B1GX81;A3KGC0;Q61036;B1GX80;A3KGC5;A3KGC1;Q61036−2

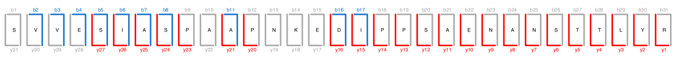

SVVESIASPAAPNKEDIPPSAENANSTTLYR
Score: 192 ; 3227.5946 m/z; 1076.8721 m/z; −0.82346 ppm; MULTI−MSMS

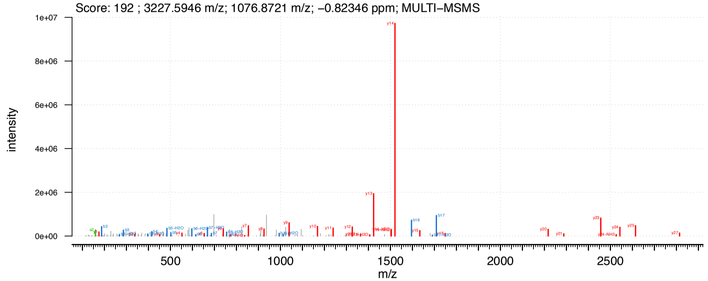

Raw File: Bibo_20111021_FEP_PD20111014_Cdc42_mouseCortex_LF_rep1_GTPgS
Scan Number: 18854
Proteins:
B1GX81;A3KGC0;Q61036;B1GX80;A3KGC5;A3KGC1;Q61036−2

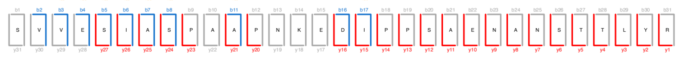

SVVESIASPAAPNKEDIPPSAENANSTTLYR
Score: 192 ; 3227.5946 m/z; 1076.8721 m/z; −0.82346 ppm; MULTI−MSMS

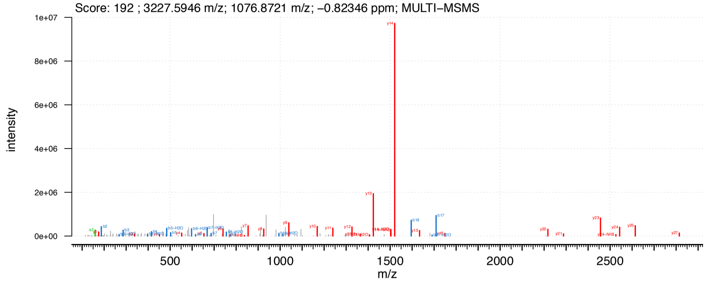

Raw File: Bibo_20111021_FEP_PD20111014_Cdc42_mouseCortex_LF_rep1_GTPgS
Scan Number: 18854
Proteins:
B1GX81;A3KGC0;Q61036;B1GX80;A3KGC5;A3KGC1;Q61036−2

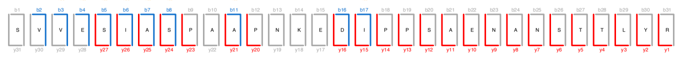

SVVESIASPAAPNKEDIPPSAENANSTTLYR
Score: 192 ; 3227.5946 m/z; 1076.8721 m/z; −0.82346 ppm; MULTI−MSMS

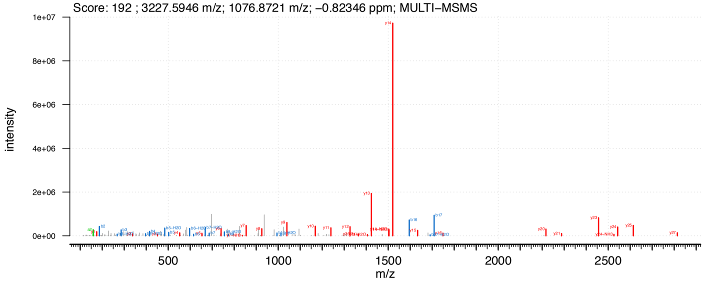

Raw File: Bibo_20111021_FEP_PD20111014_Cdc42_mouseCortex_LF_rep1_GTPgS
Scan Number: 18854
Proteins:
B1GX81;A3KGC0;Q61036;B1GX80;A3KGC5;A3KGC1;Q61036−2

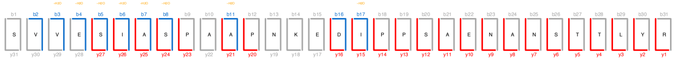

SVVESIASPAAPNKEDIPPSAENANSTTLYR
Score: 192 ; 3227.5946 m/z; 1076.8721 m/z; −0.82346 ppm; MULTI−MSMS

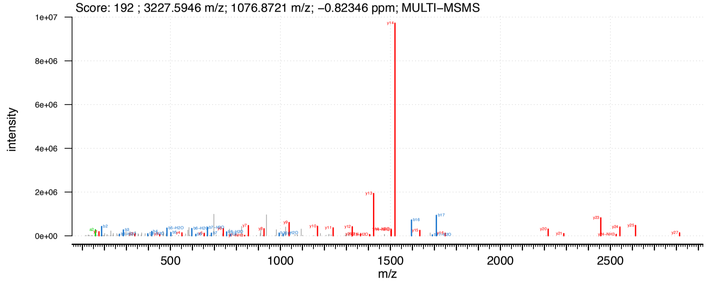

Raw File: Bibo_20111021_FEP_PD20111014_Cdc42_mouseCortex_LF_rep1_GTPgS
Scan Number: 18854
Proteins:
B1GX81;A3KGC0;Q61036;B1GX80;A3KGC5;A3KGC1;Q61036−2

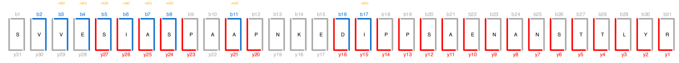

SVVESIASPAAPNKEDIPPSAENANSTTLYR
Score: 192 ; 3227.5946 m/z; 1076.8721 m/z; −0.82346 ppm; MULTI−MSMS

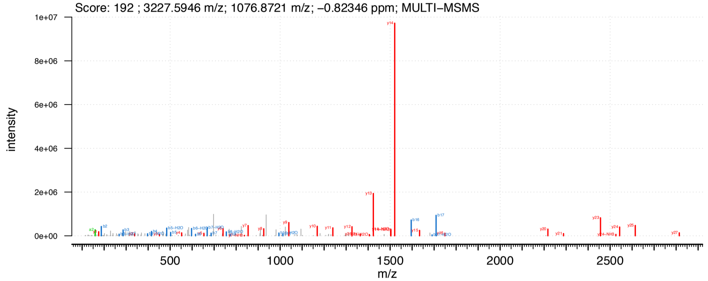

Raw File: Bibo_20111021_FEP_PD20111014_Cdc42_mouseCortex_LF_rep1_GTPgS
Scan Number: 18854
Proteins:
B1GX81;A3KGC0;Q61036;B1GX80;A3KGC5;A3KGC1;Q61036−2

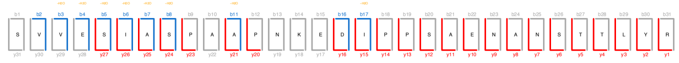

SVVESIASPAAPNKEDIPPSAENANSTTLYR
Score: 192 ; 3227.5946 m/z; 1076.8721 m/z; −0.82346 ppm; MULTI−MSMS

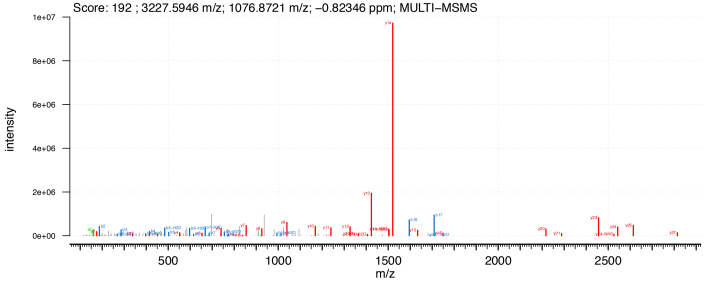

Raw File: Bibo_20111021_FEP_PD20111014_Cdc42_mouseCortex_LF_rep1_GTPgS
Scan Number: 18854
Proteins:
B1GX81;A3KGC0;Q61036;B1GX80;A3KGC5;A3KGC1;Q61036−2

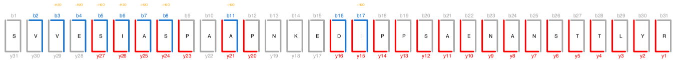

SVVESIASPAAPNKEDIPPSAENANSTTLYR
Score: 192 ; 3227.5946 m/z; 1076.8721 m/z; −0.82346 ppm; MULTI−MSMS

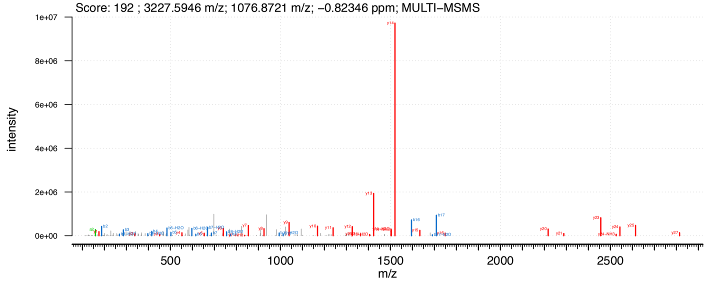

Raw File: Bibo_20111021_FEP_PD20111014_Cdc42_mouseCortex_LF_rep1_GTPgS
Scan Number: 18854
Proteins:
B1GX81;A3KGC0;Q61036;B1GX80;A3KGC5;A3KGC1;Q61036−2

SVVESIASPAAPNKEDIPPSAENANSTTLYR
Score: 192 ; 3227.5946 m/z; 1076.8721 m/z; −0.82346 ppm; MULTI−MSMS

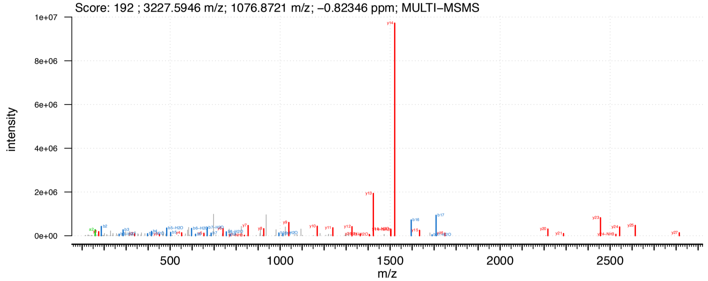

Raw File: Bibo_20111021_FEP_PD20111014_Cdc42_mouseCortex_LF_rep1_GTPgS
Scan Number: 18854
Proteins:
B1GX81;A3KGC0;Q61036;B1GX80;A3KGC5;A3KGC1;Q61036−2

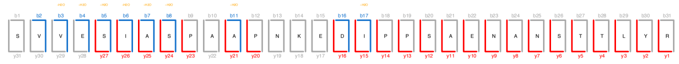

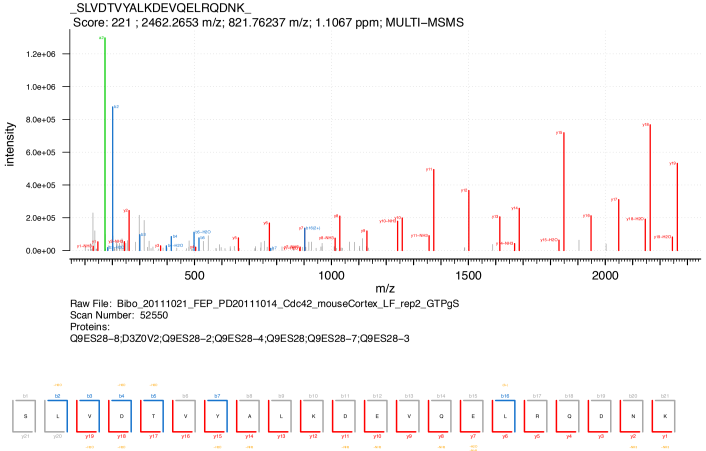
SLVDTVYALKDEVQELRQDNK
Score: 221 ; 2462.2653 m/z; 821.76237 m/z; 1.1067 ppm; MULTI−MSMS
intensity
m/z
Raw File: Bibo_20111021_FEP_PD20111014_Cdc42_mouseCortex_LF_rep2_GTPgS
Scan Number: 52550
Proteins:
Q9ES28−8;D3Z0V2;Q9ES28−2;Q9ES28−4;Q9ES28;Q9ES28−7;Q9ES28−3
S L V D T V Y A L K D E V Q E L R Q D N K

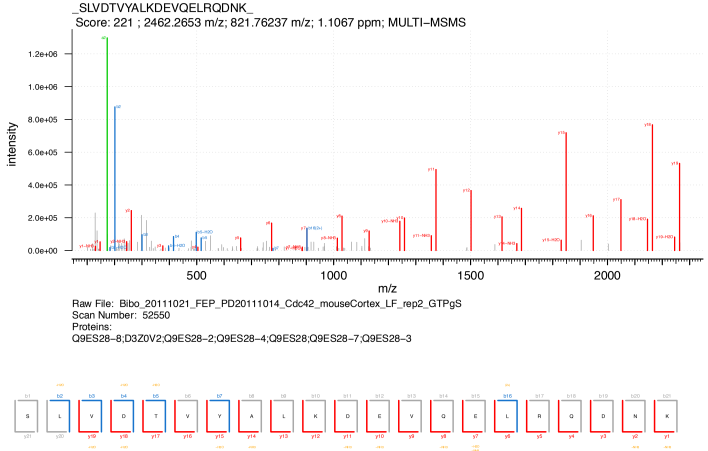
SLVDTVYALKDEVQELRQDNK
Score: 221 ; 2462.2653 m/z; 821.76237 m/z; 1.1067 ppm; MULTI−MSMS
intensity
m/z
Raw File: Bibo_20111021_FEP_PD20111014_Cdc42_mouseCortex_LF_rep2_GTPgS
Scan Number: 52550
Proteins:
Q9ES28−8;D3Z0V2;Q9ES28−2;Q9ES28−4;Q9ES28;Q9ES28−7;Q9ES28−3
S L V D T V Y A L K D E V Q E L R Q D N K

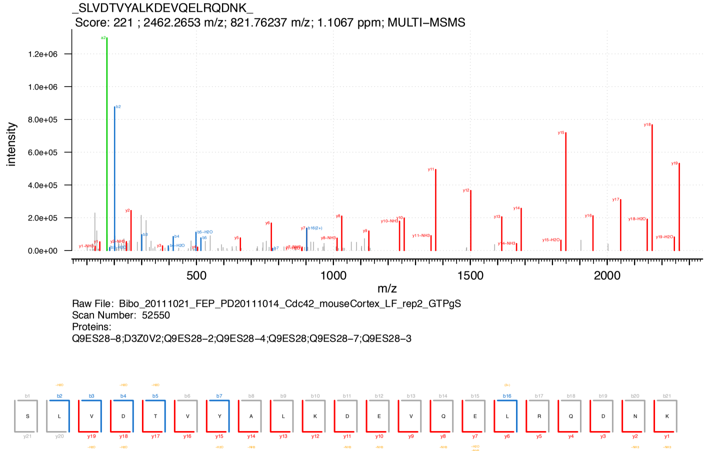
SLVDTVYALKDEVQELRQDNK
Score: 221 ; 2462.2653 m/z; 821.76237 m/z; 1.1067 ppm; MULTI−MSMS
intensity
m/z
Raw File: Bibo_20111021_FEP_PD20111014_Cdc42_mouseCortex_LF_rep2_GTPgS
Scan Number: 52550
Proteins:
Q9ES28−8;D3Z0V2;Q9ES28−2;Q9ES28−4;Q9ES28;Q9ES28−7;Q9ES28−3
S L V D T V Y A L K D E V Q E L R Q D N K

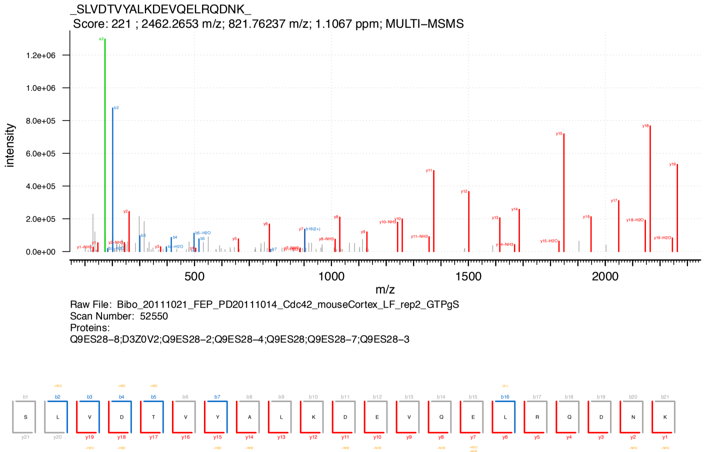
SLVDTVYALKDEVQELRQDNK
Score: 221 ; 2462.2653 m/z; 821.76237 m/z; 1.1067 ppm; MULTI−MSMS
intensity
m/z
Raw File: Bibo_20111021_FEP_PD20111014_Cdc42_mouseCortex_LF_rep2_GTPgS
Scan Number: 52550
Proteins:
Q9ES28−8;D3Z0V2;Q9ES28−2;Q9ES28−4;Q9ES28;Q9ES28−7;Q9ES28−3
S L V D T V Y A L K D E V Q E L R Q D N K

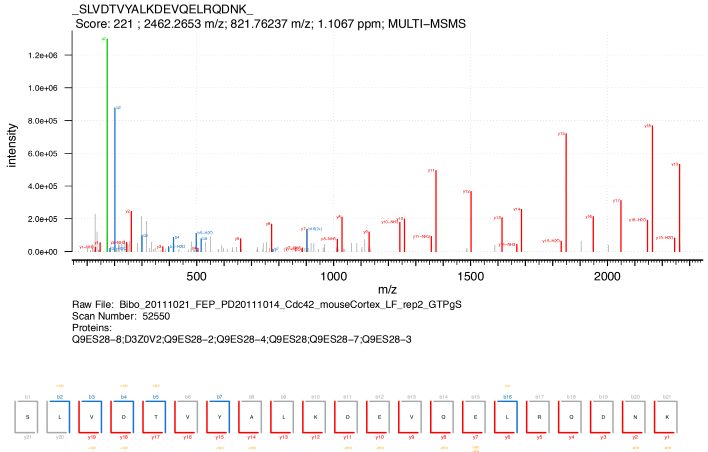
SLVDTVYALKDEVQELRQDNK
Score: 221 ; 2462.2653 m/z; 821.76237 m/z; 1.1067 ppm; MULTI−MSMS
intensity
m/z
Raw File: Bibo_20111021_FEP_PD20111014_Cdc42_mouseCortex_LF_rep2_GTPgS
Scan Number: 52550
Proteins:
Q9ES28−8;D3Z0V2;Q9ES28−2;Q9ES28−4;Q9ES28;Q9ES28−7;Q9ES28−3
S L V D T V Y A L K D E V Q E L R Q D N K

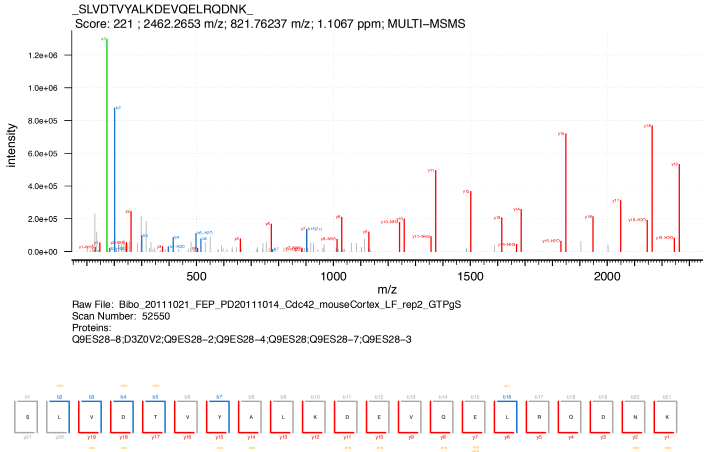
SLVDTVYALKDEVQELRQDNK
Score: 221 ; 2462.2653 m/z; 821.76237 m/z; 1.1067 ppm; MULTI−MSMS
intensity
m/z
Raw File: Bibo_20111021_FEP_PD20111014_Cdc42_mouseCortex_LF_rep2_GTPgS
Scan Number: 52550
Proteins:
Q9ES28−8;D3Z0V2;Q9ES28−2;Q9ES28−4;Q9ES28;Q9ES28−7;Q9ES28−3
S L V D T V Y A L K D E V Q E L R Q D N K

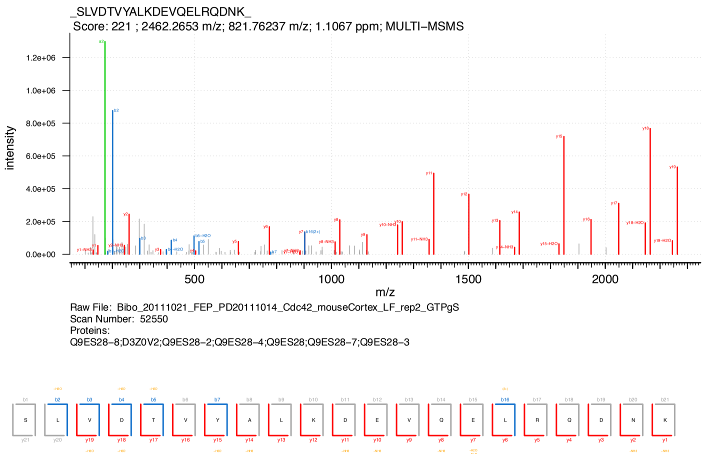
SLVDTVYALKDEVQELRQDNK
Score: 221 ; 2462.2653 m/z; 821.76237 m/z; 1.1067 ppm; MULTI−MSMS
intensity
m/z
Raw File: Bibo_20111021_FEP_PD20111014_Cdc42_mouseCortex_LF_rep2_GTPgS
Scan Number: 52550
Proteins:
Q9ES28−8;D3Z0V2;Q9ES28−2;Q9ES28−4;Q9ES28;Q9ES28−7;Q9ES28−3
S L V D T V Y A L K D E V Q E L R Q D N K

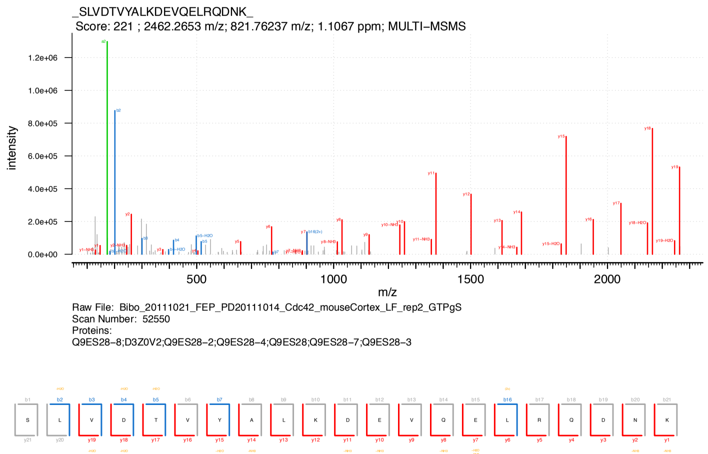
SLVDTVYALKDEVQELRQDNK
Score: 221 ; 2462.2653 m/z; 821.76237 m/z; 1.1067 ppm; MULTI−MSMS
intensity
m/z
Raw File: Bibo_20111021_FEP_PD20111014_Cdc42_mouseCortex_LF_rep2_GTPgS
Scan Number: 52550
Proteins:
Q9ES28−8;D3Z0V2;Q9ES28−2;Q9ES28−4;Q9ES28;Q9ES28−7;Q9ES28−3
S L V D T V Y A L K D E V Q E L R Q D N K

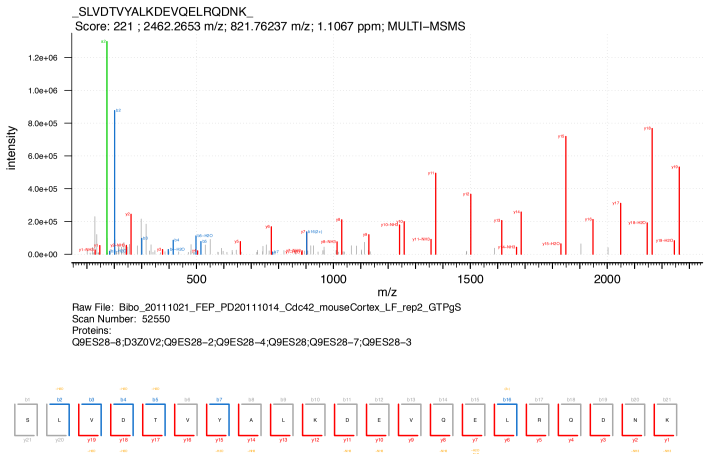
SLVDTVYALKDEVQELRQDNK
Score: 221 ; 2462.2653 m/z; 821.76237 m/z; 1.1067 ppm; MULTI−MSMS
intensity
m/z
Raw File: Bibo_20111021_FEP_PD20111014_Cdc42_mouseCortex_LF_rep2_GTPgS
Scan Number: 52550
Proteins:
Q9ES28−8;D3Z0V2;Q9ES28−2;Q9ES28−4;Q9ES28;Q9ES28−7;Q9ES28−3
S L V D T V Y A L K D E V Q E L R Q D N K

SYYNVVLQNILETEHEYSK
Score: 260 ; 2328.1274 m/z; 1165.071 m/z; −0.089837 ppm; MULTI−MSMS

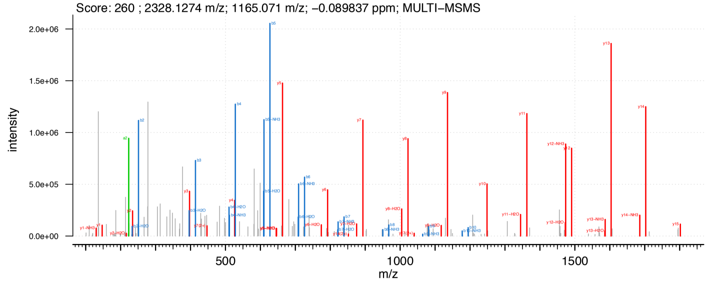

Raw File: Bibo_20111021_FEP_PD20111014_Cdc42_mouseCortex_LF_rep2_GTPgS
Scan Number: 54910
Proteins:
Q9ES28−8;D3Z0V2;Q9ES28−2;Q9ES28−4;Q9ES28−6;Q9ES28;Q9ES28−7;Q9ES28−3;Q9ES28−5

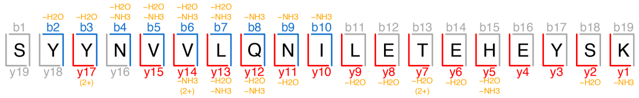

SYYNVVLQNILETEHEYSK
Score: 260 ; 2328.1274 m/z; 1165.071 m/z; −0.089837 ppm; MULTI−MSMS

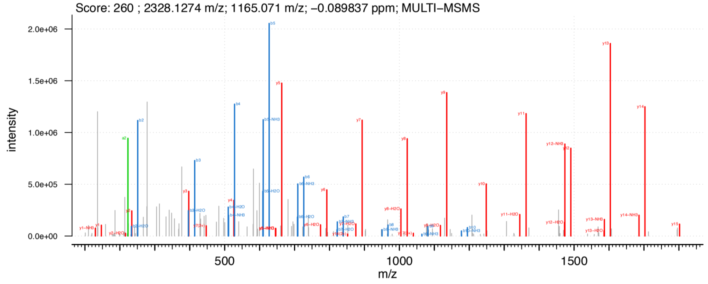

Raw File: Bibo_20111021_FEP_PD20111014_Cdc42_mouseCortex_LF_rep2_GTPgS
Scan Number: 54910
Proteins:
Q9ES28−8;D3Z0V2;Q9ES28−2;Q9ES28−4;Q9ES28−6;Q9ES28;Q9ES28−7;Q9ES28−3;Q9ES28−5

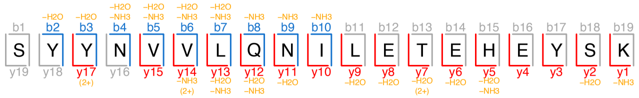

SYYNVVLQNILETEHEYSK
Score: 260 ; 2328.1274 m/z; 1165.071 m/z; −0.089837 ppm; MULTI−MSMS

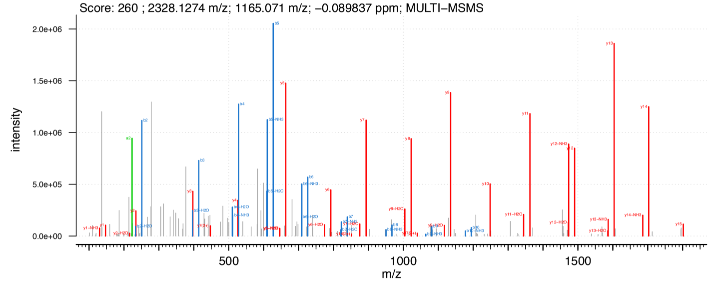

Raw File: Bibo_20111021_FEP_PD20111014_Cdc42_mouseCortex_LF_rep2_GTPgS
Scan Number: 54910
Proteins:
Q9ES28−8;D3Z0V2;Q9ES28−2;Q9ES28−4;Q9ES28−6;Q9ES28;Q9ES28−7;Q9ES28−3;Q9ES28−5

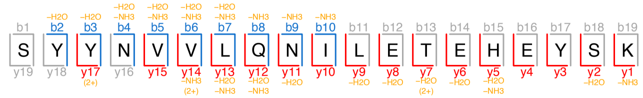

SYYNVVLQNILETEHEYSK
Score: 260 ; 2328.1274 m/z; 1165.071 m/z; −0.089837 ppm; MULTI−MSMS

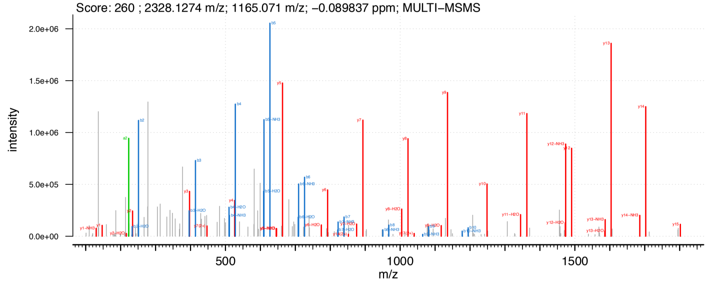

Raw File: Bibo_20111021_FEP_PD20111014_Cdc42_mouseCortex_LF_rep2_GTPgS
Scan Number: 54910
Proteins:
Q9ES28−8;D3Z0V2;Q9ES28−2;Q9ES28−4;Q9ES28−6;Q9ES28;Q9ES28−7;Q9ES28−3;Q9ES28−5

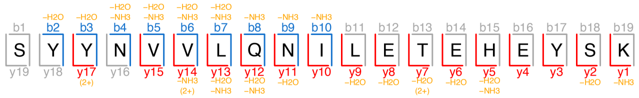

SYYNVVLQNILETEHEYSK
Score: 260 ; 2328.1274 m/z; 1165.071 m/z; −0.089837 ppm; MULTI−MSMS

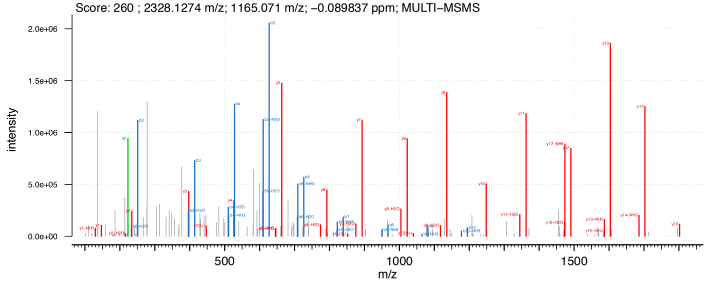

Raw File: Bibo_20111021_FEP_PD20111014_Cdc42_mouseCortex_LF_rep2_GTPgS
Scan Number: 54910
Proteins:
Q9ES28−8;D3Z0V2;Q9ES28−2;Q9ES28−4;Q9ES28−6;Q9ES28;Q9ES28−7;Q9ES28−3;Q9ES28−5

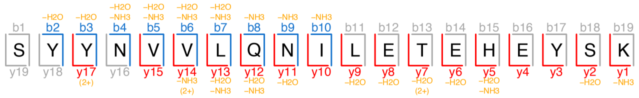

SYYNVVLQNILETEHEYSK
Score: 260 ; 2328.1274 m/z; 1165.071 m/z; −0.089837 ppm; MULTI−MSMS

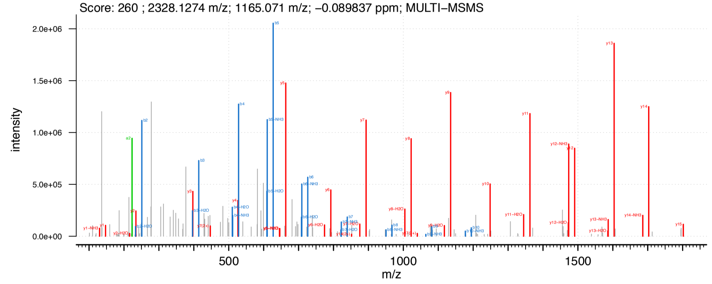

Raw File: Bibo_20111021_FEP_PD20111014_Cdc42_mouseCortex_LF_rep2_GTPgS
Scan Number: 54910
Proteins:
Q9ES28−8;D3Z0V2;Q9ES28−2;Q9ES28−4;Q9ES28−6;Q9ES28;Q9ES28−7;Q9ES28−3;Q9ES28−5

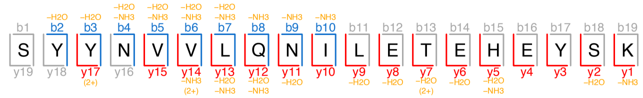

SYYNVVLQNILETEHEYSK
Score: 260 ; 2328.1274 m/z; 1165.071 m/z; −0.089837 ppm; MULTI−MSMS

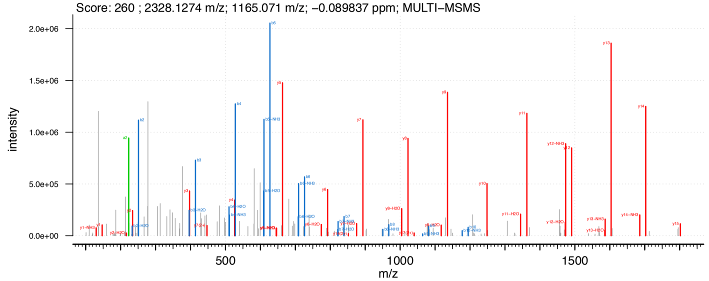

Raw File: Bibo_20111021_FEP_PD20111014_Cdc42_mouseCortex_LF_rep2_GTPgS
Scan Number: 54910
Proteins:
Q9ES28−8;D3Z0V2;Q9ES28−2;Q9ES28−4;Q9ES28−6;Q9ES28;Q9ES28−7;Q9ES28−3;Q9ES28−5

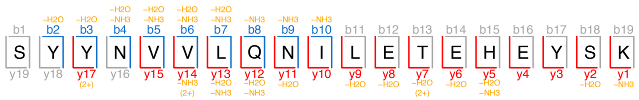

SYYNVVLQNILETEHEYSK
Score: 260 ; 2328.1274 m/z; 1165.071 m/z; −0.089837 ppm; MULTI−MSMS

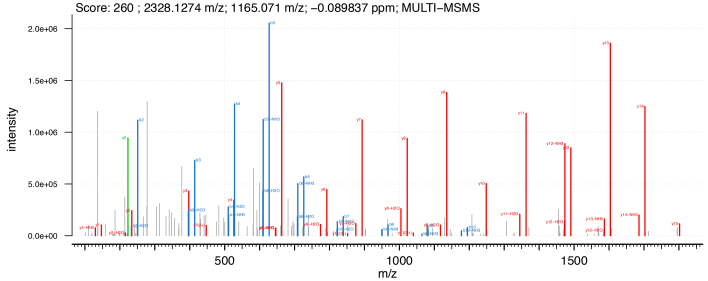

Raw File: Bibo_20111021_FEP_PD20111014_Cdc42_mouseCortex_LF_rep2_GTPgS
Scan Number: 54910
Proteins:
Q9ES28−8;D3Z0V2;Q9ES28−2;Q9ES28−4;Q9ES28−6;Q9ES28;Q9ES28−7;Q9ES28−3;Q9ES28−5

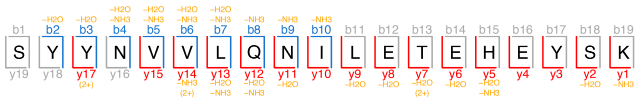

SYYNVVLQNILETEHEYSK
Score: 260 ; 2328.1274 m/z; 1165.071 m/z; −0.089837 ppm; MULTI−MSMS

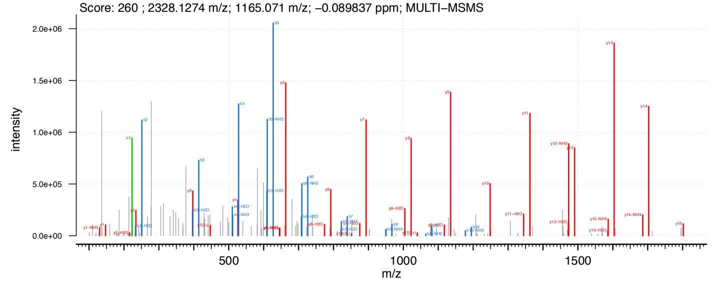

Raw File: Bibo_20111021_FEP_PD20111014_Cdc42_mouseCortex_LF_rep2_GTPgS
Scan Number: 54910
Proteins:
Q9ES28−8;D3Z0V2;Q9ES28−2;Q9ES28−4;Q9ES28−6;Q9ES28;Q9ES28−7;Q9ES28−3;Q9ES28−5

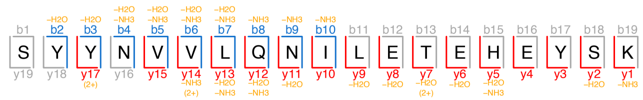

VTSVSNPTIKPHSVPSHTLPSHPLTPSSK
Score: 306 ; 3031.6091 m/z; 1011.5436 m/z; –0.74285 ppm; MULTI–MSMS

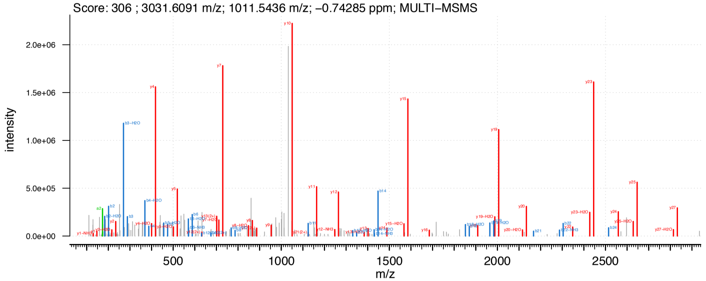

Raw File: Bibo_20111021_FEP_PD20111014_Cdc42_mouseCortex_LF_rep2_GTPgS
Scan Number: 7545
Proteins:
Q9ES28–8;Q9ES28–2;Q9ES28–4;Q9ES28–6;Q9ES28;Q9ES28–7;Q9ES28–5

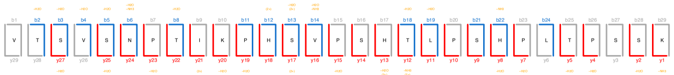

VTSVSNPTIKPHSVPSHTLPSHPLTPSSK
Score: 306 ; 3031.6091 m/z; 1011.5436 m/z; –0.74285 ppm; MULTI–MSMS

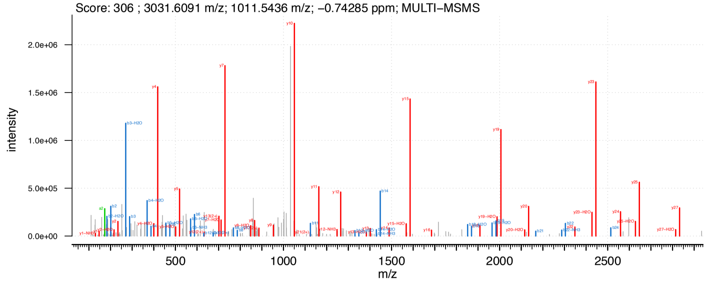

Raw File: Bibo_20111021_FEP_PD20111014_Cdc42_mouseCortex_LF_rep2_GTPgS
Scan Number: 7545
Proteins:
Q9ES28–8;Q9ES28–2;Q9ES28–4;Q9ES28–6;Q9ES28;Q9ES28–7;Q9ES28–5

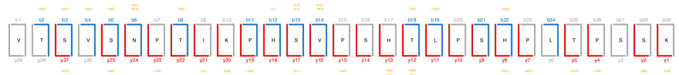

VTSVSNPTIKPHSVPSHTLPSHPLTPSSK
Score: 306 ; 3031.6091 m/z; 1011.5436 m/z; –0.74285 ppm; MULTI–MSMS

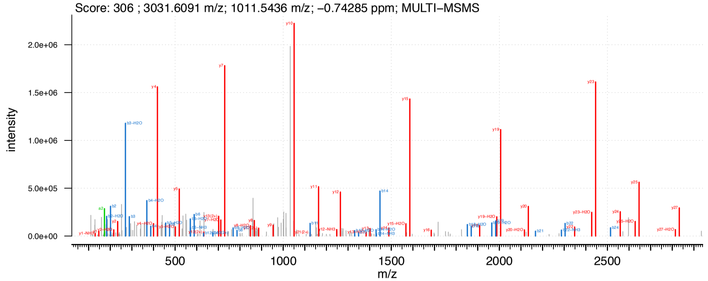

Raw File: Bibo_20111021_FEP_PD20111014_Cdc42_mouseCortex_LF_rep2_GTPgS
Scan Number: 7545
Proteins:
Q9ES28–8;Q9ES28–2;Q9ES28–4;Q9ES28–6;Q9ES28;Q9ES28–7;Q9ES28–5

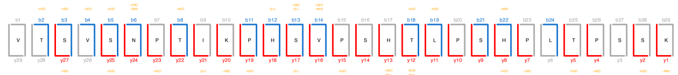

VTSVSNPTIKPHSVPSHTLPSHPLTPSSK
Score: 306 ; 3031.6091 m/z; 1011.5436 m/z; –0.74285 ppm; MULTI–MSMS

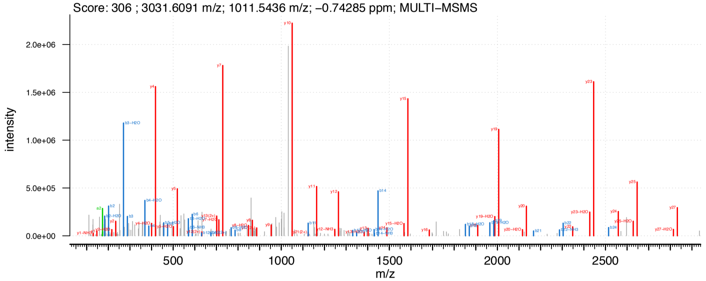

Raw File: Bibo_20111021_FEP_PD20111014_Cdc42_mouseCortex_LF_rep2_GTPgS
Scan Number: 7545
Proteins:
Q9ES28–8;Q9ES28–2;Q9ES28–4;Q9ES28–6;Q9ES28;Q9ES28–7;Q9ES28–5

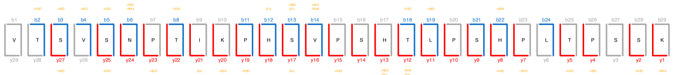

VTSVSNPTIKPHSVPSHTLPSHPLTPSSK
Score: 306 ; 3031.6091 m/z; 1011.5436 m/z; –0.74285 ppm; MULTI–MSMS

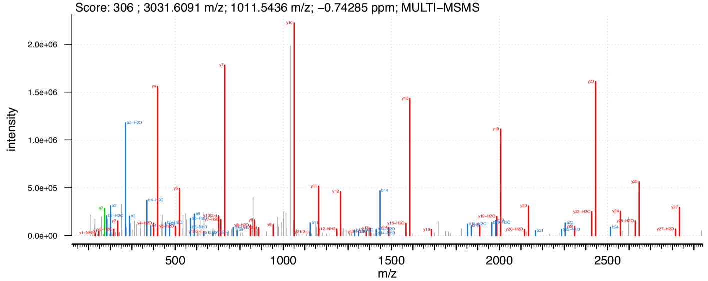

Raw File: Bibo_20111021_FEP_PD20111014_Cdc42_mouseCortex_LF_rep2_GTPgS
Scan Number: 7545
Proteins:
Q9ES28–8;Q9ES28–2;Q9ES28–4;Q9ES28–6;Q9ES28;Q9ES28–7;Q9ES28–5

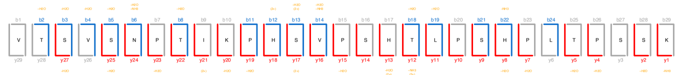

VTSVSNPTIKPHSVPSHTLPSHPLTPSSK
Score: 306 ; 3031.6091 m/z; 1011.5436 m/z; –0.74285 ppm; MULTI–MSMS

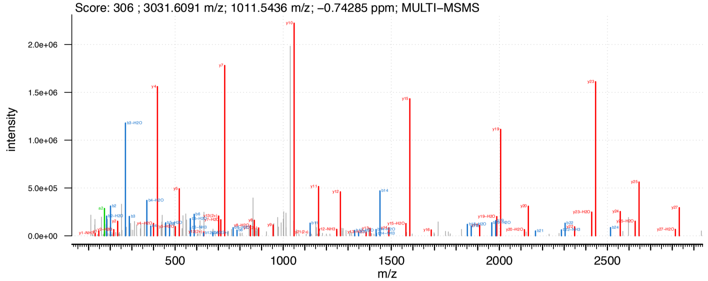

Raw File: Bibo_20111021_FEP_PD20111014_Cdc42_mouseCortex_LF_rep2_GTPgS
Scan Number: 7545
Proteins:
Q9ES28–8;Q9ES28–2;Q9ES28–4;Q9ES28–6;Q9ES28;Q9ES28–7;Q9ES28–5

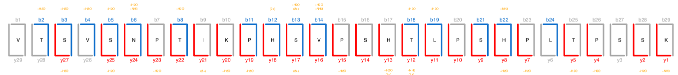

VTSVSNPTIKPHSVPSHTLPSHPLTPSSK
Score: 306 ; 3031.6091 m/z; 1011.5436 m/z; –0.74285 ppm; MULTI–MSMS

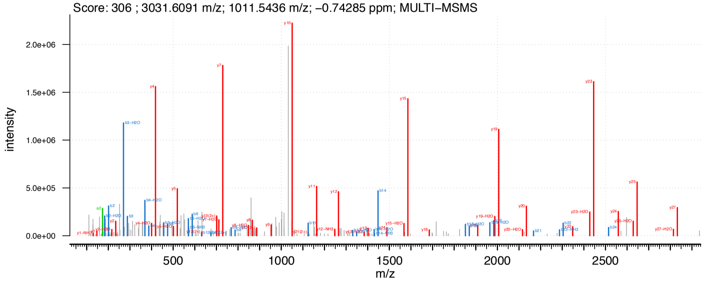

Raw File: Bibo_20111021_FEP_PD20111014_Cdc42_mouseCortex_LF_rep2_GTPgS
Scan Number: 7545
Proteins:
Q9ES28–8;Q9ES28–2;Q9ES28–4;Q9ES28–6;Q9ES28;Q9ES28–7;Q9ES28–5

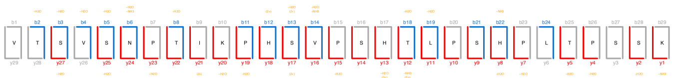

VTSVSNPTIKPHSVPSHTLPSHPLTPSSK
Score: 306 ; 3031.6091 m/z; 1011.5436 m/z; –0.74285 ppm; MULTI–MSMS

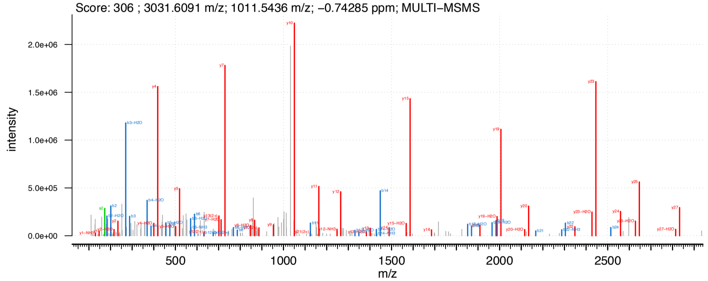

Raw File: Bibo_20111021_FEP_PD20111014_Cdc42_mouseCortex_LF_rep2_GTPgS
Scan Number: 7545
Proteins:
Q9ES28–8;Q9ES28–2;Q9ES28–4;Q9ES28–6;Q9ES28;Q9ES28–7;Q9ES28–5

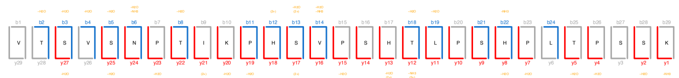

VTSVSNPTIKPHSVPSHTLPSHPLTPSSK
Score: 306 ; 3031.6091 m/z; 1011.5436 m/z; –0.74285 ppm; MULTI–MSMS

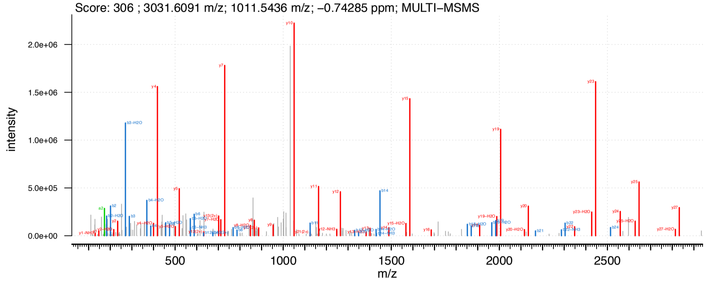

Raw File: Bibo_20111021_FEP_PD20111014_Cdc42_mouseCortex_LF_rep2_GTPgS
Scan Number: 7545
Proteins:
Q9ES28–8;Q9ES28–2;Q9ES28–4;Q9ES28–6;Q9ES28;Q9ES28–7;Q9ES28–5

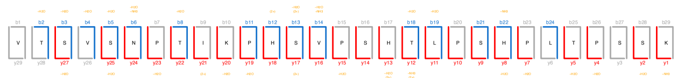

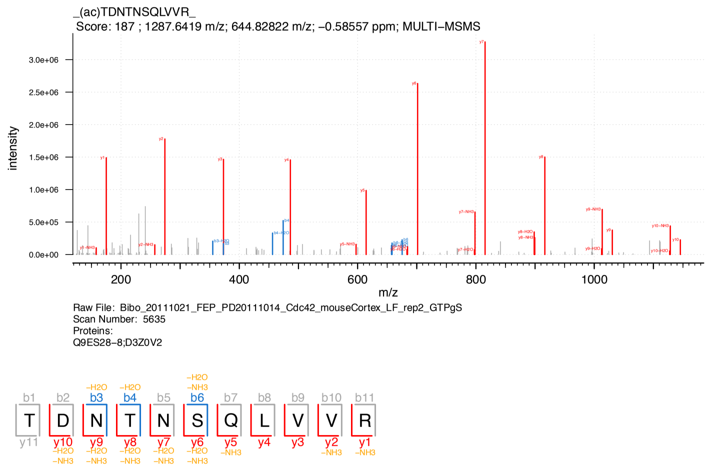
(ac)TDNTNSQLVVR
Score: 187 ; 1287.6419 m/z; 644.82822 m/z; −0.58557 ppm; MULTI−MSMS
intensity
m/z
Raw File: Bibo_20111021_FEP_PD20111014_Cdc42_mouseCortex_LF_rep2_GTPgS
Scan Number: 5635
Proteins:
Q9ES28−8;D3Z0V2

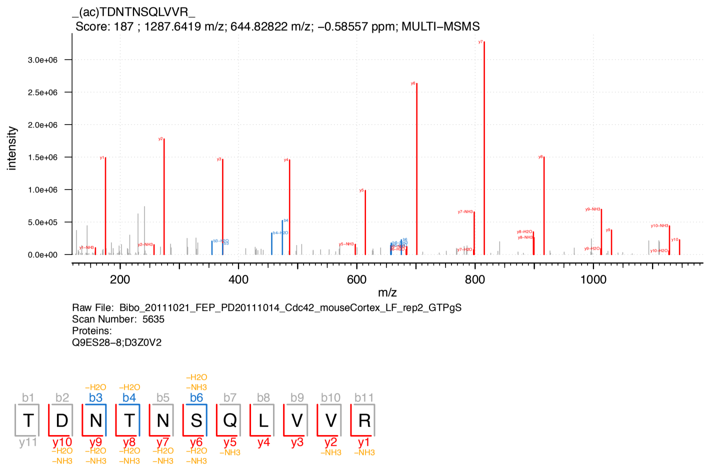
(ac)TDNTNSQLVVR
Score: 187 ; 1287.6419 m/z; 644.82822 m/z; −0.58557 ppm; MULTI−MSMS
intensity
m/z
Raw File: Bibo_20111021_FEP_PD20111014_Cdc42_mouseCortex_LF_rep2_GTPgS
Scan Number: 5635
Proteins:
Q9ES28−8;D3Z0V2

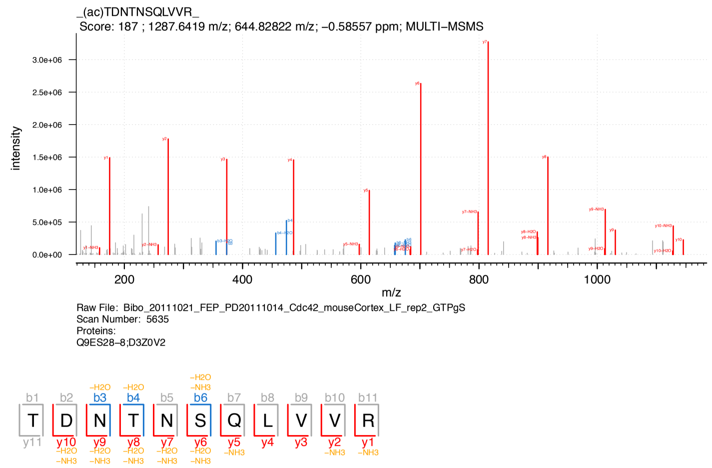
(ac)TDNTNSQLVVR
Score: 187 ; 1287.6419 m/z; 644.82822 m/z; −0.58557 ppm; MULTI−MSMS
intensity
m/z
Raw File: Bibo_20111021_FEP_PD20111014_Cdc42_mouseCortex_LF_rep2_GTPgS
Scan Number: 5635
Proteins:
Q9ES28−8;D3Z0V2

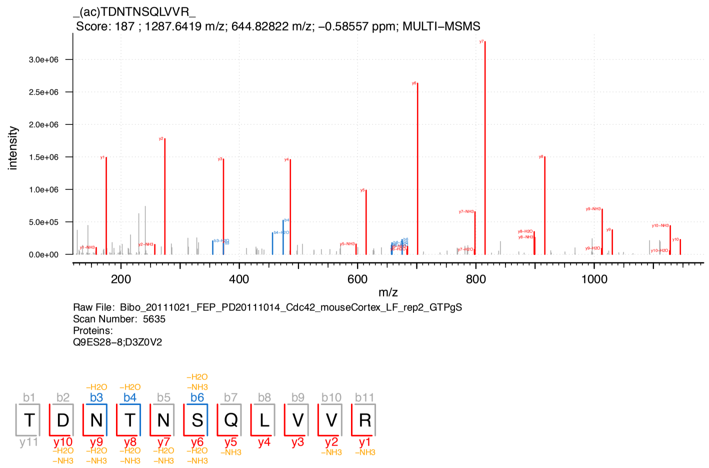
(ac)TDNTNSQLVVR
Score: 187 ; 1287.6419 m/z; 644.82822 m/z; −0.58557 ppm; MULTI−MSMS
intensity
m/z
Raw File: Bibo_20111021_FEP_PD20111014_Cdc42_mouseCortex_LF_rep2_GTPgS
Scan Number: 5635
Proteins:
Q9ES28−8;D3Z0V2

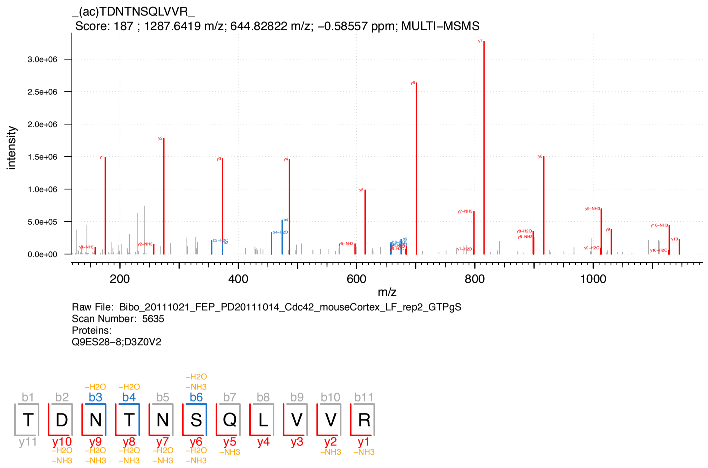
(ac)TDNTNSQLVVR
Score: 187 ; 1287.6419 m/z; 644.82822 m/z; −0.58557 ppm; MULTI−MSMS
intensity
m/z
Raw File: Bibo_20111021_FEP_PD20111014_Cdc42_mouseCortex_LF_rep2_GTPgS
Scan Number: 5635
Proteins:
Q9ES28−8;D3Z0V2

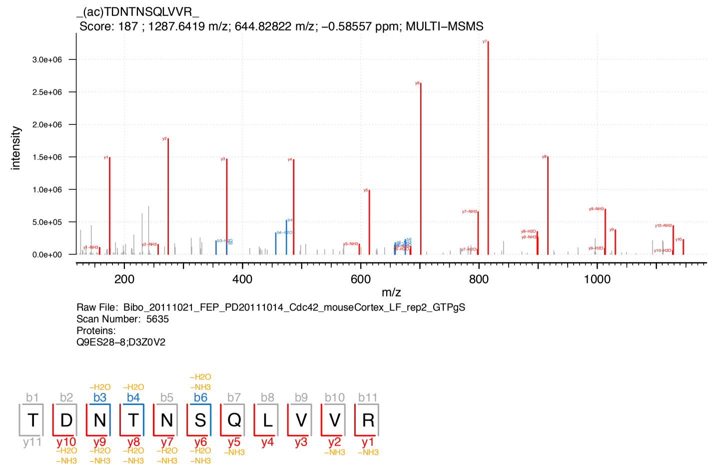
(ac)TDNTNSQLVVR
Score: 187 ; 1287.6419 m/z; 644.82822 m/z; −0.58557 ppm; MULTI−MSMS
intensity
m/z
Raw File: Bibo_20111021_FEP_PD20111014_Cdc42_mouseCortex_LF_rep2_GTPgS
Scan Number: 5635
Proteins:
Q9ES28−8;D3Z0V2

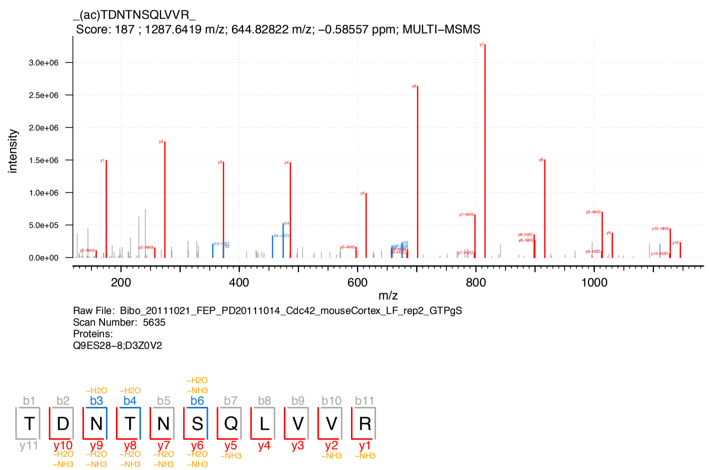
(ac)TDNTNSQLVVR
Score: 187 ; 1287.6419 m/z; 644.82822 m/z; −0.58557 ppm; MULTI−MSMS
intensity
m/z
Raw File: Bibo_20111021_FEP_PD20111014_Cdc42_mouseCortex_LF_rep2_GTPgS
Scan Number: 5635
Proteins:
Q9ES28−8;D3Z0V2

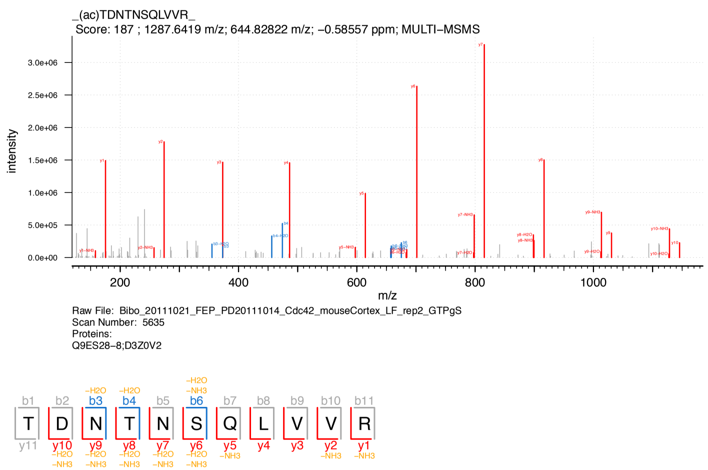
(ac)TDNTNSQLVVR
Score: 187 ; 1287.6419 m/z; 644.82822 m/z; −0.58557 ppm; MULTI−MSMS
intensity
m/z
Raw File: Bibo_20111021_FEP_PD20111014_Cdc42_mouseCortex_LF_rep2_GTPgS
Scan Number: 5635
Proteins:
Q9ES28−8;D3Z0V2

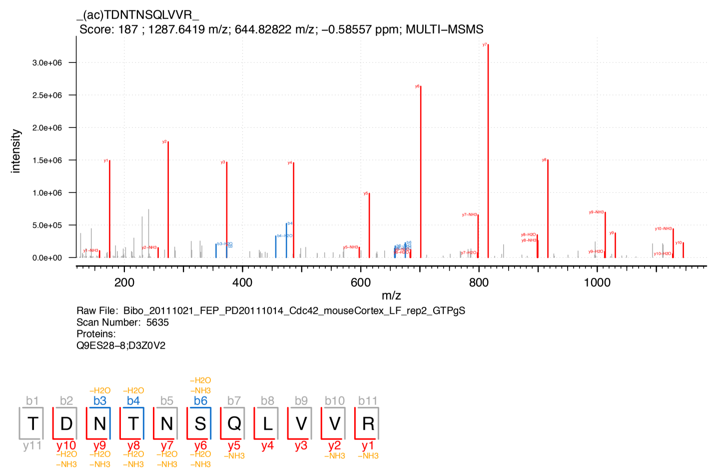
(ac)TDNTNSQLVVR
Score: 187 ; 1287.6419 m/z; 644.82822 m/z; −0.58557 ppm; MULTI−MSMS
intensity
m/z
Raw File: Bibo_20111021_FEP_PD20111014_Cdc42_mouseCortex_LF_rep2_GTPgS
Scan Number: 5635
Proteins:
Q9ES28−8;D3Z0V2

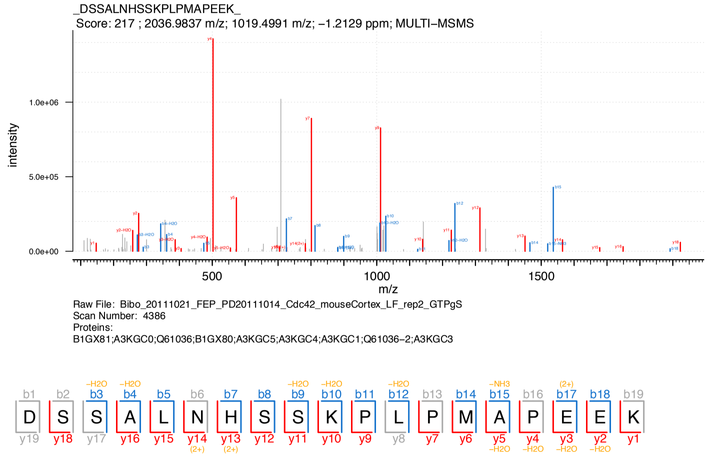
DSSALNHSSKPLPMAPEEK
Score: 217 ; 2036.9837 m/z; 1019.4991 m/z; −1.2129 ppm; MULTI−MSMS
intensity
m/z
Raw File: Bibo_20111021_FEP_PD20111014_Cdc42_mouseCortex_LF_rep2_GTPgS
Scan Number: 4386
Proteins:
B1GX81;A3KGC0;Q61036;B1GX80;A3KGC5;A3KGC4;A3KGC1;Q61036−2;A3KGC3
D S S A L N H S S K P L P M A P E E K

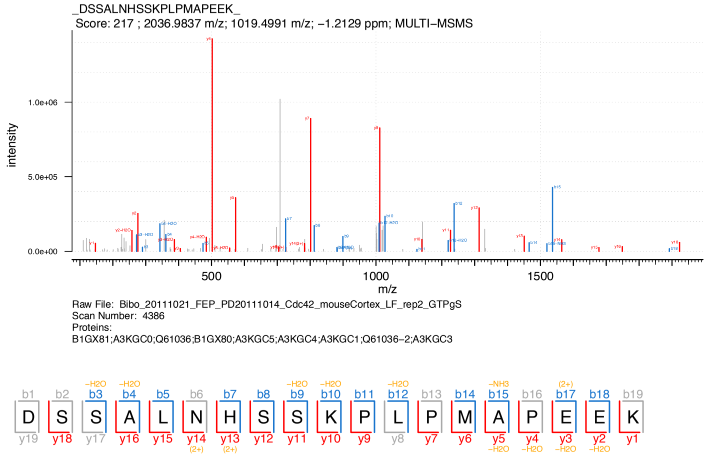
DSSALNHSSKPLPMAPEEK
Score: 217 ; 2036.9837 m/z; 1019.4991 m/z; −1.2129 ppm; MULTI−MSMS
intensity
m/z
Raw File: Bibo_20111021_FEP_PD20111014_Cdc42_mouseCortex_LF_rep2_GTPgS
Scan Number: 4386
Proteins:
B1GX81;A3KGC0;Q61036;B1GX80;A3KGC5;A3KGC4;A3KGC1;Q61036−2;A3KGC3
D S S A L N H S S K P L P M A P E E K

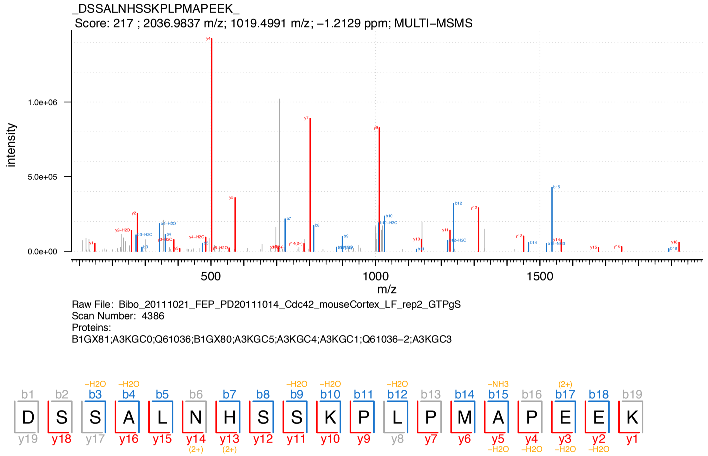
DSSALNHSSKPLPMAPEEK
Score: 217 ; 2036.9837 m/z; 1019.4991 m/z; −1.2129 ppm; MULTI−MSMS
intensity
m/z
Raw File: Bibo_20111021_FEP_PD20111014_Cdc42_mouseCortex_LF_rep2_GTPgS
Scan Number: 4386
Proteins:
B1GX81;A3KGC0;Q61036;B1GX80;A3KGC5;A3KGC4;A3KGC1;Q61036−2;A3KGC3
D S S A L N H S S K P L P M A P E E K

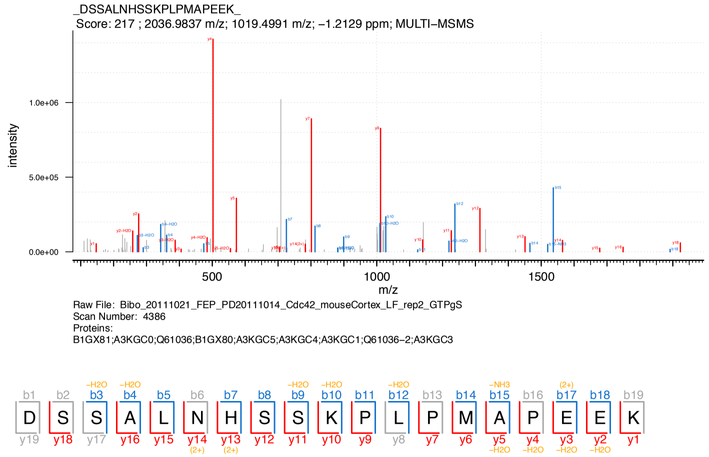
DSSALNHSSKPLPMAPEEK
Score: 217 ; 2036.9837 m/z; 1019.4991 m/z; −1.2129 ppm; MULTI−MSMS
intensity
m/z
Raw File: Bibo_20111021_FEP_PD20111014_Cdc42_mouseCortex_LF_rep2_GTPgS
Scan Number: 4386
Proteins:
B1GX81;A3KGC0;Q61036;B1GX80;A3KGC5;A3KGC4;A3KGC1;Q61036−2;A3KGC3
D S S A L N H S S K P L P M A P E E K

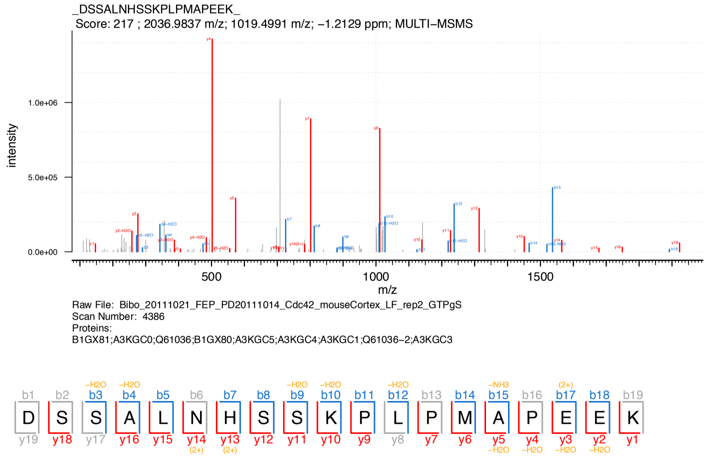
DSSALNHSSKPLPMAPEEK
Score: 217 ; 2036.9837 m/z; 1019.4991 m/z; −1.2129 ppm; MULTI−MSMS
intensity
m/z
Raw File: Bibo_20111021_FEP_PD20111014_Cdc42_mouseCortex_LF_rep2_GTPgS
Scan Number: 4386
Proteins:
B1GX81;A3KGC0;Q61036;B1GX80;A3KGC5;A3KGC4;A3KGC1;Q61036−2;A3KGC3
D S S A L N H S S K P L P M A P E E K

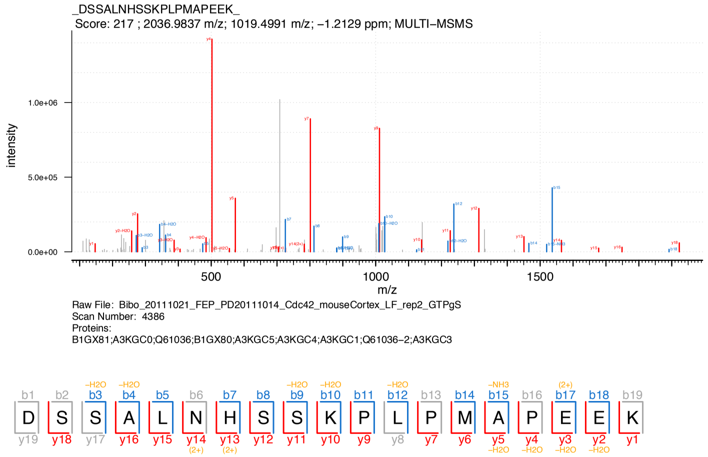
DSSALNHSSKPLPMAPEEK
Score: 217 ; 2036.9837 m/z; 1019.4991 m/z; −1.2129 ppm; MULTI−MSMS
intensity
m/z
Raw File: Bibo_20111021_FEP_PD20111014_Cdc42_mouseCortex_LF_rep2_GTPgS
Scan Number: 4386
Proteins:
B1GX81;A3KGC0;Q61036;B1GX80;A3KGC5;A3KGC4;A3KGC1;Q61036−2;A3KGC3
D S S A L N H S S K P L P M A P E E K

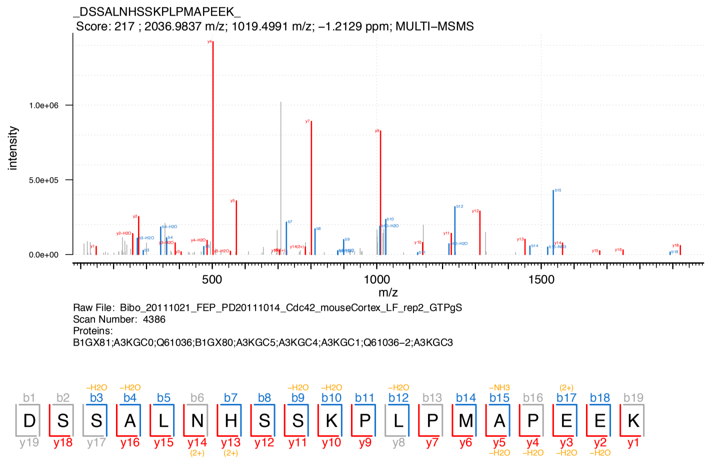
DSSALNHSSKPLPMAPEEK
Score: 217 ; 2036.9837 m/z; 1019.4991 m/z; −1.2129 ppm; MULTI−MSMS
intensity
m/z
Raw File: Bibo_20111021_FEP_PD20111014_Cdc42_mouseCortex_LF_rep2_GTPgS
Scan Number: 4386
Proteins:
B1GX81;A3KGC0;Q61036;B1GX80;A3KGC5;A3KGC4;A3KGC1;Q61036−2;A3KGC3
D S S A L N H S S K P L P M A P E E K

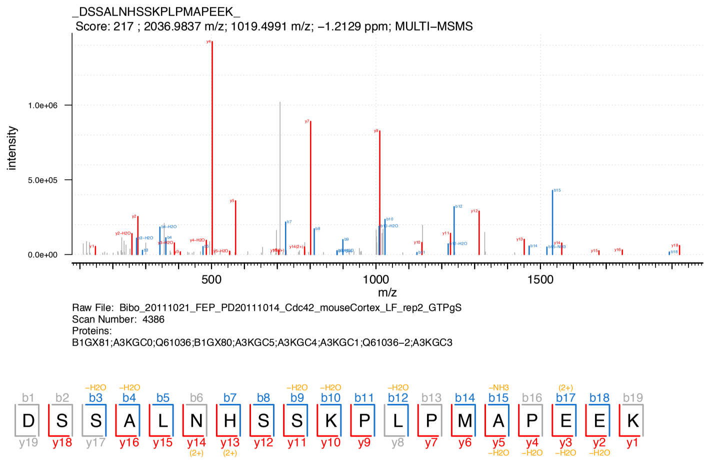
DSSALNHSSKPLPMAPEEK
Score: 217 ; 2036.9837 m/z; 1019.4991 m/z; −1.2129 ppm; MULTI−MSMS
intensity
m/z
Raw File: Bibo_20111021_FEP_PD20111014_Cdc42_mouseCortex_LF_rep2_GTPgS
Scan Number: 4386
Proteins:
B1GX81;A3KGC0;Q61036;B1GX80;A3KGC5;A3KGC4;A3KGC1;Q61036−2;A3KGC3
D S S A L N H S S K P L P M A P E E K

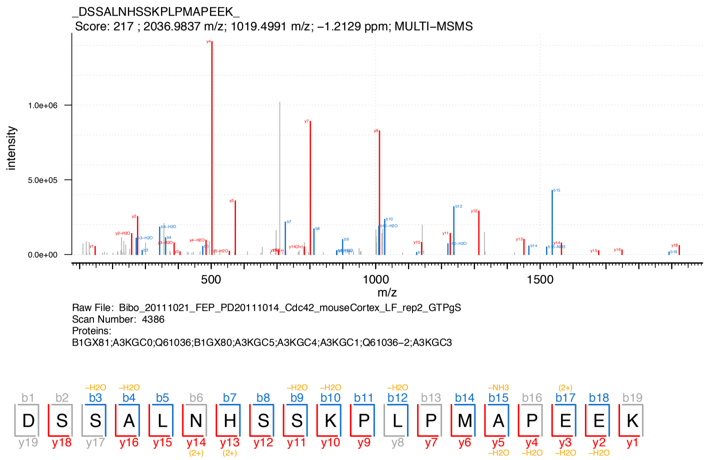
DSSALNHSSKPLPMAPEEK
Score: 217 ; 2036.9837 m/z; 1019.4991 m/z; −1.2129 ppm; MULTI−MSMS
intensity
m/z
Raw File: Bibo_20111021_FEP_PD20111014_Cdc42_mouseCortex_LF_rep2_GTPgS
Scan Number: 4386
Proteins:
B1GX81;A3KGC0;Q61036;B1GX80;A3KGC5;A3KGC4;A3KGC1;Q61036−2;A3KGC3
D S S A L N H S S K P L P M A P E E K

LLQTSNITKLEQK
Score: 214 ; 1514.8668 m/z; 758.44068 m/z; 0.21636 ppm; MULTI–MSMS

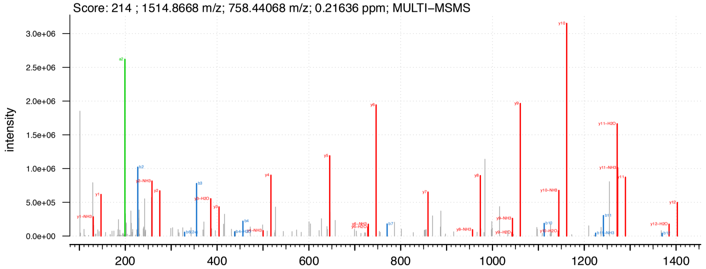

Raw File: Bibo_20111021_FEP_PD20111014_Cdc42_mouseCortex_LF_rep2_GTPgS
Scan Number: 8973
Proteins:
B1GX81;A3KGC0;Q61036;B1GX80;A3KGC5;A3KGC4;A3KGC1;Q61036–2;A3KGC3;Q8CIN4

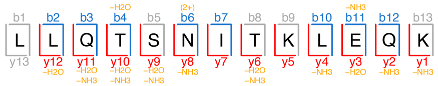

LLQTSNITKLEQK
Score: 214 ; 1514.8668 m/z; 758.44068 m/z; 0.21636 ppm; MULTI–MSMS

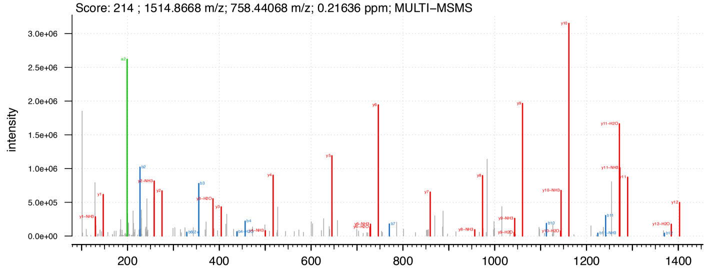

Raw File: Bibo_20111021_FEP_PD20111014_Cdc42_mouseCortex_LF_rep2_GTPgS
Scan Number: 8973
Proteins:
B1GX81;A3KGC0;Q61036;B1GX80;A3KGC5;A3KGC4;A3KGC1;Q61036–2;A3KGC3;Q8CIN4

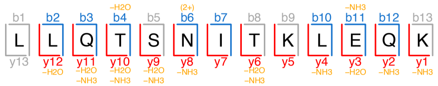

LLQTSNITKLEQK
Score: 214 ; 1514.8668 m/z; 758.44068 m/z; 0.21636 ppm; MULTI–MSMS

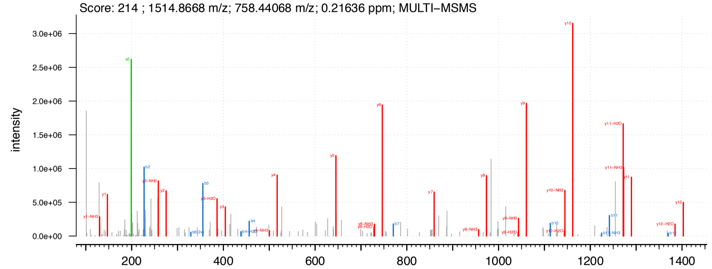

Raw File: Bibo_20111021_FEP_PD20111014_Cdc42_mouseCortex_LF_rep2_GTPgS
Scan Number: 8973
Proteins:
B1GX81;A3KGC0;Q61036;B1GX80;A3KGC5;A3KGC4;A3KGC1;Q61036–2;A3KGC3;Q8CIN4

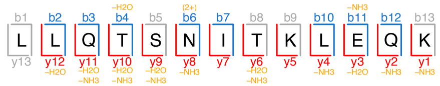

LLQTSNITKLEQK
Score: 214 ; 1514.8668 m/z; 758.44068 m/z; 0.21636 ppm; MULTI–MSMS

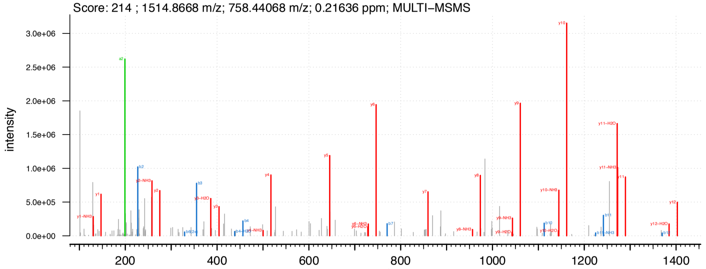

Raw File: Bibo_20111021_FEP_PD20111014_Cdc42_mouseCortex_LF_rep2_GTPgS
Scan Number: 8973
Proteins:
B1GX81;A3KGC0;Q61036;B1GX80;A3KGC5;A3KGC4;A3KGC1;Q61036–2;A3KGC3;Q8CIN4

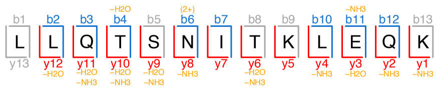

LLQTSNITKLEQK
Score: 214 ; 1514.8668 m/z; 758.44068 m/z; 0.21636 ppm; MULTI–MSMS

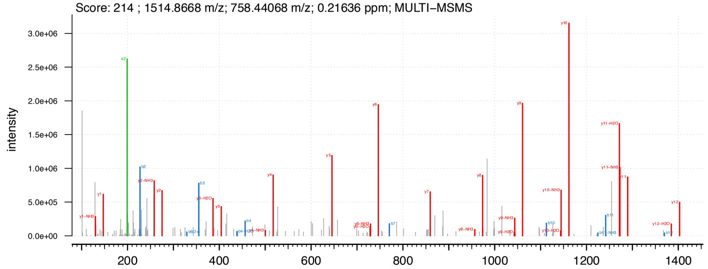

Raw File: Bibo_20111021_FEP_PD20111014_Cdc42_mouseCortex_LF_rep2_GTPgS
Scan Number: 8973
Proteins:
B1GX81;A3KGC0;Q61036;B1GX80;A3KGC5;A3KGC4;A3KGC1;Q61036–2;A3KGC3;Q8CIN4

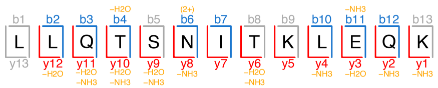

LLQTSNITKLEQK
Score: 214 ; 1514.8668 m/z; 758.44068 m/z; 0.21636 ppm; MULTI–MSMS

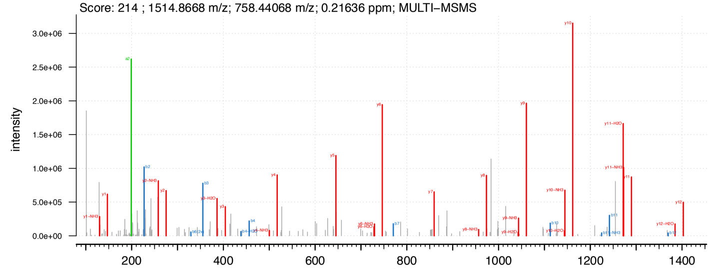

Raw File: Bibo_20111021_FEP_PD20111014_Cdc42_mouseCortex_LF_rep2_GTPgS
Scan Number: 8973
Proteins:
B1GX81;A3KGC0;Q61036;B1GX80;A3KGC5;A3KGC4;A3KGC1;Q61036–2;A3KGC3;Q8CIN4

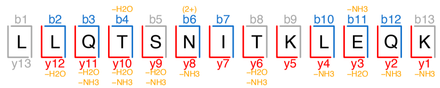

LLQTSNITKLEQK
Score: 214 ; 1514.8668 m/z; 758.44068 m/z; 0.21636 ppm; MULTI–MSMS

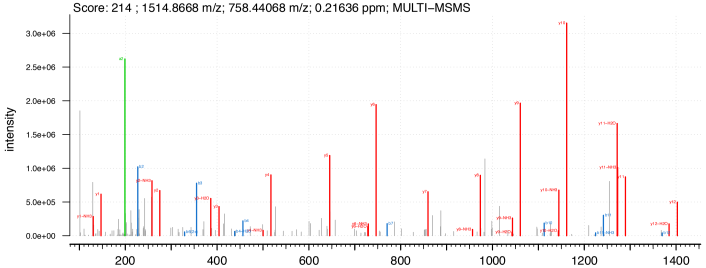

Raw File: Bibo_20111021_FEP_PD20111014_Cdc42_mouseCortex_LF_rep2_GTPgS
Scan Number: 8973
Proteins:
B1GX81;A3KGC0;Q61036;B1GX80;A3KGC5;A3KGC4;A3KGC1;Q61036–2;A3KGC3;Q8CIN4

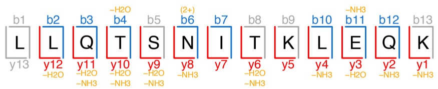

LLQTSNITKLEQK
Score: 214 ; 1514.8668 m/z; 758.44068 m/z; 0.21636 ppm; MULTI–MSMS

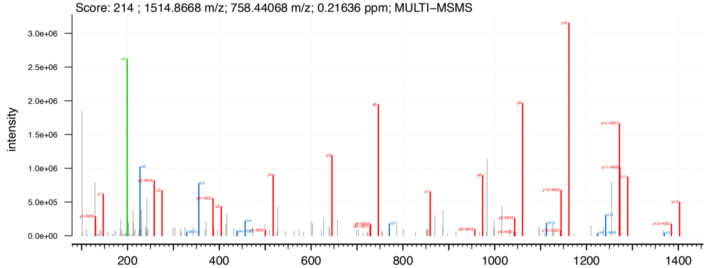

Raw File: Bibo_20111021_FEP_PD20111014_Cdc42_mouseCortex_LF_rep2_GTPgS
Scan Number: 8973
Proteins:
B1GX81;A3KGC0;Q61036;B1GX80;A3KGC5;A3KGC4;A3KGC1;Q61036–2;A3KGC3;Q8CIN4

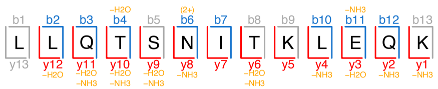

LLQTSNITKLEQK
Score: 214 ; 1514.8668 m/z; 758.44068 m/z; 0.21636 ppm; MULTI–MSMS

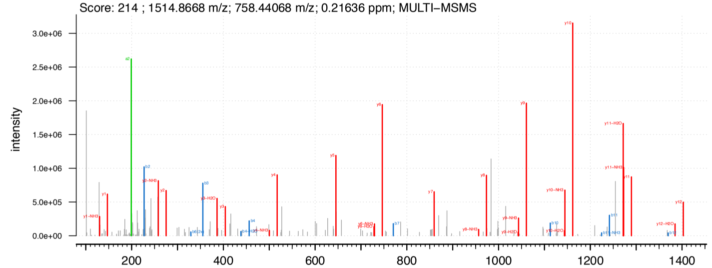

Raw File: Bibo_20111021_FEP_PD20111014_Cdc42_mouseCortex_LF_rep2_GTPgS
Scan Number: 8973
Proteins:
B1GX81;A3KGC0;Q61036;B1GX80;A3KGC5;A3KGC4;A3KGC1;Q61036–2;A3KGC3;Q8CIN4

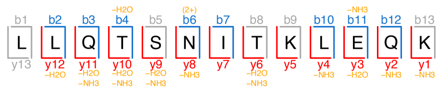

LEPSDLSEDSEYDSIWTAHSYR
Score: 206 ; 2599.1351 m/z; 867.38563 m/z; 0.5048 ppm; MULTI−MSMS

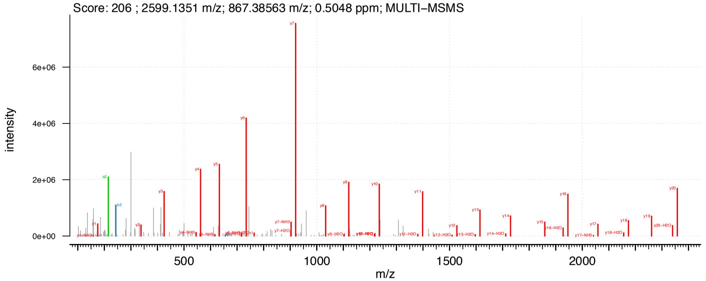

Raw File: Bibo_20111020_FEP_PD20111014_Rac1_mouseCortex_LF_rep3_GTPgS
Scan Number: 30075
Proteins:
Q9ES28−8;D3Z0V2;Q9ES28;Q9ES28−7;Q9ES28−3;Q9ES28−5

LEPSDLSEDSEYDSIWTAHSYR
Score: 206 ; 2599.1351 m/z; 867.38563 m/z; 0.5048 ppm; MULTI−MSMS

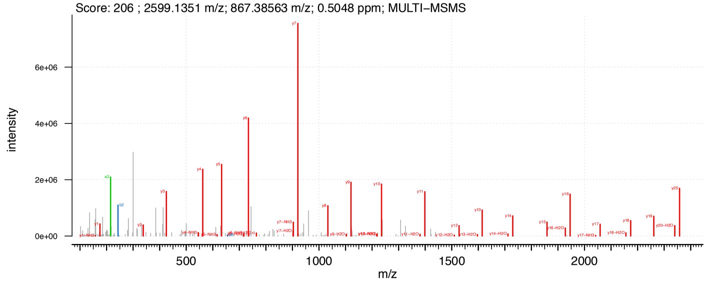

Raw File: Bibo_20111020_FEP_PD20111014_Rac1_mouseCortex_LF_rep3_GTPgS
Scan Number: 30075
Proteins:
Q9ES28−8;D3Z0V2;Q9ES28;Q9ES28−7;Q9ES28−3;Q9ES28−5

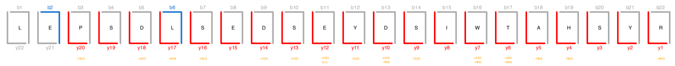

LEPSDLSEDSEYDSIWTAHSYR
Score: 206 ; 2599.1351 m/z; 867.38563 m/z; 0.5048 ppm; MULTI−MSMS

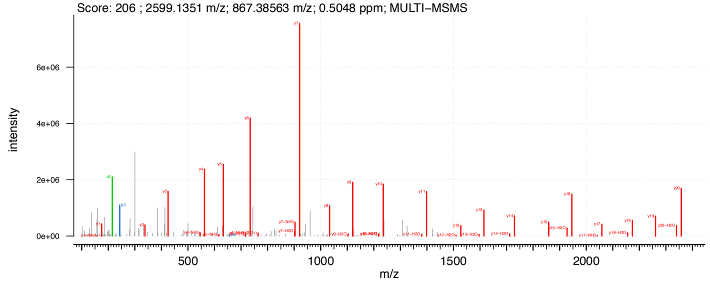

Raw File: Bibo_20111020_FEP_PD20111014_Rac1_mouseCortex_LF_rep3_GTPgS
Scan Number: 30075
Proteins:
Q9ES28−8;D3Z0V2;Q9ES28;Q9ES28−7;Q9ES28−3;Q9ES28−5

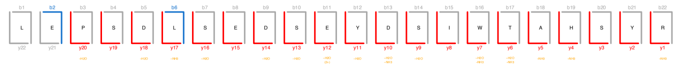

LEPSDLSEDSEYDSIWTAHSYR
Score: 206 ; 2599.1351 m/z; 867.38563 m/z; 0.5048 ppm; MULTI−MSMS

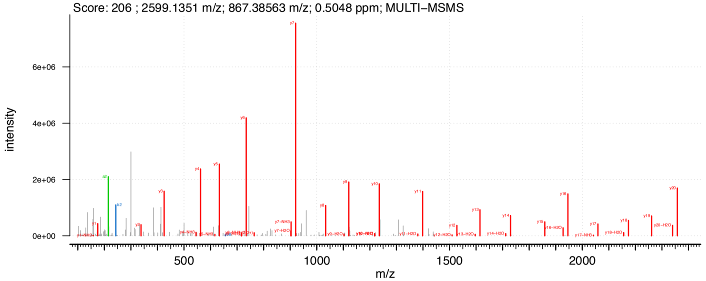

Raw File: Bibo_20111020_FEP_PD20111014_Rac1_mouseCortex_LF_rep3_GTPgS
Scan Number: 30075
Proteins:
Q9ES28−8;D3Z0V2;Q9ES28;Q9ES28−7;Q9ES28−3;Q9ES28−5

LEPSDLSEDSEYDSIWTAHSYR
Score: 206 ; 2599.1351 m/z; 867.38563 m/z; 0.5048 ppm; MULTI−MSMS

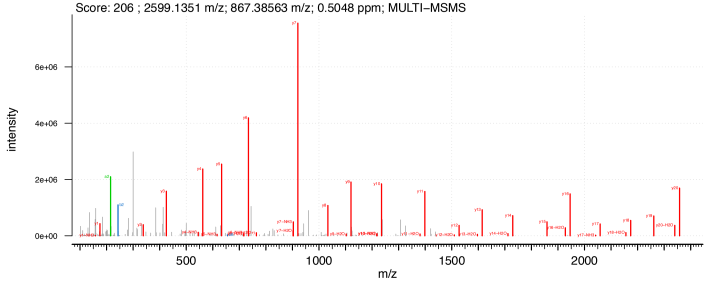

Raw File: Bibo_20111020_FEP_PD20111014_Rac1_mouseCortex_LF_rep3_GTPgS
Scan Number: 30075
Proteins:
Q9ES28−8;D3Z0V2;Q9ES28;Q9ES28−7;Q9ES28−3;Q9ES28−5

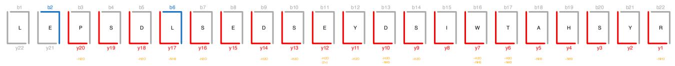

LEPSDLSEDSEYDSIWTAHSYR
Score: 206 ; 2599.1351 m/z; 867.38563 m/z; 0.5048 ppm; MULTI−MSMS

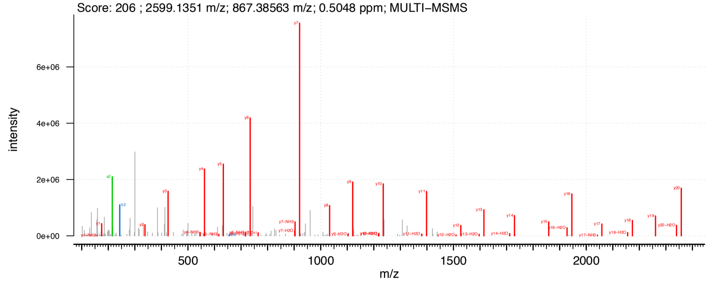

Raw File: Bibo_20111020_FEP_PD20111014_Rac1_mouseCortex_LF_rep3_GTPgS
Scan Number: 30075
Proteins:
Q9ES28−8;D3Z0V2;Q9ES28;Q9ES28−7;Q9ES28−3;Q9ES28−5

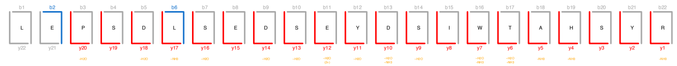

LEPSDLSEDSEYDSIWTAHSYR
Score: 206 ; 2599.1351 m/z; 867.38563 m/z; 0.5048 ppm; MULTI−MSMS

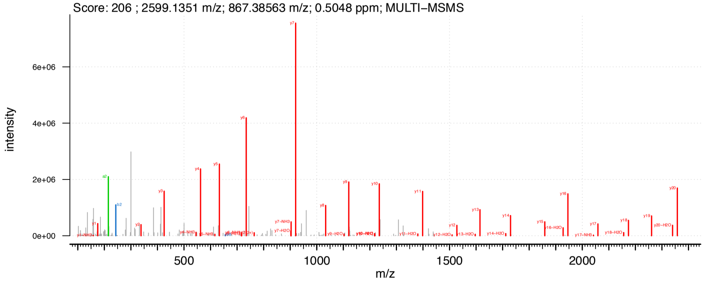

Raw File: Bibo_20111020_FEP_PD20111014_Rac1_mouseCortex_LF_rep3_GTPgS
Scan Number: 30075
Proteins:
Q9ES28−8;D3Z0V2;Q9ES28;Q9ES28−7;Q9ES28−3;Q9ES28−5

LEPSDLSEDSEYDSIWTAHSYR
Score: 206 ; 2599.1351 m/z; 867.38563 m/z; 0.5048 ppm; MULTI−MSMS

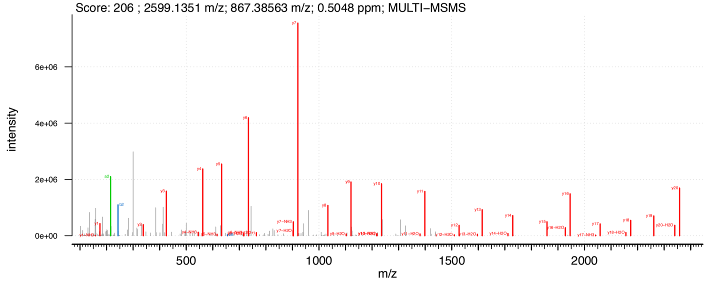

Raw File: Bibo_20111020_FEP_PD20111014_Rac1_mouseCortex_LF_rep3_GTPgS
Scan Number: 30075
Proteins:
Q9ES28−8;D3Z0V2;Q9ES28;Q9ES28−7;Q9ES28−3;Q9ES28−5

LEPSDLSEDSEYDSIWTAHSYR
Score: 206 ; 2599.1351 m/z; 867.38563 m/z; 0.5048 ppm; MULTI−MSMS

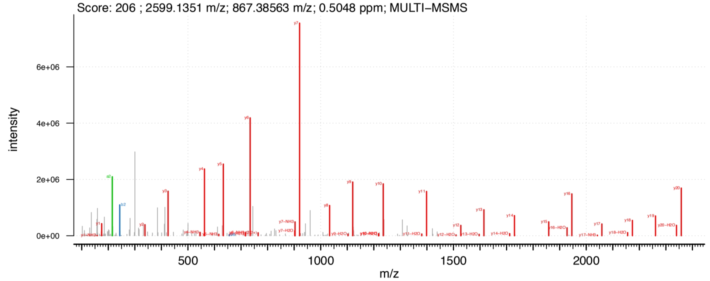

Raw File: Bibo_20111020_FEP_PD20111014_Rac1_mouseCortex_LF_rep3_GTPgS
Scan Number: 30075
Proteins:
Q9ES28−8;D3Z0V2;Q9ES28;Q9ES28−7;Q9ES28−3;Q9ES28−5

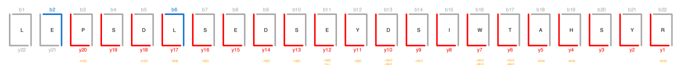

(ac)MNSAEQTVTWLITLGVLESPKK
Score: 129 ; 2486.3091 m/z; 1244.1618 m/z; 0.1843 ppm; MULTI−MSMS

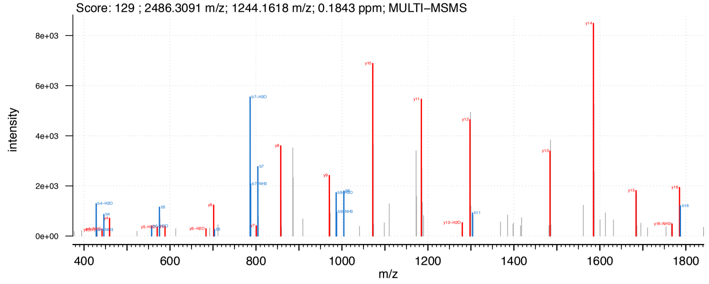

Raw File: Tiffy_20110805_FEP_259_PD20110720_Rac1_mouseCerebellum_LF_rep2_GTPgS
Scan Number: 34524
Proteins:
Q9ES28−2;Q9ES28;Q9ES28−3;Q9ES28−5

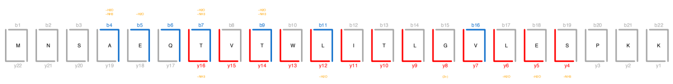

(ac)MNSAEQTVTWLITLGVLESPKK
Score: 129 ; 2486.3091 m/z; 1244.1618 m/z; 0.1843 ppm; MULTI−MSMS

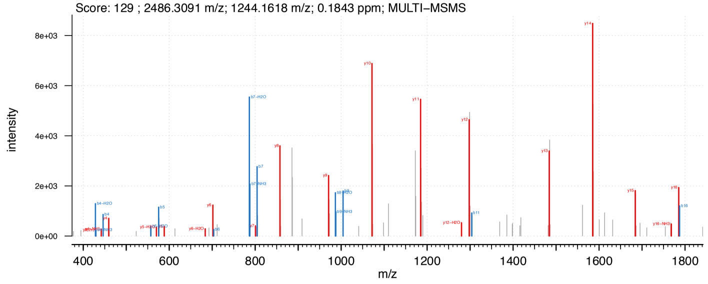

Raw File: Tiffy_20110805_FEP_259_PD20110720_Rac1_mouseCerebellum_LF_rep2_GTPgS
Scan Number: 34524
Proteins:
Q9ES28−2;Q9ES28;Q9ES28−3;Q9ES28−5

(ac)MNSAEQTVTWLITLGVLESPKK
Score: 129 ; 2486.3091 m/z; 1244.1618 m/z; 0.1843 ppm; MULTI−MSMS

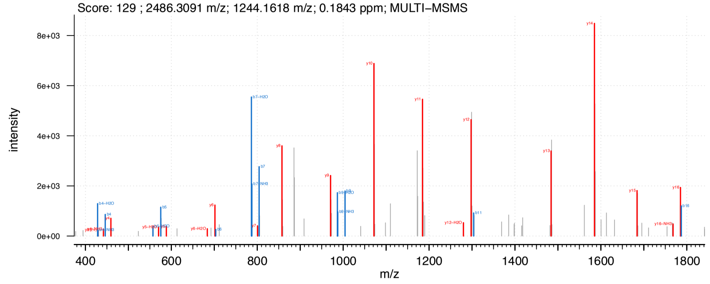

Raw File: Tiffy_20110805_FEP_259_PD20110720_Rac1_mouseCerebellum_LF_rep2_GTPgS
Scan Number: 34524
Proteins:
Q9ES28−2;Q9ES28;Q9ES28−3;Q9ES28−5

(ac)MNSAEQTVTWLITLGVLESPKK
Score: 129 ; 2486.3091 m/z; 1244.1618 m/z; 0.1843 ppm; MULTI−MSMS

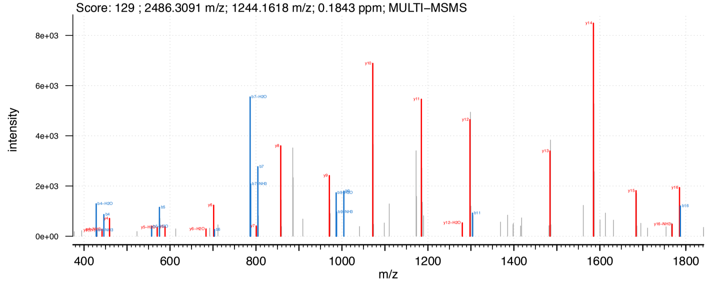

Raw File: Tiffy_20110805_FEP_259_PD20110720_Rac1_mouseCerebellum_LF_rep2_GTPgS
Scan Number: 34524
Proteins:
Q9ES28−2;Q9ES28;Q9ES28−3;Q9ES28−5

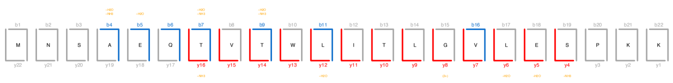

(ac)MNSAEQTVTWLITLGVLESPKK
Score: 129 ; 2486.3091 m/z; 1244.1618 m/z; 0.1843 ppm; MULTI−MSMS

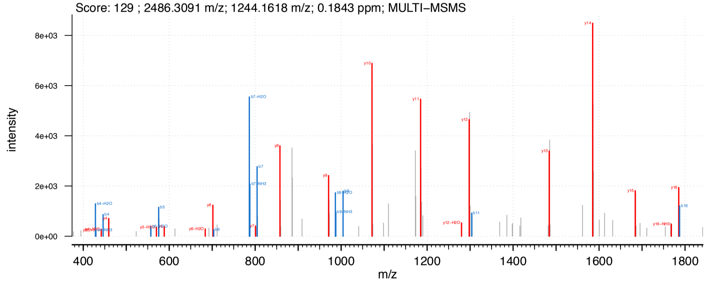

Raw File: Tiffy_20110805_FEP_259_PD20110720_Rac1_mouseCerebellum_LF_rep2_GTPgS
Scan Number: 34524
Proteins:
Q9ES28−2;Q9ES28;Q9ES28−3;Q9ES28−5

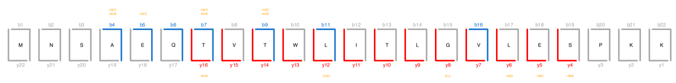

(ac)MNSAEQTVTWLITLGVLESPKK
Score: 129 ; 2486.3091 m/z; 1244.1618 m/z; 0.1843 ppm; MULTI−MSMS

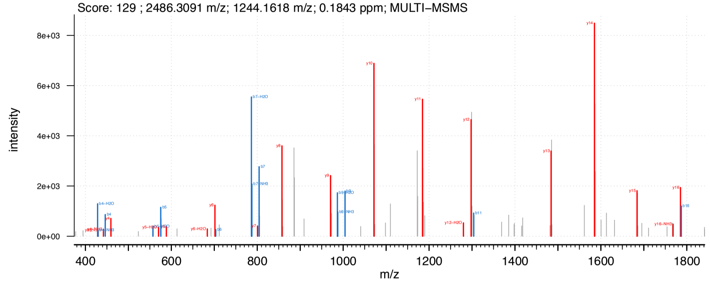

Raw File: Tiffy_20110805_FEP_259_PD20110720_Rac1_mouseCerebellum_LF_rep2_GTPgS
Scan Number: 34524
Proteins:
Q9ES28−2;Q9ES28;Q9ES28−3;Q9ES28−5

(ac)MNSAEQTVTWLITLGVLESPKK
Score: 129 ; 2486.3091 m/z; 1244.1618 m/z; 0.1843 ppm; MULTI−MSMS

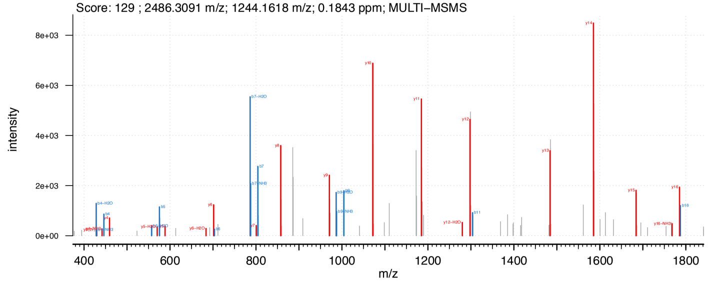

Raw File: Tiffy_20110805_FEP_259_PD20110720_Rac1_mouseCerebellum_LF_rep2_GTPgS
Scan Number: 34524
Proteins:
Q9ES28−2;Q9ES28;Q9ES28−3;Q9ES28−5

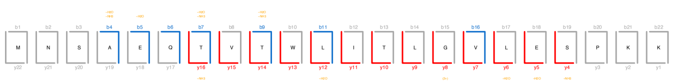

(ac)MNSAEQTVTWLITLGVLESPKK
Score: 129 ; 2486.3091 m/z; 1244.1618 m/z; 0.1843 ppm; MULTI−MSMS

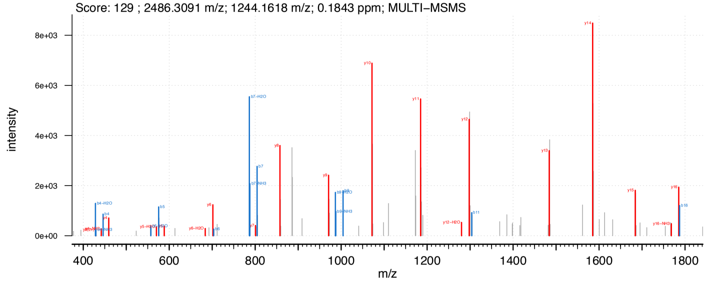

Raw File: Tiffy_20110805_FEP_259_PD20110720_Rac1_mouseCerebellum_LF_rep2_GTPgS
Scan Number: 34524
Proteins:
Q9ES28−2;Q9ES28;Q9ES28−3;Q9ES28−5

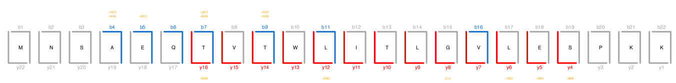

(ac)MNSAEQTVTWLITLGVLESPKK
Score: 129 ; 2486.3091 m/z; 1244.1618 m/z; 0.1843 ppm; MULTI−MSMS

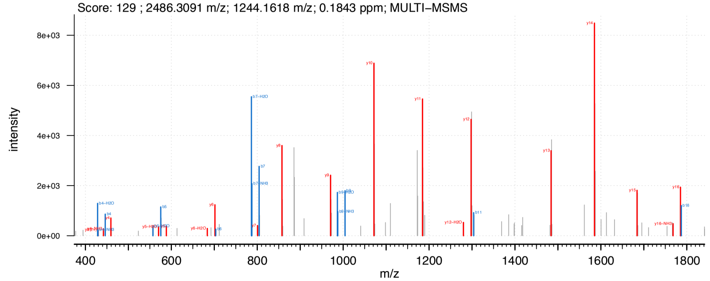

Raw File: Tiffy_20110805_FEP_259_PD20110720_Rac1_mouseCerebellum_LF_rep2_GTPgS
Scan Number: 34524
Proteins:
Q9ES28−2;Q9ES28;Q9ES28−3;Q9ES28−5

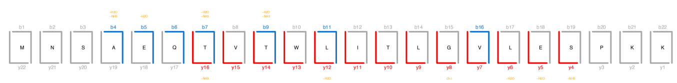

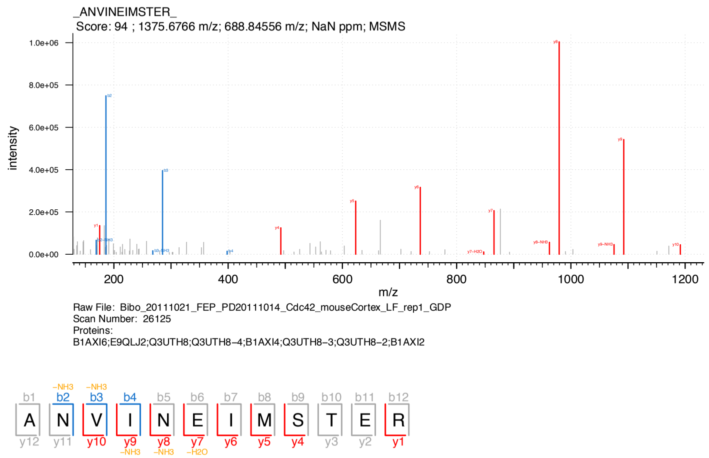
ANVINEIMSTER
Score: 94 ; 1375.6766 m/z; 688.84556 m/z; NaN ppm; MSMS
intensity
m/z
Raw File: Bibo_20111021_FEP_PD20111014_Cdc42_mouseCortex_LF_rep1_GDP
Scan Number: 26125
Proteins:
B1AXI6;E9QLJ2;Q3UTH8;Q3UTH8-4;B1AXI4;Q3UTH8-3;Q3UTH8-2;B1AXI2
A N V I N E I M S T E R

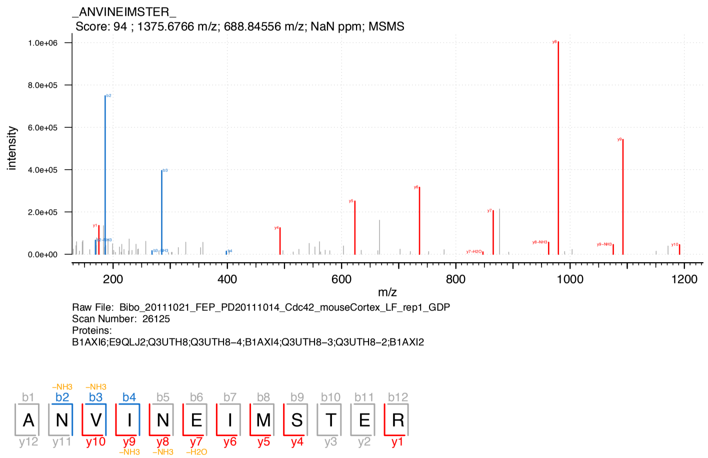
ANVINEIMSTER
Score: 94 ; 1375.6766 m/z; 688.84556 m/z; NaN ppm; MSMS
intensity
m/z
Raw File: Bibo_20111021_FEP_PD20111014_Cdc42_mouseCortex_LF_rep1_GDP
Scan Number: 26125
Proteins:
B1AXI6;E9QLJ2;Q3UTH8;Q3UTH8-4;B1AXI4;Q3UTH8-3;Q3UTH8-2;B1AXI2
A N V I N E I M S T E R

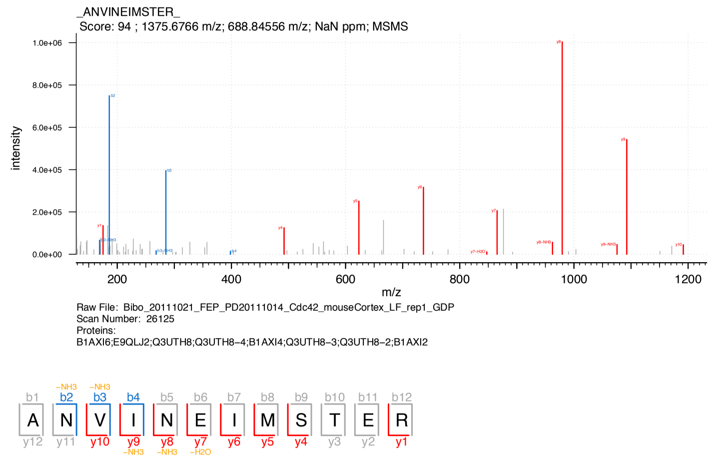
ANVINEIMSTER
Score: 94 ; 1375.6766 m/z; 688.84556 m/z; NaN ppm; MSMS
intensity
m/z
Raw File: Bibo_20111021_FEP_PD20111014_Cdc42_mouseCortex_LF_rep1_GDP
Scan Number: 26125
Proteins:
B1AXI6;E9QLJ2;Q3UTH8;Q3UTH8-4;B1AXI4;Q3UTH8-3;Q3UTH8-2;B1AXI2
A N V I N E I M S T E R

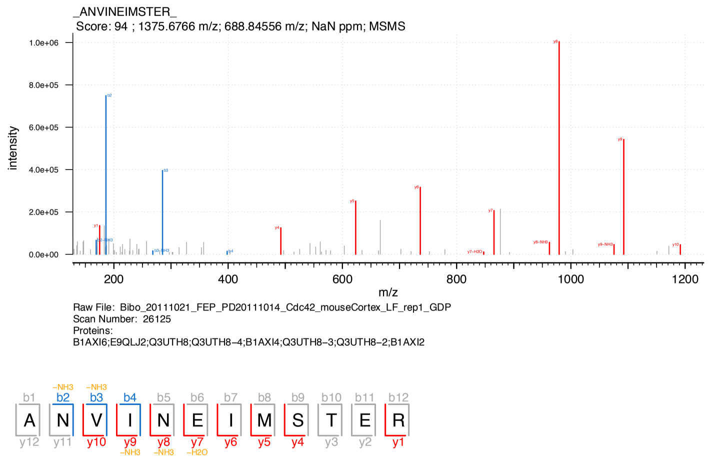
ANVINEIMSTER
Score: 94 ; 1375.6766 m/z; 688.84556 m/z; NaN ppm; MSMS
intensity
m/z
Raw File: Bibo_20111021_FEP_PD20111014_Cdc42_mouseCortex_LF_rep1_GDP
Scan Number: 26125
Proteins:
B1AXI6;E9QLJ2;Q3UTH8;Q3UTH8-4;B1AXI4;Q3UTH8-3;Q3UTH8-2;B1AXI2
A N V I N E I M S T E R

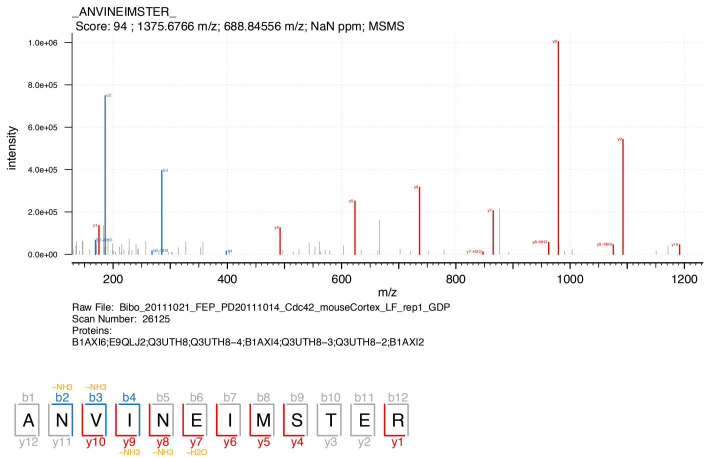
ANVINEIMSTER
Score: 94 ; 1375.6766 m/z; 688.84556 m/z; NaN ppm; MSMS
intensity
m/z
Raw File: Bibo_20111021_FEP_PD20111014_Cdc42_mouseCortex_LF_rep1_GDP
Scan Number: 26125
Proteins:
B1AXI6;E9QLJ2;Q3UTH8;Q3UTH8-4;B1AXI4;Q3UTH8-3;Q3UTH8-2;B1AXI2
A N V I N E I M S T E R

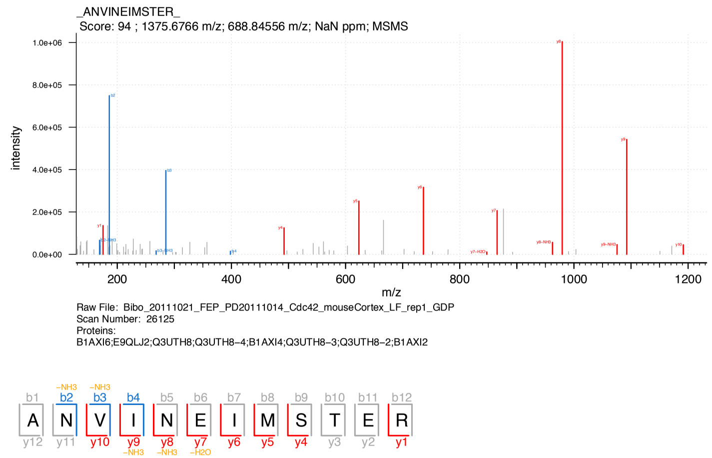
ANVINEIMSTER
Score: 94 ; 1375.6766 m/z; 688.84556 m/z; NaN ppm; MSMS
intensity
m/z
Raw File: Bibo_20111021_FEP_PD20111014_Cdc42_mouseCortex_LF_rep1_GDP
Scan Number: 26125
Proteins:
B1AXI6;E9QLJ2;Q3UTH8;Q3UTH8;Q3UTH8-4;B1AXI4;Q3UTH8-3;Q3UTH8-2;B1AXI2
A N V I N E I M S T E R

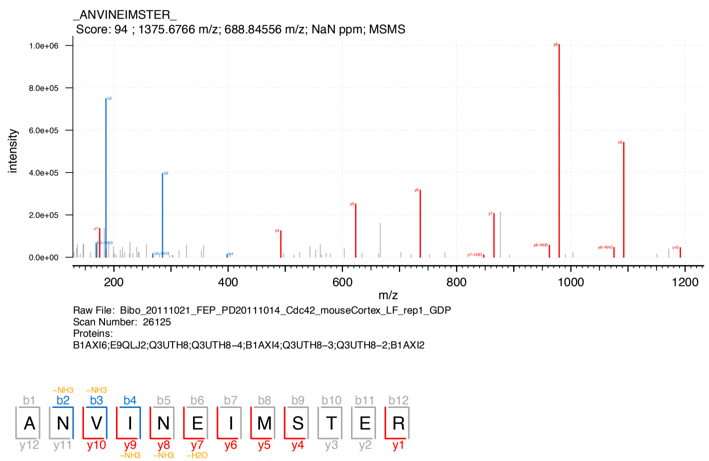
ANVINEIMSTER
Score: 94 ; 1375.6766 m/z; 688.84556 m/z; NaN ppm; MSMS
intensity
m/z
Raw File: Bibo_20111021_FEP_PD20111014_Cdc42_mouseCortex_LF_rep1_GDP
Scan Number: 26125
Proteins:
B1AXI6;E9QLJ2;Q3UTH8;Q3UTH8-4;B1AXI4;Q3UTH8-3;Q3UTH8-2;B1AXI2
A N V I N E I M S T E R

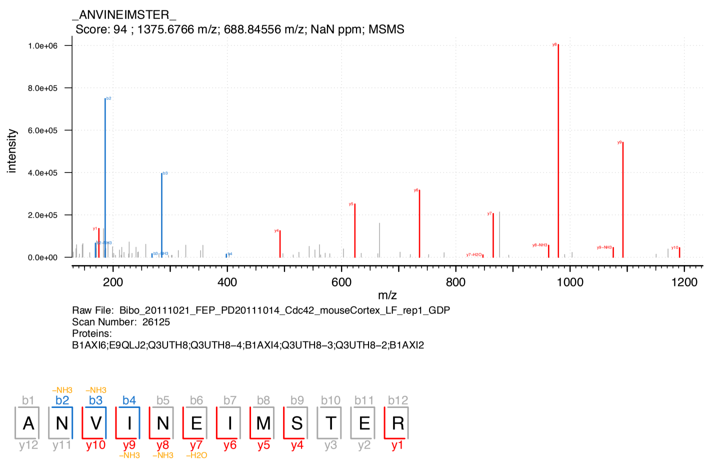
ANVINEIMSTER
Score: 94 ; 1375.6766 m/z; 688.84556 m/z; NaN ppm; MSMS
intensity
m/z
Raw File: Bibo_20111021_FEP_PD20111014_Cdc42_mouseCortex_LF_rep1_GDP
Scan Number: 26125
Proteins:
B1AXI6;E9QLJ2;Q3UTH8;Q3UTH8-4;B1AXI4;Q3UTH8-3;Q3UTH8-2;B1AXI2
A N V I N E I M S T E R

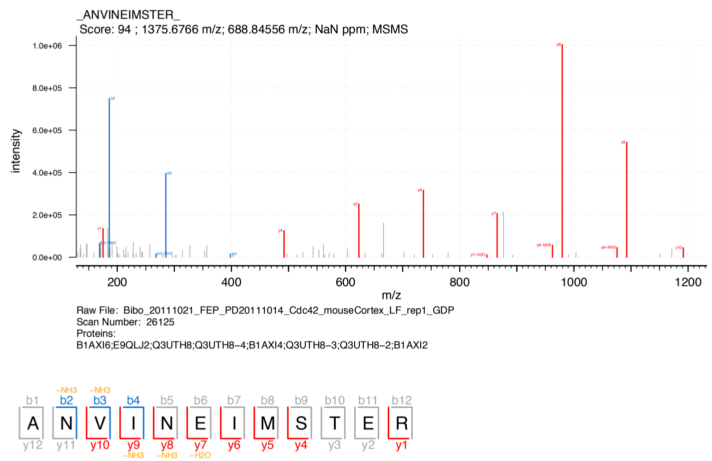
ANVINEIMSTER
Score: 94 ; 1375.6766 m/z; 688.84556 m/z; NaN ppm; MSMS
intensity
m/z
Raw File: Bibo_20111021_FEP_PD20111014_Cdc42_mouseCortex_LF_rep1_GDP
Scan Number: 26125
Proteins:
B1AXI6;E9QLJ2;Q3UTH8;Q3UTH8-4;B1AXI4;Q3UTH8-3;Q3UTH8-2;B1AXI2
A N V I N E I M S T E R

MATDPENIIK
Score: 152 ; 1130.5642 m/z; 566.28936 m/z; 0.21493 ppm; MULTI−MSMS

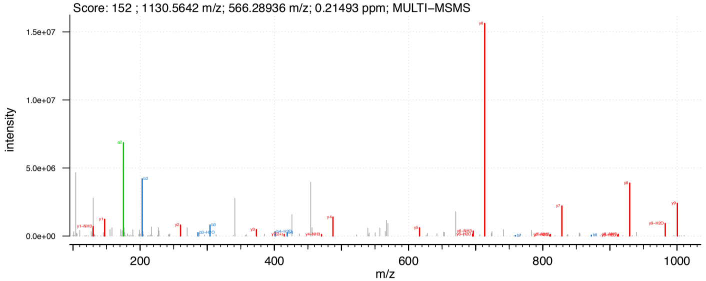

Raw File: Bibo_20111021_FEP_PD20111014_Cdc42_mouseCortex_LF_rep1_GDP
Scan Number: 9201
Proteins:
B1AVA7;Q62277;F8WGK2

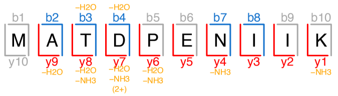

MATDPENIIK
Score: 152 ; 1130.5642 m/z; 566.28936 m/z; 0.21493 ppm; MULTI−MSMS

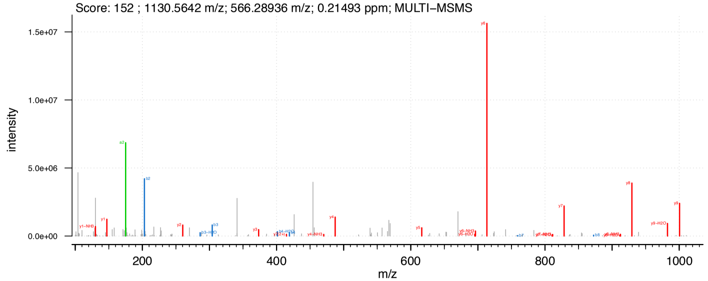

Raw File: Bibo_20111021_FEP_PD20111014_Cdc42_mouseCortex_LF_rep1_GDP
Scan Number: 9201
Proteins:
B1AVA7;Q62277;F8WGK2

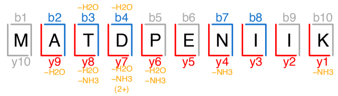

MATDPENIIK
Score: 152 ; 1130.5642 m/z; 566.28936 m/z; 0.21493 ppm; MULTI−MSMS

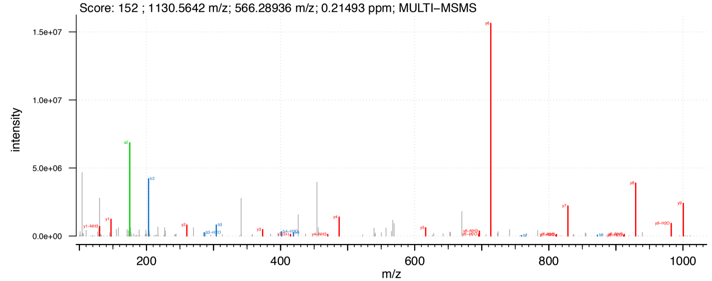

Raw File: Bibo_20111021_FEP_PD20111014_Cdc42_mouseCortex_LF_rep1_GDP
Scan Number: 9201
Proteins:
B1AVA7;Q62277;F8WGK2

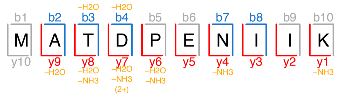

MATDPENIIK
Score: 152 ; 1130.5642 m/z; 566.28936 m/z; 0.21493 ppm; MULTI−MSMS

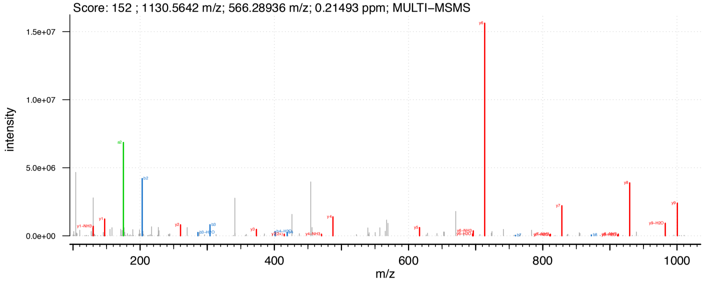

Raw File: Bibo_20111021_FEP_PD20111014_Cdc42_mouseCortex_LF_rep1_GDP
Scan Number: 9201
Proteins:
B1AVA7;Q62277;F8WGK2

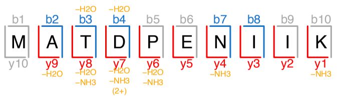

MATDPENIIK
Score: 152 ; 1130.5642 m/z; 566.28936 m/z; 0.21493 ppm; MULTI−MSMS

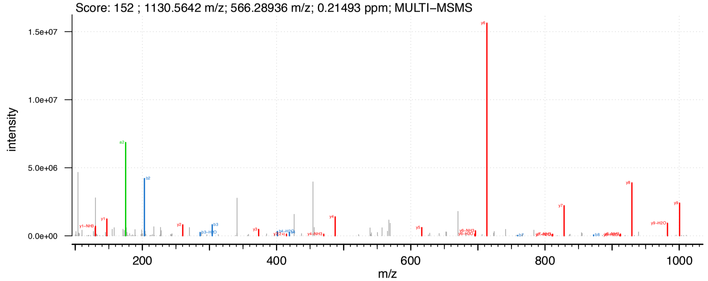

Raw File: Bibo_20111021_FEP_PD20111014_Cdc42_mouseCortex_LF_rep1_GDP
Scan Number: 9201
Proteins:
B1AVA7;Q62277;F8WGK2

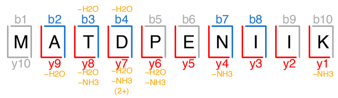

MATDPENIIK
Score: 152 ; 1130.5642 m/z; 566.28936 m/z; 0.21493 ppm; MULTI−MSMS

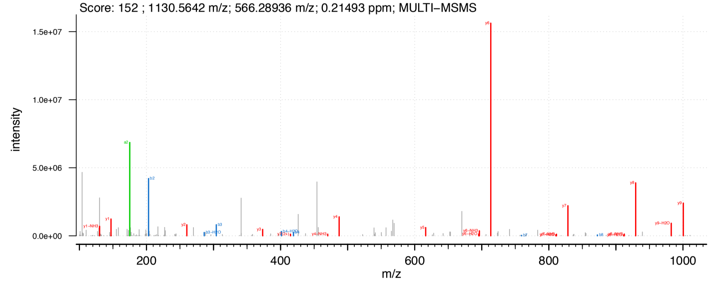

Raw File: Bibo_20111021_FEP_PD20111014_Cdc42_mouseCortex_LF_rep1_GDP
Scan Number: 9201
Proteins:
B1AVA7;Q62277;F8WGK2

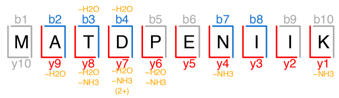

MATDPENIIK
Score: 152 ; 1130.5642 m/z; 566.28936 m/z; 0.21493 ppm; MULTI−MSMS

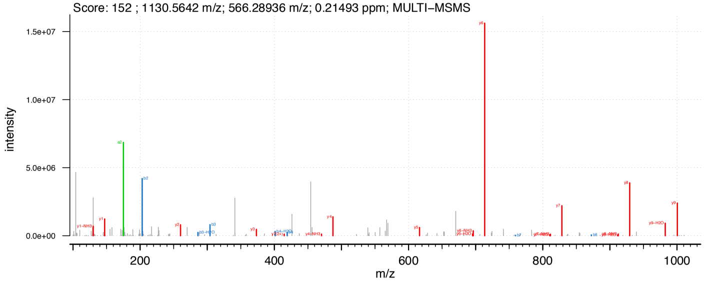

Raw File: Bibo_20111021_FEP_PD20111014_Cdc42_mouseCortex_LF_rep1_GDP
Scan Number: 9201
Proteins:
B1AVA7;Q62277;F8WGK2

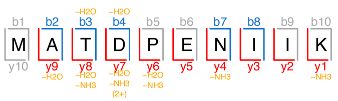

MATDPENIIK
Score: 152 ; 1130.5642 m/z; 566.28936 m/z; 0.21493 ppm; MULTI−MSMS

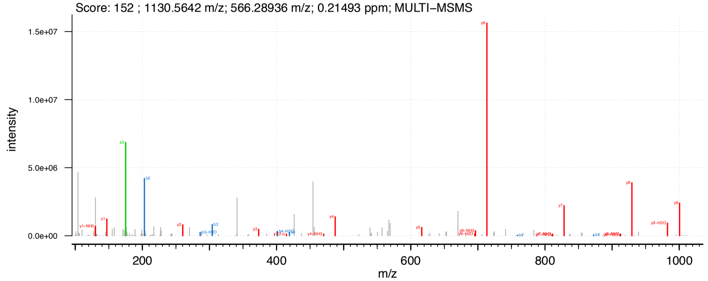

Raw File: Bibo_20111021_FEP_PD20111014_Cdc42_mouseCortex_LF_rep1_GDP
Scan Number: 9201
Proteins:
B1AVA7;Q62277;F8WGK2

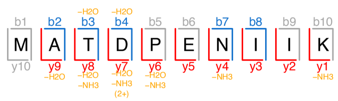

MATDPENIIK
Score: 152 ; 1130.5642 m/z; 566.28936 m/z; 0.21493 ppm; MULTI−MSMS

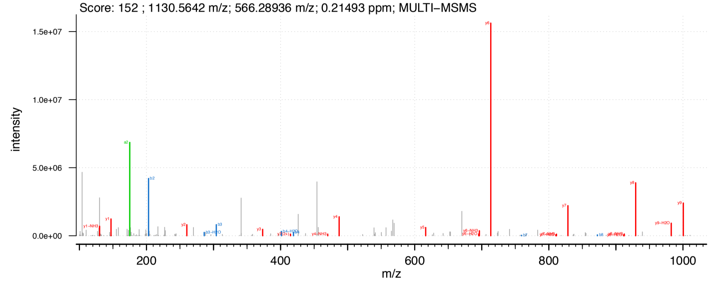

Raw File: Bibo_20111021_FEP_PD20111014_Cdc42_mouseCortex_LF_rep1_GDP
Scan Number: 9201
Proteins:
B1AVA7;Q62277;F8WGK2

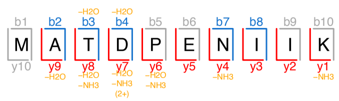

HSSDINHLVTQGR
Score: 270 ; 1462.7277 m/z; 732.37112 m/z; −0.54983 ppm; MULTI−MSMS

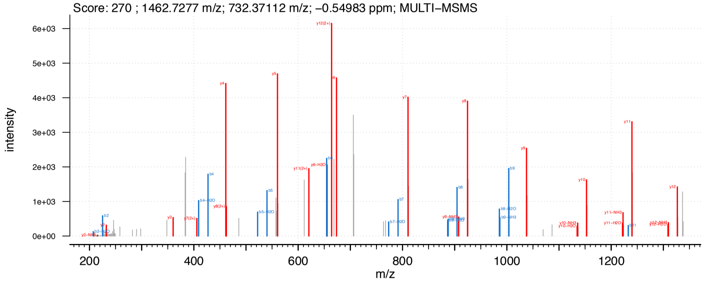

Raw File: Tiffy_20110729_FEP_267_PD20110720_Cdc42_mouseCerebellum_LF_rep3_GTPgS
Scan Number: 4490
Proteins:
E9PUK3

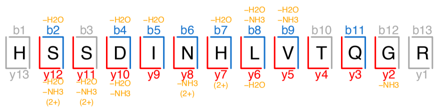

HSSDINHLVTQGR
Score: 270 ; 1462.7277 m/z; 732.37112 m/z; −0.54983 ppm; MULTI−MSMS

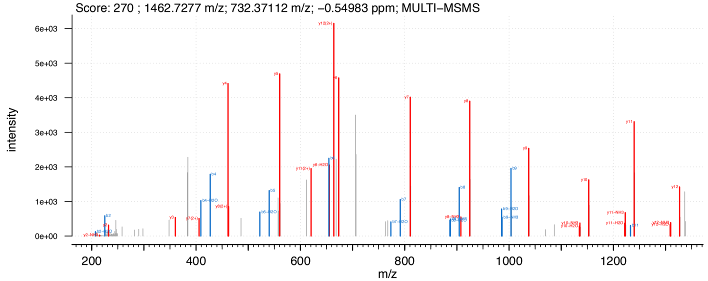

Raw File: Tiffy_20110729_FEP_267_PD20110720_Cdc42_mouseCerebellum_LF_rep3_GTPgS
Scan Number: 4490
Proteins:
E9PUK3

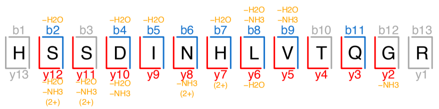

HSSDINHLVTQGR
Score: 270 ; 1462.7277 m/z; 732.37112 m/z; −0.54983 ppm; MULTI−MSMS

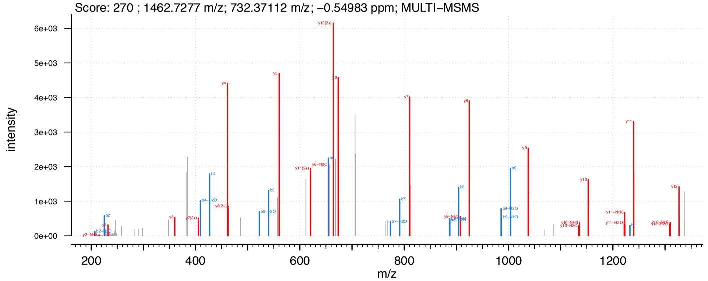

Raw File: Tiffy_20110729_FEP_267_PD20110720_Cdc42_mouseCerebellum_LF_rep3_GTPgS
Scan Number: 4490
Proteins:
E9PUK3

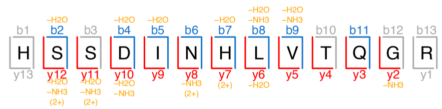

HSSDINHLVTQGR
Score: 270 ; 1462.7277 m/z; 732.37112 m/z; −0.54983 ppm; MULTI−MSMS

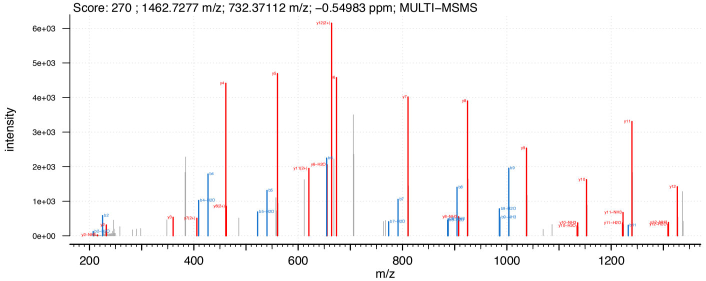

Raw File: Tiffy_20110729_FEP_267_PD20110720_Cdc42_mouseCerebellum_LF_rep3_GTPgS
Scan Number: 4490
Proteins:
E9PUK3

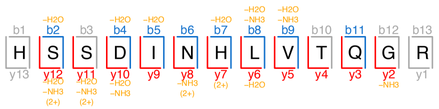

HSSDINHLVTQGR
Score: 270 ; 1462.7277 m/z; 732.37112 m/z; −0.54983 ppm; MULTI−MSMS

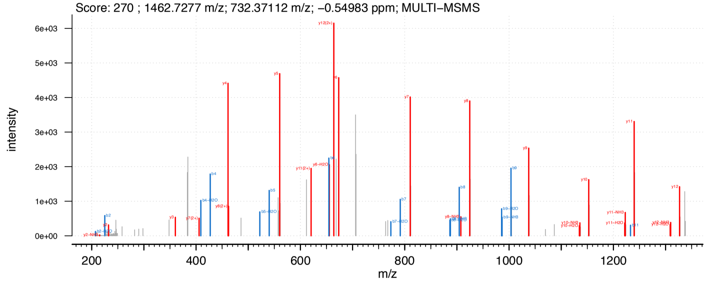

Raw File: Tiffy_20110729_FEP_267_PD20110720_Cdc42_mouseCerebellum_LF_rep3_GTPgS
Scan Number: 4490
Proteins:
E9PUK3

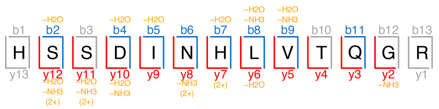

HSSDINHLVTQGR
Score: 270 ; 1462.7277 m/z; 732.37112 m/z; −0.54983 ppm; MULTI−MSMS

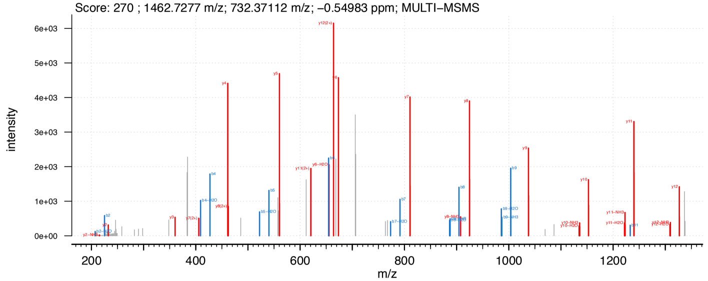

Raw File: Tiffy_20110729_FEP_267_PD20110720_Cdc42_mouseCerebellum_LF_rep3_GTPgS
Scan Number: 4490
Proteins:
E9PUK3

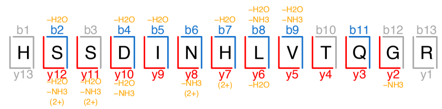

HSSDINHLVTQGR
Score: 270 ; 1462.7277 m/z; 732.37112 m/z; −0.54983 ppm; MULTI−MSMS

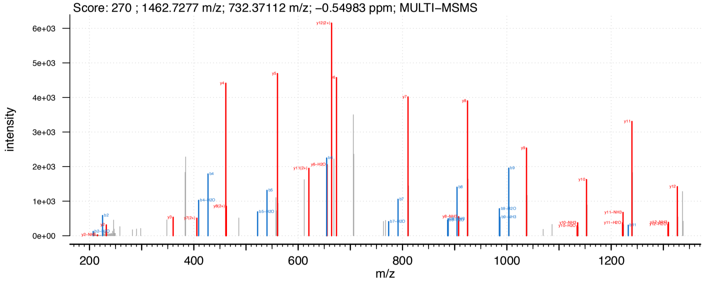

Raw File: Tiffy_20110729_FEP_267_PD20110720_Cdc42_mouseCerebellum_LF_rep3_GTPgS
Scan Number: 4490
Proteins:
E9PUK3

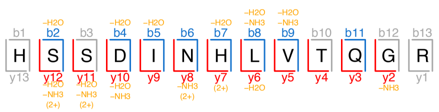

HSSDINHLVTQGR
Score: 270 ; 1462.7277 m/z; 732.37112 m/z; −0.54983 ppm; MULTI−MSMS

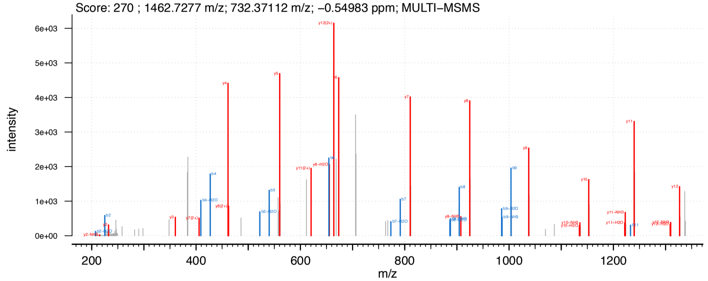

Raw File: Tiffy_20110729_FEP_267_PD20110720_Cdc42_mouseCerebellum_LF_rep3_GTPgS
Scan Number: 4490
Proteins:
E9PUK3

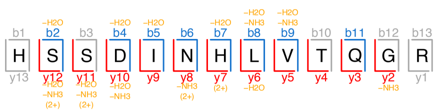

HSSDINHLVTQGR
Score: 270 ; 1462.7277 m/z; 732.37112 m/z; −0.54983 ppm; MULTI−MSMS

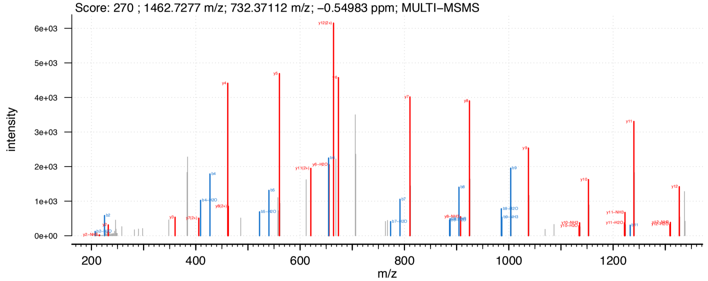

Raw File: Tiffy_20110729_FEP_267_PD20110720_Cdc42_mouseCerebellum_LF_rep3_GTPgS
Scan Number: 4490
Proteins:
E9PUK3

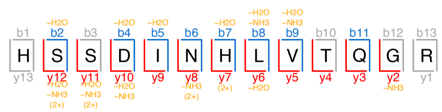

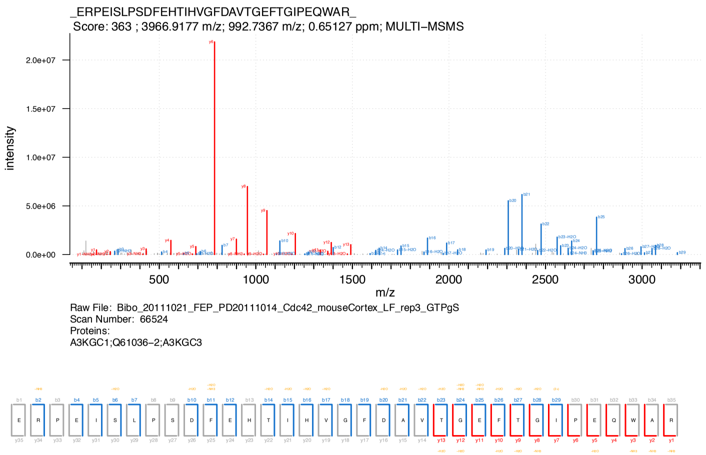
ERPEISLPSDFEHTIHVGFDAVTGEFTGIPEQWAR
Score: 363 ; 3966.9177 m/z; 992.7367 m/z; 0.65127 ppm; MULTI−MSMS
intensity
m/z
Raw File: Bibo_20111021_FEP_PD20111014_Cdc42_mouseCortex_LF_rep3_GTPgS
Scan Number: 66524
Proteins:
A3KGC1;Q61036−2;A3KGC3

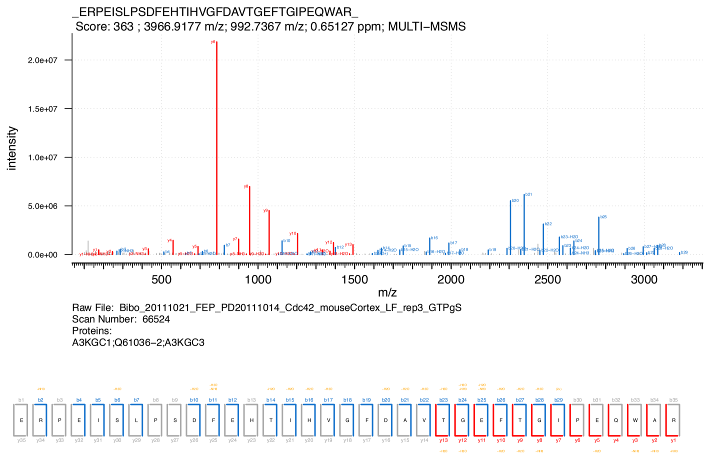
ERPEISLPSDFEHTIHVGFDAVTGEFTGIPEQWAR
Score: 363 ; 3966.9177 m/z; 992.7367 m/z; 0.65127 ppm; MULTI−MSMS
intensity
m/z
Raw File: Bibo_20111021_FEP_PD20111014_Cdc42_mouseCortex_LF_rep3_GTPgS
Scan Number: 66524
Proteins:
A3KGC1;Q61036−2;A3KGC3

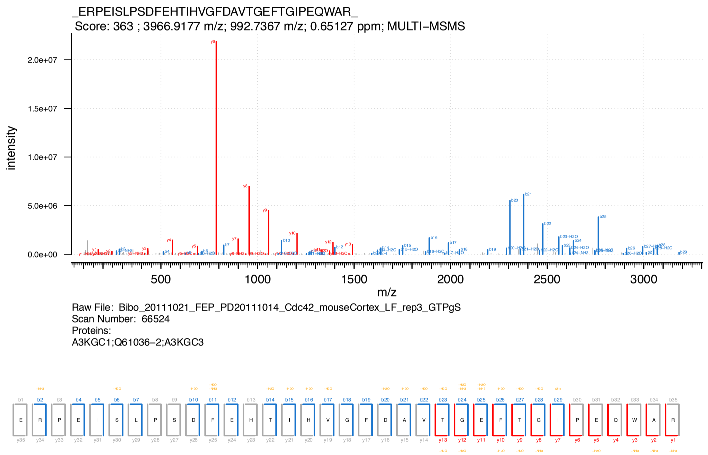
ERPEISLPSDFEHTIHVGFDAVTGEFTGIPEQWAR
Score: 363 ; 3966.9177 m/z; 992.7367 m/z; 0.65127 ppm; MULTI−MSMS
intensity
m/z
Raw File: Bibo_20111021_FEP_PD20111014_Cdc42_mouseCortex_LF_rep3_GTPgS
Scan Number: 66524
Proteins:
A3KGC1;Q61036−2;A3KGC3

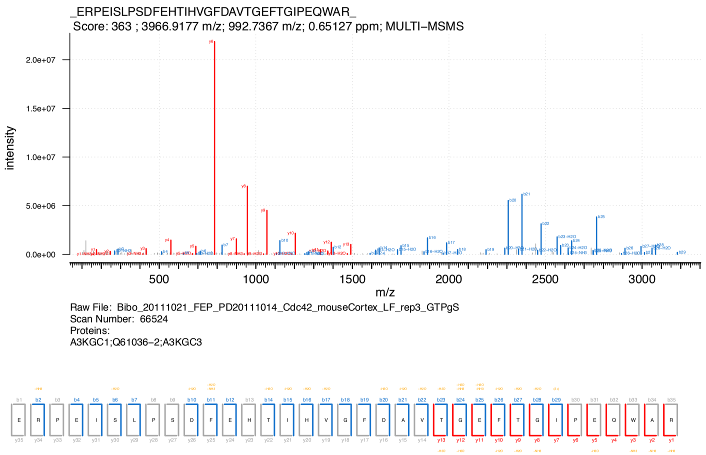
ERPEISLPSDFEHTIHVGFDAVTGEFTGIPEQWAR
Score: 363 ; 3966.9177 m/z; 992.7367 m/z; 0.65127 ppm; MULTI−MSMS
intensity
m/z
Raw File: Bibo_20111021_FEP_PD20111014_Cdc42_mouseCortex_LF_rep3_GTPgS
Scan Number: 66524
Proteins:
A3KGC1;Q61036−2;A3KGC3

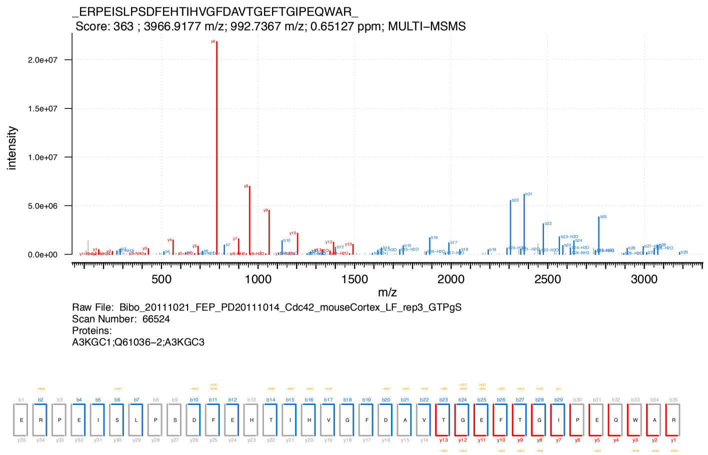
ERPEISLPSDFEHTIHVGFDAVTGEFTGIPEQWAR
Score: 363 ; 3966.9177 m/z; 992.7367 m/z; 0.65127 ppm; MULTI−MSMS
intensity
m/z
Raw File: Bibo_20111021_FEP_PD20111014_Cdc42_mouseCortex_LF_rep3_GTPgS
Scan Number: 66524
Proteins:
A3KGC1;Q61036−2;A3KGC3

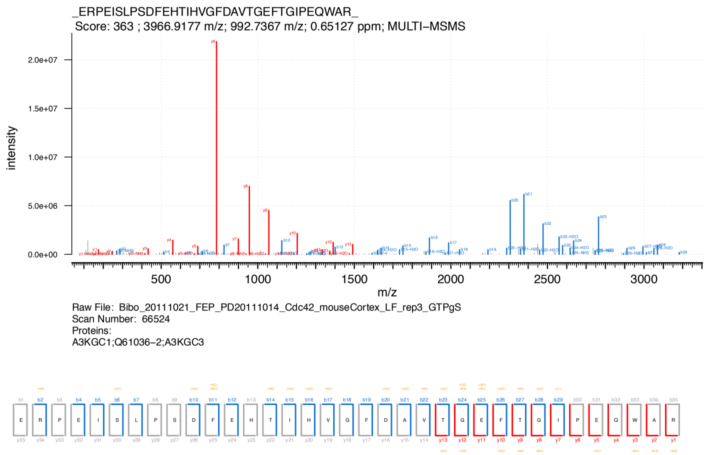
ERPEISLPSDFEHTIHVGFDAVTGEFTGIPEQWAR
Score: 363 ; 3966.9177 m/z; 992.7367 m/z; 0.65127 ppm; MULTI−MSMS
intensity
m/z
Raw File: Bibo_20111021_FEP_PD20111014_Cdc42_mouseCortex_LF_rep3_GTPgS
Scan Number: 66524
Proteins:
A3KGC1;Q61036−2;A3KGC3

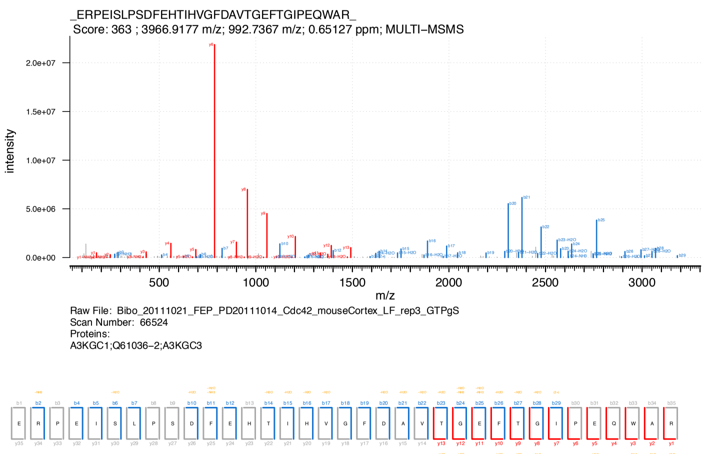
ERPEISLPSDFEHTIHVGFDAVTGEFTGIPEQWAR
Score: 363 ; 3966.9177 m/z; 992.7367 m/z; 0.65127 ppm; MULTI−MSMS
intensity
m/z
Raw File: Bibo_20111021_FEP_PD20111014_Cdc42_mouseCortex_LF_rep3_GTPgS
Scan Number: 66524
Proteins:
A3KGC1;Q61036−2;A3KGC3

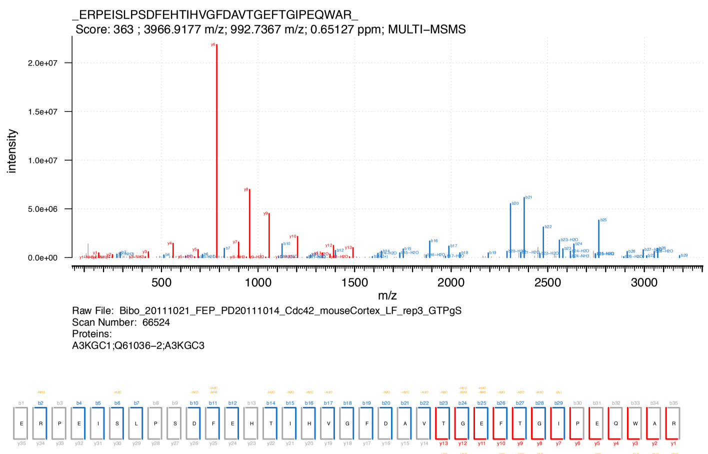
ERPEISLPSDFEHTIHVGFDAVTGEFTGIPEQWAR
Score: 363 ; 3966.9177 m/z; 992.7367 m/z; 0.65127 ppm; MULTI−MSMS
intensity
m/z
Raw File: Bibo_20111021_FEP_PD20111014_Cdc42_mouseCortex_LF_rep3_GTPgS
Scan Number: 66524
Proteins:
A3KGC1;Q61036−2;A3KGC3

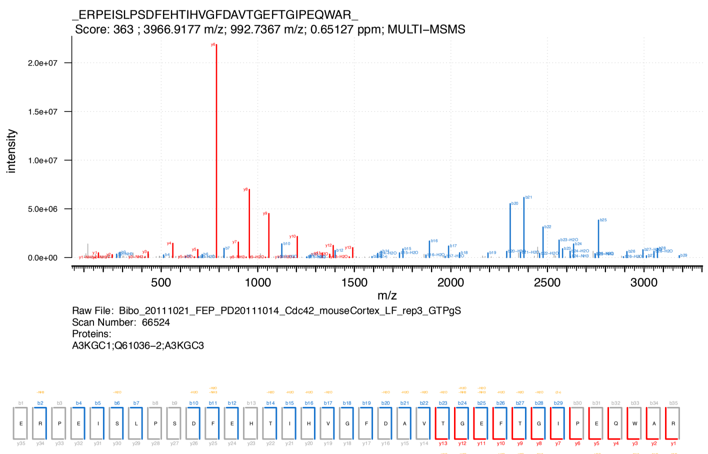
ERPEISLPSDFEHTIHVGFDAVTGEFTGIPEQWAR
Score: 363 ; 3966.9177 m/z; 992.7367 m/z; 0.65127 ppm; MULTI−MSMS
intensity
m/z
Raw File: Bibo_20111021_FEP_PD20111014_Cdc42_mouseCortex_LF_rep3_GTPgS
Scan Number: 66524
Proteins:
A3KGC1;Q61036−2;A3KGC3

LPEGIPEQWAR
Score: 100 ; 1294.667 m/z; 648.34077 m/z; 0.069884 ppm; MULTI–MSMS

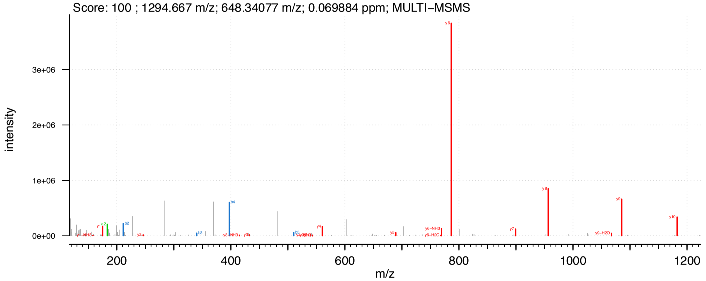

Raw File: Bibo_20111021_FEP_PD20111014_Cdc42_mouseCortex_LF_rep3_GTPgS
Scan Number: 17927
Proteins:
B1GX81;A3KGC0;Q61036;A3KGC5;A3KGC4

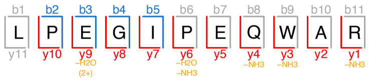

LPEGIPEQWAR
Score: 100 ; 1294.667 m/z; 648.34077 m/z; 0.069884 ppm; MULTI–MSMS

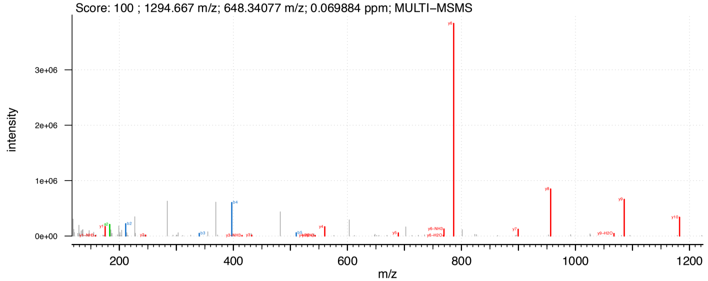

Raw File: Bibo_20111021_FEP_PD20111014_Cdc42_mouseCortex_LF_rep3_GTPgS
Scan Number: 17927
Proteins:
B1GX81;A3KGC0;Q61036;A3KGC5;A3KGC4

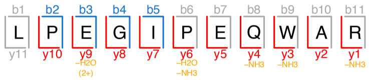

LPEGIPEQWAR
Score: 100 ; 1294.667 m/z; 648.34077 m/z; 0.069884 ppm; MULTI–MSMS

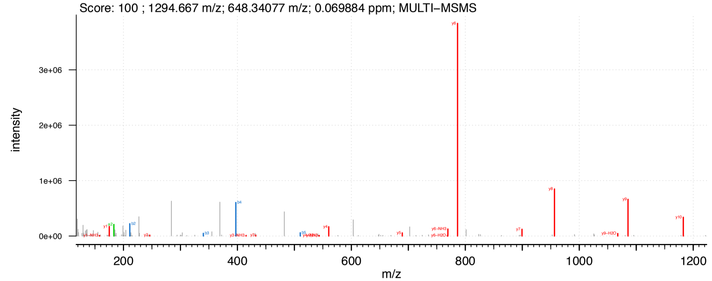

Raw File: Bibo_20111021_FEP_PD20111014_Cdc42_mouseCortex_LF_rep3_GTPgS
Scan Number: 17927
Proteins:
B1GX81;A3KGC0;Q61036;A3KGC5;A3KGC4

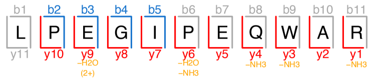

LPEGIPEQWAR
Score: 100 ; 1294.667 m/z; 648.34077 m/z; 0.069884 ppm; MULTI–MSMS

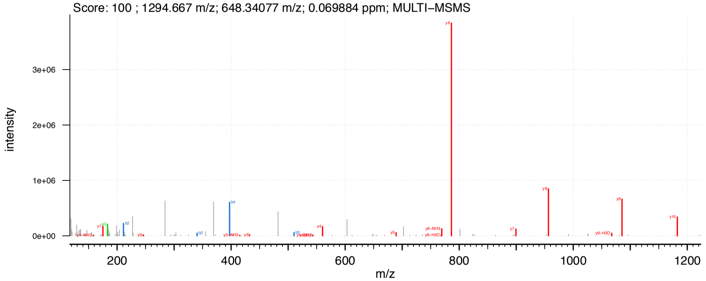

Raw File: Bibo_20111021_FEP_PD20111014_Cdc42_mouseCortex_LF_rep3_GTPgS
Scan Number: 17927
Proteins:
B1GX81;A3KGC0;Q61036;A3KGC5;A3KGC4

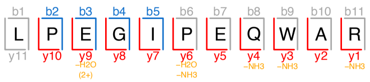

LPEGIPEQWAR
Score: 100 ; 1294.667 m/z; 648.34077 m/z; 0.069884 ppm; MULTI–MSMS

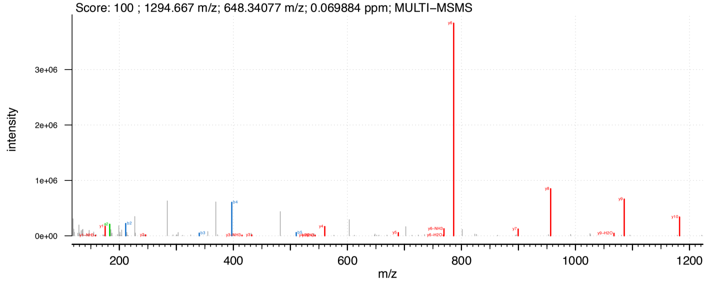

Raw File: Bibo_20111021_FEP_PD20111014_Cdc42_mouseCortex_LF_rep3_GTPgS
Scan Number: 17927
Proteins:
B1GX81;A3KGC0;Q61036;A3KGC5;A3KGC4

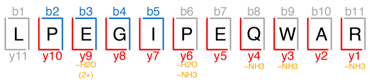

LPEGIPEQWAR
Score: 100 ; 1294.667 m/z; 648.34077 m/z; 0.069884 ppm; MULTI–MSMS

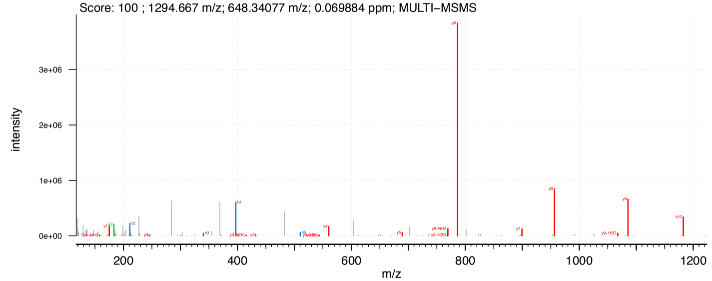

Raw File: Bibo_20111021_FEP_PD20111014_Cdc42_mouseCortex_LF_rep3_GTPgS
Scan Number: 17927
Proteins:
B1GX81;A3KGC0;Q61036;A3KGC5;A3KGC4

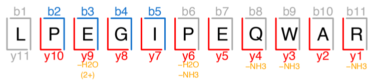

LPEGIPEQWAR
Score: 100 ; 1294.667 m/z; 648.34077 m/z; 0.069884 ppm; MULTI–MSMS

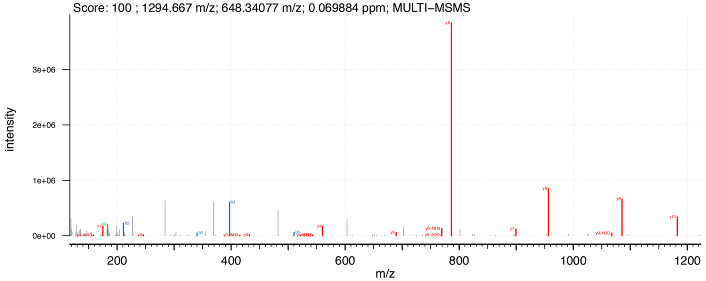

Raw File: Bibo_20111021_FEP_PD20111014_Cdc42_mouseCortex_LF_rep3_GTPgS
Scan Number: 17927
Proteins:
B1GX81;A3KGC0;Q61036;A3KGC5;A3KGC4

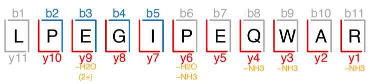

LPEGIPEQWAR
Score: 100 ; 1294.667 m/z; 648.34077 m/z; 0.069884 ppm; MULTI–MSMS

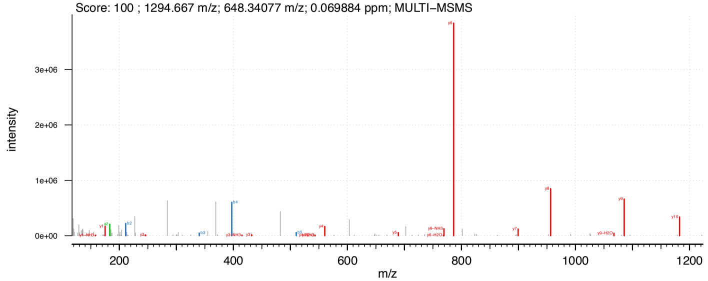

Raw File: Bibo_20111021_FEP_PD20111014_Cdc42_mouseCortex_LF_rep3_GTPgS
Scan Number: 17927
Proteins:
B1GX81;A3KGC0;Q61036;A3KGC5;A3KGC4

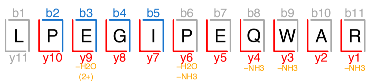

LPEGIPEQWAR
Score: 100 ; 1294.667 m/z; 648.34077 m/z; 0.069884 ppm; MULTI–MSMS

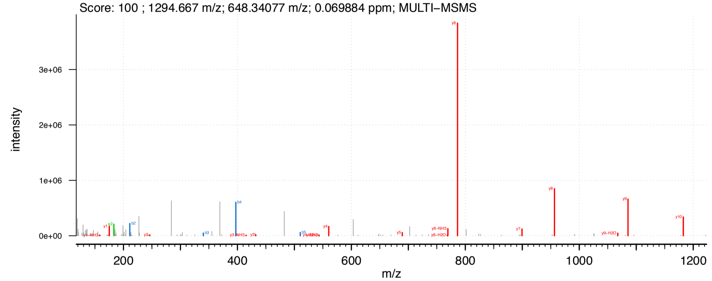

Raw File: Bibo_20111021_FEP_PD20111014_Cdc42_mouseCortex_LF_rep3_GTPgS
Scan Number: 17927
Proteins:
B1GX81;A3KGC0;Q61036;A3KGC5;A3KGC4

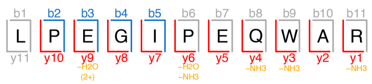

(ac)SDSLDNEEKPPAPPLR
Score: 335 ; 1805.8796 m/z; 903.94706 m/z; 0.038632 ppm; MULTI−MSMS

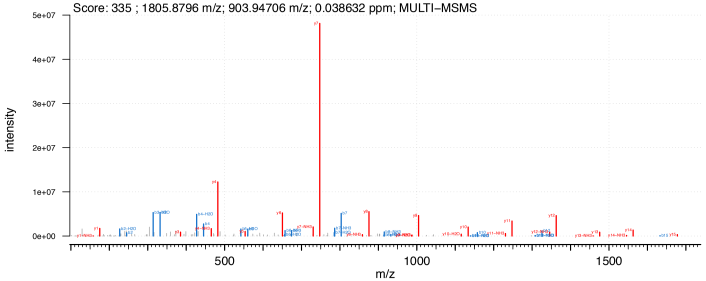

Raw File: Bibo_20111021_FEP_PD20111014_Cdc42_mouseCortex_LF_rep3_GTPgS
Scan Number: 9912
Proteins:
B1GX81;A3KGC0;Q61036;B1GX80;A3KGC5;A3KGC4;A3KGC2;A3KGC1;Q61036−2;A3KGC3

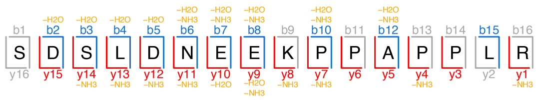

(ac)SDSLDNEEKPPAPPLR
Score: 335 ; 1805.8796 m/z; 903.94706 m/z; 0.038632 ppm; MULTI−MSMS

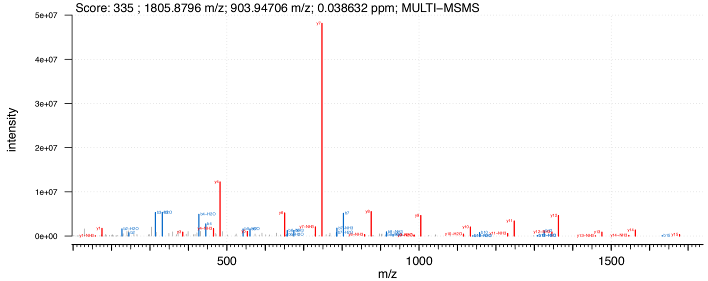

Raw File: Bibo_20111021_FEP_PD20111014_Cdc42_mouseCortex_LF_rep3_GTPgS
Scan Number: 9912
Proteins:
B1GX81;A3KGC0;Q61036;B1GX80;A3KGC5;A3KGC4;A3KGC2;A3KGC1;Q61036−2;A3KGC3

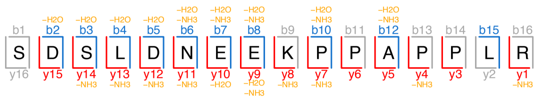

(ac)SDSLDNEEKPPAPPLR
Score: 335 ; 1805.8796 m/z; 903.94706 m/z; 0.038632 ppm; MULTI−MSMS

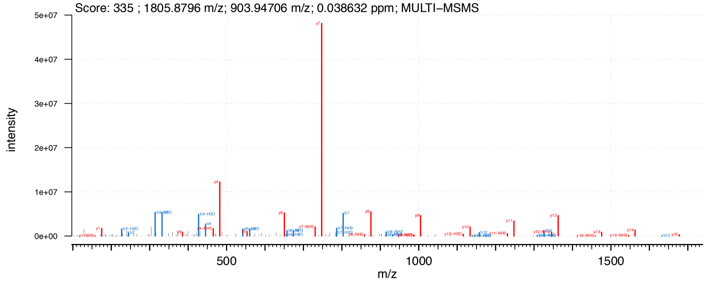

Raw File: Bibo_20111021_FEP_PD20111014_Cdc42_mouseCortex_LF_rep3_GTPgS
Scan Number: 9912
Proteins:
B1GX81;A3KGC0;Q61036;B1GX80;A3KGC5;A3KGC4;A3KGC2;A3KGC1;Q61036−2;A3KGC3

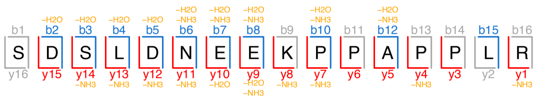

(ac)SDSLDNEEKPPAPPLR
Score: 335 ; 1805.8796 m/z; 903.94706 m/z; 0.038632 ppm; MULTI−MSMS

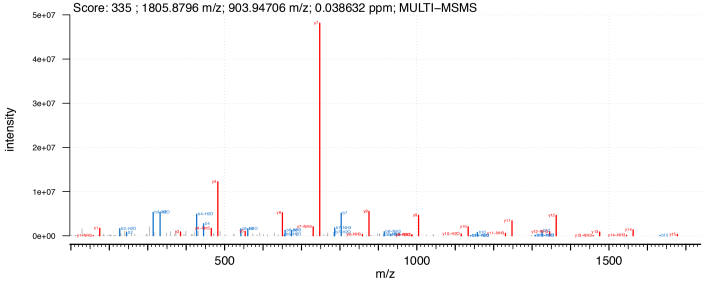

Raw File: Bibo_20111021_FEP_PD20111014_Cdc42_mouseCortex_LF_rep3_GTPgS
Scan Number: 9912
Proteins:
B1GX81;A3KGC0;Q61036;B1GX80;A3KGC5;A3KGC4;A3KGC2;A3KGC1;Q61036−2;A3KGC3

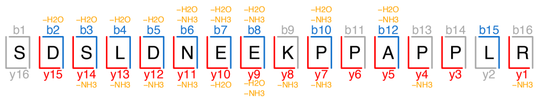

(ac)SDSLDNEEKPPAPPLR
Score: 335 ; 1805.8796 m/z; 903.94706 m/z; 0.038632 ppm; MULTI−MSMS

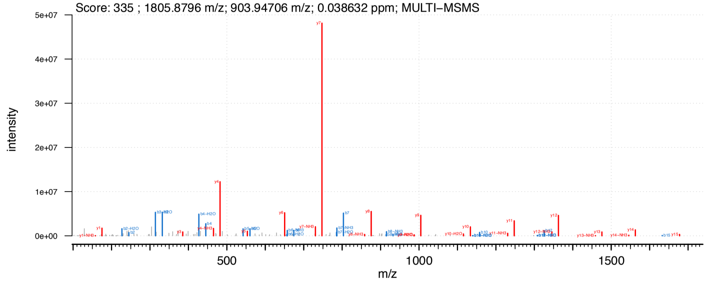

Raw File: Bibo_20111021_FEP_PD20111014_Cdc42_mouseCortex_LF_rep3_GTPgS
Scan Number: 9912
Proteins:
B1GX81;A3KGC0;Q61036;B1GX80;A3KGC5;A3KGC4;A3KGC2;A3KGC1;Q61036−2;A3KGC3

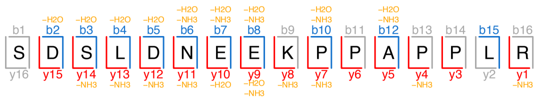

(ac)SDSLDNEEKPPAPPLR
Score: 335 ; 1805.8796 m/z; 903.94706 m/z; 0.038632 ppm; MULTI−MSMS

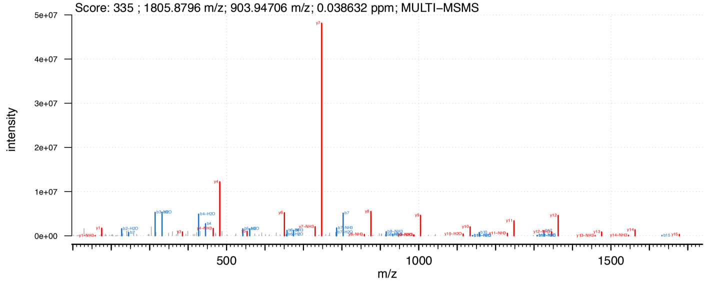

Raw File: Bibo_20111021_FEP_PD20111014_Cdc42_mouseCortex_LF_rep3_GTPgS
Scan Number: 9912
Proteins:
B1GX81;A3KGC0;Q61036;B1GX80;A3KGC5;A3KGC4;A3KGC2;A3KGC1;Q61036−2;A3KGC3

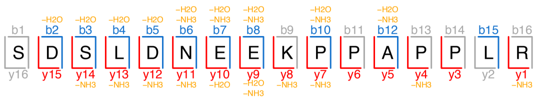

(ac)SDSLDNEEKPPAPPLR
Score: 335 ; 1805.8796 m/z; 903.94706 m/z; 0.038632 ppm; MULTI−MSMS

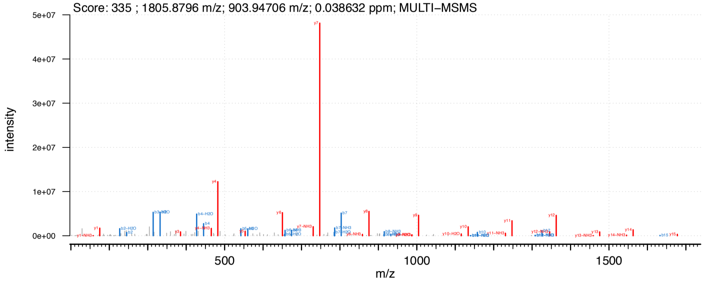

Raw File: Bibo_20111021_FEP_PD20111014_Cdc42_mouseCortex_LF_rep3_GTPgS
Scan Number: 9912
Proteins:
B1GX81;A3KGC0;Q61036;B1GX80;A3KGC5;A3KGC4;A3KGC2;A3KGC1;Q61036−2;A3KGC3

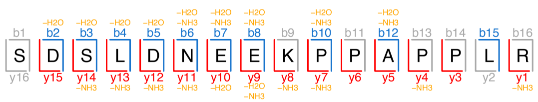

(ac)SDSLDNEEKPPAPPLR
Score: 335 ; 1805.8796 m/z; 903.94706 m/z; 0.038632 ppm; MULTI−MSMS

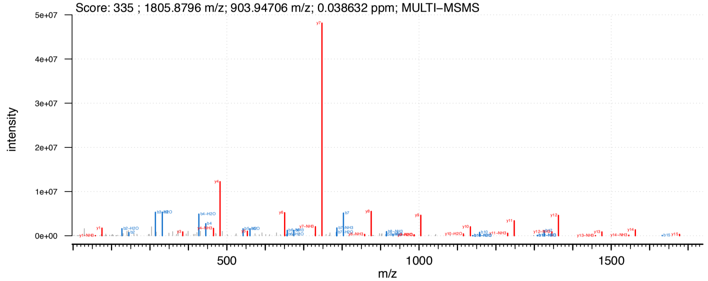

Raw File: Bibo_20111021_FEP_PD20111014_Cdc42_mouseCortex_LF_rep3_GTPgS
Scan Number: 9912
Proteins:
B1GX81;A3KGC0;Q61036;B1GX80;A3KGC5;A3KGC4;A3KGC2;A3KGC1;Q61036−2;A3KGC3

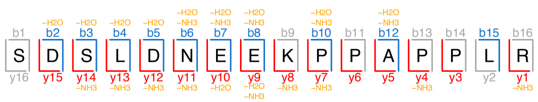

(ac)SDSLDNEEKPPAPPLR
Score: 335 ; 1805.8796 m/z; 903.94706 m/z; 0.038632 ppm; MULTI−MSMS

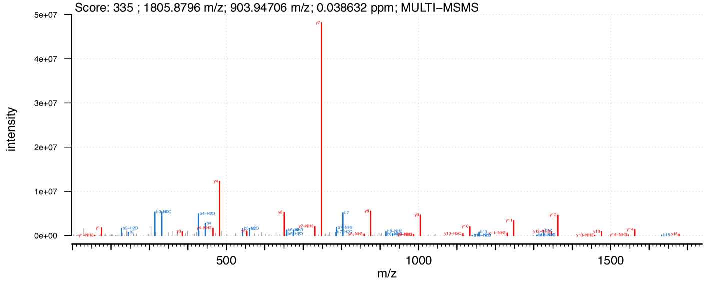

Raw File: Bibo_20111021_FEP_PD20111014_Cdc42_mouseCortex_LF_rep3_GTPgS
Scan Number: 9912
Proteins:
B1GX81;A3KGC0;Q61036;B1GX80;A3KGC5;A3KGC4;A3KGC2;A3KGC1;Q61036−2;A3KGC3

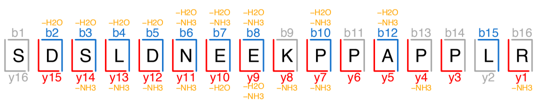

DIKSDNILLGMDGSVK
Score: 229 ; 1703.8764 m/z; 852.94547 m/z; −0.03263 ppm; MULTI−MSMS

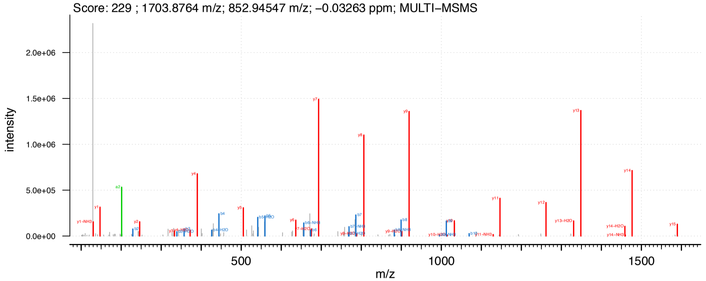

Raw File: Bibo_20111021_FEP_PD20111014_Cdc42_mouseCortex_LF_rep3_GTPgS
Scan Number: 20845
Proteins:
B1GX81;A3KGC0;Q61036;B1GX80;A3KGC1;Q61036−2;G5E884;O88643

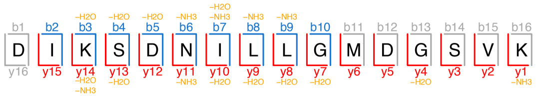

DIKSDNILLGMDGSVK
Score: 229 ; 1703.8764 m/z; 852.94547 m/z; −0.03263 ppm; MULTI−MSMS

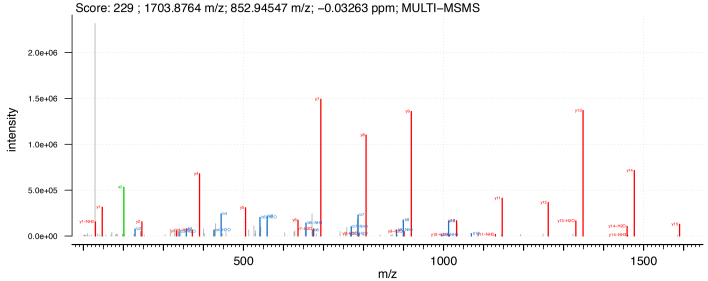

Raw File: Bibo_20111021_FEP_PD20111014_Cdc42_mouseCortex_LF_rep3_GTPgS
Scan Number: 20845
Proteins:
B1GX81;A3KGC0;Q61036;B1GX80;A3KGC1;Q61036−2;G5E884;O88643

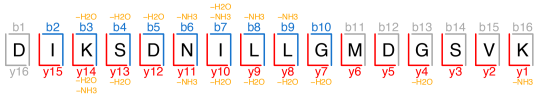

DIKSDNILLGMDGSVK
Score: 229 ; 1703.8764 m/z; 852.94547 m/z; −0.03263 ppm; MULTI−MSMS

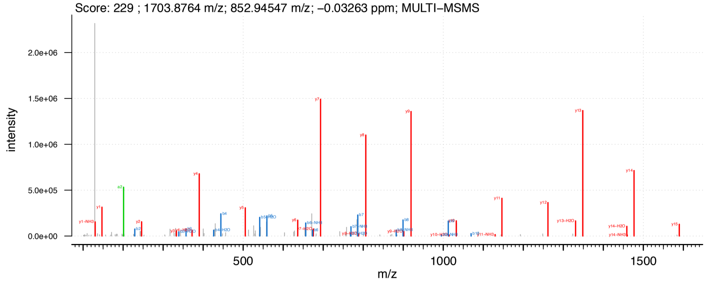

Raw File: Bibo_20111021_FEP_PD20111014_Cdc42_mouseCortex_LF_rep3_GTPgS
Scan Number: 20845
Proteins:
B1GX81;A3KGC0;Q61036;B1GX80;A3KGC1;Q61036−2;G5E884;O88643

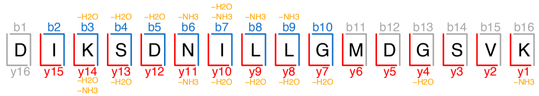

DIKSDNILLGMDGSVK
Score: 229 ; 1703.8764 m/z; 852.94547 m/z; −0.03263 ppm; MULTI−MSMS

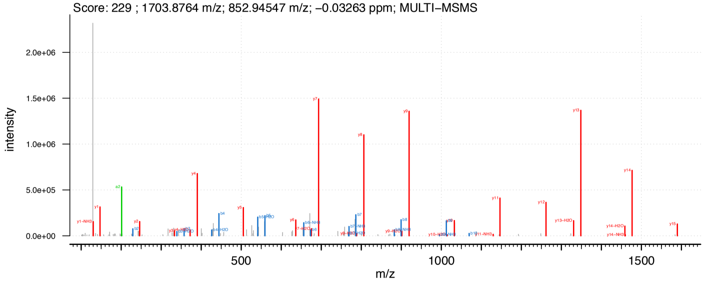

Raw File: Bibo_20111021_FEP_PD20111014_Cdc42_mouseCortex_LF_rep3_GTPgS
Scan Number: 20845
Proteins:
B1GX81;A3KGC0;Q61036;B1GX80;A3KGC1;Q61036−2;G5E884;O88643

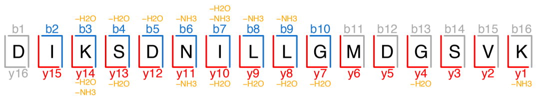

DIKSDNILLGMDGSVK
Score: 229 ; 1703.8764 m/z; 852.94547 m/z; −0.03263 ppm; MULTI−MSMS

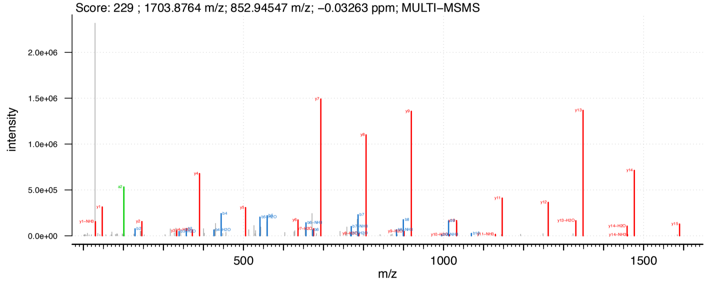

Raw File: Bibo_20111021_FEP_PD20111014_Cdc42_mouseCortex_LF_rep3_GTPgS
Scan Number: 20845
Proteins:
B1GX81;A3KGC0;Q61036;B1GX80;A3KGC1;Q61036−2;G5E884;O88643

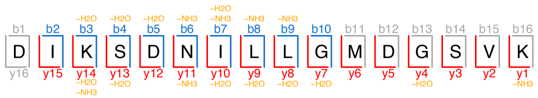

DIKSDNILLGMDGSVK
Score: 229 ; 1703.8764 m/z; 852.94547 m/z; −0.03263 ppm; MULTI−MSMS

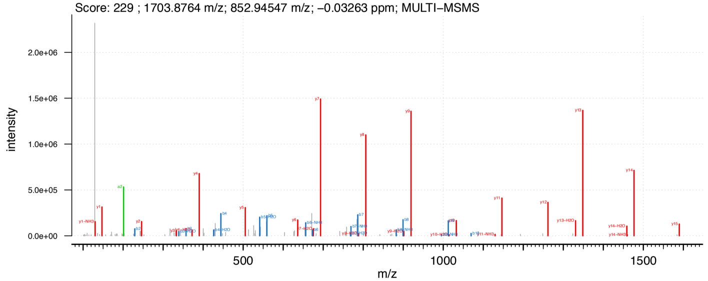

Raw File: Bibo_20111021_FEP_PD20111014_Cdc42_mouseCortex_LF_rep3_GTPgS
Scan Number: 20845
Proteins:
B1GX81;A3KGC0;Q61036;B1GX80;A3KGC1;Q61036−2;G5E884;O88643

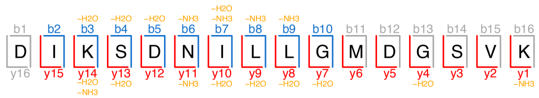

DIKSDNILLGMDGSVK
Score: 229 ; 1703.8764 m/z; 852.94547 m/z; −0.03263 ppm; MULTI−MSMS

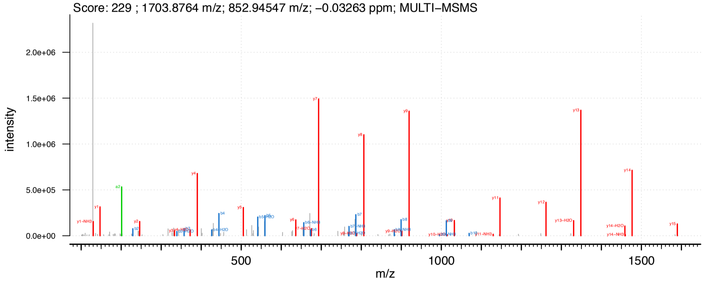

Raw File: Bibo_20111021_FEP_PD20111014_Cdc42_mouseCortex_LF_rep3_GTPgS
Scan Number: 20845
Proteins:
B1GX81;A3KGC0;Q61036;B1GX80;A3KGC1;Q61036−2;G5E884;O88643

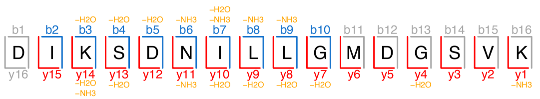

DIKSDNILLGMDGSVK
Score: 229 ; 1703.8764 m/z; 852.94547 m/z; −0.03263 ppm; MULTI−MSMS

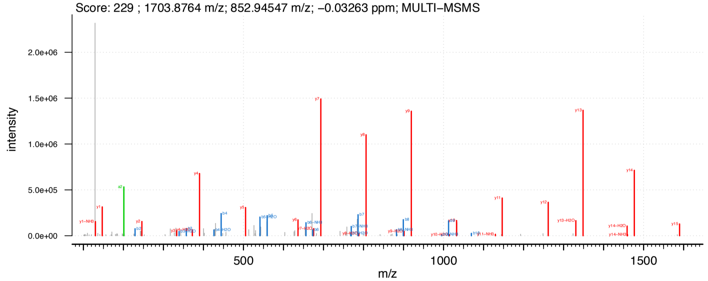

Raw File: Bibo_20111021_FEP_PD20111014_Cdc42_mouseCortex_LF_rep3_GTPgS
Scan Number: 20845
Proteins:
B1GX81;A3KGC0;Q61036;B1GX80;A3KGC1;Q61036−2;G5E884;O88643

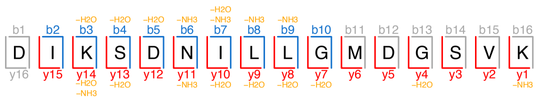

DIKSDNILLGMDGSVK
Score: 229 ; 1703.8764 m/z; 852.94547 m/z; −0.03263 ppm; MULTI−MSMS

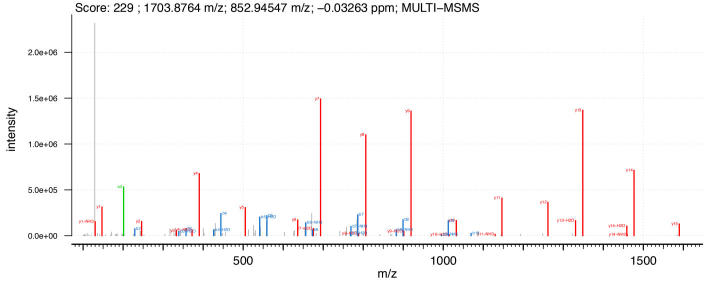

Raw File: Bibo_20111021_FEP_PD20111014_Cdc42_mouseCortex_LF_rep3_GTPgS
Scan Number: 20845
Proteins:
B1GX81;A3KGC0;Q61036;B1GX80;A3KGC1;Q61036−2;G5E884;O88643

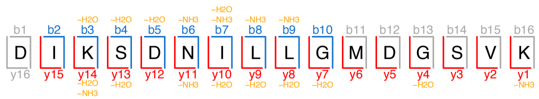

RSTMVGTPYWMAPEVVTRK
Score: 157 ; 2208.1184 m/z; 737.04673 m/z; −0.21921 ppm; MULTI−MSMS

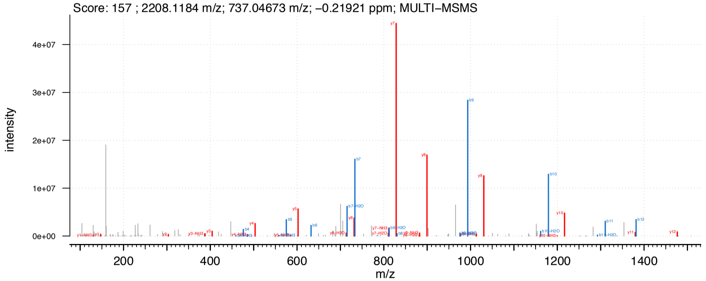

Raw File: Bibo_20111021_FEP_PD20111014_Cdc42_mouseCortex_LF_rep3_GTPgS
Scan Number: 20998
Proteins:
B1GX81;A3KGC0;Q61036;B1GX80;A3KGC1;Q61036−2;Q8CIN4;G5E884;O88643

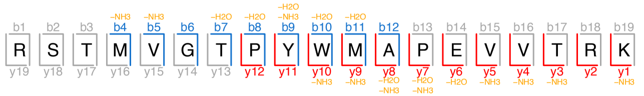

RSTMVGTPYWMAPEVVTRK
Score: 157 ; 2208.1184 m/z; 737.04673 m/z; −0.21921 ppm; MULTI−MSMS

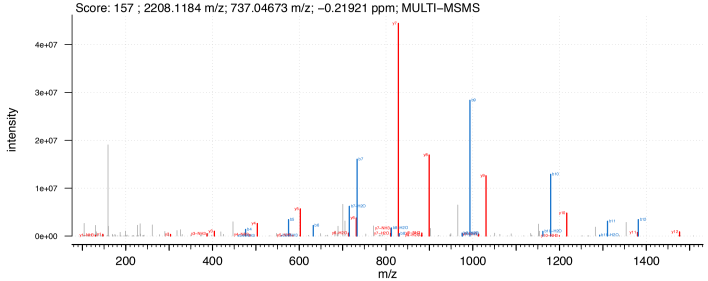

Raw File: Bibo_20111021_FEP_PD20111014_Cdc42_mouseCortex_LF_rep3_GTPgS
Scan Number: 20998
Proteins:
B1GX81;A3KGC0;Q61036;B1GX80;A3KGC1;Q61036−2;Q8CIN4;G5E884;O88643

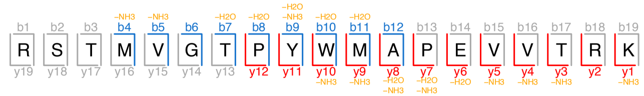

RSTMVGTPYWMAPEVVTRK
Score: 157 ; 2208.1184 m/z; 737.04673 m/z; −0.21921 ppm; MULTI−MSMS

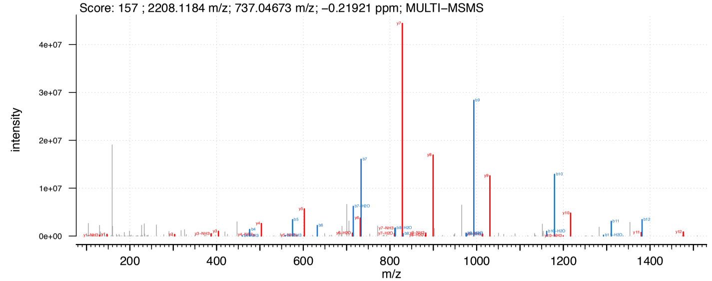

Raw File: Bibo_20111021_FEP_PD20111014_Cdc42_mouseCortex_LF_rep3_GTPgS
Scan Number: 20998
Proteins:
B1GX81;A3KGC0;Q61036;B1GX80;A3KGC1;Q61036−2;Q8CIN4;G5E884;O88643

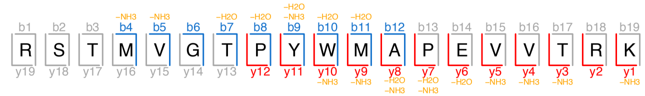

RSTMVGTPYWMAPEVVTRK
Score: 157 ; 2208.1184 m/z; 737.04673 m/z; −0.21921 ppm; MULTI−MSMS

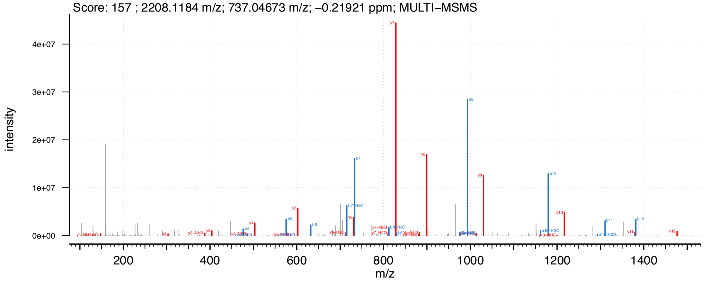

Raw File: Bibo_20111021_FEP_PD20111014_Cdc42_mouseCortex_LF_rep3_GTPgS
Scan Number: 20998
Proteins:
B1GX81;A3KGC0;Q61036;B1GX80;A3KGC1;Q61036−2;Q8CIN4;G5E884;O88643

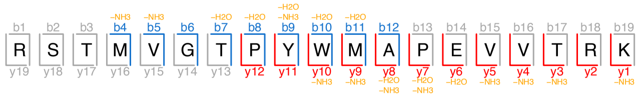

RSTMVGTPYWMAPEVVTRK
Score: 157 ; 2208.1184 m/z; 737.04673 m/z; −0.21921 ppm; MULTI−MSMS

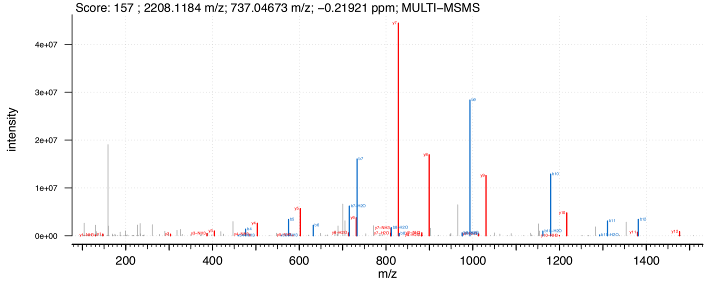

Raw File: Bibo_20111021_FEP_PD20111014_Cdc42_mouseCortex_LF_rep3_GTPgS
Scan Number: 20998
Proteins:
B1GX81;A3KGC0;Q61036;B1GX80;A3KGC1;Q61036−2;Q8CIN4;G5E884;O88643

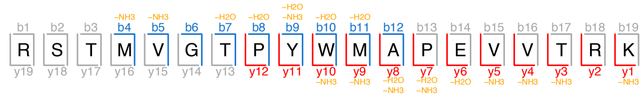

RSTMVGTPYWMAPEVVTRK
Score: 157 ; 2208.1184 m/z; 737.04673 m/z; −0.21921 ppm; MULTI−MSMS

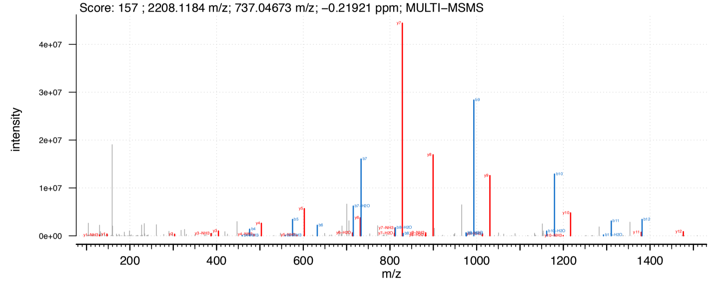

Raw File: Bibo_20111021_FEP_PD20111014_Cdc42_mouseCortex_LF_rep3_GTPgS
Scan Number: 20998
Proteins:
B1GX81;A3KGC0;Q61036;B1GX80;A3KGC1;Q61036−2;Q8CIN4;G5E884;O88643

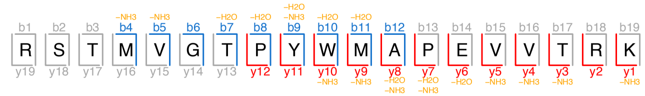

RSTMVGTPYWMAPEVVTRK
Score: 157 ; 2208.1184 m/z; 737.04673 m/z; −0.21921 ppm; MULTI−MSMS

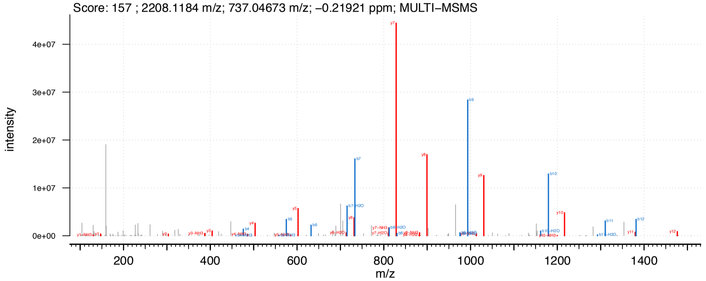

Raw File: Bibo_20111021_FEP_PD20111014_Cdc42_mouseCortex_LF_rep3_GTPgS
Scan Number: 20998
Proteins:
B1GX81;A3KGC0;Q61036;B1GX80;A3KGC1;Q61036−2;Q8CIN4;G5E884;O88643

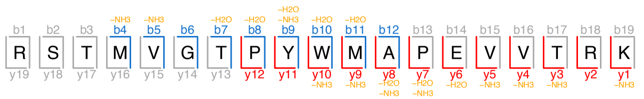

RSTMVGTPYWMAPEVVTRK
Score: 157 ; 2208.1184 m/z; 737.04673 m/z; −0.21921 ppm; MULTI−MSMS

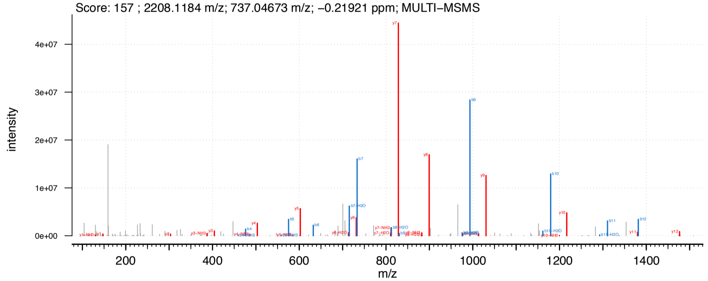

Raw File: Bibo_20111021_FEP_PD20111014_Cdc42_mouseCortex_LF_rep3_GTPgS
Scan Number: 20998
Proteins:
B1GX81;A3KGC0;Q61036;B1GX80;A3KGC1;Q61036−2;Q8CIN4;G5E884;O88643

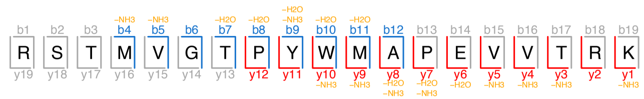

RSTMVGTPYWMAPEVVTRK
Score: 157 ; 2208.1184 m/z; 737.04673 m/z; −0.21921 ppm; MULTI−MSMS

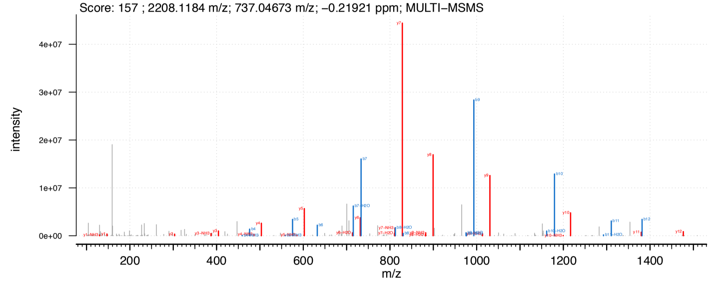

Raw File: Bibo_20111021_FEP_PD20111014_Cdc42_mouseCortex_LF_rep3_GTPgS
Scan Number: 20998
Proteins:
B1GX81;A3KGC0;Q61036;B1GX80;A3KGC1;Q61036−2;Q8CIN4;G5E884;O88643

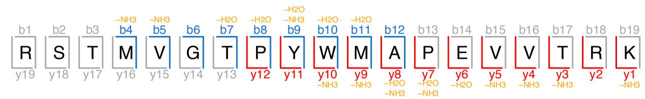

SAHGYIAAHQSNTK
Score: 330 ; 1483.7168 m/z; 742.86567 m/z; 0.067042 ppm; MULTI-MSMS

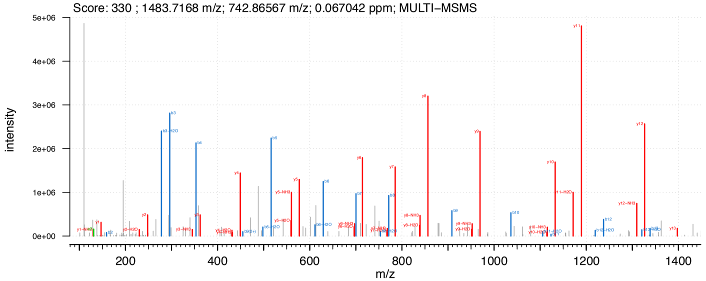

Raw File: Bibo_20111021_FEP_PD20111014_Cdc42_mouseCortex_LF_rep2_GDP
Scan Number: 393
Proteins:
B1GX81;A3KGC0;Q61036;B1GX80;A3KGC5;A3KGC4;A3KGC1;Q61036-2

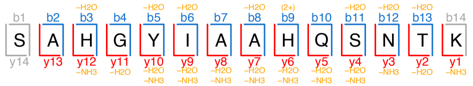

SAHGYIAAHQSNTK
Score: 330 ; 1483.7168 m/z; 742.86567 m/z; 0.067042 ppm; MULTI-MSMS

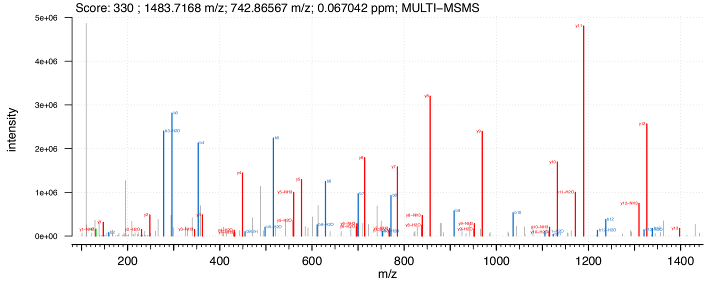

Raw File: Bibo_20111021_FEP_PD20111014_Cdc42_mouseCortex_LF_rep2_GDP
Scan Number: 393
Proteins:
B1GX81;A3KGC0;Q61036;B1GX80;A3KGC5;A3KGC4;A3KGC1;Q61036-2

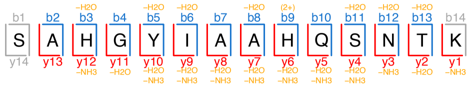

SAHGYIAAHQSNTK
Score: 330 ; 1483.7168 m/z; 742.86567 m/z; 0.067042 ppm; MULTI-MSMS

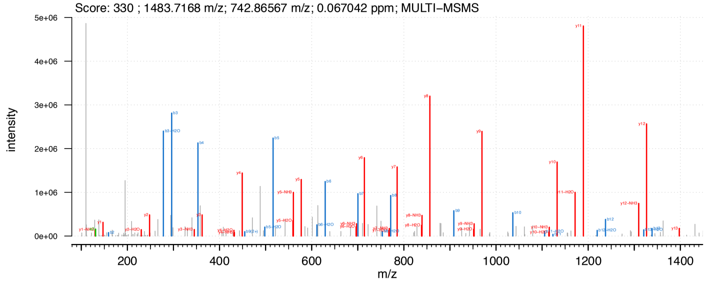

Raw File: Bibo_20111021_FEP_PD20111014_Cdc42_mouseCortex_LF_rep2_GDP
Scan Number: 393
Proteins:
B1GX81;A3KGC0;Q61036;B1GX80;A3KGC5;A3KGC4;A3KGC1;Q61036-2

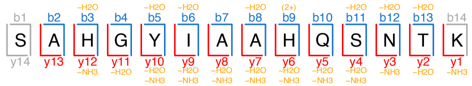

SAHGYIAAHQSNTK
Score: 330 ; 1483.7168 m/z; 742.86567 m/z; 0.067042 ppm; MULTI-MSMS

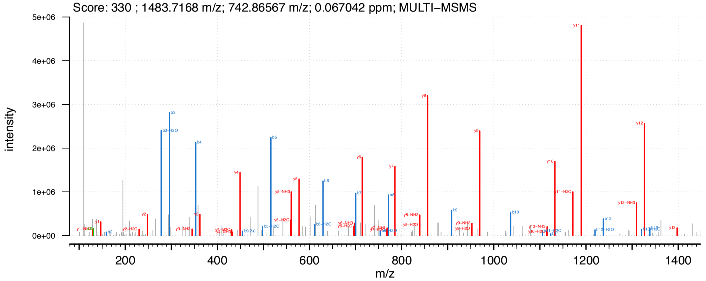

Raw File: Bibo_20111021_FEP_PD20111014_Cdc42_mouseCortex_LF_rep2_GDP
Scan Number: 393
Proteins:
B1GX81;A3KGC0;Q61036;B1GX80;A3KGC5;A3KGC4;A3KGC1;Q61036-2

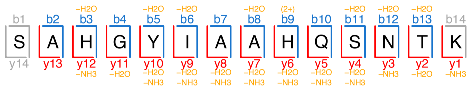

SAHGYIAAHQSNTK
Score: 330 ; 1483.7168 m/z; 742.86567 m/z; 0.067042 ppm; MULTI-MSMS

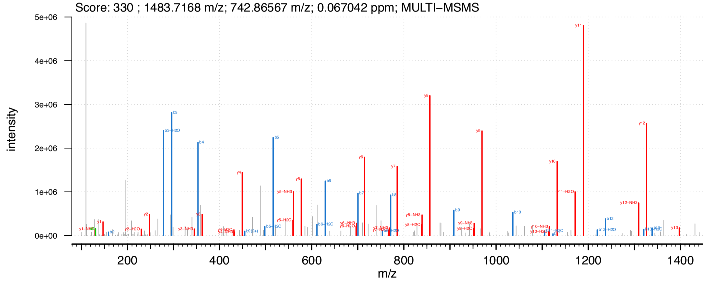

Raw File: Bibo_20111021_FEP_PD20111014_Cdc42_mouseCortex_LF_rep2_GDP
Scan Number: 393
Proteins:
B1GX81;A3KGC0;Q61036;B1GX80;A3KGC5;A3KGC4;A3KGC1;Q61036-2

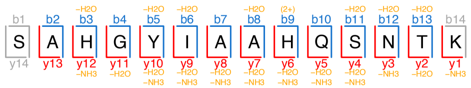

SAHGYIAAHQSNTK
Score: 330 ; 1483.7168 m/z; 742.86567 m/z; 0.067042 ppm; MULTI-MSMS

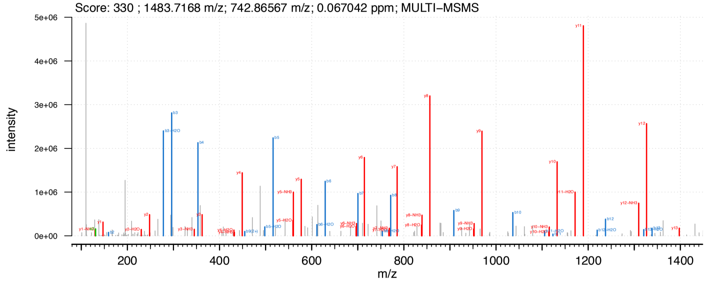

Raw File: Bibo_20111021_FEP_PD20111014_Cdc42_mouseCortex_LF_rep2_GDP
Scan Number: 393
Proteins:
B1GX81;A3KGC0;Q61036;B1GX80;A3KGC5;A3KGC4;A3KGC1;Q61036-2

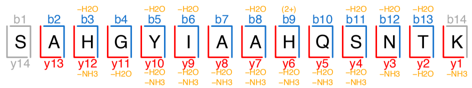

SAHGYIAAHQSNTK
Score: 330 ; 1483.7168 m/z; 742.86567 m/z; 0.067042 ppm; MULTI-MSMS

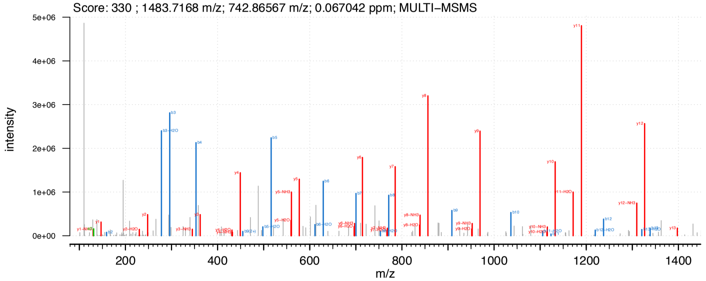

Raw File: Bibo_20111021_FEP_PD20111014_Cdc42_mouseCortex_LF_rep2_GDP
Scan Number: 393
Proteins:
B1GX81;A3KGC0;Q61036;B1GX80;A3KGC5;A3KGC4;A3KGC1;Q61036-2

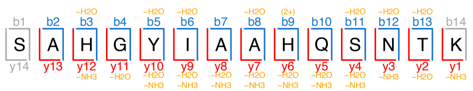

SAHGYIAAHQSNTK
Score: 330 ; 1483.7168 m/z; 742.86567 m/z; 0.067042 ppm; MULTI-MSMS

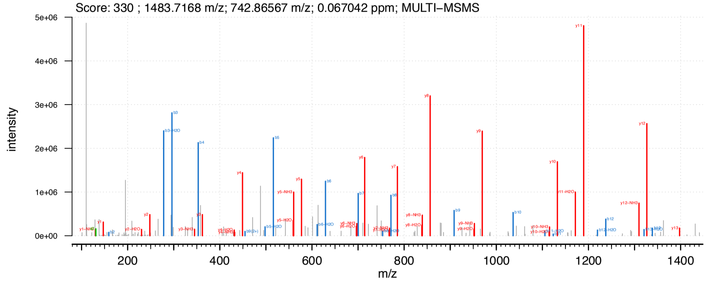

Raw File: Bibo_20111021_FEP_PD20111014_Cdc42_mouseCortex_LF_rep2_GDP
Scan Number: 393
Proteins:
B1GX81;A3KGC0;Q61036;B1GX80;A3KGC5;A3KGC4;A3KGC1;Q61036-2

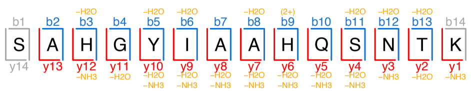

SAHGYIAAHQSNTK
Score: 330 ; 1483.7168 m/z; 742.86567 m/z; 0.067042 ppm; MULTI-MSMS

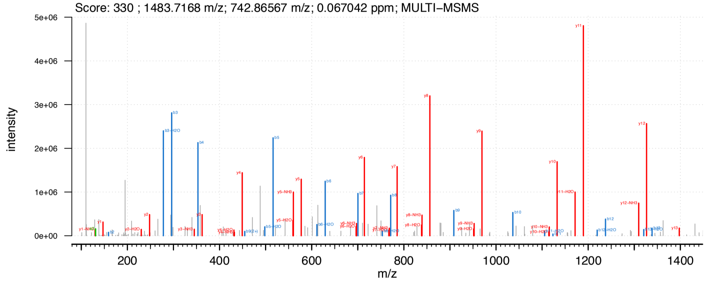

Raw File: Bibo_20111021_FEP_PD20111014_Cdc42_mouseCortex_LF_rep2_GDP
Scan Number: 393
Proteins:
B1GX81;A3KGC0;Q61036;B1GX80;A3KGC5;A3KGC4;A3KGC1;Q61036-2

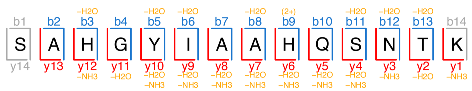

ELIINEILVMR
Score: 286 ; 1341.769 m/z; 671.89178 m/z; 1.1256 ppm; MULTI−MSMS

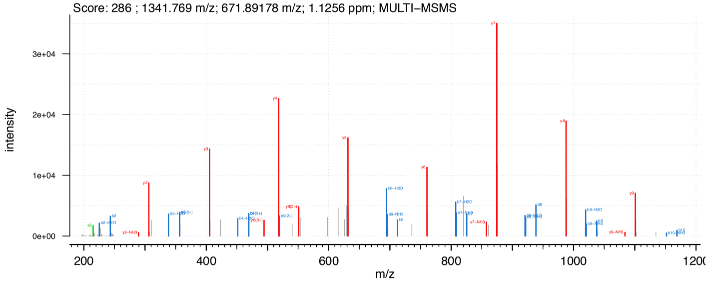

Raw File: Tiffy_20110729_FEP_265_PD20110720_Cdc42_mouseCerebellum_LF_rep2_GTPgS
Scan Number: 25078
Proteins:
B1GX81;A3KGC0;Q61036;B1GX80;A3KGC5;A3KGC1;Q61036−2;G5E884;O88643

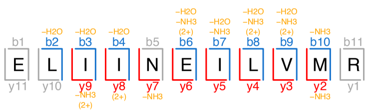

ELIINEILVMR
Score: 286 ; 1341.769 m/z; 671.89178 m/z; 1.1256 ppm; MULTI−MSMS

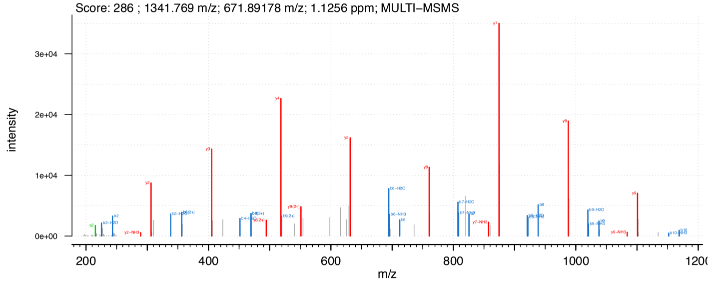

Raw File: Tiffy_20110729_FEP_265_PD20110720_Cdc42_mouseCerebellum_LF_rep2_GTPgS
Scan Number: 25078
Proteins:
B1GX81;A3KGC0;Q61036;B1GX80;A3KGC5;A3KGC1;Q61036−2;G5E884;O88643

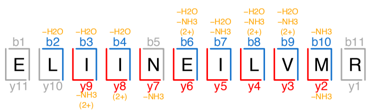

ELIINEILVMR
Score: 286 ; 1341.769 m/z; 671.89178 m/z; 1.1256 ppm; MULTI−MSMS

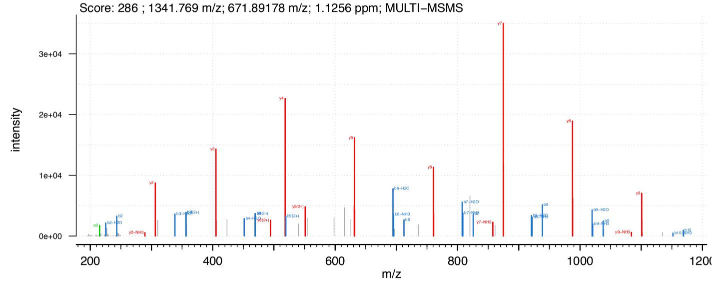

Raw File: Tiffy_20110729_FEP_265_PD20110720_Cdc42_mouseCerebellum_LF_rep2_GTPgS
Scan Number: 25078
Proteins:
B1GX81;A3KGC0;Q61036;B1GX80;A3KGC5;A3KGC1;Q61036−2;G5E884;O88643

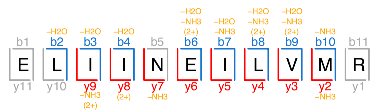

ELIINEILVMR
Score: 286 ; 1341.769 m/z; 671.89178 m/z; 1.1256 ppm; MULTI−MSMS

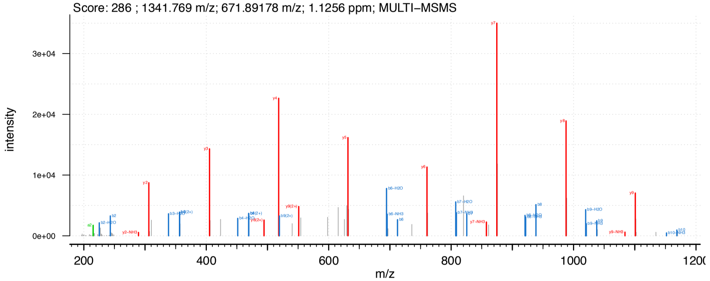

Raw File: Tiffy_20110729_FEP_265_PD20110720_Cdc42_mouseCerebellum_LF_rep2_GTPgS
Scan Number: 25078
Proteins:
B1GX81;A3KGC0;Q61036;B1GX80;A3KGC5;A3KGC1;Q61036−2;G5E884;O88643

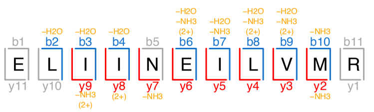

ELIINEILVMR
Score: 286 ; 1341.769 m/z; 671.89178 m/z; 1.1256 ppm; MULTI−MSMS

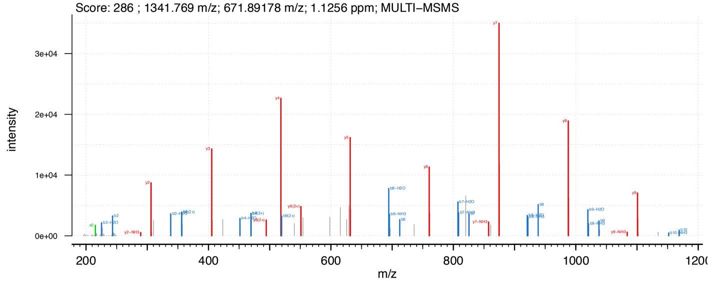

Raw File: Tiffy_20110729_FEP_265_PD20110720_Cdc42_mouseCerebellum_LF_rep2_GTPgS
Scan Number: 25078
Proteins:
B1GX81;A3KGC0;Q61036;B1GX80;A3KGC5;A3KGC1;Q61036−2;G5E884;O88643

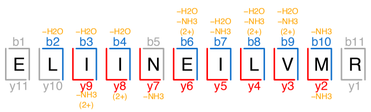

ELIINEILVMR
Score: 286 ; 1341.769 m/z; 671.89178 m/z; 1.1256 ppm; MULTI−MSMS

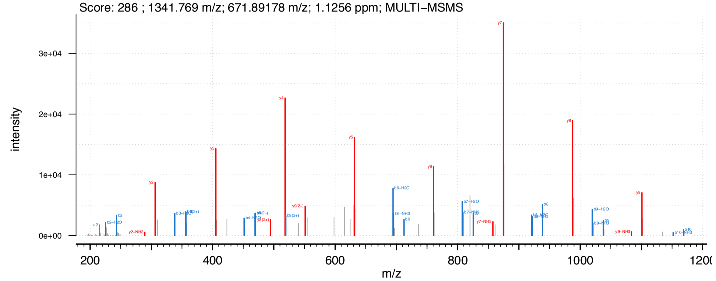

Raw File: Tiffy_20110729_FEP_265_PD20110720_Cdc42_mouseCerebellum_LF_rep2_GTPgS
Scan Number: 25078
Proteins:
B1GX81;A3KGC0;Q61036;B1GX80;A3KGC5;A3KGC1;Q61036−2;G5E884;O88643

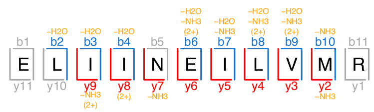

ELIINEILVMR
Score: 286 ; 1341.769 m/z; 671.89178 m/z; 1.1256 ppm; MULTI−MSMS

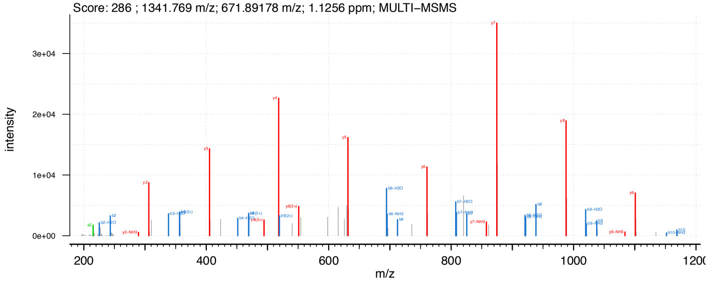

Raw File: Tiffy_20110729_FEP_265_PD20110720_Cdc42_mouseCerebellum_LF_rep2_GTPgS
Scan Number: 25078
Proteins:
B1GX81;A3KGC0;Q61036;B1GX80;A3KGC5;A3KGC1;Q61036−2;G5E884;O88643

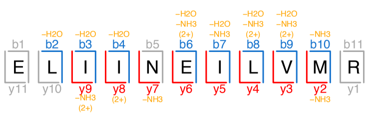

ELIINEILVMR
Score: 286 ; 1341.769 m/z; 671.89178 m/z; 1.1256 ppm; MULTI−MSMS

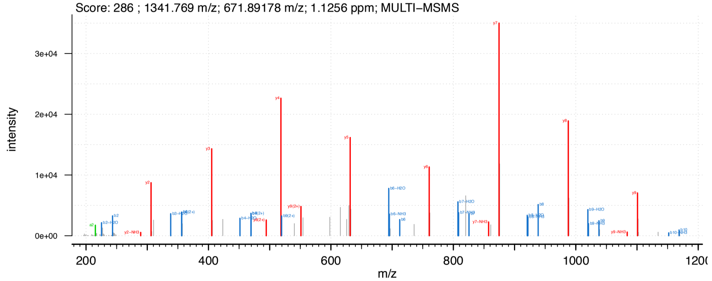

Raw File: Tiffy_20110729_FEP_265_PD20110720_Cdc42_mouseCerebellum_LF_rep2_GTPgS
Scan Number: 25078
Proteins:
B1GX81;A3KGC0;Q61036;B1GX80;A3KGC5;A3KGC1;Q61036−2;G5E884;O88643

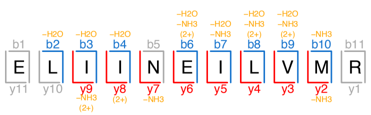

ELIINEILVMR
Score: 286 ; 1341.769 m/z; 671.89178 m/z; 1.1256 ppm; MULTI−MSMS

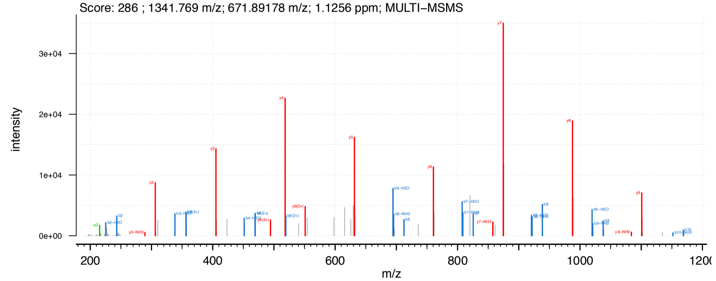

Raw File: Tiffy_20110729_FEP_265_PD20110720_Cdc42_mouseCerebellum_LF_rep2_GTPgS
Scan Number: 25078
Proteins:
B1GX81;A3KGC0;Q61036;B1GX80;A3KGC5;A3KGC1;Q61036−2;G5E884;O88643

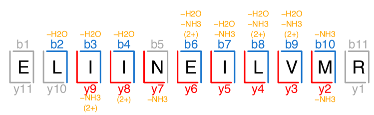

LLQTSNITK
Score: 202 ; 1016.5866 m/z; 509.30058 m/z; 0.43983 ppm; MULTI−MSMS

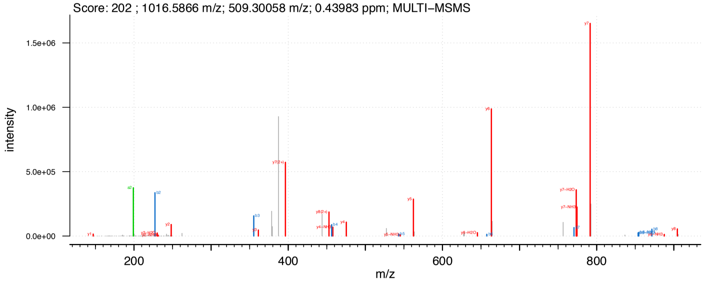

Raw File: Tiffy_20110729_FEP_265_PD20110720_Cdc42_mouseCerebellum_LF_rep2_GTPgS
Scan Number: 4184
Proteins:
B1GX81;A3KGC0;Q61036;B1GX80;A3KGC5;A3KGC4;A3KGC1;Q61036−2;A3KGC3;Q8CIN4;G5E884;O88643

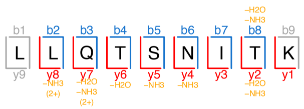

LLQTSNITK
Score: 202 ; 1016.5866 m/z; 509.30058 m/z; 0.43983 ppm; MULTI−MSMS

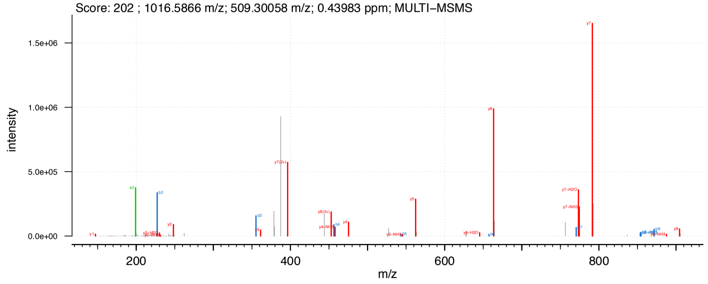

Raw File: Tiffy_20110729_FEP_265_PD20110720_Cdc42_mouseCerebellum_LF_rep2_GTPgS
Scan Number: 4184
Proteins:
B1GX81;A3KGC0;Q61036;B1GX80;A3KGC5;A3KGC4;A3KGC1;Q61036−2;A3KGC3;Q8CIN4;G5E884;O88643

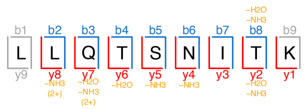

LLQTSNITK
Score: 202 ; 1016.5866 m/z; 509.30058 m/z; 0.43983 ppm; MULTI−MSMS

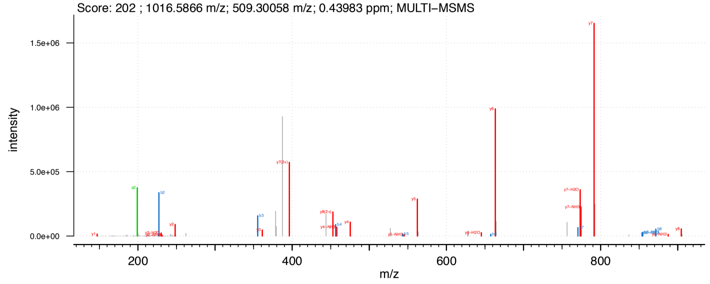

Raw File: Tiffy_20110729_FEP_265_PD20110720_Cdc42_mouseCerebellum_LF_rep2_GTPgS
Scan Number: 4184
Proteins:
B1GX81;A3KGC0;Q61036;B1GX80;A3KGC5;A3KGC4;A3KGC1;Q61036−2;A3KGC3;Q8CIN4;G5E884;O88643

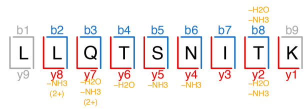

LLQTSNITK
Score: 202 ; 1016.5866 m/z; 509.30058 m/z; 0.43983 ppm; MULTI−MSMS

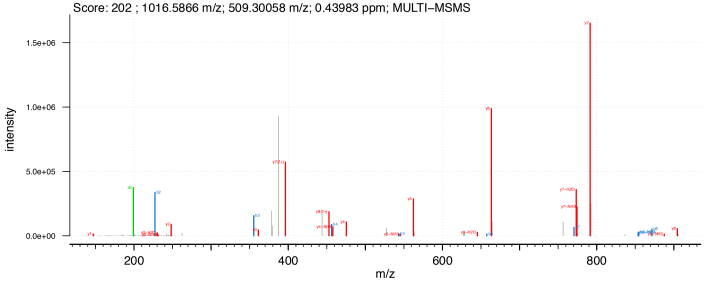

Raw File: Tiffy_20110729_FEP_265_PD20110720_Cdc42_mouseCerebellum_LF_rep2_GTPgS
Scan Number: 4184
Proteins:
B1GX81;A3KGC0;Q61036;B1GX80;A3KGC5;A3KGC4;A3KGC1;Q61036−2;A3KGC3;Q8CIN4;G5E884;O88643

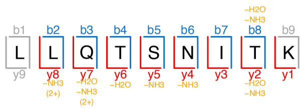

LLQTSNITK
Score: 202 ; 1016.5866 m/z; 509.30058 m/z; 0.43983 ppm; MULTI−MSMS

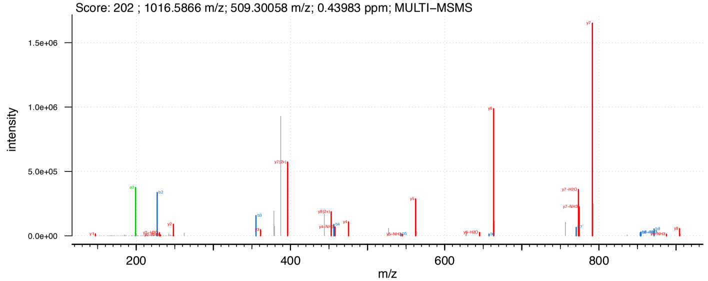

Raw File: Tiffy_20110729_FEP_265_PD20110720_Cdc42_mouseCerebellum_LF_rep2_GTPgS
Scan Number: 4184
Proteins:
B1GX81;A3KGC0;Q61036;B1GX80;A3KGC5;A3KGC4;A3KGC1;Q61036−2;A3KGC3;Q8CIN4;G5E884;O88643

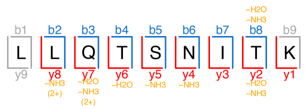

LLQTSNITK
Score: 202 ; 1016.5866 m/z; 509.30058 m/z; 0.43983 ppm; MULTI−MSMS

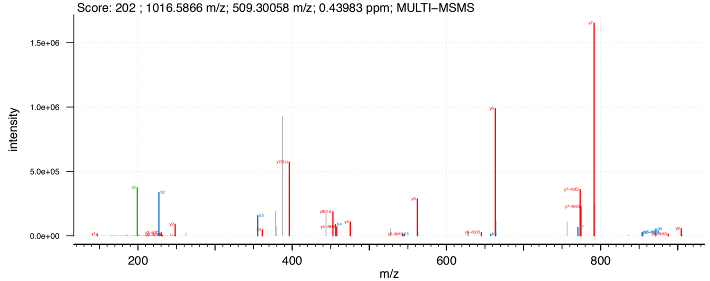

Raw File: Tiffy_20110729_FEP_265_PD20110720_Cdc42_mouseCerebellum_LF_rep2_GTPgS
Scan Number: 4184
Proteins:
B1GX81;A3KGC0;Q61036;B1GX80;A3KGC5;A3KGC4;A3KGC1;Q61036−2;A3KGC3;Q8CIN4;G5E884;O88643

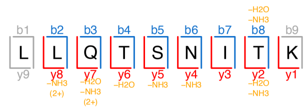

LLQTSNITK
Score: 202 ; 1016.5866 m/z; 509.30058 m/z; 0.43983 ppm; MULTI−MSMS

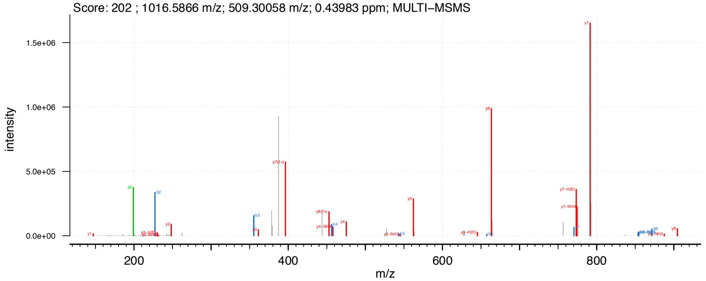

Raw File: Tiffy_20110729_FEP_265_PD20110720_Cdc42_mouseCerebellum_LF_rep2_GTPgS
Scan Number: 4184
Proteins:
B1GX81;A3KGC0;Q61036;B1GX80;A3KGC5;A3KGC4;A3KGC1;Q61036−2;A3KGC3;Q8CIN4;G5E884;O88643

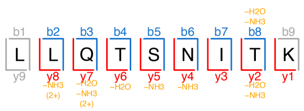

LLQTSNITK
Score: 202 ; 1016.5866 m/z; 509.30058 m/z; 0.43983 ppm; MULTI−MSMS

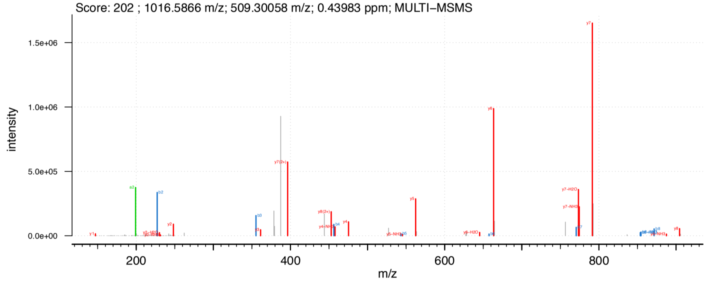

Raw File: Tiffy_20110729_FEP_265_PD20110720_Cdc42_mouseCerebellum_LF_rep2_GTPgS
Scan Number: 4184
Proteins:
B1GX81;A3KGC0;Q61036;B1GX80;A3KGC5;A3KGC4;A3KGC1;Q61036−2;A3KGC3;Q8CIN4;G5E884;O88643

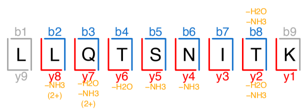

LLQTSNITK
Score: 202 ; 1016.5866 m/z; 509.30058 m/z; 0.43983 ppm; MULTI−MSMS

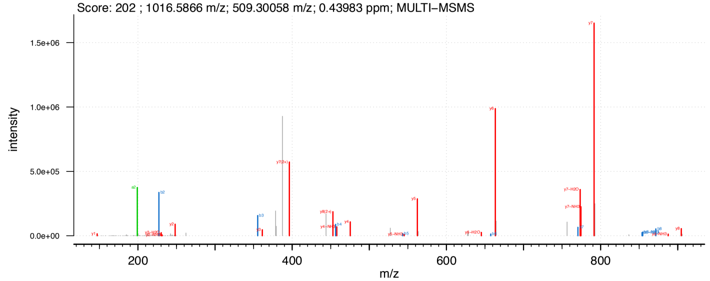

Raw File: Tiffy_20110729_FEP_265_PD20110720_Cdc42_mouseCerebellum_LF_rep2_GTPgS
Scan Number: 4184
Proteins:
B1GX81;A3KGC0;Q61036;B1GX80;A3KGC5;A3KGC4;A3KGC1;Q61036−2;A3KGC3;Q8CIN4;G5E884;O88643

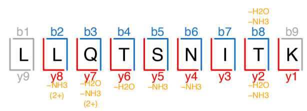

ELLQHPFLK
Score: 166 ; 1123.639 m/z; 562.82677 m/z; 0.512 ppm; MULTI−MSMS

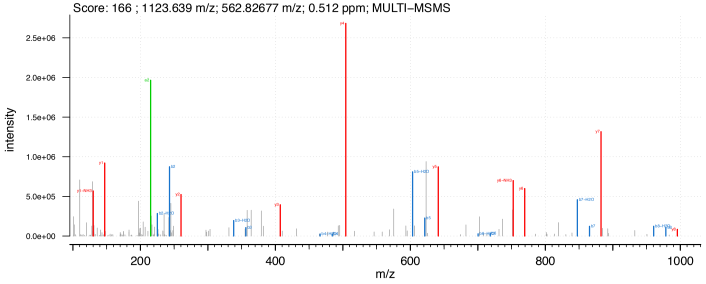

Raw File: Bibo_20111020_FEP_PD20111014_Rac1_mouseCortex_LF_rep2_GTPgS
Scan Number: 10996
Proteins:
B1GX81;A3KGC0;Q61036;B1GX80;A3KGC1;Q61036−2;Q8CIN4

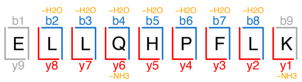

ELLQHPFLK
Score: 166 ; 1123.639 m/z; 562.82677 m/z; 0.512 ppm; MULTI−MSMS

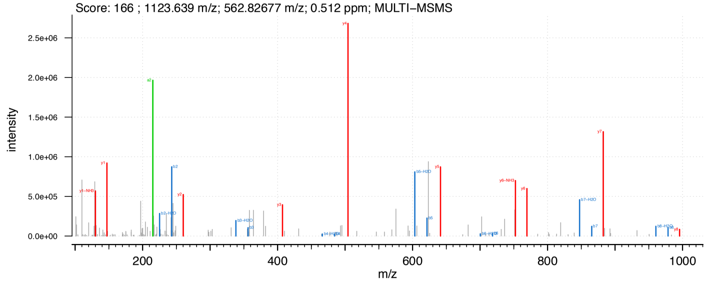

Raw File: Bibo_20111020_FEP_PD20111014_Rac1_mouseCortex_LF_rep2_GTPgS
Scan Number: 10996
Proteins:
B1GX81;A3KGC0;Q61036;B1GX80;A3KGC1;Q61036−2;Q8CIN4

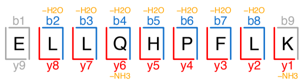

ELLQHPFLK
Score: 166 ; 1123.639 m/z; 562.82677 m/z; 0.512 ppm; MULTI−MSMS

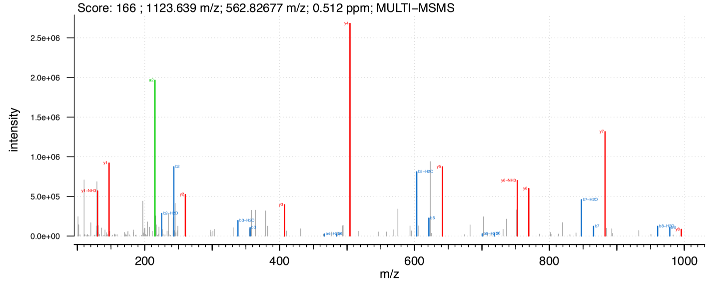

Raw File: Bibo_20111020_FEP_PD20111014_Rac1_mouseCortex_LF_rep2_GTPgS
Scan Number: 10996
Proteins:
B1GX81;A3KGC0;Q61036;B1GX80;A3KGC1;Q61036−2;Q8CIN4

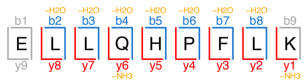

ELLQHPFLK
Score: 166 ; 1123.639 m/z; 562.82677 m/z; 0.512 ppm; MULTI−MSMS

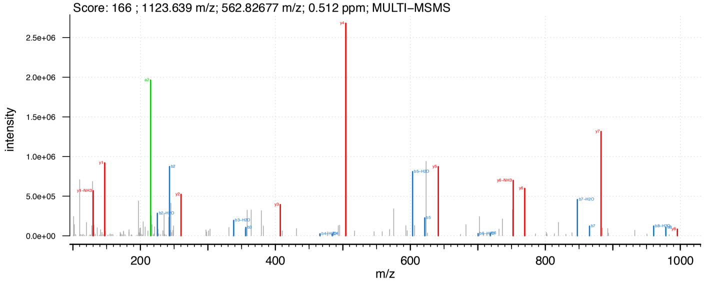

Raw File: Bibo_20111020_FEP_PD20111014_Rac1_mouseCortex_LF_rep2_GTPgS
Scan Number: 10996
Proteins:
B1GX81;A3KGC0;Q61036;B1GX80;A3KGC1;Q61036−2;Q8CIN4

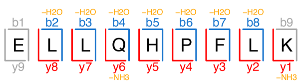

ELLQHPFLK
Score: 166 ; 1123.639 m/z; 562.82677 m/z; 0.512 ppm; MULTI−MSMS

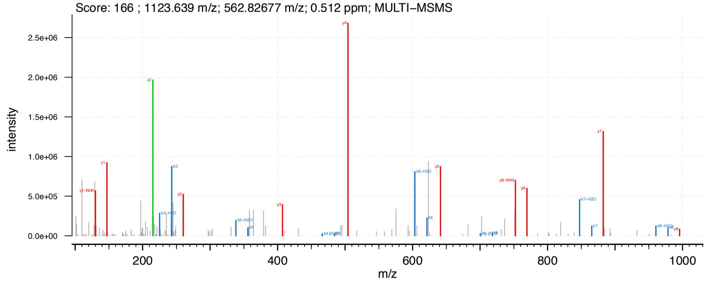

Raw File: Bibo_20111020_FEP_PD20111014_Rac1_mouseCortex_LF_rep2_GTPgS
Scan Number: 10996
Proteins:
B1GX81;A3KGC0;Q61036;B1GX80;A3KGC1;Q61036−2;Q8CIN4

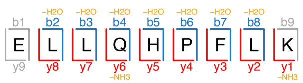

ELLQHPFLK
Score: 166 ; 1123.639 m/z; 562.82677 m/z; 0.512 ppm; MULTI−MSMS

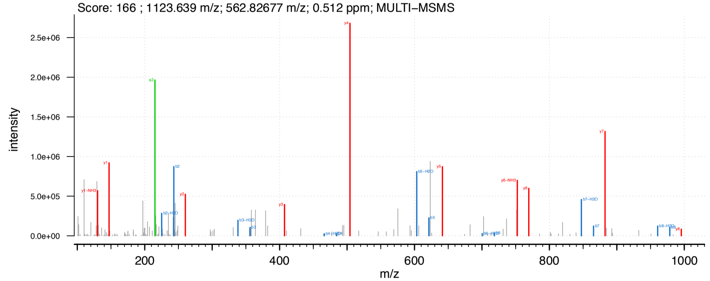

Raw File: Bibo_20111020_FEP_PD20111014_Rac1_mouseCortex_LF_rep2_GTPgS
Scan Number: 10996
Proteins:
B1GX81;A3KGC0;Q61036;B1GX80;A3KGC1;Q61036−2;Q8CIN4

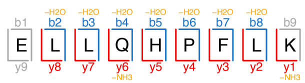

ELLQHPFLK
Score: 166 ; 1123.639 m/z; 562.82677 m/z; 0.512 ppm; MULTI−MSMS

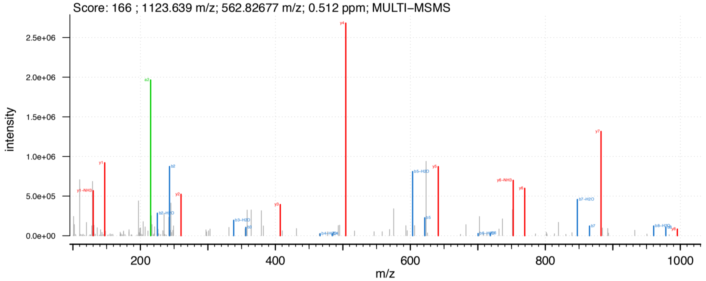

Raw File: Bibo_20111020_FEP_PD20111014_Rac1_mouseCortex_LF_rep2_GTPgS
Scan Number: 10996
Proteins:
B1GX81;A3KGC0;Q61036;B1GX80;A3KGC1;Q61036−2;Q8CIN4

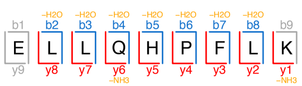

ELLQHPFLK
Score: 166 ; 1123.639 m/z; 562.82677 m/z; 0.512 ppm; MULTI−MSMS

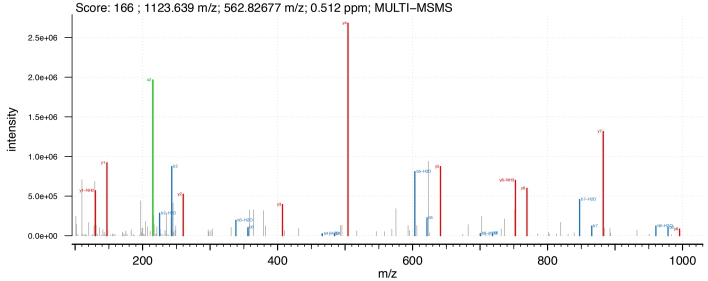

Raw File: Bibo_20111020_FEP_PD20111014_Rac1_mouseCortex_LF_rep2_GTPgS
Scan Number: 10996
Proteins:
B1GX81;A3KGC0;Q61036;B1GX80;A3KGC1;Q61036−2;Q8CIN4

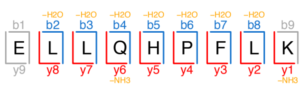

ELLQHPFLK
Score: 166 ; 1123.639 m/z; 562.82677 m/z; 0.512 ppm; MULTI−MSMS

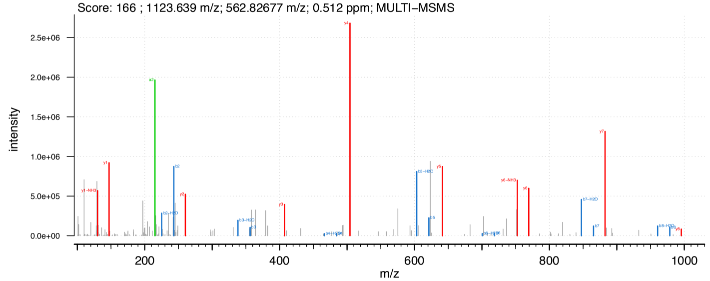

Raw File: Bibo_20111020_FEP_PD20111014_Rac1_mouseCortex_LF_rep2_GTPgS
Scan Number: 10996
Proteins:
B1GX81;A3KGC0;Q61036;B1GX80;A3KGC1;Q61036−2;Q8CIN4

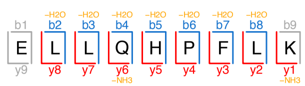

DLLHPSPEEEK
Score: 170 ; 1292.6248 m/z; 647.3197 m/z; 0.73712 ppm; MULTI−MSMS

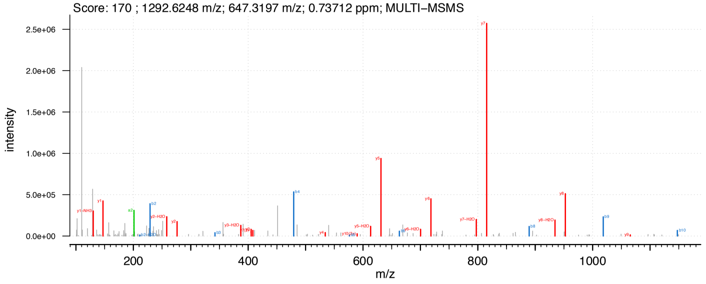

Raw File: Bibo_20111023_FEP_PD20111014_RhoA_mouseCortex_LF_rep1_GDP
Scan Number: 5016
Proteins:
Q6ZWU9

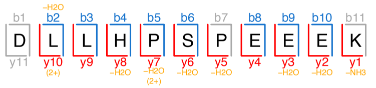

DLLHPSPEEEK
Score: 170 ; 1292.6248 m/z; 647.3197 m/z; 0.73712 ppm; MULTI−MSMS

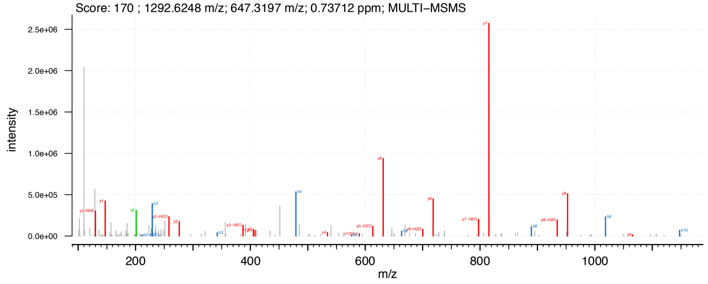

Raw File: Bibo_20111023_FEP_PD20111014_RhoA_mouseCortex_LF_rep1_GDP
Scan Number: 5016
Proteins:
Q6ZWU9

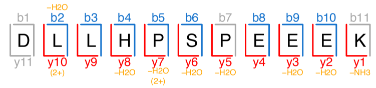

DLLHPSPEEEK
Score: 170 ; 1292.6248 m/z; 647.3197 m/z; 0.73712 ppm; MULTI−MSMS

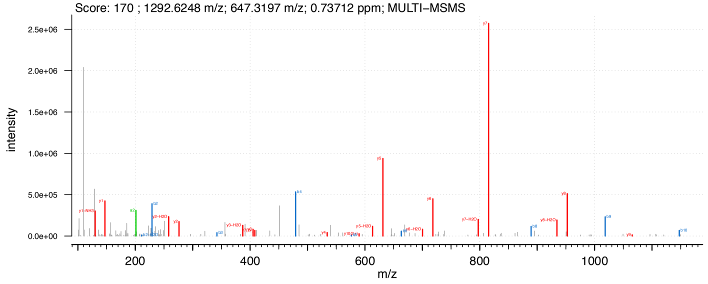

Raw File: Bibo_20111023_FEP_PD20111014_RhoA_mouseCortex_LF_rep1_GDP
Scan Number: 5016
Proteins:
Q6ZWU9

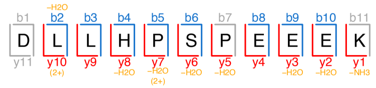

DLLHPSPEEEK
Score: 170 ; 1292.6248 m/z; 647.3197 m/z; 0.73712 ppm; MULTI−MSMS

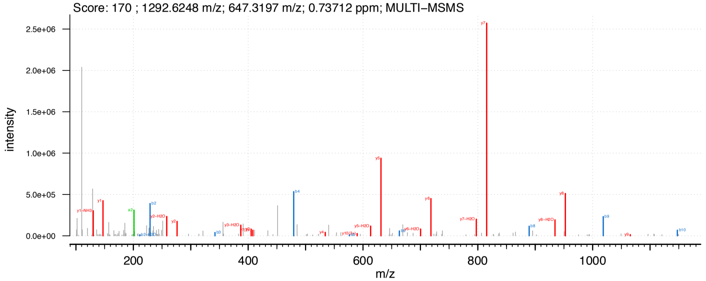

Raw File: Bibo_20111023_FEP_PD20111014_RhoA_mouseCortex_LF_rep1_GDP
Scan Number: 5016
Proteins:
Q6ZWU9

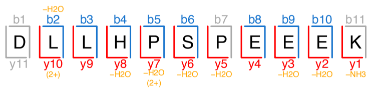

DLLHPSPEEEK
Score: 170 ; 1292.6248 m/z; 647.3197 m/z; 0.73712 ppm; MULTI−MSMS

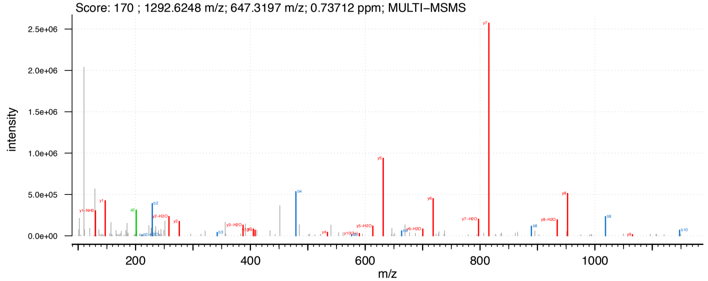

Raw File: Bibo_20111023_FEP_PD20111014_RhoA_mouseCortex_LF_rep1_GDP
Scan Number: 5016
Proteins:
Q6ZWU9

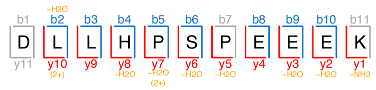

DLLHPSPEEEK
Score: 170 ; 1292.6248 m/z; 647.3197 m/z; 0.73712 ppm; MULTI−MSMS

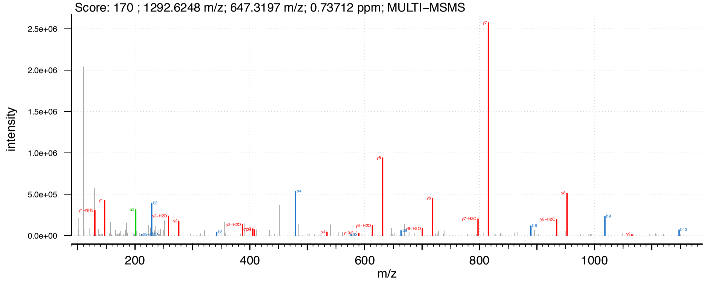

Raw File: Bibo_20111023_FEP_PD20111014_RhoA_mouseCortex_LF_rep1_GDP
Scan Number: 5016
Proteins:
Q6ZWU9

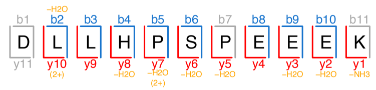

DLLHPSPEEEK
Score: 170 ; 1292.6248 m/z; 647.3197 m/z; 0.73712 ppm; MULTI−MSMS

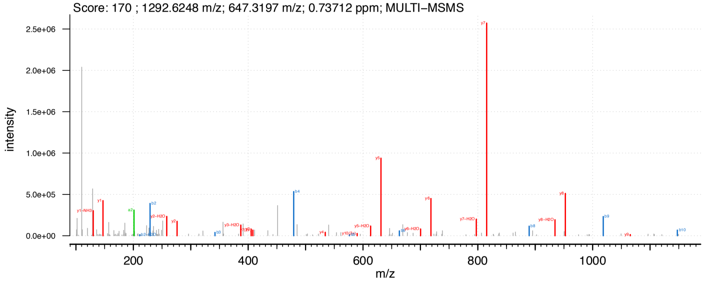

Raw File: Bibo_20111023_FEP_PD20111014_RhoA_mouseCortex_LF_rep1_GDP
Scan Number: 5016
Proteins:
Q6ZWU9

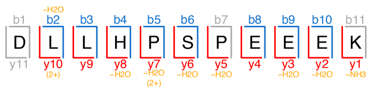

DLLHPSPEEEK
Score: 170 ; 1292.6248 m/z; 647.3197 m/z; 0.73712 ppm; MULTI−MSMS

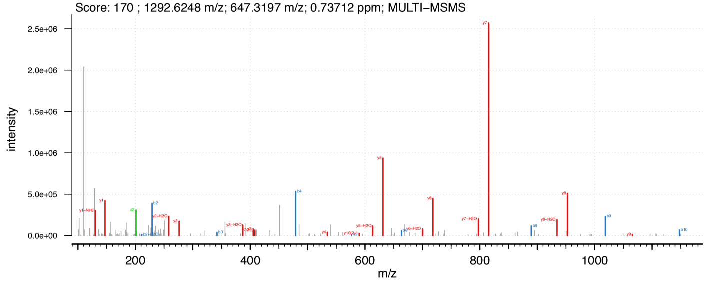

Raw File: Bibo_20111023_FEP_PD20111014_RhoA_mouseCortex_LF_rep1_GDP
Scan Number: 5016
Proteins:
Q6ZWU9

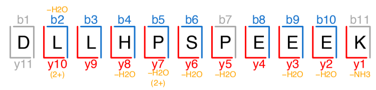

DLLHPSPEEEK
Score: 170 ; 1292.6248 m/z; 647.3197 m/z; 0.73712 ppm; MULTI−MSMS

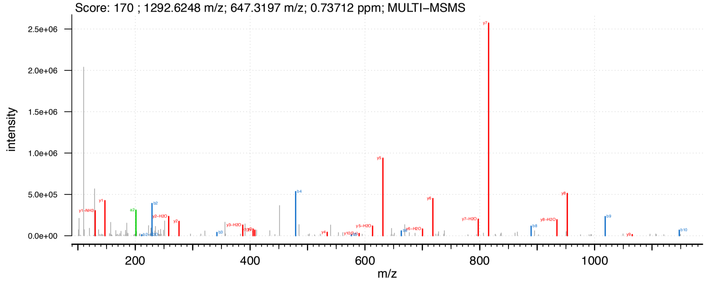

Raw File: Bibo_20111023_FEP_PD20111014_RhoA_mouseCortex_LF_rep1_GDP
Scan Number: 5016
Proteins:
Q6ZWU9

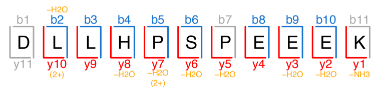

MLLLADMDVVNQLVAGGQFR
Score: 84 ; 2189.1337 m/z; 730.7185 m/z; −0.90365 ppm; MULTI−MSMS

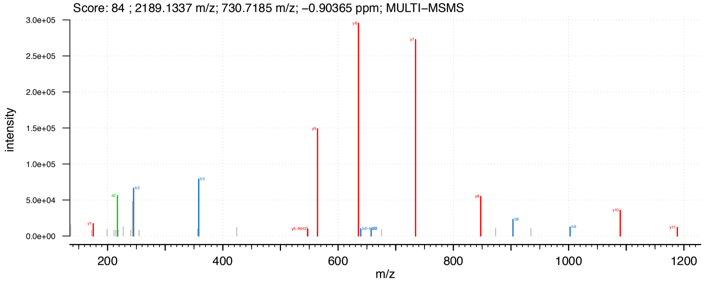

Raw File: Bibo_20111023_FEP_PD20111014_RhoA_mouseCortex_LF_rep1_GDP
Scan Number: 74090
Proteins:
B1AVA7;Q62277

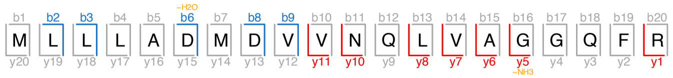

MLLLADMDVVNQLVAGGQFR
Score: 84 ; 2189.1337 m/z; 730.7185 m/z; −0.90365 ppm; MULTI−MSMS

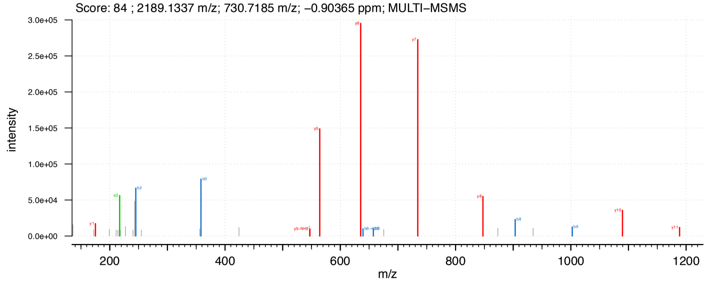

Raw File: Bibo_20111023_FEP_PD20111014_RhoA_mouseCortex_LF_rep1_GDP
Scan Number: 74090
Proteins:
B1AVA7;Q62277

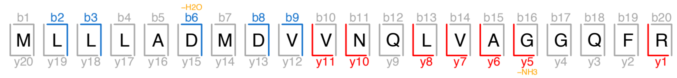

MLLLADMDVVNQLVAGGQFR
Score: 84 ; 2189.1337 m/z; 730.7185 m/z; −0.90365 ppm; MULTI−MSMS

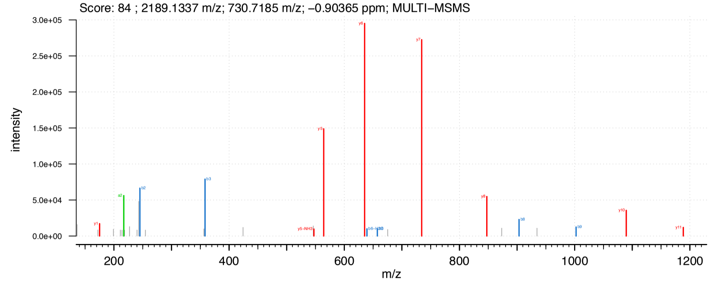

Raw File: Bibo_20111023_FEP_PD20111014_RhoA_mouseCortex_LF_rep1_GDP
Scan Number: 74090
Proteins:
B1AVA7;Q62277

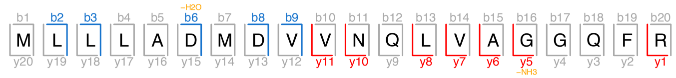

MLLLADMDVVNQLVAGGQFR
Score: 84 ; 2189.1337 m/z; 730.7185 m/z; −0.90365 ppm; MULTI−MSMS

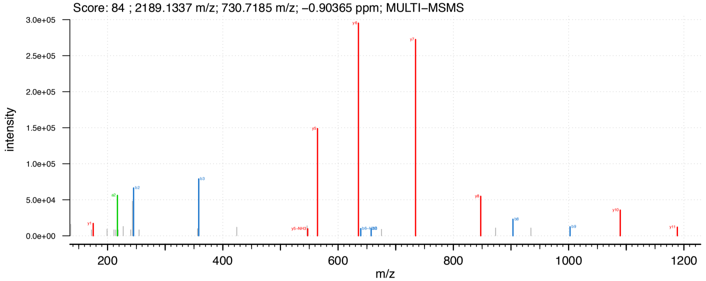

Raw File: Bibo_20111023_FEP_PD20111014_RhoA_mouseCortex_LF_rep1_GDP
Scan Number: 74090
Proteins:
B1AVA7;Q62277

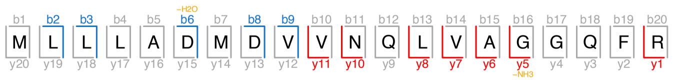

MLLLADMDVVNQLVAGGQFR
Score: 84 ; 2189.1337 m/z; 730.7185 m/z; −0.90365 ppm; MULTI−MSMS

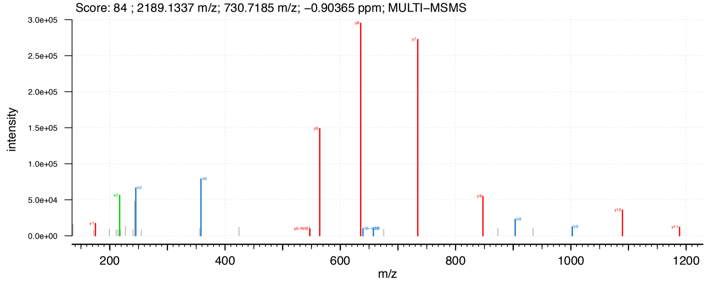

Raw File: Bibo_20111023_FEP_PD20111014_RhoA_mouseCortex_LF_rep1_GDP
Scan Number: 74090
Proteins:
B1AVA7;Q62277

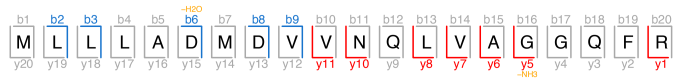

MLLLADMDVVNQLVAGGQFR
Score: 84 ; 2189.1337 m/z; 730.7185 m/z; −0.90365 ppm; MULTI−MSMS

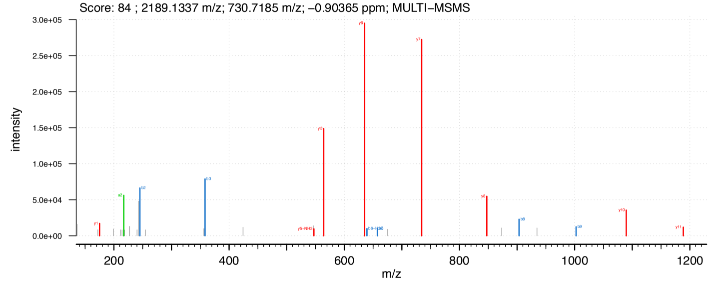

Raw File: Bibo_20111023_FEP_PD20111014_RhoA_mouseCortex_LF_rep1_GDP
Scan Number: 74090
Proteins:
B1AVA7;Q62277

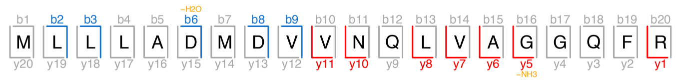

MLLLADMDVVNQLVAGGQFR
Score: 84 ; 2189.1337 m/z; 730.7185 m/z; −0.90365 ppm; MULTI−MSMS

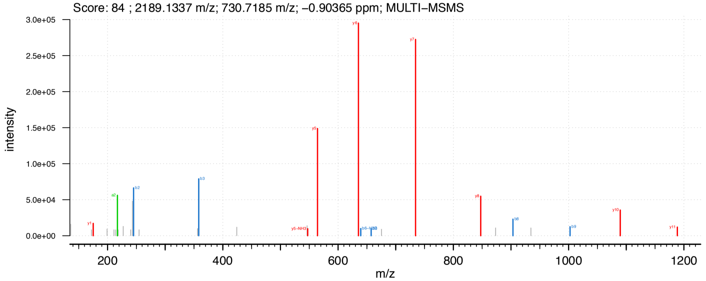

Raw File: Bibo_20111023_FEP_PD20111014_RhoA_mouseCortex_LF_rep1_GDP
Scan Number: 74090
Proteins:
B1AVA7;Q62277

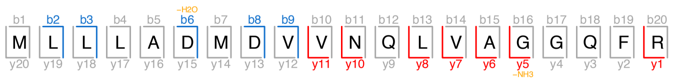

MLLLADMDVVNQLVAGGQFR
Score: 84 ; 2189.1337 m/z; 730.7185 m/z; −0.90365 ppm; MULTI−MSMS

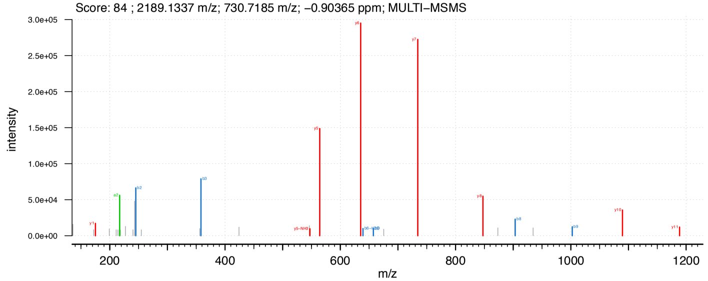

Raw File: Bibo_20111023_FEP_PD20111014_RhoA_mouseCortex_LF_rep1_GDP
Scan Number: 74090
Proteins:
B1AVA7;Q62277

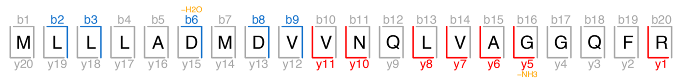

MLLLADMDVVNQLVAGGQFR
Score: 84 ; 2189.1337 m/z; 730.7185 m/z; −0.90365 ppm; MULTI−MSMS

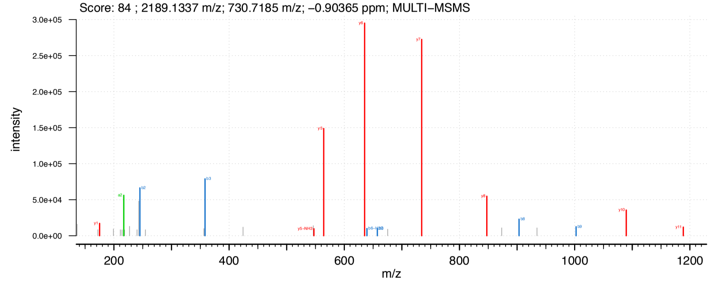

Raw File: Bibo_20111023_FEP_PD20111014_RhoA_mouseCortex_LF_rep1_GDP
Scan Number: 74090
Proteins:
B1AVA7;Q62277

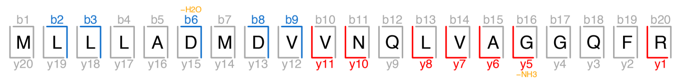

RLVQSPNSYFMDVK
Score: 170 ; 1682.845 m/z; 842.42979 m/z; –0.07078 ppm; MULTI–MSMS

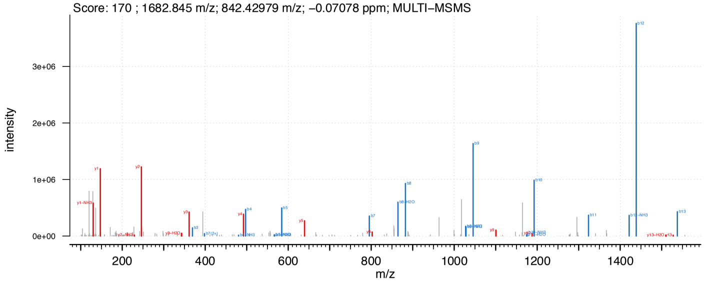

Raw File: Bibo_20111019_FEP_PD20111014_RhoA_mouseCortex_LF_rep3_GDP
Scan Number: 13895
Proteins:
Q6ZWU9;E9QAB4

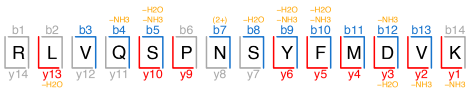

RLVQSPNSYFMDVK
Score: 170 ; 1682.845 m/z; 842.42979 m/z; –0.07078 ppm; MULTI–MSMS

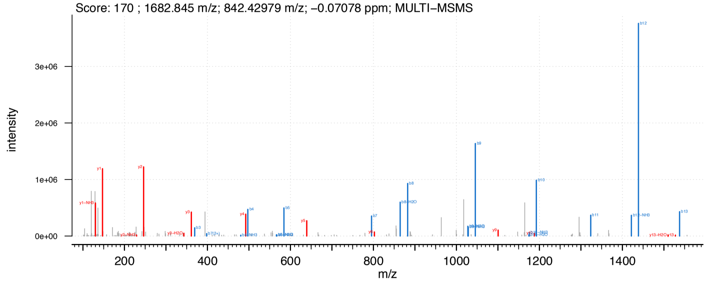

Raw File: Bibo_20111019_FEP_PD20111014_RhoA_mouseCortex_LF_rep3_GDP
Scan Number: 13895
Proteins:
Q6ZWU9;E9QAB4

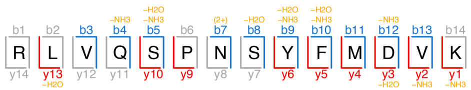

RLVQSPNSYFMDVK
Score: 170 ; 1682.845 m/z; 842.42979 m/z; –0.07078 ppm; MULTI–MSMS

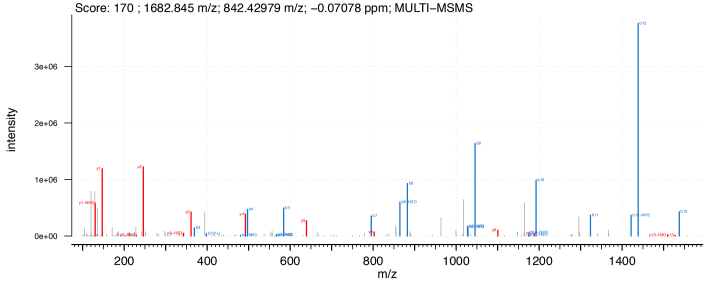

Raw File: Bibo_20111019_FEP_PD20111014_RhoA_mouseCortex_LF_rep3_GDP
Scan Number: 13895
Proteins:
Q6ZWU9;E9QAB4

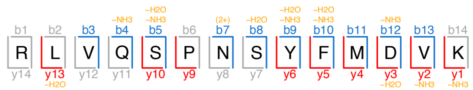

RLVQSPNSYFMDVK
Score: 170 ; 1682.845 m/z; 842.42979 m/z; –0.07078 ppm; MULTI–MSMS

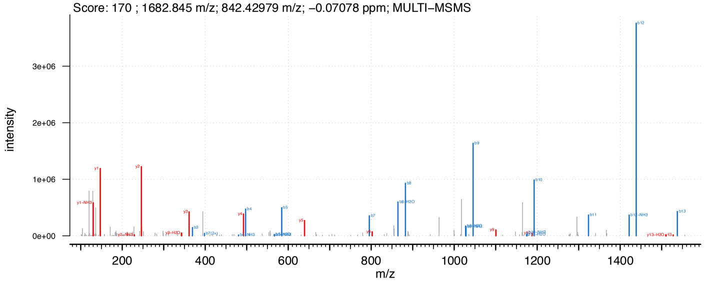

Raw File: Bibo_20111019_FEP_PD20111014_RhoA_mouseCortex_LF_rep3_GDP
Scan Number: 13895
Proteins:
Q6ZWU9;E9QAB4

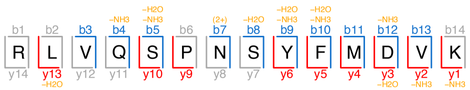

RLVQSPNSYFMDVK
Score: 170 ; 1682.845 m/z; 842.42979 m/z; –0.07078 ppm; MULTI–MSMS

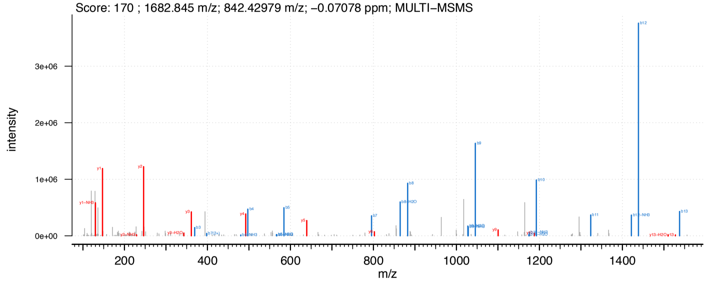

Raw File: Bibo_20111019_FEP_PD20111014_RhoA_mouseCortex_LF_rep3_GDP
Scan Number: 13895
Proteins:
Q6ZWU9;E9QAB4

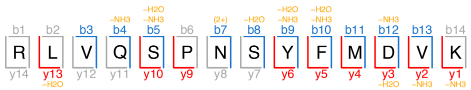

RLVQSPNSYFMDVK
Score: 170 ; 1682.845 m/z; 842.42979 m/z; –0.07078 ppm; MULTI–MSMS

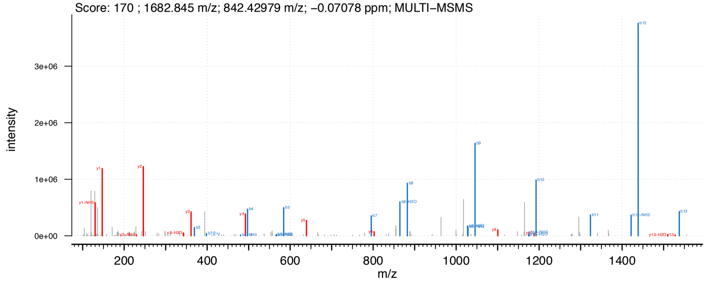

Raw File: Bibo_20111019_FEP_PD20111014_RhoA_mouseCortex_LF_rep3_GDP
Scan Number: 13895
Proteins:
Q6ZWU9;E9QAB4

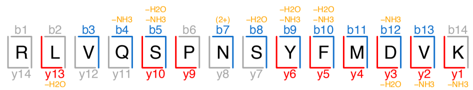

RLVQSPNSYFMDVK
Score: 170 ; 1682.845 m/z; 842.42979 m/z; –0.07078 ppm; MULTI–MSMS

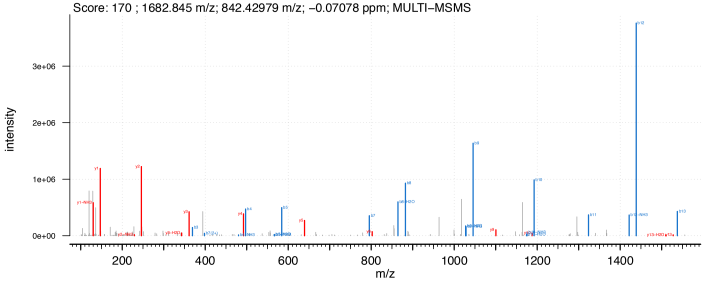

Raw File: Bibo_20111019_FEP_PD20111014_RhoA_mouseCortex_LF_rep3_GDP
Scan Number: 13895
Proteins:
Q6ZWU9;E9QAB4

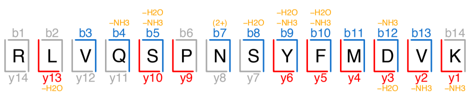

RLVQSPNSYFMDVK
Score: 170 ; 1682.845 m/z; 842.42979 m/z; –0.07078 ppm; MULTI–MSMS

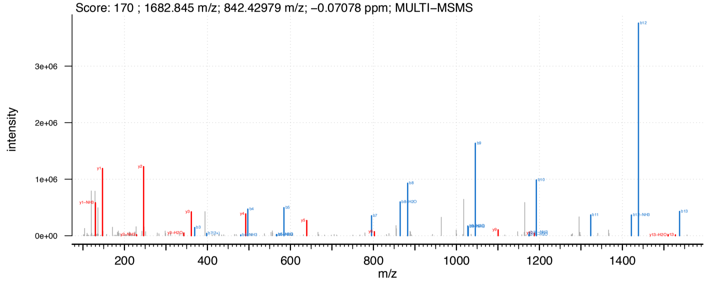

Raw File: Bibo_20111019_FEP_PD20111014_RhoA_mouseCortex_LF_rep3_GDP
Scan Number: 13895
Proteins:
Q6ZWU9;E9QAB4

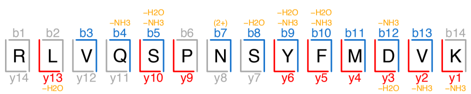

RLVQSPNSYFMDVK
Score: 170 ; 1682.845 m/z; 842.42979 m/z; –0.07078 ppm; MULTI–MSMS

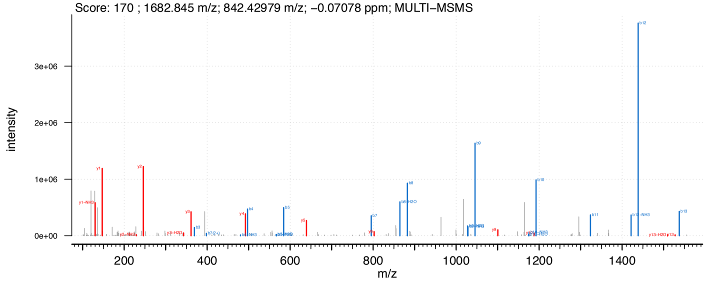

Raw File: Bibo_20111019_FEP_PD20111014_RhoA_mouseCortex_LF_rep3_GDP
Scan Number: 13895
Proteins:
Q6ZWU9;E9QAB4

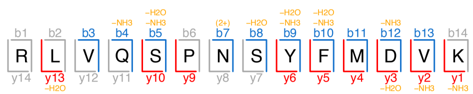

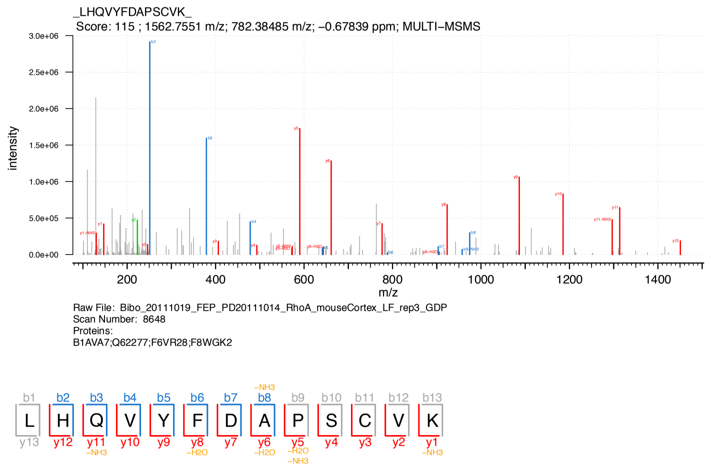
LHQVYFDAPSCVK
Score: 115 ; 1562.7551 m/z; 782.38485 m/z; −0.67839 ppm; MULTI−MSMS
intensity
m/z
Raw File: Bibo_20111019_FEP_PD20111014_RhoA_mouseCortex_LF_rep3_GDP
Scan Number: 8648
Proteins:
B1AVA7;Q62277;F6VR28;F8WGK2
L H Q V Y F D A P S C V K

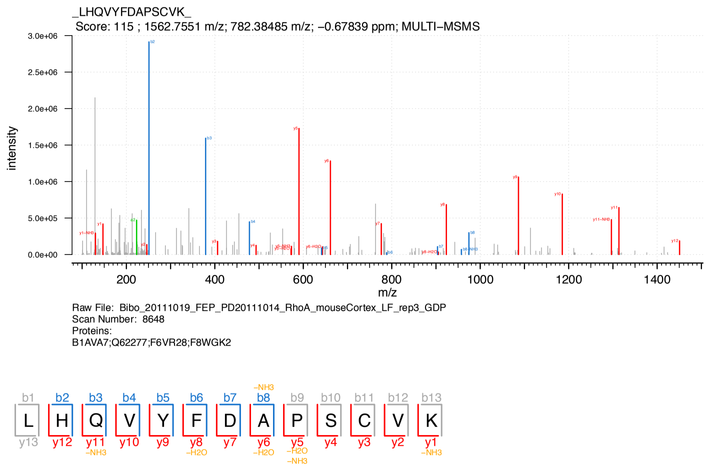
LHQVYFDAPSCVK
Score: 115 ; 1562.7551 m/z; 782.38485 m/z; −0.67839 ppm; MULTI−MSMS
intensity
m/z
Raw File: Bibo_20111019_FEP_PD20111014_RhoA_mouseCortex_LF_rep3_GDP
Scan Number: 8648
Proteins:
B1AVA7;Q62277;F6VR28;F8WGK2
L H Q V Y F D A P S C V K

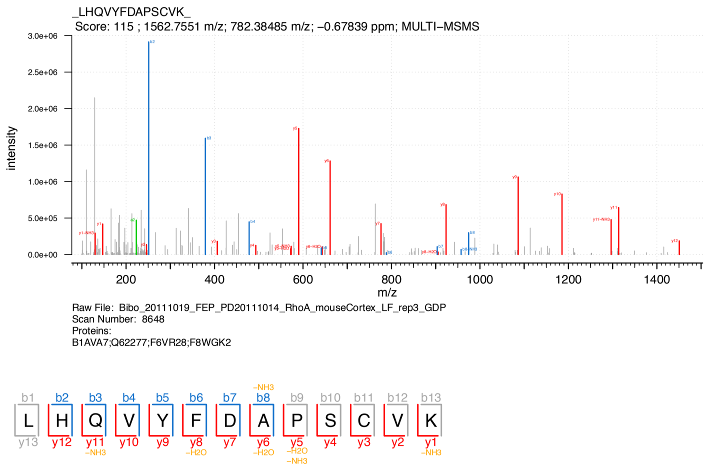
LHQVYFDAPSCVK
Score: 115 ; 1562.7551 m/z; 782.38485 m/z; −0.67839 ppm; MULTI−MSMS
intensity
m/z
Raw File: Bibo_20111019_FEP_PD20111014_RhoA_mouseCortex_LF_rep3_GDP
Scan Number: 8648
Proteins:
B1AVA7;Q62277;F6VR28;F8WGK2
L H Q V Y F D A P S C V K

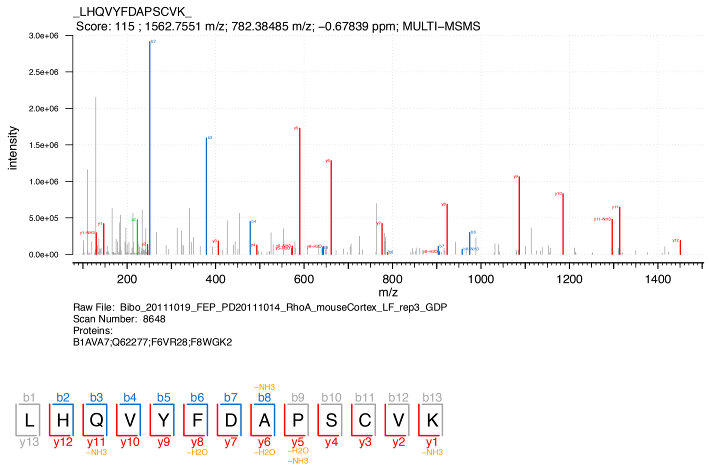
LHQVYFDAPSCVK
Score: 115 ; 1562.7551 m/z; 782.38485 m/z; −0.67839 ppm; MULTI−MSMS
intensity
m/z
Raw File: Bibo_20111019_FEP_PD20111014_RhoA_mouseCortex_LF_rep3_GDP
Scan Number: 8648
Proteins:
B1AVA7;Q62277;F6VR28;F8WGK2
L H Q V Y F D A P S C V K

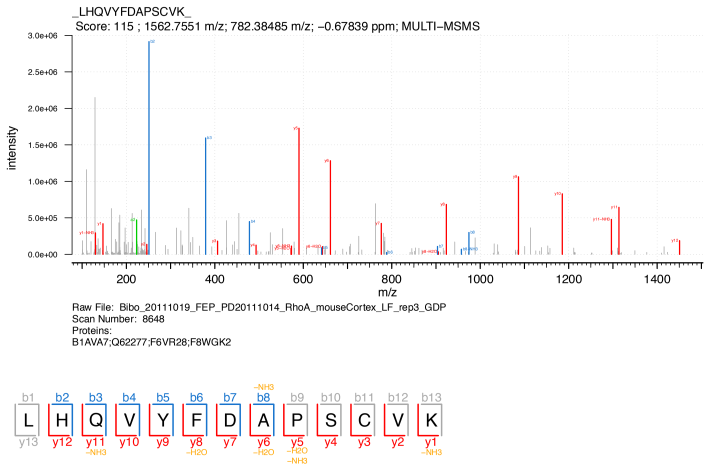
LHQVYFDAPSCVK
Score: 115 ; 1562.7551 m/z; 782.38485 m/z; −0.67839 ppm; MULTI−MSMS
intensity
m/z
Raw File: Bibo_20111019_FEP_PD20111014_RhoA_mouseCortex_LF_rep3_GDP
Scan Number: 8648
Proteins:
B1AVA7;Q62277;F6VR28;F8WGK2
L H Q V Y F D A P S C V K

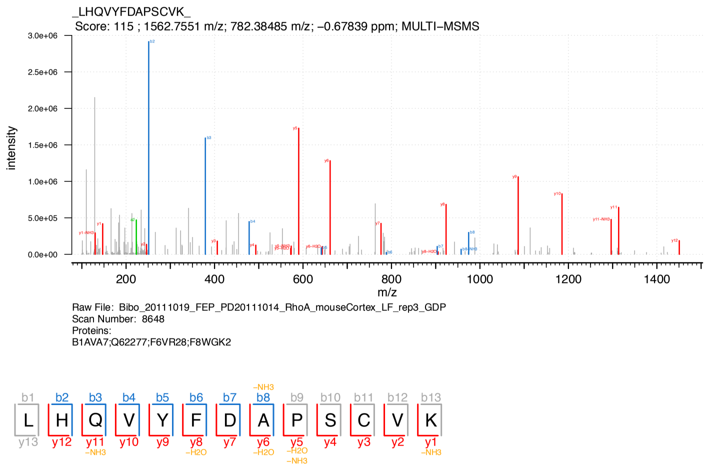
LHQVYFDAPSCVK
Score: 115 ; 1562.7551 m/z; 782.38485 m/z; −0.67839 ppm; MULTI−MSMS
intensity
m/z
Raw File: Bibo_20111019_FEP_PD20111014_RhoA_mouseCortex_LF_rep3_GDP
Scan Number: 8648
Proteins:
B1AVA7;Q62277;F6VR28;F8WGK2
L H Q V Y F D A P S C V K

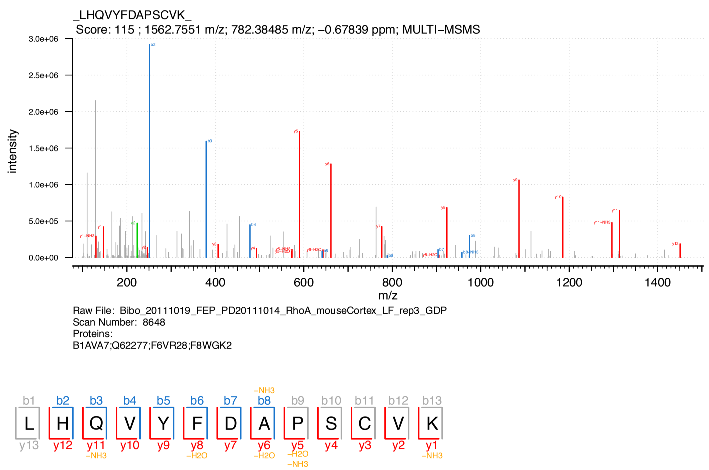
LHQVYFDAPSCVK
Score: 115 ; 1562.7551 m/z; 782.38485 m/z; −0.67839 ppm; MULTI−MSMS
intensity
m/z
Raw File: Bibo_20111019_FEP_PD20111014_RhoA_mouseCortex_LF_rep3_GDP
Scan Number: 8648
Proteins:
B1AVA7;Q62277;F6VR28;F8WGK2
L H Q V Y F D A P S C V K

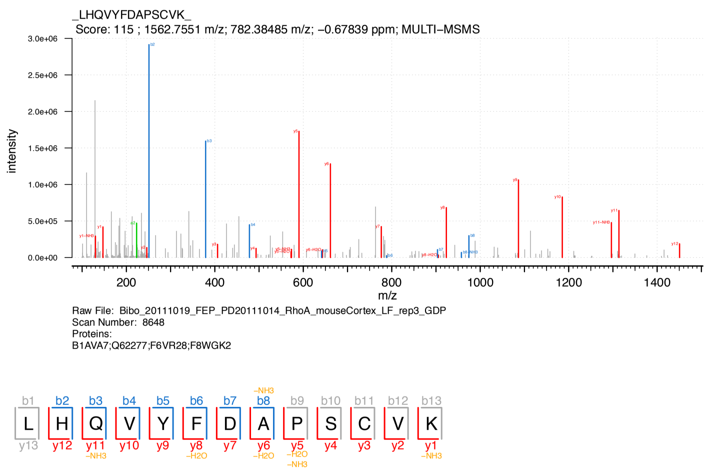
LHQVYFDAPSCVK
Score: 115 ; 1562.7551 m/z; 782.38485 m/z; −0.67839 ppm; MULTI−MSMS
intensity
m/z
Raw File: Bibo_20111019_FEP_PD20111014_RhoA_mouseCortex_LF_rep3_GDP
Scan Number: 8648
Proteins:
B1AVA7;Q62277;F6VR28;F8WGK2
L H Q V Y F D A P S C V K

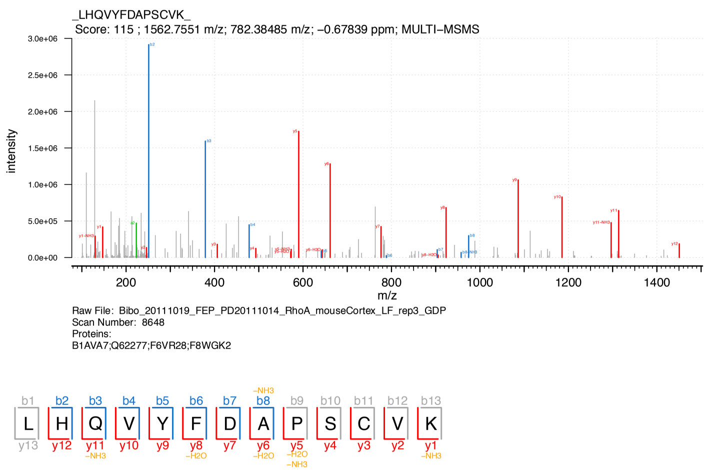
LHQVYFDAPSCVK
Score: 115 ; 1562.7551 m/z; 782.38485 m/z; −0.67839 ppm; MULTI−MSMS
intensity
m/z
Raw File: Bibo_20111019_FEP_PD20111014_RhoA_mouseCortex_LF_rep3_GDP
Scan Number: 8648
Proteins:
B1AVA7;Q62277;F6VR28;F8WGK2
L H Q V Y F D A P S C V K

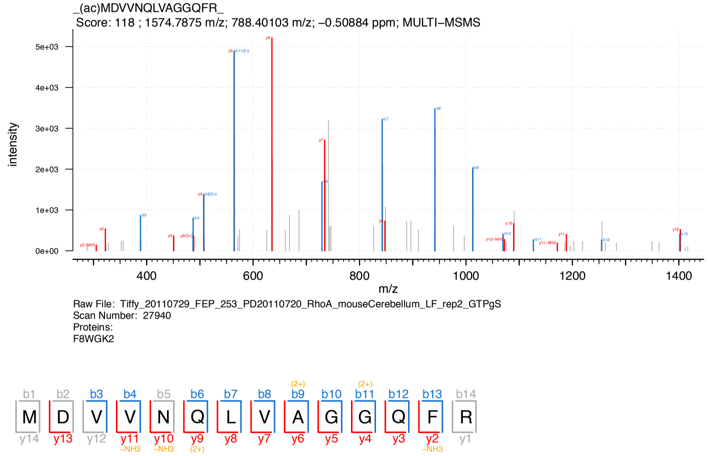
(ac)MDVVNQLVAGGQFR
Score: 118 ; 1574.7875 m/z; 788.40103 m/z; −0.50884 ppm; MULTI−MSMS
intensity
m/z
Raw File: Tiffy_20110729_FEP_253_PD20110720_RhoA_mouseCerebellum_LF_rep2_GTPgS
Scan Number: 27940
Proteins:
F8WGK2
M D V V N Q L V A G G Q F R
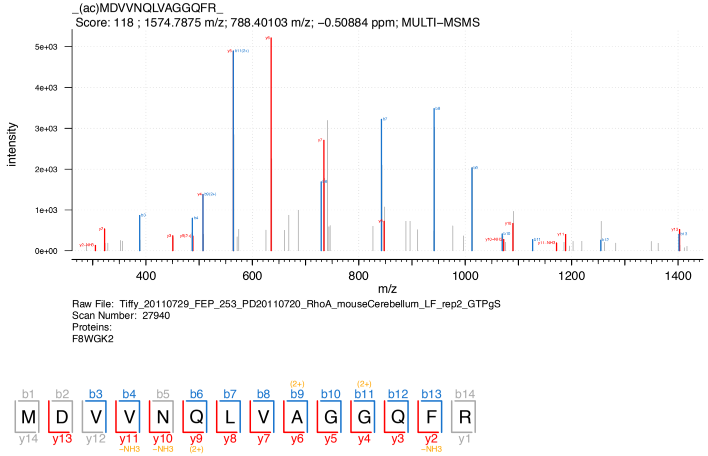
(ac)MDVVNQLVAGGQFR
Score: 118 ; 1574.7875 m/z; 788.40103 m/z; −0.50884 ppm; MULTI−MSMS
intensity
m/z
Raw File: Tiffy_20110729_FEP_253_PD20110720_RhoA_mouseCerebellum_LF_rep2_GTPgS
Scan Number: 27940
Proteins:
F8WGK2
M D V V N Q L V A G G Q F R
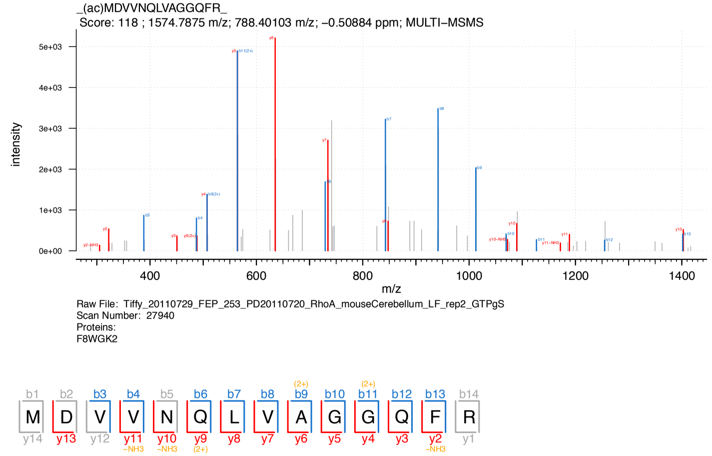
(ac)MDVVNQLVAGGQFR
Score: 118 ; 1574.7875 m/z; 788.40103 m/z; −0.50884 ppm; MULTI−MSMS
intensity
m/z
Raw File: Tiffy_20110729_FEP_253_PD20110720_RhoA_mouseCerebellum_LF_rep2_GTPgS
Scan Number: 27940
Proteins:
F8WGK2
M D V V N Q L V A G G Q F R
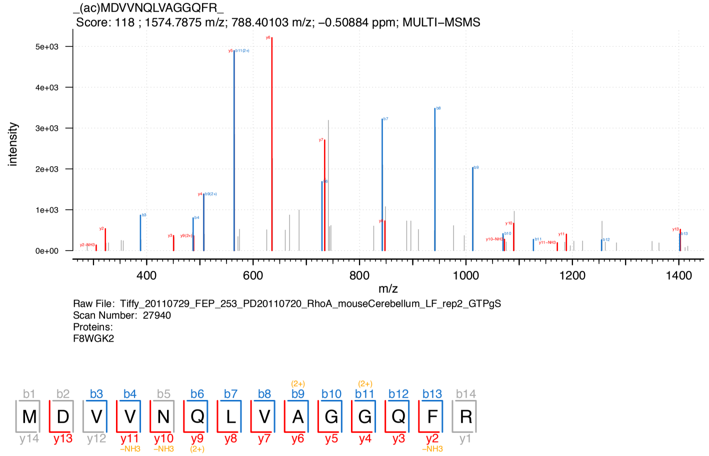
(ac)MDVVNQLVAGGQFR
Score: 118 ; 1574.7875 m/z; 788.40103 m/z; −0.50884 ppm; MULTI−MSMS
intensity
m/z
Raw File: Tiffy_20110729_FEP_253_PD20110720_RhoA_mouseCerebellum_LF_rep2_GTPgS
Scan Number: 27940
Proteins:
F8WGK2
M D V V N Q L V A G G Q F R
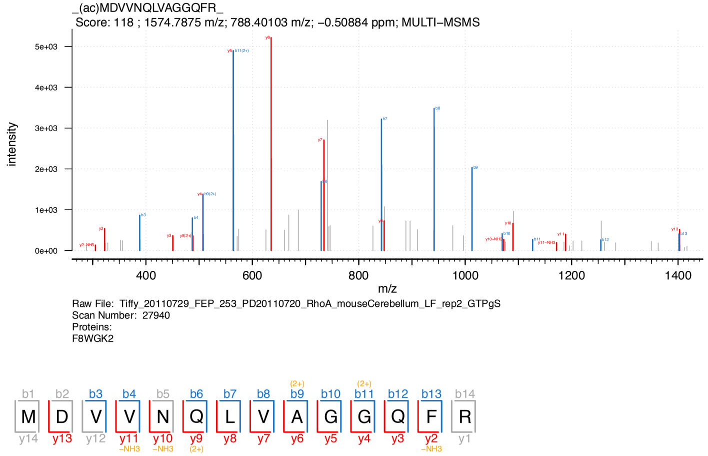
(ac)MDVVNQLVAGGQFR
Score: 118 ; 1574.7875 m/z; 788.40103 m/z; −0.50884 ppm; MULTI−MSMS
intensity
m/z
Raw File: Tiffy_20110729_FEP_253_PD20110720_RhoA_mouseCerebellum_LF_rep2_GTPgS
Scan Number: 27940
Proteins:
F8WGK2
M D V V N Q L V A G G Q F R
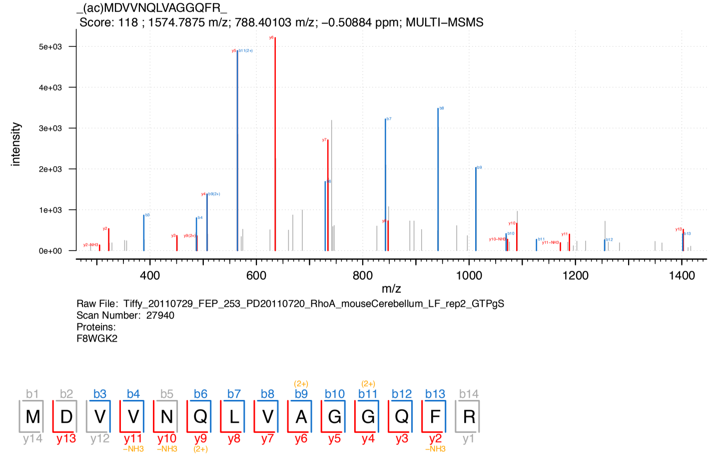
(ac)MDVVNQLVAGGQFR
Score: 118 ; 1574.7875 m/z; 788.40103 m/z; −0.50884 ppm; MULTI−MSMS
intensity
m/z
Raw File: Tiffy_20110729_FEP_253_PD20110720_RhoA_mouseCerebellum_LF_rep2_GTPgS
Scan Number: 27940
Proteins:
F8WGK2
M D V V N Q L V A G G Q F R
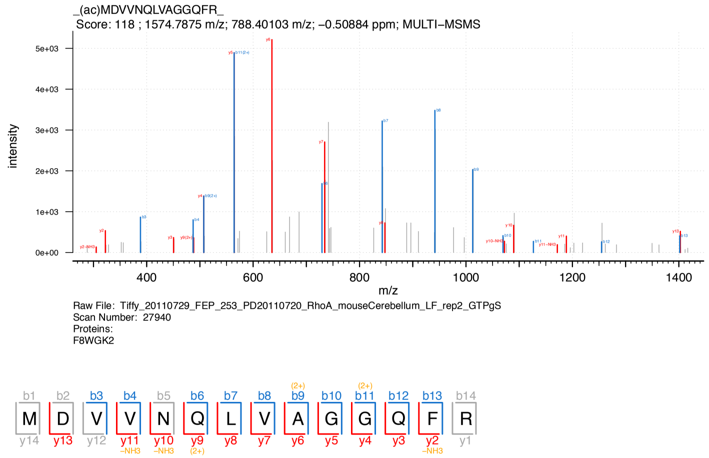
(ac)MDVVNQLVAGGQFR
Score: 118 ; 1574.7875 m/z; 788.40103 m/z; −0.50884 ppm; MULTI−MSMS
intensity
m/z
Raw File: Tiffy_20110729_FEP_253_PD20110720_RhoA_mouseCerebellum_LF_rep2_GTPgS
Scan Number: 27940
Proteins:
F8WGK2
M D V V N Q L V A G G Q F R
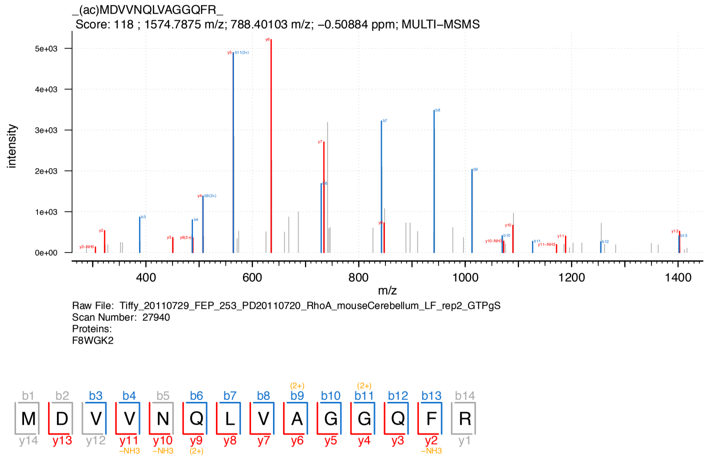
(ac)MDVVNQLVAGGQFR
Score: 118 ; 1574.7875 m/z; 788.40103 m/z; −0.50884 ppm; MULTI−MSMS
intensity
m/z
Raw File: Tiffy_20110729_FEP_253_PD20110720_RhoA_mouseCerebellum_LF_rep2_GTPgS
Scan Number: 27940
Proteins:
F8WGK2
M D V V N Q L V A G G Q F R
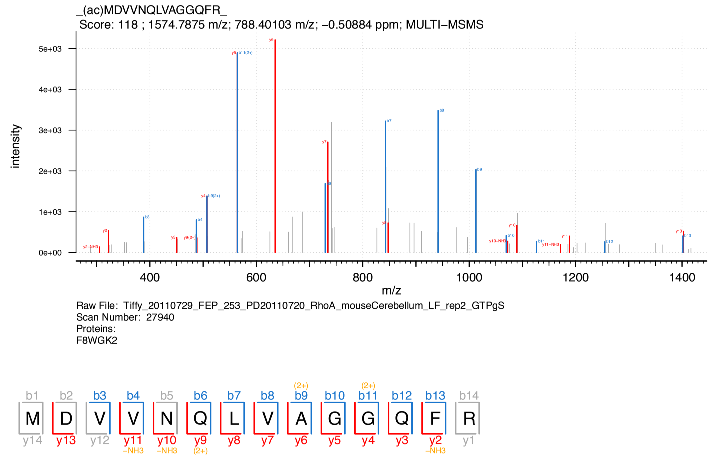
(ac)MDVVNQLVAGGQFR
Score: 118 ; 1574.7875 m/z; 788.40103 m/z; −0.50884 ppm; MULTI−MSMS
intensity
m/z
Raw File: Tiffy_20110729_FEP_253_PD20110720_RhoA_mouseCerebellum_LF_rep2_GTPgS
Scan Number: 27940
Proteins:
F8WGK2
M D V V N Q L V A G G Q F R

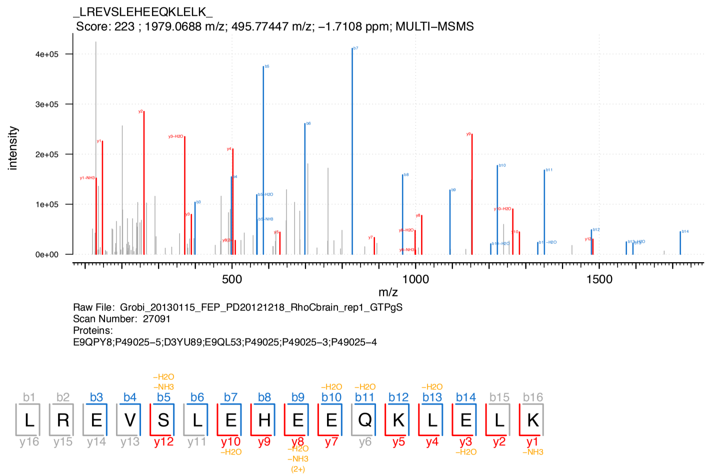
LREVSLEHEEQKLELK
Score: 223 ; 1979.0688 m/z; 495.77447 m/z; −1.7108 ppm; MULTI−MSMS
intensity
m/z
Raw File: Grobi_20130115_FEP_PD20121218_RhoCbrain_rep1_GTPgS
Scan Number: 27091
Proteins:
E9QPY8;P49025−5;D3YU89;E9QL53;P49025;P49025−3;P49025−4
L R E V S L E H E E Q K L E L K
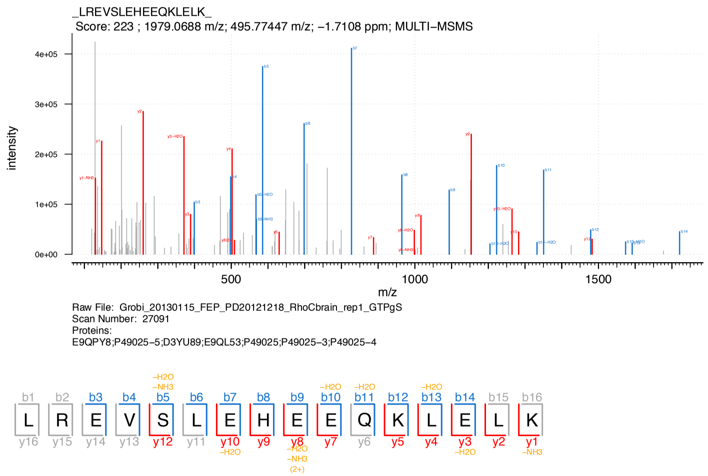
LREVSLEHEEQKLELK
Score: 223 ; 1979.0688 m/z; 495.77447 m/z; −1.7108 ppm; MULTI−MSMS
intensity
m/z
Raw File: Grobi_20130115_FEP_PD20121218_RhoCbrain_rep1_GTPgS
Scan Number: 27091
Proteins:
E9QPY8;P49025−5;D3YU89;E9QL53;P49025;P49025−3;P49025−4
L R E V S L E H E E Q K L E L K
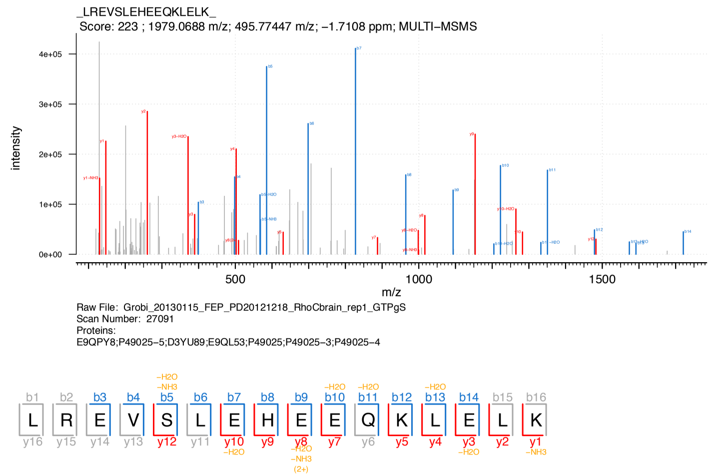
LREVSLEHEEQKLELK
Score: 223 ; 1979.0688 m/z; 495.77447 m/z; −1.7108 ppm; MULTI−MSMS
intensity
m/z
Raw File: Grobi_20130115_FEP_PD20121218_RhoCbrain_rep1_GTPgS
Scan Number: 27091
Proteins:
E9QPY8;P49025−5;D3YU89;E9QL53;P49025;P49025−3;P49025−4
L R E V S L E H E E Q K L E L K
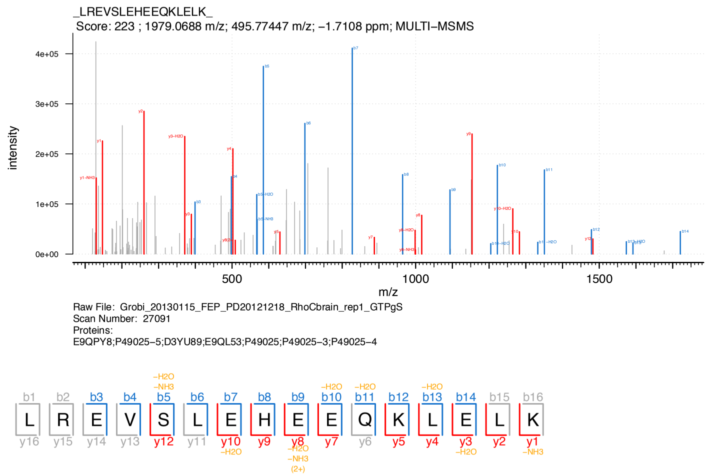
LREVSLEHEEQKLELK
Score: 223 ; 1979.0688 m/z; 495.77447 m/z; −1.7108 ppm; MULTI−MSMS
intensity
m/z
Raw File: Grobi_20130115_FEP_PD20121218_RhoCbrain_rep1_GTPgS
Scan Number: 27091
Proteins:
E9QPY8;P49025−5;D3YU89;E9QL53;P49025;P49025−3;P49025−4
L R E V S L E H E E Q K L E L K
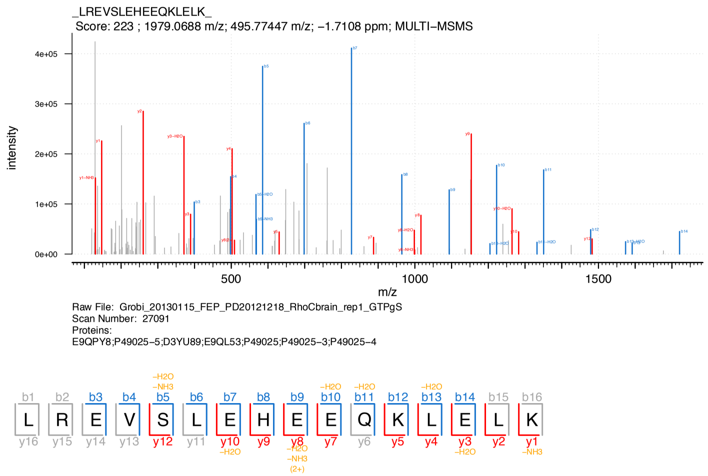
LREVSLEHEEQKLELK
Score: 223 ; 1979.0688 m/z; 495.77447 m/z; −1.7108 ppm; MULTI−MSMS
intensity
m/z
Raw File: Grobi_20130115_FEP_PD20121218_RhoCbrain_rep1_GTPgS
Scan Number: 27091
Proteins:
E9QPY8;P49025−5;D3YU89;E9QL53;P49025;P49025−3;P49025−4
L R E V S L E H E E Q K L E L K
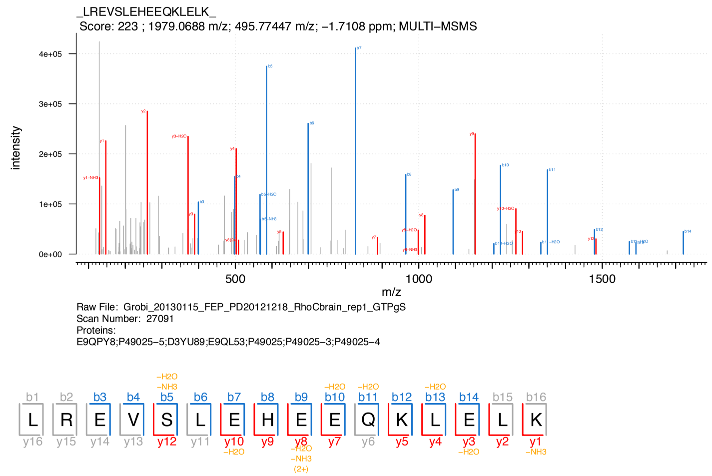
LREVSLEHEEQKLELK
Score: 223 ; 1979.0688 m/z; 495.77447 m/z; −1.7108 ppm; MULTI−MSMS
intensity
m/z
Raw File: Grobi_20130115_FEP_PD20121218_RhoCbrain_rep1_GTPgS
Scan Number: 27091
Proteins:
E9QPY8;P49025−5;D3YU89;E9QL53;P49025;P49025−3;P49025−4
L R E V S L E H E E Q K L E L K
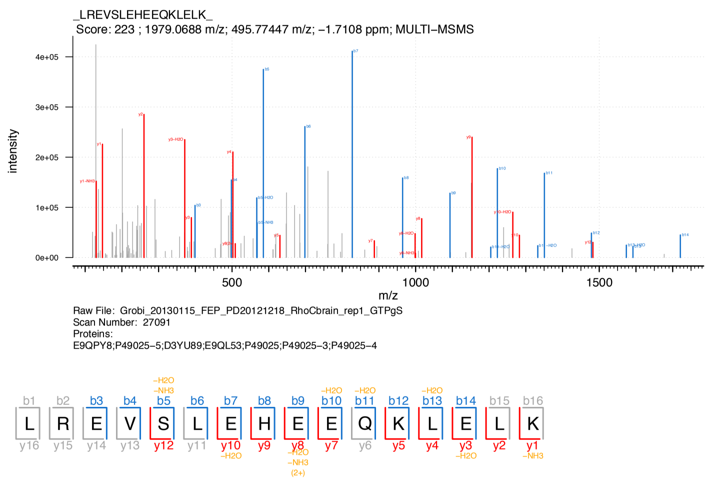
LREVSLEHEEQKLELK
Score: 223 ; 1979.0688 m/z; 495.77447 m/z; −1.7108 ppm; MULTI−MSMS
intensity
m/z
Raw File: Grobi_20130115_FEP_PD20121218_RhoCbrain_rep1_GTPgS
Scan Number: 27091
Proteins:
E9QPY8;P49025−5;D3YU89;E9QL53;P49025;P49025−3;P49025−4
L R E V S L E H E E Q K L E L K
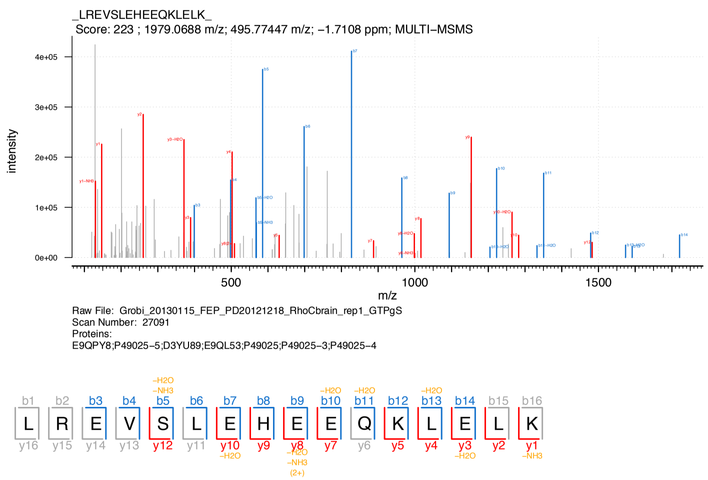
LREVSLEHEEQKLELK
Score: 223 ; 1979.0688 m/z; 495.77447 m/z; −1.7108 ppm; MULTI−MSMS
intensity
m/z
Raw File: Grobi_20130115_FEP_PD20121218_RhoCbrain_rep1_GTPgS
Scan Number: 27091
Proteins:
E9QPY8;P49025−5;D3YU89;E9QL53;P49025;P49025−3;P49025−4
L R E V S L E H E E Q K L E L K
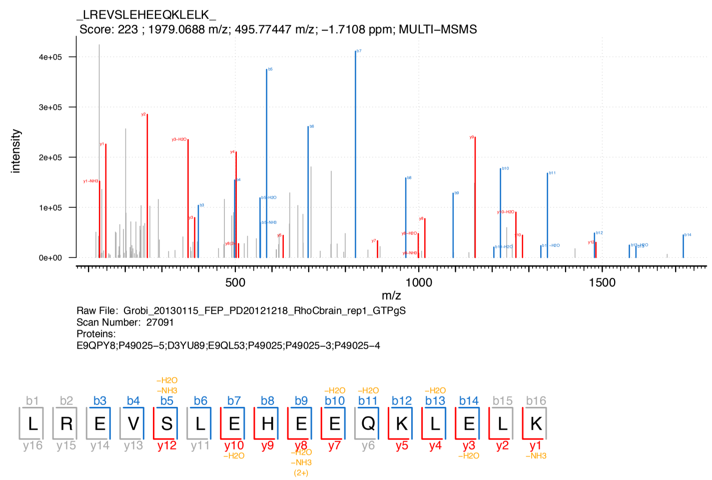
LREVSLEHEEQKLELK
Score: 223 ; 1979.0688 m/z; 495.77447 m/z; −1.7108 ppm; MULTI−MSMS
intensity
m/z
Raw File: Grobi_20130115_FEP_PD20121218_RhoCbrain_rep1_GTPgS
Scan Number: 27091
Proteins:
E9QPY8;P49025−5;D3YU89;E9QL53;P49025;P49025−3;P49025−4
L R E V S L E H E E Q K L E L K

Table legends

Supplemental Table 1: Interaction partners of Rho GTPases. For the six Rho GT identified repeatedly in different tissues.

Experiment			Interaction Partner		
GTPase	Nucleotide	Tissue	Gene names	Protein names	Protein IDs
Cdc42	GTP	Cerebellum	1520402A15Rik;I	Leucine rich adapt	A2A8F6;Q9
Cdc42	GTP	Cerebrum	1520402A15Rik;I	Leucine rich adapt	A2A8F6;Q9
Rac1	GTP	Cerebrum	1520402A15Rik;I	Leucine rich adapt	A2A8F6;Q9
RhoD	GDP	Whole Brain	2700060E02Rik	UPF0568 protein C	Q4VA29;Q
Rac1	GTP	Cerebrum	Abi1	Abl interactor 1	B7ZCT9;Q8
Rac1	GTP	Cerebellum	Abi1	Abl interactor 1	B7ZCT9;Q8
RhoA	GTP	Cerebrum	Abi1	Abl interactor 1	B7ZCT9;Q8
RhoA	GTP	Cerebellum	Abi1	Abl interactor 1	B7ZCT9;Q8
Rac1	GTP	Cerebrum	Abi2	Abl interactor 2	P62484;Q6
Rac1	GTP	Cerebellum	Abi2	Abl interactor 2	P62484;Q6
RhoA	GTP	Cerebrum	Abi2	Abl interactor 2	P62484;Q6
RhoA	GTP	Cerebrum	Abr	Active breakpoint	Q5SSL4-2;(
Cdc42	GTP	Cerebrum	Acadl	Long-chain specifi	P51174
Cdc42	GTP	Hippocampus	Acadl	Long-chain specifi	P51174
Cdc42	GTP	Cerebellum	Acadl	Long-chain specifi	P51174
RhoA	GTP	Cerebrum	Acat1	Acetyl-CoA acetylt	Q8QZT1
RhoA	GTP	Cerebellum	Acat1	Acetyl-CoA acetylt	Q8QZT1
RhoB	GTP	Whole Brain	Acat1	Acetyl-CoA acetylt	Q8QZT1
RhoC	GTP	Whole Brain	Acat1	Acetyl-CoA acetylt	Q8QZT1
RhoA	GTP	Cerebrum	Acat2;Acat3	Acetyl-CoA acetylt	Q8CAY6;Q
Rac1	GTP	Cerebrum	Adam23	Disintegrin and me	Q5SRA0;Q9
RhoB	GTP	Whole Brain	Akap13		E9Q474;E9
RhoA	GTP	Cerebellum	Anln	Actin-binding prot	Q8K298
RhoA	GTP	Cerebrum	Anln	Actin-binding prot	Q8K298
Rac1	GDP	Cerebellum	Arf3;Arf1;Arf2	ADP-ribosylation f	P61205;P8
Cdc42	GTP	Cerebrum	Arhgap32	Rho GTPase-activa	Q811P8;Q8
Rac1	GTP	Cerebrum	Arhgap32	Rho GTPase-activa	Q811P8;Q8
RhoA	GTP	Cerebrum	Arhgap32	Rho GTPase-activa	Q811P8;Q8
RhoC	GTP	Whole Brain	Arhgap32	Rho GTPase-activa	Q811P8;Q8
RhoD	GTP	Whole Brain	Arhgap32	Rho GTPase-activa	Q811P8;Q8
Cdc42	GTP	Cerebellum	Arhgap5	Rho GTPase-activa	E9PYT0;P9
Rac1	GTP	Cerebrum	Arhgap5	Rho GTPase-activa	E9PYT0;P9
Rac1	GTP	Cerebellum	Arhgap5	Rho GTPase-activa	E9PYT0;P9
RhoA	GTP	Cerebrum	Arhgap5	Rho GTPase-activa	E9PYT0;P9
RhoA	GTP	Cerebellum	Arhgap5	Rho GTPase-activa	E9PYT0;P9
RhoB	GTP	Whole Brain	Arhgap5	Rho GTPase-activa	E9PYT0;P9
RhoC	GTP	Whole Brain	Arhgap5	Rho GTPase-activa	E9PYT0;P9
Rac1	GDP	Cerebellum	Arhgdia	Rho GDP-dissociat	Q99PT1
RhoA	GDP	Cerebellum	Arhgdia	Rho GDP-dissociat	Q99PT1
RhoA	GDP	Cerebrum	Arhgdia	Rho GDP-dissociat	Q99PT1
RhoB	GDP	Whole Brain	Arhgdia	Rho GDP-dissociat	Q99PT1
RhoA	GTP	Cerebrum	Arhgef1	Rho guanine nucle	Q61210-5;
RhoA	GTP	Cerebellum	Arhgef1	Rho guanine nucle	Q61210-5;
RhoB	GTP	Whole Brain	Arhgef1	Rho guanine nucle	E9PUF7;Q6

Cdc42	GTP	Cerebrum	Arhgef11		Q68FM7;D
Cdc42	GTP	Cerebellum	Arhgef11		Q68FM7;D
Cdc42	GTP	Hippocampus	Arhgef11		Q68FM7;D
Rac1	GTP	Cerebellum	Arhgef11		Q68FM7;D
Rac1	GTP	Cerebrum	Arhgef11		Q68FM7;D
RhoA	GTP	Cerebellum	Arhgef11		Q68FM7;D
RhoB	GTP	Whole Brain	Arhgef11		Q68FM7;D
RhoC	GTP	Whole Brain	Arhgef11		Q68FM7;D
Cdc42	GTP	Cerebrum	Arhgef12	Rho guanine nucle	Q8R4H2
Cdc42	GTP	Hippocampus	Arhgef12	Rho guanine nucle	Q8R4H2
Cdc42	GTP	Cerebellum	Arhgef12	Rho guanine nucle	Q8R4H2
Rac1	GTP	Cerebellum	Arhgef12	Rho guanine nucle	Q8R4H2
Rac1	GTP	Cerebrum	Arhgef12	Rho guanine nucle	Q8R4H2
RhoA	GTP	Cerebellum	Arhgef12	Rho guanine nucle	Q8R4H2
RhoA	GDP	Cerebellum	Arhgef17	Rho guanine nucle	Q80U35;Q
RhoB	GDP	Whole Brain	Arhgef17	Rho guanine nucle	Q80U35-2;
RhoC	GDP	Whole Brain	Arhgef17	Rho guanine nucle	Q80U35-2;
RhoA	GTP	Cerebellum	Arhgef18	Rho guanine nucle	Q6P9R4;Q
RhoA	GTP	Cerebrum	Arhgef18	Rho guanine nucle	Q6P9R4;Q
RhoB	GTP	Whole Brain	Arhgef18	Rho guanine nucle	Q6P9R4;Q
Cdc42	GTP	Cerebrum	Arhgef2	Rho guanine nucle	Q60875;H3
Rac1	GTP	Cerebrum	Arhgef2	Rho guanine nucle	Q60875;H3
RhoA	GTP	Cerebrum	Arhgef2	Rho guanine nucle	Q60875;H3
RhoA	GTP	Cerebellum	Arhgef2	Rho guanine nucle	Q60875;H3
RhoB	GTP	Whole Brain	Arhgef2	Rho guanine nucle	Q60875;H3
RhoC	GTP	Whole Brain	Arhgef2	Rho guanine nucle	Q60875;H3
RhoD	GTP	Whole Brain	Arhgef2	Rho guanine nucle	Q60875;H3
Cdc42	GTP	Cerebrum	Arhgef6	Rho guanine nucle	F6WMJ3;C
Cdc42	GTP	Cerebellum	Arhgef6	Rho guanine nucle	F6WMJ3;C
Cdc42	GTP	Hippocampus	Arhgef6	Rho guanine nucle	F6WMJ3;C
Rac1	GTP	Cerebellum	Arhgef6	Rho guanine nucle	F6WMJ3;C
Rac1	GTP	Cerebrum	Arhgef6	Rho guanine nucle	F6WMJ3;C
Cdc42	GTP	Cerebrum	Arhgef7	Rho guanine nucle	Q9ES28;Q9
Cdc42	GTP	Hippocampus	Arhgef7	Rho guanine nucle	Q9ES28;Q9
Cdc42	GTP	Cerebellum	Arhgef7	Rho guanine nucle	Q9ES28;Q9
Rac1	GTP	Cerebrum	Arhgef7	Rho guanine nucle	Q9ES28;Q9
Rac1	GTP	Cerebellum	Arhgef7	Rho guanine nucle	Q9ES28;Q9
RhoA	GTP	Cerebrum	Arhgef7	Rho guanine nucle	Q9ES28;Q9
RhoC	GDP	Whole Brain	Arl2	ADP-ribosylation f	Q9D0J4
RhoA	GTP	Cerebrum	Ass1	Argininosuccinate	P16460;Q3
Cdc42	GTP	Cerebrum	Atl1	Atlastin-1	Q8BH66
RhoA	GDP	Cerebellum	Atp5d	ATP synthase subu	Q4FK74;Q9
RhoD	GDP	Whole Brain	Atp6v1f	V-type proton ATP	Q9D1K2;F7
RhoD	GDP	Whole Brain	Baiap2	Brain-specific angi	B1AZ47;Q8
Cdc42	GTP	Cerebrum	Baiap2		B1AZ45;Q8
Cdc42	GTP	Cerebrum	Baiap2	Brain-specific angi	Q3UKP6;Q
Cdc42	GTP	Cerebellum	Baiap2	Brain-specific angi	Q3UKP6;Q
Cdc42	GTP	Hippocampus	Baiap2	Brain-specific angi	Q3UKP6;Q
Rac1	GTP	Cerebrum	Bckdk	[3-methyl-2-oxobu	O55028;Q3
Rac1	GTP	Cerebellum	Brk1	Protein BRICK1	Q91VR8

Rac1	GTP	Cerebrum	Brk1	Protein BRICK1	Q91VR8
RhoA	GTP	Cerebrum	Brk1	Protein BRICK1	Q91VR8
RhoC	GTP	Whole Brain	Cadm3	Cell adhesion mole	Q99N28;E9
Cdc42	GTP	Cerebellum	Camk2b	Calcium/calmoduli	Q5SVJ0;P2
RhoA	GTP	Cerebrum	Capza1	F-actin-capping pr	E9PWZ5;P4
RhoA	GTP	Cerebrum	Ccdc6	Coiled-coil domain	D3YZP9
RhoB	GDP	Whole Brain	Cdc42	Cell division contr	P60766;Q3
Cdc42	GTP	Cerebrum	Cdc42bpa	Serine/threonine-p	E9PVY0;D3
Cdc42	GTP	Hippocampus	Cdc42bpa	Serine/threonine-p	E9PVY0;D3
Cdc42	GTP	Cerebellum	Cdc42bpa	Serine/threonine-p	E9PVY0;D3
Rac1	GTP	Cerebrum	Cdc42bpa	Serine/threonine-p	E9PVY0;D3
Cdc42	GTP	Cerebrum	Cdc42bpb	Serine/threonine-p	Q7TT50;P5
Cdc42	GTP	Hippocampus	Cdc42bpb	Serine/threonine-p	Q7TT50;P5
Cdc42	GTP	Cerebellum	Cdc42bpb	Serine/threonine-p	Q7TT50;P5
Rac1	GTP	Cerebellum	Cdc42bpb	Serine/threonine-p	Q7TT50;P5
Rac1	GTP	Cerebrum	Cdc42bpb	Serine/threonine-p	Q7TT50;P5
Cdc42	GTP	Cerebellum	Cdc42ep1	Cdc42 effector pro	Q91W92
Rac1	GTP	Cerebellum	Cdc42ep1	Cdc42 effector pro	Q91W92
Cdc42	GTP	Cerebellum	Cdc42ep4	Cdc42 effector pro	A2A6Q1;Q
Rac1	GTP	Cerebellum	Cdc42ep4	Cdc42 effector pro	A2A6Q1;Q
Rac1	GTP	Cerebrum	Cdc42ep4	Cdc42 effector pro	A2A6Q1;Q
Rac1	GTP	Cerebrum	Cdc42se2	CDC42 small effect	Q8BGH7
Rac1	GTP	Cerebrum	Cit	Citron Rho-interac	E9QL53;P4
RhoA	GTP	Cerebellum	Cit	Citron Rho-interac	E9QL53;P4
RhoA	GTP	Cerebrum	Cit	Citron Rho-interac	E9QL53;P4
RhoB	GTP	Whole Brain	Cit	Citron Rho-interac	E9QPY8;P4
RhoC	GTP	Whole Brain	Cit	Citron Rho-interac	E9QPY8;P4
Rac1	GTP	Cerebrum	Cryzl1	Quinone oxidored	Q921W4;D
RhoB	GDP	Whole Brain	Ctnnd1	Catenin delta-1	E9Q8Z8;E9
Rac1	GTP	Cerebrum	Cyfip2	Cytoplasmic FMR1	Q5SQX6;E9
Rac1	GTP	Cerebellum	Cyfip2	Cytoplasmic FMR1	Q5SQX6;E9
RhoA	GTP	Cerebrum	Cyfip2	Cytoplasmic FMR1	Q5SQX6;E9
RhoB	GTP	Whole Brain	Daam1	Disheveled-associa	Q8BPM0;C
RhoC	GTP	Whole Brain	Daam1	Disheveled-associa	Q8BPM0;C
RhoB	GTP	Whole Brain	Daam2	Disheveled-associa	Q80U19;Q
RhoC	GTP	Whole Brain	Daam2	Disheveled-associa	Q80U19;Q
RhoD	GTP	Whole Brain	Daam2	Disheveled-associa	Q80U19;Q
RhoD	GTP	Whole Brain	Diap1;Diaph1	Protein diaphanou	E9PV41;E9
Cdc42	GTP	Cerebellum	Diap2;Diaph2	Protein diaphanou	E9Q4U7;Q
Cdc42	GTP	Cerebrum	Diap2;Diaph2	Protein diaphanou	E9Q4U7;Q
RhoB	GDP	Whole Brain	Diras2	GTP-binding prote	Q3UWU7;(
Cdc42	GTP	Hippocampus	Dock9		E9QMR2
Rac1	GTP	Cerebellum	Dock9		E9QMR2
Rac1	GTP	Cerebrum	Dock9		E9QMR2
Cdc42	GTP	Cerebrum	Dync1i2	Cytoplasmic dynei	A2BFF9;Q3
Cdc42	GTP	Cerebellum	Dynll2	Dynein light chain	B2KGQ2;Q
Rac1	GTP	Cerebellum	Dynll2	Dynein light chain	B2KGQ2;Q
RhoB	GTP	Whole Brain	Ech1	Delta(3,5)-Delta(2,	O35459;F7
Rac1	GTP	Cerebellum	Echdc1	Ethylmalonyl-CoA	Q9D9V3;Q
Rac1	GTP	Cerebrum	Echdc1	Ethylmalonyl-CoA	Q9D9V3;Q

RhoB	GDP	Whole Brain	Eef1a2	Elongation factor 1	P62631;B7
RhoC	GDP	Whole Brain	Eef1a2	Elongation factor 1	P62631;B7
RhoD	GDP	Whole Brain	Eef1a2	Elongation factor 1	P62631;B7
Cdc42	GDP	Cerebrum	Eif5a;Eif5a2	Eukaryotic translat	P63242;Q8
Rac1	GTP	Cerebrum	Elmo1	Engulfment and ce	F8WIL9;Q8
Rac1	GTP	Cerebrum	Elmo2	Engulfment and ce	Q8BHL5-2;
Rac1	GTP	Cerebellum	Elmo2	Engulfment and ce	Q8BHL5-2;
Cdc42	GDP	Cerebrum	Eps15l1	Epidermal growth	Q60902;F8
RhoB	GTP	Whole Brain	Exoc3	Exocyst complex c	Q6KAR6;Q
RhoB	GDP	Whole Brain	Fahd1	Acylpyruvase FAHI	Q3UQY4;Q
RhoA	GTP	Cerebrum	Fam65a	Protein FAM65A	G5E8A2;Q(
RhoA	GTP	Cerebellum	Fam65a	Protein FAM65A	G5E8A2;Q(
RhoB	GTP	Whole Brain	Fam65a	Protein FAM65A	G5E8A2;Q(
RhoC	GTP	Whole Brain	Fam65a	Protein FAM65A	G5E8A2;Q(
RhoB	GTP	Whole Brain	Fam65b	Protein FAM65B	Q80U16
Cdc42	GTP	Cerebrum	Fam89b		Q9QUI1;Q
RhoA	GTP	Cerebellum	Fh	Fumarate hydratas	P97807;P9
RhoD	GDP	Whole Brain	Fkbp2	Peptidyl-prolyl cis-	P45878;Q3
Cdc42	GTP	Hippocampus	Fnbp1	Formin-binding pr(	Q80TY0;A2
Cdc42	GTP	Cerebrum	Fnbp1	Formin-binding pr(	Q80TY0;A2
Cdc42	GTP	Cerebellum	Fnbp1	Formin-binding pr(	Q80TY0;A2
Rac1	GTP	Cerebellum	Fnbp1	Formin-binding pr(	Q80TY0;A2
Cdc42	GTP	Hippocampus	Fnbp1l		E9PUK3
Cdc42	GTP	Cerebellum	Fnbp1l		E9PUK3
Cdc42	GTP	Cerebrum	Fnbp1l		E9PUK3
RhoD	GDP	Whole Brain	Gabbr1	Gamma-aminobut	Q9WV18;C
Cdc42	GDP	Cerebrum	Gad2	Glutamate decarb(	P48320;Q5
RhoA	GDP	Cerebrum	Gart	Trifunctional purin	Q64737;Q3
RhoB	GTP	Whole Brain	Gdap1	Ganglioside-induc(	O88741;O8
Cdc42	GTP	Cerebrum	Git1	ARF GTPase-activa	Q68FF6
Cdc42	GTP	Hippocampus	Git1	ARF GTPase-activa	Q68FF6
Cdc42	GTP	Cerebellum	Git1	ARF GTPase-activa	Q68FF6
Rac1	GTP	Cerebrum	Git1	ARF GTPase-activa	Q68FF6
Rac1	GTP	Cerebellum	Git1	ARF GTPase-activa	Q68FF6
Cdc42	GTP	Cerebrum	Git2		E9PVA6;Q8
Cdc42	GTP	Cerebellum	Git2		E9PVA6;Q8
Rac1	GTP	Cerebrum	Git2		E9PVA6;Q8
Rac1	GTP	Cerebellum	Git2		E9PVA6;Q8
RhoB	GTP	Whole Brain	Gnao1	Guanine nucleotid	P18872;Q5
RhoC	GTP	Whole Brain	Gpm6b	Neuronal membra	A2AEG6;P3
RhoB	GDP	Whole Brain	Gpn1	GPN-loop GTPase	Q4VAB2;Q
Cdc42	GTP	Cerebrum	Grb2	Growth factor rec(	Q3U5I5;Q(
RhoA	GTP	Cerebrum	Grlf1;Arhgap35	Rho GTPase-activa	B2RTN5;Q5
RhoB	GTP	Whole Brain	Gsn	Gelsolin	A2AL35;P1
RhoB	GDP	Whole Brain	Gtpbp10	GTP-binding prote	Q8K013;F8
RhoC	GTP	Whole Brain	Gucy1a2		F8VQK3;F(
RhoD	GTP	Whole Brain	Hexdc	Hexosaminidase D	Q3U4H6-2
Cdc42	GTP	Cerebellum	Homer3	Homer protein ho	Q99JP6-2;(
Rac1	GTP	Cerebellum	Homer3	Homer protein ho	Q99JP6-2;(
RhoA	GTP	Cerebellum	Homer3	Homer protein ho	Q99JP6-2;(

Cdc42	GDP	Cerebellum	Hspe1	10 kDa heat shock	Q4KL76;Q6
Cdc42	GDP	Cerebellum	Igsf5;Pcp4	Purkinje cell prote	D3YXH0;P6
RhoB	GTP	Whole Brain	Igtp		Q9DCE9;E9
Rac1	GTP	Cerebrum	Inppl1	Phosphatidylinosit	Q6P549
RhoA	GTP	Cerebellum	Inppl1	Phosphatidylinosit	Q6P549
RhoA	GTP	Cerebrum	Inppl1	Phosphatidylinosit	Q6P549
RhoB	GTP	Whole Brain	Inppl1	Phosphatidylinosit	Q6P549
RhoC	GTP	Whole Brain	Inppl1	Phosphatidylinosit	Q6P549
RhoA	GTP	Cerebrum	Iqsec2	IQ motif and SEC7	E9QAD8;A4
Cdc42	GTP	Cerebrum	Iqsec3	IQ motif and SEC7	Q3TES0;D6
Rac1	GTP	Cerebellum	Iqsec3	IQ motif and SEC7	Q3TES0;D6
Rac1	GTP	Cerebrum	Iqsec3	IQ motif and SEC7	Q3TES0;D6
RhoA	GTP	Cerebrum	Iqsec3	IQ motif and SEC7	Q3TES0;D6
Cdc42	GDP	Cerebrum	Isca2	Iron-sulfur cluster	Q9DCB8
Rac1	GDP	Cerebrum	Kalrn	Kalirin	A2CG49-7;
Cdc42	GDP	Cerebrum	Kcnab2	Voltage-gated pota	E0CXZ9;P6
RhoA	GTP	Cerebrum	Kif2a	Kinesin-like protei	E0CZ72;P2
RhoB	GDP	Whole Brain	Lgalsla	Galectin-related pı	Q8VED9
Rac1	GTP	Cerebellum	Lin7a	Protein lin-7 homc	Q8JZS0;Q3
Cdc42	GTP	Cerebrum	Llgl1	Lethal(2) giant larv	Q80Y17
Cdc42	GTP	Cerebellum	Llgl1	Lethal(2) giant larv	Q80Y17
RhoB	GTP	Whole Brain	Lrpap1	Alpha-2-macroglol	F6SY09;P5
RhoB	GTP	Whole Brain	Lrrc47	Leucine-rich repea	E9PV22;B1
Cdc42	GTP	Cerebrum	Lurap1l	Leucine rich adapt	Q8K2P1
Cdc42	GDP	Cerebrum	Lypla2	Acyl-protein thioe:	B1AV56;Q9
RhoD	GDP	Whole Brain	Map4;Mtap4	Microtubule-assoc	P27546;P2
RhoA	GDP	Cerebrum	Mat2b	Methionine adeno	Q99LB6;Q9
RhoA	GDP	Cerebrum	Mccc1	Methylcrotonoyl-C	Q99MR8;F
RhoD	GTP	Whole Brain	Mettl21d	Methyltransferase	Q8C436;Q8
RhoB	GTP	Whole Brain	Mpdz	Multiple PDZ dom:	F8WGE8;Q
RhoD	GDP	Whole Brain	Mpi	Mannose-6-phosp	Q3V100;Q9
Rac1	GDP	Cerebrum	Mpp1	55 kDa erythrocyte	P70290;Q5
RhoD	GTP	Whole Brain	Mtap4	Microtubule-assoc	F6XPV7;F6
Cdc42	GTP	Cerebrum	Myl6;Gm8894	Myosin light polyp	Q60605;Q6
Cdc42	GTP	Cerebrum	Mzt2	Mitotic-spindle or	Q9CQ25
Rac1	GTP	Cerebrum	Mzt2	Mitotic-spindle or	Q9CQ25
Cdc42	GDP	Cerebrum	Ncald	Neurocalcin-delta	Q91X97;D3
RhoA	GDP	Cerebrum	Nceh1	Neutral cholesterc	Q8BLF1
RhoB	GTP	Whole Brain	Nceh1	Neutral cholesterc	Q8BLF1;Q8
Rac1	GTP	Cerebrum	Nckap1	Nck-associated pr	A2AS98;A2
Rac1	GTP	Cerebellum	Nckap1	Nck-associated pr	A2AS98;A2
RhoA	GDP	Cerebrum	Ndufa4	NADH dehydrogen	Q62425
RhoA	GDP	Cerebrum	Ndufa8	NADH dehydrogen	Q9DCJ5
RhoC	GTP	Whole Brain	Ndufs2	NADH dehydrogen	Q91WD5;D
RhoA	GTP	Cerebrum	Nefh	Neurofilament hea	P19246;F7
RhoB	GDP	Whole Brain	Nudt16	U8 snoRNA-decap	Q6P3D0;Q
RhoC	GDP	Whole Brain	Nudt16	U8 snoRNA-decap	Q6P3D0;Q
RhoD	GDP	Whole Brain	Nudt16	U8 snoRNA-decap	Q6P3D0;Q
Cdc42	GTP	Cerebrum	Opa1	Dynamin-like 120 l	P58281-2;I
Cdc42	GTP	Cerebellum	Opa1	Dynamin-like 120 l	P58281-2;I

Cdc42	GTP	Hippocampus	Opa1	Dynamin-like 120	P58281-2;I
Rac1	GTP	Cerebrum	Opa1	Dynamin-like 120	P58281-2;I
Rac1	GTP	Cerebellum	Opa1	Dynamin-like 120	P58281-2;I
Rac1	GDP	Cerebrum	Pacsin2	Protein kinase C a	Q3TDA7;Q
Rac1	GDP	Cerebellum	Pacsin2	Protein kinase C a	Q3TDA7;Q
Cdc42	GTP	Cerebrum	Pak1	Serine/threonine-p	G5E884;O8
Cdc42	GTP	Hippocampus	Pak1	Serine/threonine-p	G5E884;O8
Cdc42	GTP	Cerebellum	Pak1	Serine/threonine-p	G5E884;O8
Rac1	GTP	Cerebrum	Pak1	Serine/threonine-p	G5E884;O8
Rac1	GTP	Cerebellum	Pak1	Serine/threonine-p	G5E884;O8
Cdc42	GTP	Cerebrum	Pak2	Serine/threonine-p	Q8CIN4
Cdc42	GTP	Cerebellum	Pak2	Serine/threonine-p	Q8CIN4
Cdc42	GTP	Hippocampus	Pak2	Serine/threonine-p	Q8CIN4
Rac1	GTP	Cerebrum	Pak2	Serine/threonine-p	Q8CIN4
Cdc42	GTP	Hippocampus	Pak3		A3KGC1;Q
Cdc42	GTP	Cerebrum	Pak3		A3KGC1;Q
Cdc42	GTP	Cerebellum	Pak3		A3KGC1;Q
Rac1	GTP	Cerebrum	Pak3		A3KGC1;Q
Rac1	GTP	Cerebellum	Pak3		A3KGC1;Q
Cdc42	GTP	Cerebellum	Pak4	Serine/threonine-p	Q8BTW9
Rac1	GTP	Cerebrum	Pak6	Serine/threonine-p	Q3ULB5
Cdc42	GTP	Cerebrum	Pak7	Serine/threonine-p	B1AYC2;Q8
Cdc42	GTP	Cerebellum	Pard6a	Partitioning defect	Q9Z101;D3
Rac1	GTP	Cerebrum	Pard6a	Partitioning defect	Q9Z101;D3
Rac1	GTP	Cerebrum	Pddc1	Parkinson disease	Q8BFQ8
RhoB	GDP	Whole Brain	Pde6d	Retinal rod rhodop	O55057;Q3
RhoB	GTP	Whole Brain	Pi4ka		E9Q3L2;F6
Cdc42	GTP	Cerebrum	Pik3cb	Phosphatidylinosit	Q8BTI9
Cdc42	GTP	Cerebellum	Pik3r1	Phosphatidylinosit	P26450;Q8
Cdc42	GTP	Cerebrum	Pik3r1	Phosphatidylinosit	P26450;Q8
Rac1	GTP	Cerebellum	Pik3r1	Phosphatidylinosit	P26450;Q8
Rac1	GTP	Cerebrum	Pik3r1	Phosphatidylinosit	P26450;Q8
Rac1	GTP	Cerebrum	Pip4k2b	Phosphatidylinosit	Q3UJ95;Q8
RhoA	GTP	Cerebrum	Pkn1	Serine/threonine-p	P70268-2;I
RhoB	GTP	Whole Brain	Pkn1	Serine/threonine-p	P70268-2;I
RhoD	GTP	Whole Brain	Pkn1	Serine/threonine-p	P70268-2;I
RhoB	GTP	Whole Brain	Plcxd3	PI-PLC X domain-c	G3X9A7;Q8
Cdc42	GDP	Cerebrum	Pld3	Phospholipase D3	O35405
RhoA	GTP	Cerebrum	Plekhg5	Pleckstrin homolo	Q66T02;B1
RhoB	GTP	Whole Brain	Plekhg5	Pleckstrin homolo	Q66T02;B1
RhoD	GTP	Whole Brain	Plekhg5	Pleckstrin homolo	Q66T02;B1
Rac1	GTP	Cerebrum	Plxnb1	Plexin-B1	Q8CJH3
RhoD	GTP	Whole Brain	Plxnb2	Plexin-B2	B2RXS4;E9
RhoC	GTP	Whole Brain	Pnpo	Pyridoxine-5-phos	Q91XF0;A2
Cdc42	GTP	Cerebellum	Ppm1h	Protein phosphata	Q3UYC0;Q
Cdc42	GTP	Cerebellum	Ppp1ca	Serine/threonine-p	P62137;Q3
Rac1	GTP	Cerebellum	Ppp1r21	Protein phosphata	Q3TDD9;Q
Rac1	GTP	Cerebrum	Ppp1r21	Protein phosphata	Q3TDD9;Q
RhoC	GTP	Whole Brain	Ppp2r5c	Serine/threonine-p	Q60996;Q
Cdc42	GDP	Cerebrum	Prex1	Phosphatidylinosit	Q69ZK0

Cdc42	GTP	Cerebrum	Prkci	Protein kinase C io	Q5DTK3;Q
Cdc42	GTP	Cerebellum	Prkci	Protein kinase C io	Q5DTK3;Q
RhoB	GTP	Whole Brain	Prrt3	Proline-rich transn	Q6PE13
RhoB	GTP	Whole Brain	Psd3	PH and SEC7 doma	Q8C0E9;E9
Cdc42	GDP	Cerebrum	Psma6	Proteasome subur	Q9QUM9;I
Rac1	GTP	Cerebrum	Psmd9	26S proteasome n	Q9CR00
RhoB	GTP	Whole Brain	Psme2	Proteasome activa	P97372;Q5
RhoB	GDP	Whole Brain	Ran	GTP-binding nucle	P62827;A6
RhoC	GDP	Whole Brain	Ran	GTP-binding nucle	P62827;A6
RhoD	GDP	Whole Brain	Ran	GTP-binding nucle	P62827;A6
RhoC	GTP	Whole Brain	Rap1b;Rap1a	Ras-related protei	Q52L50;Q9
RhoC	GDP	Whole Brain	Rap1gds1		E9Q912;E9
Cdc42	GTP	Cerebrum	Raph1		F2Z408;G5
RhoD	GTP	Whole Brain	Rbfox1	RNA binding prote	Q9JJ43-3;C
Cdc42	GTP	Hippocampus	Rgs14	Regulator of G-pro	P97492
Cdc42	GTP	Cerebrum	Rgs14	Regulator of G-pro	P97492
Rac1	GTP	Cerebrum	Rgs14	Regulator of G-pro	P97492
RhoB	GTP	Whole Brain	Rhpn2	Rhophilin-2	Q8BWR8
RhoB	GTP	Whole Brain	Rock1	Rho-associated pr	P70335;P7
Cdc42	GTP	Cerebrum	Rock2	Rho-associated pr	F8VPK5;P7
Rac1	GTP	Cerebrum	Rock2	Rho-associated pr	F8VPK5;P7
RhoA	GTP	Cerebellum	Rock2	Rho-associated pr	F8VPK5;P7
RhoA	GTP	Cerebrum	Rock2	Rho-associated pr	F8VPK5;P7
RhoB	GTP	Whole Brain	Rock2	Rho-associated pr	E9PYM9;F8
RhoC	GTP	Whole Brain	Rock2	Rho-associated pr	E9PYM9;F8
RhoD	GDP	Whole Brain	Rpl22	60S ribosomal pro	P67984;Q4
RhoA	GDP	Cerebellum	Rps27;Gm17241	40S ribosomal pro	Q6ZWU9;E
RhoA	GTP	Cerebellum	Rtkn	Rhotekin	Q8C6B2-2;
RhoA	GTP	Cerebrum	Rtkn	Rhotekin	Q8C6B2-2;
RhoB	GTP	Whole Brain	Rtkn	Rhotekin	Q8C6B2;Q
RhoB	GTP	Whole Brain	Scamp3	Secretory carrier-a	Q3UXS0;O
Rac1	GTP	Cerebrum	Sccpdh	Saccharopine deh	Q8R127;D3
Cdc42	GTP	Cerebellum	Sept4	Septin-4	P28661;P2
Cdc42	GTP	Cerebellum	Sept7	Septin-7	E9Q9F5;O5
Cdc42	GTP	Cerebellum	Sept8	Septin-8	B1AQZ0;B1
Cdc42	GTP	Cerebellum	Sestd1	SEC14 domain and	Q80UK0
Cdc42	GTP	Cerebrum	Sestd1	SEC14 domain and	Q80UK0
Rac1	GTP	Cerebrum	Sestd1	SEC14 domain and	Q80UK0
Rac1	GTP	Cerebrum	Sh3rf1	E3 ubiquitin-prote	Q69ZI1;E9
RhoA	GDP	Cerebellum	Slc25a18	Mitochondrial glut	Q9DB41;Q
RhoA	GTP	Cerebrum	Slk	STE20-like serine/t	O54988;A2
Cdc42	GTP	Cerebellum	Snap91	Clathrin coat asser	Q61548;Q
RhoC	GTP	Whole Brain	Snx27	Sorting nexin-27	Q3UHD6;C
Cdc42	GTP	Cerebellum	Sowahc	Ankyrin repeat do	Q8C0J6
Cdc42	GTP	Cerebrum	Sowahc	Ankyrin repeat do	Q8C0J6
Rac1	GTP	Cerebrum	Srgap3	SLIT-ROBO Rho GT	F8VPQ4;Q8
RhoB	GDP	Whole Brain	Srp54;Srp54c	Signal recognition	P14576;E9
RhoA	GTP	Cerebrum	St13	Hsc70-interacting	Q99L47;F8
Rac1	GDP	Cerebrum	Stam	Signal transducing	P70297;Q3
RhoB	GTP	Whole Brain	Stx16	Syntaxin-16	E9QM25;C

RhoA	GTP	Cerebrum	Sult4a1	Sulfotransferase 4	P63046;P6
RhoA	GDP	Cerebellum	Syp		F8WGK2
Cdc42	GTP	Cerebellum	Taok2	Serine/threonine-p	Q6ZQ29-2;
Cdc42	GTP	Cerebrum	Taok2	Serine/threonine-p	Q6ZQ29-2;
Rac1	GDP	Cerebrum	Tiam2	T-lymphoma invas	Q6ZPF3;Q6
Rac1	GDP	Cerebellum	Traf7	E3 ubiquitin-prote	F8WJF7;Q8
Rac1	GTP	Cerebrum	Trim3	Tripartite motif-co	Q9R1R2;Q
Rac1	GTP	Cerebellum	Trim3	Tripartite motif-co	Q9R1R2;Q
Rac1	GDP	Cerebrum	Trio	Triple functional d	Q0KL02-4;
Cdc42	GTP	Hippocampus	Trip10	Cdc42-interacting	Q8CJ53;Q8
Cdc42	GTP	Cerebellum	Trip10	Cdc42-interacting	Q8CJ53;Q8
Cdc42	GTP	Cerebrum	Trip10	Cdc42-interacting	Q8CJ53;Q8
RhoC	GTP	Whole Brain	Tsn	Translin	Q545E6;Q6
RhoB	GTP	Whole Brain	Tsnax	Translin-associate	Q9QZE7
RhoD	GDP	Whole Brain	Ufc1	Ubiquitin-fold mo	Q9CR09
Rac1	GTP	Cerebrum	Wasf1	Wiskott-Aldrich sy	Q8R5H6;B3
Rac1	GTP	Cerebellum	Wasf1	Wiskott-Aldrich sy	Q8R5H6;B3
RhoA	GTP	Cerebrum	Wasf1	Wiskott-Aldrich sy	Q8R5H6;B3
Rac1	GTP	Cerebrum	Wasf3	Wiskott-Aldrich sy	Q8VHI6;D3
Rac1	GTP	Cerebellum	Wasf3	Wiskott-Aldrich sy	Q8VHI6;D3
RhoA	GTP	Cerebrum	Wasf3	Wiskott-Aldrich sy	Q8VHI6;D3
Cdc42	GTP	Cerebrum	Wasl	Neural Wiskott-Al	Q3TXX8;Q9
Cdc42	GTP	Cerebellum	Wasl	Neural Wiskott-Al	Q3TXX8;Q9
Cdc42	GTP	Hippocampus	Wasl	Neural Wiskott-Al	Q3TXX8;Q9
RhoA	GDP	Cerebrum	Wbp2	WW domain-bindi	E9Q1S7;P9
Cdc42	GTP	Cerebrum	Wipf1	WAS/WASL-intera	A2ATB9;Q8
Cdc42	GTP	Cerebellum	Wipf2	WAS/WASL-intera	Q6PEV3;D3
Cdc42	GTP	Cerebrum	Wipf2	WAS/WASL-intera	Q6PEV3;D3
Cdc42	GTP	Hippocampus	Wipf2	WAS/WASL-intera	Q6PEV3;D3
Cdc42	GTP	Cerebrum	Wipf3	WAS/WASL-intera	P0C7L0;E9
Cdc42	GTP	Hippocampus	Wipf3	WAS/WASL-intera	P0C7L0;E9
Cdc42	GTP	Cerebellum	Wipf3	WAS/WASL-intera	P0C7L0;E9
Cdc42	GTP	Cerebrum		Uncharacterized p	Q8C3W1
RhoB	GTP	Whole Brain			Q80U16-5;
RhoB	GTP	Whole Brain		Uncharacterized p	Q8C3W1
RhoC	GTP	Whole Brain		Uncharacterized p	Q8C3W1
RhoD	GTP	Whole Brain		Uncharacterized p	Q8C3W1

Pases RhoA, RhoB, RhoC, RhoD, Rac1 and Cdc42 a total number of 293 distinct i

							Results mass spectı	
Majority p	LFQ intens	LFQ intens	LFQ intens	LFQ intens	LFQ intens	LFQ intens	Peptides	Razor + un
A2A8F6;Q9	26,7144	24,8568	24,3541	27,7072	29,0261	27,6589	9	9
A2A8F6;Q9	26,103	24,001	24,1774	28,114	28,7797	29,1471	9	9
A2A8F6;Q9	24,0402	23,955	23,3534	26,3918	26,3188	26,1309	9	9
Q4VA29;Q	24,2248	23,8377	25,0461	21,5993	21,9763	22,6614	8	8
B7ZCT9;Q8	29,4318	28,9221	29,4554	33,0053	33,7752	33,4501	20	20
B7ZCT9;Q8	27,1735	27,0548	26,2609	33,0809	32,9178	32,6433	20	20
B7ZCT9;Q8	28,9457	29,6813	29,2684	30,6671	30,7975	31,027	20	20
B7ZCT9;Q8	27,4278	27,184	25,7252	28,7182	29,7158	29,5531	20	20
P62484;Q6	27,7149	27,5261	27,3545	32,3513	32,9999	32,7189	19	14
P62484;Q6	24,0128	24,6245	25,4851	31,0749	31,4696	30,769	19	14
P62484;Q6	26,8876	27,2019	27,9978	28,9739	30,027	29,9408	19	14
Q5SSL4-2;(	25,7241	24,328	23,6758	27,1176	26,3712	26,6047	10	10
P51174	28,2785	27,4064	27,5851	30,9035	31,2396	31,2904	16	16
P51174	26,2354	26,1121	26,6682	29,4417	29,8698	30,0161	16	16
P51174	28,3998	27,5064	27,6793	31,7403	32,1335	31,9478	16	16
Q8QZT1	32,4212	31,9864	32,2419	36,2045	36,5458	36,3435	32	32
Q8QZT1	31,4219	31,1635	31,2171	36,9963	37,6617	37,0694	32	32
Q8QZT1	28,5669	28,7721	28,5608	30,8271	30,5858	30,1503	24	24
Q8QZT1	28,8845	28,5187	28,923	31,223	30,7321	30,7663	24	24
Q8CAY6;Q8	24,4378	24,9038	24,3826	26,9768	27,0752	27,119	6	6
Q5SRA0;Q9	23,8806	24,4027	24,3418	26,7967	26,6786	27,0385	5	5
E9Q474;E9	21,7996	23,6361	21,2988	24,8006	25,4305	26,021	12	12
Q8K298	26,0585	26,3797	25,6635	27,2602	28,6342	28,3776	11	11
Q8K298	23,6278	25,5042	23,9479	26,0371	27,7595	28,4481	11	11
P61205;P8	30,1326	28,8862	29,5733	27,3634	26,5539	27,7687	10	10
Q811P8;Q8	26,7367	26,7167	24,0727	31,4999	30,9978	31,3584	28	28
Q811P8;Q8	24,2684	23,54	24,5196	29,6697	30,2397	29,7885	28	28
Q811P8;Q8	24,1841	24,34	24,7877	28,3694	28,6	28,5205	28	28
Q811P8;Q8	22,7986	23,851	23,8435	26,228	25,9613	26,5869	31	31
Q811P8;Q8	25,2048	24,4963	23,949	28,3637	27,6138	28,8439	31	31
E9PYT0;P9	25,7505	25,4051	24,6669	27,1046	27,275	27,5442	48	48
E9PYT0;P9	23,8042	25,6346	27,9559	30,5384	30,9817	30,9041	48	48
E9PYT0;P9	24,9483	25,9081	25,0086	31,8133	32,1457	31,9672	48	48
E9PYT0;P9	26,443	23,1835	25,9507	30,0878	30,7069	31,0829	48	48
E9PYT0;P9	26,4408	25,7397	25,5039	30,8284	32,0866	32,0247	48	48
E9PYT0;P9	23,6065	23,179	23,9389	25,6518	25,9859	26,3764	23	23
E9PYT0;P9	22,7425	23,1175	24,1878	26,0187	25,4909	26,1927	23	23
Q99PT1	29,6284	29,6673	29,5755	28,0182	27,3527	27,6115	13	13
Q99PT1	31,1526	31,4984	32,3304	27,2925	25,4624	28,9325	13	13
Q99PT1	31,7337	31,6256	32,3336	30,0288	29,589	29,4944	13	13
Q99PT1	29,5408	29,6502	29,1115	28,4462	28,4161	27,9086	14	14
Q61210-5;	22,7258	28,2202	28,1739	30,0104	31,6156	31,3287	33	33
Q61210-5;	24,0586	24,232	24,4934	28,8167	30,8581	31,1701	33	33
E9PUF7;Q6	28,1501	28,1497	28,2229	29,9924	30,3526	30,3907	49	49

Q68FM7	27,6711	28,257	28,0774	32,6095	32,8532	32,662	73	73
Q68FM7	27,6253	26,2082	26,6919	32,6953	32,8186	32,8563	73	73
Q68FM7	26,9561	27,265	25,5845	33,1527	33,3197	33,459	73	73
Q68FM7	24,6035	24,8462	25,1126	29,2088	29,9048	28,9566	73	73
Q68FM7	23,6502	25,055	23,969	29,2511	30,4178	30,1891	73	73
Q68FM7	27,7403	29,6232	30,2645	32,0944	32,978	33,2457	73	73
Q68FM7	28,4122	28,7026	28,6702	30,7889	31,0835	31,5791	80	80
Q68FM7	28,1474	27,5786	27,485	30,007	29,1453	30,1521	80	80
Q8R4H2	29,8516	24,602	29,9393	33,2988	33,734	33,6016	77	77
Q8R4H2	27,2432	26,8546	25,8668	34,2937	33,9202	33,6519	77	77
Q8R4H2	25,7708	25,3214	26,8723	33,4545	33,6292	33,6119	77	77
Q8R4H2	25,4881	25,2442	25,0199	27,9474	28,8528	29,0529	77	77
Q8R4H2	24,0802	24,6002	24,4918	29,5874	30,5481	30,1224	77	77
Q8R4H2	31,4343	31,7327	31,6196	33,6698	34,1709	34,07	77	77
Q80U35;Q	29,3547	30,6503	30,7424	25,2959	27,4317	27,8442	19	19
Q80U35-2;	29,613	29,6722	29,5418	26,885	26,7104	26,8006	25	25
Q80U35-2;	29,1387	29,1596	28,4739	23,0582	22,9207	24,6684	25	25
Q6P9R4;Q(	24,8948	25,1712	26,0049	27,3968	29,7069	29,8688	20	20
Q6P9R4;Q(	23,7185	24,9447	23,4294	28,5728	29,3683	29,9721	20	20
Q6P9R4;Q(	23,3445	23,1021	22,4562	26,4681	27,3457	27,1846	24	24
Q60875;H3	28,3046	26,4998	26,3564	30,02	29,6779	29,7653	47	47
Q60875;H3	28,0504	27,1375	27,1474	30,268	30,29	30,4339	47	47
Q60875;H3	29,4564	31,0678	31,0776	32,9833	33,6895	33,4717	47	47
Q60875;H3	24,3544	28,2787	26,987	28,7385	31,0224	30,3602	47	47
Q60875;H3	31,6975	31,6064	31,2212	33,3552	33,4995	33,7747	78	78
Q60875;H3	30,6733	30,6965	30,2937	32,4501	31,8412	32,3398	78	78
Q60875;H3	24,2116	20,5982	23,7973	30,5475	30,4382	31,0588	78	78
F6WMJ3;C	26,2087	25,4498	24,574	29,9964	30,5361	30,4109	23	20
F6WMJ3;C	24,6054	24,7306	25,9328	29,6826	30,4283	30,3224	23	20
F6WMJ3;C	25,0346	26,9492	27,3245	31,5935	31,6518	31,9271	23	20
F6WMJ3;C	25,1856	25,3166	25,6607	30,3216	31,0433	30,6532	23	20
F6WMJ3;C	24,4002	24,967	25,4784	29,4027	30,6655	30,8441	23	20
Q9ES28;Q9	30,3102	28,7208	27,3787	35,3431	35,4225	35,3608	68	68
Q9ES28;Q9	26,9065	25,9222	25,1191	35,3948	35,2447	35,1034	68	68
Q9ES28;Q9	25,2788	25,8294	25,2457	34,8591	35,1369	35,0312	68	68
Q9ES28;Q9	29,8619	30,496	29,7755	34,5412	35,4402	35,3508	68	68
Q9ES28;Q9	29,0465	29,8161	28,9969	35,8181	35,8452	35,1766	68	68
Q9ES28;Q9	25,1104	24,6964	24,7361	27,5014	27,6791	26,9781	68	68
Q9D0J4	29,1258	28,978	28,3819	27,3874	26,7332	27,0243	10	10
P16460;Q3	24,0716	24,6628	23,5854	26,3806	26,0682	26,5715	2	2
Q8BH66	24,4693	24,6326	23,8939	25,8075	25,778	25,6015	6	6
Q4FK74;Q9	29,6103	30,2947	30,0892	26,4991	25,1975	25,2266	4	4
Q9D1K2;F7	24,3844	25,3281	26,74	22,0192	20,9762	21,3082	4	4
B1AZ47;Q8	23,7399	22,9137	23,7967	21,7572	22,0027	22,0675	8	8
B1AZ45;Q8	24,2545	24,6604	23,7654	30,1236	29,9366	29,829	42	2
Q3UKP6;Q	29,2851	29,4925	29,0407	36,2609	36,2124	36,076	43	43
Q3UKP6;Q	24,7086	24,6286	24,3025	33,3155	33,6748	33,2003	43	43
Q3UKP6;Q	25,612	23,6096	26,1024	35,2293	35,3443	35,431	43	43
O55028;Q3	23,9001	24,4767	24,6109	26,4503	27,7758	27,2593	4	4
Q91VR8	26,9347	26,4047	24,8612	30,5484	32,3383	31,3002	12	12

Q91VR8	27,9279	26,2961	27,3432	32,4582	33,3956	33,1474	12	12
Q91VR8	25,3551	24,8311	25,8092	29,7158	29,3552	27,6497	12	12
Q99N28;E9	25,6469	25,6325	26,3344	27,7118	27,076	27,2922	7	7
Q5SVJ0;P2	25,2587	28,3149	24,4845	28,3106	28,7993	29,3048	21	15
E9PWZ5;P4	24,3836	23,9482	23,0254	27,114	26,9392	26,4841	7	4
D3YZP9	25,4742	25,218	23,8193	27,8081	27,8412	28,1355	2	2
P60766;Q3	25,6322	25,5516	26,1199	24,8245	24,3056	22,9113	3	3
E9PVY0;D3	30,0569	29,8555	29,8382	32,9718	33,571	33,4727	72	64
E9PVY0;D3	27,4929	26,2378	27,6672	30,9188	31,9055	30,5076	72	64
E9PVY0;D3	26,2803	26,0549	24,6337	31,7853	33,2083	32,4922	72	64
E9PVY0;D3	26,3562	25,4182	25,7307	29,5117	30,794	30,7209	72	64
Q7TT50	32,6407	32,5108	32,4814	35,1895	35,3021	35,4176	105	105
Q7TT50	26,3861	27,0178	27,4921	34,0888	34,4611	34,3078	105	105
Q7TT50	28,1775	27,0562	25,3377	34,0413	34,7645	34,5059	105	105
Q7TT50	25,325	25,3016	25,252	28,9928	29,5787	29,6142	105	105
Q7TT50	25,6366	26,3279	25,3289	31,6507	31,8931	32,0661	105	105
Q91W92	29,4228	28,8667	29,3866	30,8549	31,4858	31,6099	14	13
Q91W92	26,9483	26,3836	24,5485	28,4848	29,3655	29,0275	14	13
A2A6Q1;Q	34,1325	33,2844	33,7551	36,0805	35,5699	35,7225	27	27
A2A6Q1;Q	28,6646	27,6649	28,0338	33,0086	32,4042	32,2371	27	27
A2A6Q1;Q	25,1658	24,7431	24,4512	29,3849	29,851	29,9665	27	27
Q8BGH7	25,8599	25,015	24,7582	27,5851	28,4296	28,071	2	2
E9QL53;P4	25,8912	24,2883	23,8924	28,0541	29,3414	29,6081	86	86
E9QL53;P4	26,5625	24,1583	24,5156	28,8382	32,4674	31,7681	86	86
E9QL53;P4	25,5675	26,5388	25,5677	32,7594	33,3739	33,447	86	86
E9QPY8;P4	22,6555	22,1928	21,4416	27,7505	28,0379	28,4545	56	56
E9QPY8;P4	23,1359	25,9143	23,2759	28,5925	26,8592	27,4479	56	56
Q921W4;D	24,6343	25,8541	23,5751	27,9756	28,2648	28,6396	7	7
E9Q8Z8;E9	24,1684	24,2592	24,5918	22,0307	21,8302	23,7358	6	6
Q5SQX6;E9	29,486	29,4056	29,569	32,6156	33,1557	32,6565	51	51
Q5SQX6;E9	27,4273	27,6147	27,7342	30,0165	32,44	32,5691	51	51
Q5SQX6;E9	29,2895	28,9869	29,0917	30,3354	30,7008	30,2344	51	51
Q8BPM0;C	22,4334	21,0426	23,4721	26,9412	26,8504	27,3198	42	42
Q8BPM0;C	22,2374	22,6913	23,2914	28,4308	27,445	28,1899	42	42
Q80U19	21,7287	22,1458	20,768	27,3199	27,1019	27,6038	40	38
Q80U19	24,5366	25,1054	25,7554	27,9296	26,9909	27,6771	40	38
Q80U19	23,7007	24,6168	25,2783	26,4338	26,6033	27,4167	40	38
E9PV41;E9	22,4059	21,5128	22,9812	24,6145	24,0463	23,7535	12	12
E9Q4U7;Q	25,2775	25,6037	25,5929	27,9213	29,2786	28,8453	17	17
E9Q4U7;Q	24,8192	24,7554	24,5957	28,577	28,7168	29,3162	17	17
Q3UWU7;(	27,3467	27,2148	27,2704	26,0923	25,7934	26,2217	9	9
E9QMR2	26,7636	25,909	26,5362	28,8742	31,0816	29,3813	80	80
E9QMR2	25,4659	26,3907	25,5215	30,2518	33,089	32,4595	80	80
E9QMR2	23,5209	24,8519	24,2843	30,5771	31,3431	30,8044	80	80
A2BFF9;Q3	24,0001	26,0386	23,1049	26,7593	27,2578	27,1415	6	6
B2KGQ2;Q	24,8118	24,7341	29,2702	30,5852	29,2539	29,7256	4	4
B2KGQ2;Q	28,6307	28,6385	24,6044	30,8962	30,7811	30,1585	4	4
O35459	21,5872	21,9357	20,5006	24,1112	22,9421	22,8557	5	5
Q9D9V3;Q	24,6253	26,2448	26,1497	29,1837	29,8085	29,3013	14	14
Q9D9V3;Q	25,6335	25,0583	24,5737	28,4749	28,9504	29,2432	14	14

P62631;B7	35,7865	35,3184	35,6441	31,6667	31,6249	31,8712	46	46
P62631;B7	36,0333	35,6234	35,0792	31,4784	31,1382	31,3606	46	46
P62631;B7	34,5191	34,4589	34,5626	31,9486	31,3838	31,4715	46	46
P63242;Q8	27,8239	27,8921	27,915	26,7966	26,7094	26,6782	5	5
F8WIL9;Q8	28,5222	29,4792	29,1635	30,0859	31,1191	31,1439	29	21
Q8BHL5-2;	29,324	29,9195	29,8331	30,6423	32,4272	32,1908	32	32
Q8BHL5-2;	28,4377	29,3808	29,6772	30,4449	32,0849	31,7418	32	32
Q60902;F8	30,7094	31,0854	31,307	28,6961	29,3507	29,6265	31	31
Q6KAR6;Q	21,7289	21,8582	22,7144	24,2711	23,6738	24,2965	12	12
Q3UQY4;Q	23,3339	23,1331	23,8709	22,3654	22,4522	21,7273	3	3
G5E8A2;Q(	25,444	28,5469	28,1	29,5296	30,7768	30,3426	19	19
G5E8A2;Q(	25,8624	23,7925	26,5588	27,7279	28,6813	29,88	19	19
G5E8A2;Q(	22,2242	22,052	22,8074	28,3944	28,2592	28,099	33	33
G5E8A2;Q(	23,7906	23,4956	23,3019	29,24	28,208	28,8648	33	33
Q80U16	21,8925	22,8338	22,5303	25,634	25,9257	26,1643	17	16
Q9QUI1;Q	26,6737	26,2483	24,2258	28,7993	29,1497	28,9244	6	6
P97807;P9	29,5662	30,0569	29,8223	31,1197	31,0364	31,3478	21	21
P45878;Q3	23,5573	24,5892	23,8033	21,9972	21,6691	22,2384	3	3
Q80TY0;A2	26,8729	26,8492	26,6829	28,3243	28,6258	28,9448	21	21
Q80TY0;A2	24,8992	25,3817	23,8405	29,9448	29,6868	29,6418	21	21
Q80TY0;A2	26,272	24,7208	24,9743	31,4474	31,2554	31,4471	21	21
Q80TY0;A2	25,6012	26,5199	25,7575	28,442	28,809	29,2503	21	21
E9PUK3	26,4507	26,3635	26,4721	30,3168	30,7844	30,8623	30	30
E9PUK3	24,8079	25,6061	25,9209	31,3869	31,4081	31,8154	30	30
E9PUK3	24,6504	23,9053	24,8415	31,5084	31,5989	31,6399	30	30
Q9WV18;C	23,4193	23,8369	23,2372	22,129	21,9444	21,849	6	6
P48320;Q5	26,932	26,2931	26,944	24,9126	23,9053	24,9149	4	3
Q64737;Q3	27,075	27,1792	27,2772	26,2262	25,9909	25,9981	6	6
O88741	21,7151	22,1419	23,3097	24,26	24,642	23,7256	9	9
Q68FF6	30,669	30,4246	30,3414	34,4125	35,2557	35,0532	52	52
Q68FF6	26,7686	28,7085	29,1668	34,9429	35,2101	34,8323	52	52
Q68FF6	25,3936	25,2601	26,9222	33,8362	34,0143	34,3625	52	52
Q68FF6	30,2404	30,9826	31,2049	34,4692	35,6106	35,3668	52	52
Q68FF6	29,2627	29,8381	29,3633	34,5658	34,991	34,5657	52	52
E9PVA6;Q8	24,1284	24,976	24,6117	28,7769	29,7737	29,7308	29	25
E9PVA6;Q8	24,8404	25,7943	25,4007	32,2496	31,8891	32,271	29	25
E9PVA6;Q8	25,3501	25,5801	24,2166	28,8933	30,3188	30,2948	29	25
E9PVA6;Q8	27,4418	28,0044	28,0593	33,5332	34,2057	33,2716	29	25
P18872;Q5	30,0842	30,4096	30,0818	31,6102	31,5894	31,3887	25	25
A2AEG6;P3	22,8752	22,7993	24,5803	25,3159	25,672	25,6886	8	8
Q4VAB2;Q	23,6736	24,6222	24,2908	21,5675	22,8632	22,1724	5	5
Q3U5I5;Q6	25,7189	26,3917	27,6503	29,113	29,0201	28,4785	16	16
B2RTN5;Q9	23,5303	25,2297	24,4283	29,0699	28,6952	28,971	9	9
A2AL35;P1	21,5814	21,8497	22,6028	23,2127	23,1107	23,8207	6	6
Q8K013;F8	25,0414	25,4239	25,1173	21,2788	22,1144	23,3455	6	6
F8VQK3	22,2567	23,0778	23,5097	24,7991	24,8129	25,0491	11	11
Q3U4H6-2	22,0772	22,4765	22,5918	24,5845	24,6487	24,8377	8	8
Q99JP6-2;(	30,7453	29,7738	30,0597	34,4051	33,2249	33,2312	26	26
Q99JP6-2;(	31,1258	29,4441	28,6973	35,5093	34,736	34,2858	26	26
Q99JP6-2;(	31,7488	30,1166	29,7076	34,266	33,3478	33,2909	26	26

Q4KL76;Q6	28,3777	28,0492	27,9576	25,2146	27,2744	25,3971	8	8
D3YXH0;P6	27,3127	28,2214	28,0455	25,0954	26,9453	25,9199	4	4
Q9DCE9	21,9688	21,1691	22,0057	24,0127	24,294	24,0563	6	6
Q6P549	23,8183	23,781	24,8866	28,214	28,9828	29,1427	17	17
Q6P549	24,2768	25,9508	25,6862	26,7167	29,0198	28,9018	17	17
Q6P549	24,3065	24,4596	24,2335	28,3001	28,7914	28,2373	17	17
Q6P549	23,2974	23,6141	21,5945	25,1865	24,8417	25,1202	16	16
Q6P549	23,2462	23,5404	22,1356	26,3622	25,1747	25,7342	16	16
E9QAD8;A4	23,4165	25,0666	24,3519	27,5055	27,5881	28,0491	6	6
Q3TES0;D6	25,2962	23,9398	24,0218	26,9668	28,0685	27,4001	7	7
Q3TES0;D6	25,5886	25,2	26,5198	28,8083	30,5925	29,6802	7	7
Q3TES0;D6	26,7964	23,9354	23,9357	30,047	30,8797	30,5713	7	7
Q3TES0;D6	24,2793	23,4818	25,4268	28,7406	27,6242	28,8766	7	7
Q9DCB8	28,1842	27,9155	28,9502	24,7482	23,63	25,5393	4	4
A2CG49-7;	30,4872	32,0608	31,5368	28,3771	28,9949	28,6462	34	27
E0CXZ9;P6	27,0485	27,1837	26,8076	25,1362	24,8906	24,74	8	8
E0CZ72;P2	22,6143	23,7449	24,6386	26,2237	26,8469	26,4219	8	8
Q8VED9	24,0601	24,4981	24,0772	21,8087	22,2815	21,5976	4	3
Q8JZS0	24,3422	25,4622	26,4592	28,1874	27,9572	27,5165	9	9
Q80Y17	24,8048	25,4692	25,3773	28,9614	29,1265	28,478	13	13
Q80Y17	25,1101	25,5766	25,2908	28,5618	29,5483	29,1695	13	13
F6SY09;P5	22,9438	23,7171	22,7882	24,581	24,6464	24,3245	7	7
E9PV22;B1	21,1778	22,6456	22,4218	23,6412	24,0083	23,4751	7	7
Q8K2P1	25,1543	24,4858	23,6295	29,2643	29,0212	28,9703	7	7
B1AV56;Q9	26,3264	25,6863	26,3452	23,682	24,1959	24,598	7	7
P27546;P2	23,6078	24,5593	24,0605	22,7691	22,6621	22,367	17	7
Q99LB6;Q9	26,7537	26,5584	26,5154	24,392	25,3393	24,2095	5	5
Q99MR8;F	26,5393	26,9451	27,3279	24,9025	24,4329	25,0981	9	9
Q8C436;Q8	24,9223	24,5835	23,9549	29,1376	26,212	27,0654	7	7
F8WGE8;Q	21,4966	21,0324	21,7429	23,341	23,8792	24,2808	13	13
Q3V100;Q9	24,2618	23,8444	23,8456	21,7622	22,0741	22,4286	7	7
P70290;Q5	25,6025	26,4966	26,4011	23,164	24,2782	23,0919	8	8
F6XPV7;F6	20,8556	21,2217	21,7769	23,8457	23,1693	24,3253	5	4
Q60605;Q6	26,7827	28,0026	27,1588	28,8738	29,7723	29,1161	9	9
Q9CQ25	24,4898	24,0945	23,2866	26,4393	26,8373	27,05	3	3
Q9CQ25	24,726	24,2074	23,4173	27,9468	28,6234	28,7223	3	3
Q91X97;D3	27,3977	27,4126	27,4171	23,7081	24,6255	23,9134	7	4
Q8BLF1	28,2411	27,6272	27,4797	25,5996	24,7103	24,6456	5	5
Q8BLF1	25,9224	25,8058	25,4329	26,8506	26,5643	26,9618	13	13
A2AS98;A2	29,23	28,9982	28,8523	32,9192	34,5641	33,5494	59	59
A2AS98;A2	25,9991	25,7203	26,1107	32,1372	33,9234	33,13	59	59
Q62425	30,6551	30,2364	30,6608	28,8495	28,8409	28,7219	8	8
Q9DCJ5	27,1347	27,2082	27,4168	25,0207	23,9332	23,8632	7	7
Q91WD5;D	22,4135	21,8375	21,5786	23,0328	24,8239	24,5089	5	5
P19246;F7	25,1889	24,4588	23,8874	28,3267	28,0597	27,0139	11	8
Q6P3D0	27,1795	27,8131	27,0284	23,8232	23,4129	22,6138	13	13
Q6P3D0	26,767	27,2961	26,6223	20,3651	22,8614	23,8606	13	13
Q6P3D0	25,6076	26,8576	26,4079	22,3146	22,4351	22,6829	13	13
P58281-2;I	30,1642	30,2141	30,3218	31,3672	32,0048	31,8159	50	50
P58281-2;I	29,279	29,5079	29,0826	31,6771	31,6041	31,5468	50	50

P58281-2;I	28,5179	28,1339	27,6163	32,2522	32,0275	31,8102	50	50
P58281-2;I	30,2445	30,0441	30,2225	32,3552	33,1811	32,9239	50	50
P58281-2;I	29,5431	29,8907	28,6778	32,2043	32,9169	32,1939	50	50
Q3TDA7;Q	29,2422	30,0201	30,4246	25,7257	24,0689	25,5135	16	14
Q3TDA7;Q	29,0054	29,372	28,831	24,1109	24,9511	25,4187	16	14
G5E884;O8	32,7505	32,6441	32,7858	35,9129	36,1638	36,059	42	42
G5E884;O8	31,0777	32,0078	31,6831	34,8872	35,2617	35,2873	42	42
G5E884;O8	31,4419	31,9578	30,7591	35,3169	35,3904	35,4967	42	42
G5E884;O8	30,25	30,2534	30,4937	32,5848	33,3663	33,1777	42	42
G5E884;O8	28,6729	28,0246	29,0213	32,2142	32,6772	32,1397	42	42
Q8CIN4	30,4934	29,5585	29,3035	32,5716	32,6619	32,8163	27	15
Q8CIN4	28,9489	28,118	28,8174	32,6399	32,6133	32,7167	27	15
Q8CIN4	27,944	27,3459	26,6813	32,9282	33,504	32,772	27	15
Q8CIN4	25,1332	24,7275	26,5235	29,8237	31,0223	30,9257	27	15
A3KGC1;Q	31,9759	32,4468	31,2745	33,9588	34,0217	34,2668	37	21
A3KGC1;Q	31,5662	31,305	31,9686	33,9087	33,8959	33,8915	37	21
A3KGC1;Q	29,197	29,6864	28,5726	32,8029	33,3348	32,7714	37	21
A3KGC1;Q	28,6119	28,1588	28,3546	31,975	32,2548	31,9815	37	21
A3KGC1;Q	25,7301	25,1339	25,8056	29,0097	30,2621	29,556	37	21
Q8BTW9	26,0078	25,8113	26,1093	28,1603	28,4836	27,817	9	9
Q3ULB5	23,8585	24,028	24,4668	25,473	25,9748	26,043	3	2
B1AYC2;Q8	26,9726	26,8098	27,0364	28,1576	28,3827	28,259	8	7
Q9Z101;D3	25,0309	24,9168	25,1567	28,6065	27,068	26,308	7	7
Q9Z101;D3	23,8762	24,5273	24,489	25,7401	27,0952	25,8793	7	7
Q8BFQ8	25,3066	24,2893	24,7663	27,8407	28,7127	27,7418	4	4
O55057;Q3	24,3372	24,2485	24,7024	23,5013	23,1515	23,3969	4	4
E9Q3L2	24,0336	24,368	23,4257	25,1344	25,5655	25,0808	22	22
Q8BTI9	25,4108	24,1283	24,8687	26,9053	28,2008	28,385	11	11
P26450;Q8	25,3896	25,9067	26,1492	28,8041	29,0871	30,2447	11	11
P26450;Q8	24,2941	24,2735	25,317	28,1002	29,6719	29,3613	11	11
P26450;Q8	25,7579	25,7876	25,4961	27,6735	27,4981	27,944	11	11
P26450;Q8	23,9916	24,4784	23,2036	27,4417	27,4518	27,5346	11	11
Q3UJ95;Q8	26,9225	25,2787	23,9653	27,663	27,9356	28,0024	9	9
P70268-2;I	24,3829	25,3213	25,1449	27,7427	29,6541	28,8216	18	18
P70268-2;I	22,9373	23,538	22,9715	25,0984	24,2372	25,612	13	13
P70268-2;I	22,3595	21,5714	22,3414	24,5308	23,7728	24,032	13	13
G3X9A7;Q8	22,4302	22,3442	22,236	25,3023	23,7232	25,0118	8	8
O35405	28,1181	28,2649	27,9241	27,2295	24,9715	24,432	5	5
Q66T02;B1	26,4431	23,4091	24,4345	28,4534	29,0858	29,358	8	8
Q66T02;B1	24,7063	24,5894	25,3936	27,7765	27,943	29,0536	30	30
Q66T02;B1	26,8178	27,0164	26,4948	28,5445	28,1401	28,9183	30	30
Q8CJH3	25,3195	23,0082	25,4993	26,6726	28,1129	27,8022	5	5
B2RXS4;E9	23,5105	24,1338	22,9912	26,4725	25,7856	26,3537	14	14
Q91XF0	22,1407	21,8915	22,0549	24,484	24,9748	24,3284	6	6
Q3UYC0;Q	27,3279	27,6946	27,6969	28,7748	28,5417	28,9593	16	16
P62137;Q3	25,3686	25,6275	24,5916	27,7456	27,7902	27,7677	9	9
Q3TDD9	25,6834	25,3034	26,3567	29,1523	30,1264	28,8315	14	14
Q3TDD9	24,1234	23,9825	23,7306	27,9843	28,6731	28,717	14	14
Q60996;Q	21,7732	22,5216	23,9882	24,9253	25,035	24,7231	8	8
Q69ZK0	28,1534	27,8774	28,5158	24,1872	23,6294	24,8871	11	11

Q5DTK3;Q	25,9325	26,0665	25,8582	27,0664	28,1822	27,7466	8	8
Q5DTK3;Q	26,0743	24,6683	25,8402	27,1433	27,1655	27,8986	8	8
Q6PE13	21,8219	22,0098	21,682	23,249	23,0874	22,9114	3	3
Q8C0E9;E9	22,1836	21,4465	22,9206	23,3768	23,6161	24,1834	5	5
Q9QUM9;I	26,5461	26,9513	26,197	24,7349	24,4033	24,791	5	5
Q9CR00	24,1841	24,902	23,8323	26,3893	26,0277	26,041	4	4
P97372;Q5	22,3598	22,6346	22,5312	24,1839	23,7274	24,0096	5	4
P62827	29,7327	29,7655	29,9168	27,9163	27,3894	27,6063	18	18
P62827	30,2343	29,8905	29,2494	27,9795	28,0416	27,9459	18	18
P62827	29,3426	29,498	29,2378	27,584	28,0753	27,2519	18	18
Q52L50;Q9	22,4866	22,4953	23,8563	25,4138	24,4895	25,2423	6	6
E9Q912;E9	31,5589	30,6844	30,6046	29,2318	28,7537	28,9112	27	27
F2Z408;G5	23,2059	24,7232	23,6093	27,2371	27,3054	27,6028	8	8
Q9JJ43-3;C	21,872	21,3311	22,5293	24,1536	24,0189	24,3508	12	2
P97492	27,0299	25,2866	25,0275	28,3647	28,2824	28,7287	12	12
P97492	25,9668	25,954	25,8819	29,2711	29,6579	29,4308	12	12
P97492	25,7741	26,0432	26,5949	27,7144	28,4099	28,146	12	12
Q8BWR8	21,9053	22,9494	21,6192	23,9762	23,7046	24,9162	12	12
P70335;P7	21,0926	22,8838	21,874	23,6673	23,9162	24,1253	13	7
F8VPK5;P7	26,1883	26,4891	23,2215	29,0742	29,0721	29,8596	78	78
F8VPK5;P7	26,7955	25,622	26,3999	29,2431	28,0968	28,2774	78	78
F8VPK5;P7	25,3277	26,7337	26,4013	29,8978	32,1701	31,7473	78	78
F8VPK5;P7	26,5603	27,0314	28,176	33,6193	34,0758	34,0645	78	78
E9PYM9;F8	26,0174	26,0218	26,1176	29,4731	29,389	28,9697	65	65
E9PYM9;F8	26,4132	25,7472	26,7987	29,8985	28,6115	29,1193	65	65
P67984;Q4	25,3611	24,7334	25,3805	22,7747	22,4312	23,6978	5	3
Q6ZWU9;E	28,312	27,2619	28,1822	25,8787	25,4772	26,0668	3	3
Q8C6B2-2;	26,2945	25,9151	25,1475	27,2295	28,5938	28,3772	12	12
Q8C6B2-2;	24,8242	26,3305	27,0496	27,8266	29,0406	29,7056	12	12
Q8C6B2;Q8	22,0756	21,9931	22,2584	23,494	23,4639	23,1574	4	4
Q3UXS0;O	22,7436	22,0311	23,057	23,8206	23,8109	24,0462	4	4
Q8R127;D3	25,1334	24,5764	23,8885	26,7529	26,6197	26,8021	3	3
P28661;P2	27,9252	28,1864	29,0163	30,3045	29,9054	30,9384	16	14
E9Q9F5;O5	31,0877	31,1349	30,0115	32,3458	32,4577	32,2702	22	22
B1AQZ0;B1	27,9132	28,8357	28,0801	29,6569	31,1264	31,5157	18	13
Q80UK0	24,861	26,1062	25,2564	27,1763	28,6002	28,0432	13	13
Q80UK0	25,0818	25,3553	25,3175	29,178	29,7191	29,4859	13	13
Q80UK0	25,3998	24,8792	24,3288	27,1379	27,8642	27,8634	13	13
Q69ZI1;E9(	24,7767	24,0347	23,2971	26,7889	27,6309	27,3724	4	4
Q9DB41;Q	27,3016	26,7142	27,1005	24,0864	24,8316	25,8527	6	3
O54988;A2	24,2853	25,7165	26,1147	26,7927	28,6999	28,3995	10	10
Q61548;Q(	25,0771	26,2796	25,2908	27,2923	29,5633	28,4756	16	16
Q3UHD6;C	22,1333	22,2157	22,9702	23,7826	24,5004	24,3745	11	11
Q8C0J6	24,385	25,7524	25,6146	27,3265	27,0277	27,0871	8	8
Q8C0J6	24,4714	24,6497	24,098	27,8726	27,5376	27,5053	8	8
F8VPQ4;Q8	24,473	24,6051	24,5638	25,5182	26,8393	26,54	5	5
P14576;E9	24,4893	25,1576	23,8925	21,3858	22,806	23,0729	13	13
Q99L47;F8	22,8326	24,0456	24,7776	27,4588	26,7371	27,1053	7	7
P70297;Q3	25,9608	26,8008	27,544	25,1568	23,6733	24,3256	3	3
E9QM25;C	21,3674	22,4256	21,9938	23,1476	23,1935	23,7792	3	3

P63046;P6	24,8363	25,2037	23,941	27,673	28,1865	28,8375	5	5
F8WGK2	28,4191	30,6554	30,4025	26,1446	27,9568	24,7002	5	5
Q6ZQ29-2;	25,5207	25,8112	25,5467	28,1032	27,0689	27,3901	9	9
Q6ZQ29-2;	24,6483	23,9438	24,9669	26,8854	27,0973	27,1562	9	9
Q6ZPF3;Q6	29,3082	29,8391	30,1726	26,1086	27,1434	26,8295	14	14
F8WJF7;Q8	27,6809	29,1111	27,4231	25,2887	25,8054	26,1876	4	4
Q9R1R2;Q	26,2773	25,4919	25,0893	28,0003	28,1931	28,5507	17	17
Q9R1R2;Q	24,3475	24,9908	24,517	28,8114	28,2975	28,4197	17	17
Q0KL02-4;(	30,8915	32,2817	32,074	28,5354	29,7782	29,4747	38	38
Q8CJ53;Q8	27,117	27,4383	25,5746	30,4841	31,0674	30,8689	20	20
Q8CJ53;Q8	24,9423	24,2383	26,1101	30,7368	30,5384	31,1146	20	20
Q8CJ53;Q8	25,0645	26,4126	22,8407	30,8079	30,6976	30,7443	20	20
Q545E6;Q6	23,0731	22,2853	23,1057	26,2791	26,0898	26,1207	6	6
Q9QZE7	22,3383	21,8759	22,9996	23,7003	25,4824	23,9485	9	9
Q9CR09	23,6312	23,4912	23,0902	22,1618	21,9063	22,0253	4	4
Q8R5H6	29,3197	28,521	29,7536	33,0654	33,8916	33,4645	24	24
Q8R5H6	27,5362	25,8656	26,0234	31,8696	31,8488	31,8638	24	24
Q8R5H6	28,2054	28,2571	28,4662	30,6383	30,3708	30,2835	24	24
Q8VHI6	27,3739	26,7503	26,7262	31,1943	32,3378	32,2341	15	15
Q8VHI6	25,7375	27,7191	26,4006	32,7701	33,2671	33,032	15	15
Q8VHI6	26,6606	26,8048	26,3279	28,0436	27,9725	28,0166	15	15
Q3TXX8;Q9	31,7529	32,0837	32,3153	34,1241	34,7047	34,3238	32	32
Q3TXX8;Q9	29,3043	28,6118	29,3082	33,8514	33,8378	33,8747	32	32
Q3TXX8;Q9	28,1433	29,9051	29,1246	34,6893	34,7172	34,7513	32	32
E9Q1S7;P9	27,2398	27,4344	27,1614	24,7197	22,9878	24,6674	4	4
A2ATB9;Q8	25,043	24,2741	25,249	28,9368	28,916	28,7133	6	6
Q6PEV3	27,3378	28,3613	29,3083	32,7319	32,8431	31,4298	29	29
Q6PEV3	29,1067	29,8339	28,9539	33,5494	33,4693	33,6285	29	29
Q6PEV3	27,4625	26,8181	26,0282	31,9032	31,5362	32,2731	29	29
P0C7L0;E9	29,0374	29,6961	29,2648	32,4668	32,3234	32,3164	17	17
P0C7L0;E9	29,0157	30,4487	28,9732	33,1523	32,9859	33,2298	17	17
P0C7L0;E9	24,9355	25,1631	25,4076	30,3987	29,7998	29,9994	17	17
Q8C3W1	24,4117	24,505	24,7764	27,5458	27,7489	27,6485	12	12
Q80U16-5;	21,9288	23,2	22,2916	23,3022	24,3688	25,0613	15	3
Q8C3W1	24,1401	23,8173	24,0772	26,804	26,8843	27,7556	19	19
Q8C3W1	25,8105	25,364	25,3513	27,3169	26,7236	27,4353	19	19
Q8C3W1	25,1438	25,463	25,215	26,7933	26,3659	26,803	19	19

nteractions were identified with LF-qGAP. A number of interactions were

rometry							Statistics	
Unique pe	Sequence (	Mol. weigh	Sequence l	PEP	Intensity	Proteins	-Log t-test p va	t-test Diffe
9	49,4	25,83	239	2,05E-58	6,17E+08	2	1,53832	2,82228
9	49,4	25,83	239	2,05E-58	6,17E+08	2	2,21896	3,9198
9	49,4	25,83	239	2,05E-58	6,17E+08	2	3,3915	2,49764
8	47,1	28,152	244	7,68E-43	1,63E+09	2	2,077	-2,29053
15	44,1	52,287	481	0	2,14E+10	15	3,89665	4,14041
15	44,1	52,287	481	0	2,14E+10	15	4,37118	6,05094
15	44,1	52,287	481	0	2,14E+10	15	2,5273	1,53206
15	44,1	52,287	481	0	2,14E+10	15	1,84488	2,55006
14	44,8	49,387	446	0	1,07E+10	2	4,74953	5,15818
14	44,8	49,387	446	0	1,07E+10	2	3,76298	6,39705
14	44,8	49,387	446	0	1,07E+10	2	2,07479	2,28479
9	21,7	98,987	859	1,91E-44	5,56E+08	8	1,52354	2,12188
16	41,9	47,907	430	0	3,94E+09	1	3,49919	3,38787
16	41,9	47,907	430	0	3,94E+09	1	3,85202	3,43732
16	41,9	47,907	430	0	3,94E+09	1	3,79269	4,07868
32	84	44,816	424	0	2,79E+11	1	4,87644	4,14807
32	84	44,816	424	0	2,79E+11	1	4,9233	5,97495
24	64,9	44,816	424	0	8,29E+10	1	3,07268	1,88783
24	64,9	44,816	424	0	8,29E+10	1	3,32401	2,13176
6	17,4	41,297	397	3,04E-12	5,19E+08	4	3,88716	2,48226
5	9,9	93,042	837	6,05E-39	8,31E+08	8	3,74882	2,62959
12	7,1	306	2776	6,95E-44	5,61E+08	7	1,7925	3,17257
11	12,4	122,79	1121	1,83E-88	7,24E+08	1	1,92447	2,05678
11	12,4	122,79	1121	1,83E-88	7,24E+08	1	1,52939	3,05488
6	65,2	20,601	181	0	1,04E+10	11	1,97796	-2,30203
28	18,3	229,72	2089	3,55E-253	4,62E+09	7	2,4285	5,44331
28	18,3	229,72	2089	3,55E-253	4,62E+09	7	4,15039	5,78996
28	18,3	229,72	2089	3,55E-253	4,62E+09	7	4,51887	4,05938
31	21,4	229,72	2089	1,83E-293	1,15E+10	7	2,66196	2,76102
31	21,4	229,72	2089	1,83E-293	1,15E+10	7	2,72741	3,72379
48	43,2	172,47	1503	0	8,1E+09	2	2,3863	2,03378
48	43,2	172,47	1503	0	8,1E+09	2	1,84364	5,00985
48	43,2	172,47	1503	0	8,1E+09	2	4,48262	6,68706
48	43,2	172,47	1503	0	8,1E+09	2	2,17097	5,43348
48	43,2	172,47	1503	0	8,1E+09	2	3,4975	5,75175
23	19,6	172,47	1503	1,10E-104	2,06E+09	2	2,8785	2,42991
23	19,6	172,47	1503	1,10E-104	2,06E+09	2	2,21465	2,55146
13	67,2	23,407	204	0	1,45E+10	1	3,25707	-1,96296
13	67,2	23,407	204	0	1,45E+10	1	1,85464	-4,43133
13	67,2	23,407	204	0	1,45E+10	1	2,8735	-2,19356
14	60,8	23,407	204	0	3,88E+10	1	2,09814	-1,17724
33	46,2	109,25	920	0	6,91E+09	8	1,14772	4,61158
33	46,2	109,25	920	0	6,91E+09	8	2,88653	6,02028
49	52,9	108,69	976	0	2,18E+10	8	4,05268	2,07102

4	61,5	171,8	1552	0	3,66E+10	2	4,81635	4,70642
4	61,5	171,8	1552	0	3,66E+10	2	3,84594	5,9483
4	61,5	171,8	1552	0	3,66E+10	2	3,66862	6,70859
4	61,5	171,8	1552	0	3,66E+10	2	3,83286	4,50265
4	61,5	171,8	1552	0	3,66E+10	2	3,30292	5,72796
4	61,5	171,8	1552	0	3,66E+10	2	1,88945	3,5634
6	56,6	171,8	1552	0	3,88E+10	3	3,29949	2,5555
6	56,6	171,8	1552	0	3,88E+10	3	2,24422	2,03114
2	61,6	172,35	1543	0	6,97E+10	1	1,42404	5,41382
2	61,6	172,35	1543	0	6,97E+10	1	4,07341	7,30041
2	61,6	172,35	1543	0	6,97E+10	1	4,08441	7,57708
2	61,6	172,35	1543	0	6,97E+10	1	3,11044	3,36696
2	61,6	172,35	1543	0	6,97E+10	1	4,23301	5,69524
2	61,6	172,35	1543	0	6,97E+10	1	3,75773	2,37471
19	13	221,67	2057	0	5,03E+09	2	1,69479	-3,3919
25	30	114,37	2057	0	9,56E+09	2	5,82285	-2,81034
25	30	114,37	2057	0	9,56E+09	2	3,05334	-5,37496
20	27,6	114,33	1021	2,32E-182	2,17E+09	3	1,86327	3,63385
20	27,6	114,33	1021	2,32E-182	2,17E+09	3	2,98946	5,27357
23	29,4	114,33	1021	5,22E-134	1,74E+09	3	3,35805	4,03187
47	55,8	111,97	985	0	3,68E+10	17	1,91751	2,76746
47	55,8	111,97	985	0	3,68E+10	17	3,14584	2,88552
47	55,8	111,97	985	0	3,68E+10	17	2,10325	2,84754
47	55,8	111,97	985	0	3,68E+10	17	1,22775	3,50038
78	68,3	111,97	985	0	3,13E+11	17	3,35778	2,03478
78	68,3	111,97	985	0	3,13E+11	17	2,71691	1,65589
78	68,3	111,97	985	0	3,13E+11	17	2,59978	7,81244
8	38,7	89,811	795	0	4,71E+09	4	3,2187	4,90366
8	38,7	89,811	795	0	4,71E+09	4	3,32676	5,05483
8	38,7	89,811	795	0	4,71E+09	4	2,74557	5,288
8	38,7	89,811	795	0	4,71E+09	4	4,51418	5,28509
8	38,7	89,811	795	0	4,71E+09	4	3,20487	5,35555
0	81,9	97,055	862	0	9,39E+10	4	2,82661	6,57224
0	81,9	97,055	862	0	9,39E+10	4	4,22224	9,26503
0	81,9	97,055	862	0	9,39E+10	4	5,89005	9,55775
0	81,9	97,055	862	0	9,39E+10	4	3,80543	5,06625
0	81,9	97,055	862	0	9,39E+10	4	4,29091	6,32679
0	81,9	97,055	862	0	9,39E+10	4	3,2874	2,5386
10	50,5	20,864	184	5,63E-128	2,11E+10	1	2,41571	-1,78023
2	11,2	46,584	412	5,20E-58	3,04E+08	2	2,53586	2,23347
6	14,5	63,377	558	9,21E-28	4,23E+08	1	2,40935	1,3971
4	41,1	17,6	168	3,47E-234	1,48E+10	3	3,10693	-4,35699
4	32,8	13,37	119	1,89E-12	2,74E+09	2	2,24375	-4,04965
8	17	59,236	535	4,12E-18	7,98E+08	9	2,16409	-1,54096
2	78,8	53,274	390	0	1,32E+09	2	4,52038	5,73629
3	77,6	57,595	522	0	8,52E+10	7	5,97402	6,91036
3	77,6	57,595	522	0	8,52E+10	7	5,90223	8,85031
3	77,6	57,595	522	0	8,52E+10	7	3,74294	10,2269
4	11,7	46,587	412	2,43E-11	1,84E+08	3	2,51237	2,83259
12	88	8,7608	75	0	1,24E+10	1	2,55852	5,32876

12	88	8,7608	75	0	1,24E+10	1	3,332	5,81134
12	88	8,7608	75	0	1,24E+10	1	2,16473	3,57511
7	30,8	42,964	396	4,18E-203	1,58E+10	2	2,12704	1,48876
10	47,4	72,902	666	0	1,42E+10	10	1,08767	2,78551
4	32,4	33,328	286	5,87E-72	5,3E+08	3	2,64031	3,06002
2	7,2	52,938	469	1,40E-07	7,07E+08	1	2,38181	3,09112
2	20,4	21,258	191	8,87E-37	1,04E+09	2	1,36948	-1,75411
64	45,7	196,92	1732	0	1,66E+10	10	4,17849	3,42163
64	45,7	196,92	1732	0	1,66E+10	10	2,53861	3,97801
64	45,7	196,92	1732	0	1,66E+10	10	3,31244	6,83894
64	45,7	196,92	1732	0	1,66E+10	10	3,08	4,50713
96	63,9	194,75	1713	0	6,54E+10	15	5,33083	2,75875
96	63,9	194,75	1713	0	6,54E+10	15	4,57021	7,32055
96	63,9	194,75	1713	0	6,54E+10	15	3,05356	7,58008
96	63,9	194,75	1713	0	6,54E+10	15	4,45434	4,10236
96	63,9	194,75	1713	0	6,54E+10	15	4,35733	6,1055
13	39,1	43,095	409	6,04E-57	8,87E+08	1	2,68111	2,09148
13	39,1	43,095	409	6,04E-57	8,87E+08	1	1,75695	2,99913
26	82,5	37,869	349	0	2,65E+10	4	2,69844	2,06691
26	82,5	37,869	349	0	2,65E+10	4	3,53452	4,42884
26	82,5	37,869	349	0	2,65E+10	4	4,26232	4,9474
2	66,7	9,2234	84	6,77E-124	3,77E+09	1	2,61706	2,81757
86	39,9	235,36	2055	0	2,8E+10	11	2,28721	4,3106
86	39,9	235,36	2055	0	2,8E+10	11	1,94414	5,94572
86	39,9	235,36	2055	0	2,8E+10	11	4,31828	7,30212
1	28,9	238,82	724	6,00E-276	6,13E+09	8	3,89847	5,98439
1	28,9	238,82	1552	6,00E-276	6,13E+09	8	1,56353	3,52454
7	25,9	38,725	348	8,65E-32	4,05E+08	6	2,20272	3,60551
6	6,8	108,17	967	3,95E-13	8,56E+08	19	1,36596	-1,80756
32	45,9	145,66	1253	0	1,57E+10	6	4,29573	3,32237
32	45,9	145,66	1253	0	1,57E+10	6	2,09145	4,08314
32	45,9	145,66	1253	0	1,57E+10	6	2,83264	1,30088
40	41,3	123,37	1077	0	7,15E+09	3	2,55703	4,72112
40	41,3	123,37	1077	0	7,15E+09	3	3,61524	5,28185
38	42,1	128,37	1115	1,69E-201	8,6E+09	2	3,7438	5,79436
38	42,1	128,37	1115	1,69E-201	8,6E+09	2	2,22492	2,40004
38	42,1	128,37	1115	1,69E-201	8,6E+09	2	1,85124	2,28601
12	13,3	140,4	1264	4,42E-36	9,84E+08	7	1,68238	1,83812
17	25,8	125,41	1102	6,03E-135	7,56E+08	6	2,81529	3,19038
17	25,8	125,41	1102	6,03E-135	7,56E+08	6	4,20832	4,14663
9	45,2	22,498	199	1,17E-50	6,09E+09	2	3,14122	-1,24151
3	47,9	234,91	2058	0	1,24E+10	1	2,0386	3,37612
3	47,9	234,91	2058	0	1,24E+10	1	2,59809	6,14076
3	47,9	234,91	2058	0	1,24E+10	1	3,93291	6,68916
6	21,5	71,424	638	2,79E-145	1,01E+09	7	1,41242	2,67162
2	34,8	10,35	89	3,83E-26	9,08E+09	4	1,0874	3,58289
2	34,8	10,35	89	3,83E-26	9,08E+09	4	1,14591	3,32073
5	23,9	36,118	327	7,18E-14	3,67E+08	2	1,52909	1,96183
14	57,8	35,467	322	4,17E-142	8,93E+08	3	2,59458	3,75795
14	57,8	35,467	322	4,17E-142	8,93E+08	3	3,25336	3,80102

25	71,5	50,454	463	0	1,47E+12	2	4,77847	-3,86207
25	71,5	50,454	463	0	1,47E+12	2	3,87816	-4,25292
25	71,5	50,454	463	0	1,47E+12	2	4,08752	-2,91227
5	56,5	16,832	154	2,70E-68	2,02E+09	2	4,86315	-1,14895
21	41	85,559	727	0	3,16E+09	5	1,73976	1,72803
24	45,3	82,542	732	0	4,73E+09	9	1,60186	2,06119
24	45,3	82,542	732	0	4,73E+09	9	1,65103	2,25863
31	50,5	99,307	907	5,52E-255	3,58E+09	7	2,28587	-1,80947
12	20,1	86,454	755	2,56E-40	1,23E+09	2	2,22991	1,97993
3	20,7	25,172	227	2,05E-13	1,48E+08	2	1,78637	-1,26431
18	24,9	132,35	1223	1,27E-292	4,11E+09	2	1,29187	2,85267
18	24,9	132,35	1223	1,27E-292	4,11E+09	2	1,49732	3,35852
32	35,2	132,35	1223	0	9,76E+09	2	4,75764	5,88968
32	35,2	132,35	1223	0	9,76E+09	2	4,01952	5,24156
4	20,2	118,97	1078	1,49E-70	1,19E+09	1	3,41231	3,48915
6	39,2	20,14	189	9,51E-65	6,1E+08	3	1,88225	3,24187
21	59,6	54,356	507	0	1,31E+10	3	2,87414	1,35286
3	24,3	15,344	140	2,40E-09	1,57E+09	2	2,33547	-2,01504
21	44	71,343	616	1,70E-157	1,35E+09	14	3,19724	1,82998
21	44	71,343	616	1,70E-157	1,35E+09	14	3,39018	5,05066
21	44	71,343	616	1,70E-157	1,35E+09	14	3,62864	6,06094
21	44	71,343	616	1,70E-157	1,35E+09	14	2,84032	2,87424
1	64,6	63,974	551	0	4,82E+09	1	4,77253	4,22575
1	64,6	63,974	551	0	4,82E+09	1	4,14864	6,09188
1	64,6	63,974	551	0	4,82E+09	1	4,79667	7,11668
6	9,1	108,21	960	2,57E-66	5,43E+08	5	2,83393	-1,52363
3	10,3	65,223	585	5,01E-79	2,77E+08	2	2,238	-2,14546
6	10,7	107,5	1010	2,90E-171	6,44E+08	4	3,47367	-1,1054
8	26	41,31	358	8,26E-34	2,38E+09	2	1,53838	1,82033
2	81,6	85,299	770	0	8,8E+10	1	4,07654	4,42884
2	81,6	85,299	770	0	8,8E+10	1	3,09574	6,78048
2	81,6	85,299	770	0	8,8E+10	1	3,91528	8,21238
2	81,6	85,299	770	0	8,8E+10	1	3,17706	4,33958
2	81,6	85,299	770	0	8,8E+10	1	4,67284	5,21947
4	53	84,456	759	0	4,25E+09	5	3,546	4,8551
4	53	84,456	759	0	4,25E+09	5	4,62838	6,79143
4	53	84,456	759	0	4,25E+09	5	2,7875	4,78671
4	53	84,456	759	0	4,25E+09	5	4,16445	5,83498
3	60,2	40,084	354	0	1,81E+11	4	3,30128	1,33755
8	19,2	36,196	328	5,65E-114	3,87E+09	15	1,64422	2,14055
5	18	41,598	372	1,10E-36	3,17E+08	4	1,89053	-1,99452
16	68,7	25,238	217	1,76E-251	9,8E+09	6	1,72204	2,28355
9	8,9	170,39	1499	2,08E-90	1,39E+09	3	3,06805	4,51593
6	10,3	85,941	780	3,55E-48	1,51E+09	6	1,65377	1,37005
6	22,4	40,141	366	4,44E-27	3,01E+08	6	2,06964	-2,94796
11	26	81,83	730	7,47E-135	3,45E+09	2	2,17186	1,93898
8	24,9	62,22	486	4,60E-33	7,53E+08	5	3,73459	2,30845
25	79,7	40,064	356	1,53E-291	8,43E+09	3	2,66838	3,42744
25	79,7	40,064	356	1,53E-291	8,43E+09	3	2,49979	5,08798
25	79,7	40,064	356	1,53E-291	8,43E+09	3	1,94895	3,11059

8	73,5	10,963	102	1,82E-86	6,27E+09	2	1,49534	-2,16614
4	9,4	32,627	298	9,14E-66	2,74E+09	2	1,44344	-1,87298
6	20,8	48,493	423	3,48E-27	4,61E+08	3	2,95842	2,40648
17	22,8	138,97	1257	2,52E-211	1,83E+09	1	3,249	4,61787
17	22,8	138,97	1257	2,52E-211	1,83E+09	1	1,47904	2,90814
17	22,8	138,97	1257	2,52E-211	1,83E+09	1	4,59174	4,10973
16	19,3	138,97	1257	1,51E-55	1,27E+09	1	1,59656	2,21413
16	19,3	138,97	1257	1,51E-55	1,27E+09	1	2,14867	2,78299
5	4,6	162,83	1488	2,51E-56	5,51E+08	5	2,60718	3,43591
7	9,2	129,12	1195	2,95E-149	2,89E+09	3	2,3094	3,05917
7	9,2	129,12	1195	2,95E-149	2,89E+09	3	2,42799	3,92425
7	9,2	129,12	1195	2,95E-149	2,89E+09	3	2,32982	5,61018
7	9,2	129,12	1195	2,95E-149	2,89E+09	3	2,36335	4,01783
4	36,4	16,718	154	2,24E-211	1,94E+09	1	2,36976	-3,71076
2	16	338,88	2964	0	2,33E+09	15	2,25086	-2,68889
8	27,5	42,734	382	5,53E-158	1,38E+09	6	3,70927	-2,09099
8	16,3	83,86	743	2,76E-20	3,6E+08	7	2,00279	2,83154
3	20,9	18,955	172	1,55E-14	2,16E+09	1	3,13687	-2,31589
5	44,6	25,992	233	4,83E-246	7,06E+09	2	1,73329	2,46581
13	20	112,62	1036	5,06E-68	6,18E+08	1	3,66538	3,63819
13	20	112,62	1036	5,06E-68	6,18E+08	1	3,53781	3,76736
7	24,9	42,499	360	8,79E-20	1,18E+09	4	1,96731	1,3676
7	16,1	65,903	603	1,94E-52	9,34E+08	3	1,55117	1,62647
7	33,9	23,728	221	2,18E-49	6,43E+08	1	3,30795	4,66208
7	39,4	24,794	231	1,99E-119	8,81E+08	2	2,33729	-1,96068
7	22,3	117,43	1125	1,39E-98	7,01E+08	5	2,10164	-1,47647
5	17,1	37,392	334	4,70E-23	5,03E+08	3	2,26904	-1,96222
9	22,5	79,343	717	3,78E-68	5,99E+08	3	2,67203	-2,12627
7	30,3	25,535	228	1,43E-172	8,1E+09	2	1,51027	2,98477
13	8,9	220,45	545	1,65E-33	3,3E+08	24	2,66601	2,40971
7	27,7	46,575	423	3,43E-94	1,07E+09	3	2,87506	-1,89563
8	24,2	52,227	466	5,25E-37	5,66E+08	9	2,29149	-2,65538
3	72	7,9609	228	1,32E-98	8,49E+08	3	2,3611	2,49533
9	60,3	16,93	151	1,71E-67	2,6E+09	5	1,90277	1,9394
3	44,7	16,524	159	1,85E-127	7,11E+08	1	2,6832	2,81855
3	44,7	16,524	159	1,85E-127	7,11E+08	1	3,17252	4,31394
4	47,2	22,245	193	0	2,01E+09	4	3,5535	-3,32679
5	27,2	45,739	408	2,86E-46	1,36E+09	1	2,71532	-2,79752
13	44,4	45,739	408	7,18E-146	7,48E+09	2	2,31965	1,07187
59	57,6	129,51	1134	0	2,42E+10	6	3,1571	4,65073
59	57,6	129,51	1134	0	2,42E+10	6	3,75193	7,12015
8	86,6	9,3267	82	2,75E-74	6,75E+09	1	3,51553	-1,71332
7	50	19,992	172	3,31E-72	1,44E+09	1	2,82798	-2,98086
5	12,1	52,625	463	9,01E-23	2,06E+09	3	1,64398	2,17866
8	12,8	116,99	1090	3,45E-80	1,51E+09	2	2,40579	3,28841
13	55,9	21,825	195	5,13E-199	4,62E+09	4	3,15738	-4,05707
13	55,9	21,825	195	5,13E-199	4,62E+09	4	1,89064	-4,53279
13	55,9	21,825	195	5,13E-199	4,62E+09	4	3,25064	-3,8135
50	57,8	115,59	960	0	3,02E+10	6	2,81147	1,49593
50	57,8	115,59	960	0	3,02E+10	6	4,25599	2,31947

50	57,8	115,59	960	0	3,02E+10	6	3,76585	3,9406
50	57,8	115,59	960	0	3,02E+10	6	3,33407	2,64971
50	57,8	115,59	960	0	3,02E+10	6	2,67964	3,06783
14	45,1	55,832	486	3,94E-169	4,08E+09	2	2,80699	-4,79295
14	45,1	55,832	486	3,94E-169	4,08E+09	2	3,28943	-4,24254
24	77,6	60,607	544	0	1E+11	3	5,60417	3,31844
24	77,6	60,607	544	0	1E+11	3	3,5281	3,55587
24	77,6	60,607	544	0	1E+11	3	3,47697	4,01502
24	77,6	60,607	544	0	1E+11	3	3,39396	2,71056
24	77,6	60,607	544	0	1E+11	3	3,43991	3,77076
15	62,2	57,93	524	0	1,04E+10	1	2,84913	2,8981
15	62,2	57,93	524	0	1,04E+10	1	3,99631	4,02854
15	62,2	57,93	524	0	1,04E+10	1	3,75189	5,74434
15	62,2	57,93	524	0	1,04E+10	1	2,81544	5,12915
1	69,9	60,78	946	0	3,22E+10	3	2,45804	2,18338
1	69,9	60,78	322	0	3,22E+10	3	3,53515	2,28543
1	69,9	60,78	559	0	3,22E+10	3	3,30061	3,81772
1	69,9	60,78	744	0	3,22E+10	3	4,67771	3,69533
1	69,9	60,78	239	0	3,22E+10	3	3,18956	4,05273
8	22,3	64,622	593	7,90E-93	5,03E+08	1	3,29999	2,17747
2	6,7	74,866	682	3,85E-20	2,15E+08	1	2,59016	1,71249
7	17,2	80,947	719	4,51E-40	4,7E+08	2	3,83952	1,32685
5	32,1	37,333	346	1,77E-28	3,01E+08	4	1,55357	2,29267
5	32,1	37,333	346	1,77E-28	3,01E+08	4	1,81003	1,94067
4	28,2	23,277	220	4,90E-26	4,05E+08	1	2,83034	3,31099
4	24,7	17,348	150	4,46E-11	1,46E+09	2	2,47046	-1,07949
22	16,2	231,35	2105	4,64E-104	4,35E+09	4	1,85486	1,31779
11	15	121,71	1064	4,68E-47	3,4E+08	1	2,15058	3,0278
10	18,9	83,516	724	1,68E-62	1,13E+09	6	2,707	3,56346
10	18,9	83,516	724	1,68E-62	1,13E+09	6	2,76513	4,41627
10	18,9	83,516	724	1,68E-62	1,13E+09	6	3,65534	2,02467
10	18,9	83,516	724	1,68E-62	1,13E+09	6	3,18554	3,58478
6	26,7	47,318	416	4,99E-79	1,25E+09	2	1,34481	2,47812
18	23,7	105,01	946	1,90E-299	1,34E+09	3	2,43087	3,78972
13	17,5	105,01	946	1,13E-110	1,1E+09	3	1,83261	1,83358
13	17,5	105,01	946	1,13E-110	1,1E+09	3	2,38686	2,0211
8	40,5	36,314	321	3,10E-43	2,97E+09	3	2,06142	2,3423
5	13,7	54,388	488	4,42E-22	1,94E+09	1	1,38387	-2,55805
8	10,5	118,92	1073	1,41E-66	1,34E+09	4	1,97156	4,2035
30	29,6	118,92	1073	2,14E-200	2,15E+10	4	2,68414	3,36125
30	29,6	118,92	1073	2,14E-200	2,15E+10	4	2,53422	1,75801
5	5,2	231,37	2119	1,07E-64	2,98E+08	1	1,48115	2,92026
14	10,8	206,23	1842	5,08E-96	3,31E+09	3	2,60597	2,65876
6	37,2	30,114	261	7,00E-27	9,18E+08	2	3,60558	2,56669
16	37,8	56,379	513	3,19E-163	2,42E+09	7	2,63269	1,18545
4	29,7	37,54	330	7,06E-159	2,14E+09	2	2,93023	2,57198
14	26,5	88,337	780	2,90E-148	6,44E+08	3	2,71174	3,58895
14	26,5	88,337	780	2,90E-148	6,44E+08	3	4,1655	4,51262
5	20,4	60,824	524	1,05E-33	2,58E+09	5	1,50251	2,1335
6	8,8	184,93	1650	9,37E-37	4,48E+08	1	3,19444	-3,94763

8	15,9	77,221	674	2,88E-96	3,31E+08	5	2,18132	1,71266
8	15,9	77,221	674	2,88E-96	3,31E+08	5	1,69791	1,87488
3	4,5	101,22	971	3,53E-23	1,05E+09	1	3,1007	1,24475
5	16,2	43,76	390	6,19E-29	1,37E+09	10	1,46557	1,54184
5	26	27,372	246	2,23E-17	4,95E+08	3	2,81704	-1,92171
4	23,9	24,72	222	4,02E-14	3,71E+08	1	2,27088	1,84656
4	27,2	27,057	239	5,84E-17	8,9E+08	5	3,15285	1,4651
9	50	24,423	216	8,16E-280	5,3E+10	3	3,73274	-2,16769
9	50	24,423	216	8,16E-280	5,3E+10	3	2,46733	-1,80242
9	50	24,423	216	8,16E-280	5,3E+10	3	2,62782	-1,72239
6	42,4	20,825	184	2,74E-53	4,42E+09	3	1,76309	2,10246
27	59	66,076	607	0	4,62E+10	2	2,383	-1,98375
8	16,8	80,782	679	5,88E-88	5,61E+08	4	2,78589	3,53558
2	29,7	44,728	396	5,60E-207	7,02E+08	5	2,48757	2,2636
12	29,3	59,846	547	5,51E-124	1,5E+09	1	1,84948	2,6773
12	29,3	59,846	547	5,51E-124	1,5E+09	1	5,16327	3,51903
12	29,3	59,846	547	5,51E-124	1,5E+09	1	2,4611	1,95265
12	18,8	76,956	686	4,73E-24	2,19E+08	1	1,69557	2,04105
7	11,4	158,17	1354	6,41E-34	1,5E+08	2	1,66186	1,95278
71	55,5	160,61	1388	0	4,58E+10	5	1,70148	4,03564
71	55,5	160,61	1388	0	4,58E+10	5	1,99056	2,26665
71	55,5	160,61	1388	0	4,58E+10	5	2,48041	5,11748
71	55,5	160,61	1388	0	4,58E+10	5	3,72766	6,66399
59	43,8	166,88	1388	0	2,15E+10	5	4,45629	3,22498
59	43,8	166,88	1388	0	2,15E+10	5	2,40269	2,89005
3	27,3	14,759	128	1,29E-16	1,92E+09	2	2,14051	-2,19044
1	29,8	9,461	84	1,40E-61	8,43E+08	2	2,31643	-2,11114
12	35,6	61,557	564	0	1,65E+09	5	1,86834	2,28117
12	35,6	61,557	564	0	1,65E+09	5	1,50719	2,78953
4	12,4	63,012	564	8,62E-19	2,57E+08	5	3,1623	1,26275
4	19,1	38,586	350	2,89E-113	1,47E+09	3	1,8261	1,28197
3	16,3	47,129	429	6,72E-142	1,13E+09	4	2,41624	2,1921
14	46,2	54,935	478	4,63E-106	9,6E+08	9	1,96655	2,00679
20	58,6	50,648	437	0	4,29E+10	4	1,91506	1,61324
12	59,3	55,874	484	0	5,55E+09	8	1,76789	2,48995
13	25,9	79,375	696	2,27E-102	1,26E+09	1	1,98981	2,53203
13	25,9	79,375	696	2,27E-102	1,26E+09	1	4,71703	4,20948
13	25,9	79,375	696	2,27E-102	1,26E+09	1	2,66164	2,75257
4	7,8	93,446	892	9,27E-23	2,33E+08	6	2,54616	3,2279
3	17,5	34,166	320	6,53E-28	1,88E+08	3	1,76164	-2,1152
10	11,8	141,46	1233	3,75E-86	8,44E+08	3	1,47971	2,59183
14	28,2	91,85	901	0	7,56E+09	8	1,73499	2,89459
8	29,1	60,988	539	1,62E-39	1,88E+09	4	2,16773	1,77942
8	23,8	54,937	512	2,55E-40	2,51E+08	1	1,88766	1,89641
8	23,8	54,937	512	2,55E-40	2,51E+08	1	4,0622	3,23212
5	6,6	124,45	1099	2,97E-36	2,03E+08	5	1,91852	1,75187
2	36,7	55,72	504	8,55E-41	1,09E+09	4	1,51404	-2,09161
7	20,5	41,655	371	1,04E-64	6,81E+08	4	2,22178	3,21514
3	12,8	59,771	548	1,07E-09	3,05E+08	4	1,71872	-2,38329
3	17,5	37,066	326	3,14E-90	5,69E+08	6	1,76369	1,4445

5	21,1	33,053	284	1,05E-48	8,72E+08	2	2,67894	3,57202
1	24,5	25,977	2055	1,43E-46	1,2E+10	1	1,40755	-3,55848
9	12,9	119,96	1240	3,03E-87	1,87E+08	2	2,39243	1,89454
9	12,9	119,96	1240	3,03E-87	1,87E+08	2	2,89179	2,52665
13	12,9	192,56	1715	4,42E-133	6,76E+08	3	2,82945	-3,07947
4	8,4	74,455	669	1,32E-11	1,77E+08	4	1,77188	-2,31111
17	27,7	80,774	744	5,31E-281	8,67E+08	3	2,62151	2,62855
17	27,7	80,774	744	5,31E-281	8,67E+08	3	4,02197	3,89108
31	17,4	347,94	3102	0	4,08E+09	5	1,91357	-2,48628
20	41,6	68,489	603	0	2,47E+09	4	2,61827	4,09685
20	41,6	68,489	603	0	2,47E+09	4	3,24598	5,69973
20	41,6	68,489	603	0	2,47E+09	4	2,33981	5,97729
6	46,1	26,201	228	3,88E-79	3,98E+09	2	3,58273	3,34181
9	35,9	32,926	290	6,34E-100	1,71E+09	1	1,42193	1,97247
4	34,1	19,481	167	4,32E-32	1,05E+09	1	2,81691	-1,37308
24	50,6	61,508	559	0	2,14E+10	4	3,23029	4,27576
24	50,6	61,508	559	0	2,14E+10	4	3,2692	5,38568
24	50,6	61,508	559	0	2,14E+10	4	4,04126	2,12129
15	40,5	55,203	501	0	6,88E+09	2	3,52642	4,97187
15	40,5	55,203	501	0	6,88E+09	2	3,36055	6,40397
15	40,5	55,203	501	0	6,88E+09	2	3,23365	1,4132
32	68,9	54,274	501	0	2,89E+10	3	3,23215	2,33355
32	68,9	54,274	501	0	2,89E+10	3	4,48616	4,77987
32	68,9	54,274	501	0	2,89E+10	3	3,42644	5,66159
4	18,8	36,943	261	2,26E-19	4,01E+08	4	2,27024	-3,15362
6	18,5	50,08	493	8,13E-28	5,29E+08	2	3,70893	4,00003
29	78,9	46,297	440	0	1,55E+10	2	2,27212	3,99915
29	78,9	46,297	440	0	1,55E+10	2	3,98838	4,25088
29	78,9	46,297	440	0	1,55E+10	2	3,41332	5,13459
17	50,9	49,452	485	0	9,56E+09	4	3,96563	3,0361
17	50,9	49,452	485	0	9,56E+09	4	2,75699	3,64346
17	50,9	49,452	485	0	9,56E+09	4	4,59703	4,8972
12	62,7	35,316	322	7,31E-82	1,78E+09	1	4,80753	3,08332
2	29,7	70,406	1078	4,13E-74	1,76E+08	5	1,30407	1,77061
19	69,6	35,316	322	4,40E-187	7,63E+09	1	3,21491	3,13639
19	69,6	35,316	322	4,40E-187	7,63E+09	1	2,45817	1,65002
19	69,6	35,316	322	4,40E-187	7,63E+09	1	2,86812	1,38016

PLA-tested	reference	Listed in Hippie
	http://www.biochemsoctrans.org/content/34/1/73.long http://www.biochemsoctrans.org/content/34/1/73.long	
	http://www.biochemsoctrans.org/content/34/1/73.long http://www.biochemsoctrans.org/content/34/1/73.long http://www.jbc.org/cgi/pmidlookup?view=long&pmid=8349582	
yes yes		
	http://www.jbc.org/content/276/47/44247.full	
		+
		+
		+
		+
		+
		+
http://scri		+
http://scri		+
		+
		+
		+
		+

+
+
+

http://ww +

+

+
+

+
+
+

+
+
+
+
+
+
+
+
+
http://eur +
http://eur +

http://ww +
http://ww +
http://ww +
http://ww +

http://www.plosone.org/article/info%3Adoi%2F10.1371%2Fjournal.pone.000

http://eur +
http://eur +
http://eur +

+
+
+

http://eur +

http://ww +

+
http://onli +
http://onli +
http://onli +
+
+

+
+

+
http://ww +
http://ww +

+
http://www.nature.com/ncb/journal/v4/n9/full/ncb835.html
http://www.nature.com/ncb/journal/v4/n9/full/ncb835.html

+
http://ac.els-cdn.com/S0092867401005207/1-s2.0-S0092867401005207-mai
http://ac.els-cdn.com/S0092867401005207/1-s2.0-S0092867401005207-mai

http://ww +
http://ww +
http://ww +

+
+
+

http://ww +
http://ww +

+
http://pub +

yes
yes
yes
yes

http://ww +

yes
yes

+
+

yes (negative)
yes (negative)

yes (negative)
yes
yes

http://ww+
http://ww+
http://ww+
http://onli+
http://onli+
http://ww+
http://ww+
http://ww+
http://onli+
http://eur+
http://eur+
http://eur+
http://ww+
http://ww+
http://emb+
+
+
http://ww+
http://onli+

+

+
+
+
+

http://ww+

http://www.nature.com/onc/journal/v20/n50/full/1204921a.html

http://ww+
+

http://ww +
http://ww +

+
http://mcb.asm.org/content/16/10/5313.long
yes
yes
yes http://ww +
yes http://ww +
http://mcb.asm.org/content/16/10/5313.long
http://mcb.asm.org/content/16/10/5313.long

http://ww +
http://ww +

yes
yes
yes
http://eur +

http://ww +
http://ww +
http://ww +
http://ww +

http://ww +
http://ww +

http://www.ncbi.nlm.nih.gov/pubmed/16417486

+
http://ww +
http://ww +

+

yes

)2462

n.pdf?_tid=39f8bef6-4b10-11e3-bd22-00000aacb361&acdnat=1384202061_6ff1ea34f83a469f29a6a
n.pdf?_tid=39f8bef6-4b10-11e3-bd22-00000aacb361&acdnat=1384202061_6ff1ea34f83a469f29a6a

ab91c66c5692
ab91c66c5692

Antibodies used in PLA

Name (clone)	Host species	Working dilution PLA	Company	Recommended by manufacturer for	Reference link
ACAT1 (HPA004428)	Rabbit	1:400	Atlas antibodies	IF	http://www.sigmaaldrich.com/catalog/product/sigma/hpa004428?lang=de&region=DE
C1Orf198 (HPA004798)	Rabbit	1:400	Sigma	IF	http://www.sigmaaldrich.com/catalog/product/sigma/hpa004798?lang=de&region=DE
Cdc42 (B-8)	Mouse	1:400	Santa Cruz	IF	https://www3.scbt.com/scbt/product/cdc42-antibody-b-8
Cdc42 (P-1)	Rabbit	1:300	Santa Cruz	IF	https://www3.scbt.com/scbt/de/product/cdc42-antibody-p1
IQSEC3	Rabbit	1:400	Atlas antibodies		
Mzt2 (C-14)	Rabbit	1:200	Santa Cruz	IF	https://www3.scbt.com/scbt/de/product/mzt2a-b-antibody-c-14
Opa1 (55772)	Mouse	1:400	Abcam	IF	http://www.abcam.com/OPA1-antibody-ab55772.pdf
Rac1 (23A8)	Mouse	1:500	Upstate	IHC	http://www.abcam.com/rac-antibody-23a8-ab13048.html (immunohistochemistry)
Rac1 (20571-1-AP)	Rabbit	1:300	Proteintech	ELISA	http://www.ptglab.com/Products/RAC1-Antibody-20571-1-AP.htm (ELISA)
RhoA (26C4)	Mouse	1:400	Santa Cruz	IF	https://www.scbt.com/scbt/product/rho-a-antibody-26c4
RhoA (119)	Rabbit	1:300	Santa Cruz	IF	https://www.scbt.com/scbt/product/rho-a-antibody-119
Rock2 (1E12)	Rabbit	1:200	Abnova	IF	http://www.novusbio.com/ROCK2-Antibody-1E12_H00009475-M02.html
SESTD1 (LS-B5489)	Rabbit	1:1,000	LS Bio	IHC	https://www.lsbio.com/antibodies/antibody-ihc-plus-ls-b5489/140038 (immunohistochemistry)

Legends to Supplemental Figures and Tables

Fig S1: GTPase activity of purified recombinant RhoA, Cdc42, and Rac1 under different conditions. GTPase activity was determined by monitoring GTP to GDP ratios over time by HPLC measurements. GTP-loaded GTPases were incubated with either buffer (greyline) or cell lysates of Citrine (green line) or Citrine-GAP (blue line) transfected cells. Samples were collected at different time intervals, immediately treated with TCA for protein precipitation and neutralized with NaOH. Guanine nucleotide ratios were determined by HPLC and relative GTP ratios calculated from GTP/(GTP+GDP). Rate constants (k_{cat}) of intrinsic GTP hydrolysis were calculated from exponential fittings on the data. All three GTPases showed GTPase activity that was further stimulated by the respective GAP.

Fig S2: LF-qGAP from brain lysates from additional tissues for (A) Rac1 (Cerebellum), (B) RhoA (Cerebellum) and (C) Cdc42 (Hippocampus). Specific interactors (colored in orange) are distinguished from background proteins based on a combination of the log2 fold change and the t-test p-value. GTPγS-specific interactors are expected in the upper right corner, interactors of the GDP-form in the upper left corner.

Fig S3: Validation of loading state dependent interactions *in situ* with the proximity ligation assay (PLA) (details given in Fig. 5A). This figure is complementary to figure 5.

Fig S4: Fragment spectra of Rho GTPase interactors identified by only one peptide sequence. For each protein the best available spectrum of the corresponding peptide was selected. All spectra are shown in the mass to charge deconvoluted version as listed in the msms.txt as provided by MaxQuant. Red peaks belong to the y-ion series, blue peaks to the b-ion series and grey peaks are unidentified background peaks of each spectrum. Orange labels indicate a modification of the corresponding fragment.

Table legends

Supplemental Table 1: Interaction partners of Rho GTPases. For the six Rho GTPases RhoA, RhoB, RhoC, RhoD, Rac1 and Cdc42 a total number of 293 distinct interactions were identified with LF-qGAP. A number of interactions were identified repeatedly in different tissues.

Supplemental Table 2: List of antibodies used for the proximity ligation assays. This list gives additional information about suppliers, used dilutions and reference links.